UNIVERSIDADE DE LISBOA
FACULDADE DE CIÊNCIAS

Ciências
ULisboa

Combined brain language connectivity and intraoperative neurophysiologic techniques in awake craniotomy for eloquent-area brain tumor resection

"Documento Definitivo"

Doutoramento em Engenharia Biomédica e Biofísica

João Carlos Leote Rebocho

Tese orientada por:
Doutor Hugo A. Ferreira
Doutora Rita G. Nunes
Doutor Josep Valls Solé

Documento especialmente elaborado para a obtenção do grau de doutor

2019

UNIVERSIDADE DE LISBOA
FACULDADE DE CIÊNCIAS

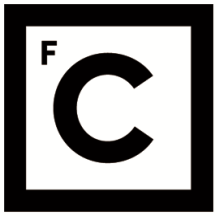

Ciências
ULisboa

Combined brain language connectivity and intraoperative neurophysiologic techniques in awake craniotomy for eloquent-area brain tumor resection

Doutoramento em Engenharia Biomédica e Biofísica

João Carlos Leote Rebocho

Tese orientada por:
Doutor Hugo A. Ferreira
Doutora Rita G. Nunes
Doutor Josep Valls Solé

Júri

Presidente: Doutor José Manuel Nunes Vicente Rebordão, Investigador Coordenador da Faculdade de Ciências da Universidade de Lisboa;

Vogais: Doutor Josep Valls Solé, retired Associate Professor da Faculty of Medicine da University of Barcelona (Espanha) (Orientador);

Doutor Albino Jorge Oliveira-Maia, Professor Auxiliar Convidado da Nova Medical School da Universidade Nova de Lisboa;

Doutor Rafael Neto Henriques, Postdoctoral Researcher na Fundação Champalimaud;

Doutor Martin Lauterbach, Médico especialista em Neurologia e Psiquiatria, na qualidade de individualidade de reconhecida competência na área científica em que se insere a tese;

Doutor Pedro Michael Cavaleiro de Miranda, Professor Associado da Faculdade de Ciências da Universidade de Lisboa;

Doutor Alexandre da Rocha Freire de Andrade, Professor Auxiliar da Faculdade de Ciências da Universidade de Lisboa.

Documento especialmente elaborado para a obtenção do grau de doutor

2019

PREFACE

Modern neuro-oncology comprises the management of various types of tumors within the central nervous system by a multidisciplinary healthcare team. Cerebral primary brain tumors invade white and grey matter tissues disrupting neural circuits and imposing local functional reorganization. At some point, secondary to brain tumor growth, symptoms become more obvious, especially affecting speech and language function. Moreover, the location of brain tumors entails broader concerns due to the high probability of neurological morbidity following surgical treatment.

Knowledge about speech and language brain structure went through an unprecedented growth due to recent advances in neuroimaging tools and analysis methods. These allowed to integrate neuroscience research procedures with clinical management. Nowadays, the paradigm of surgical treatment of brain tumors involving eloquent brain tissue is to avoid neurological morbidity achieving the maximum tumor resection (i.e. the gross resection). Particularly when facing tumors involving the speech area, a variety of procedures and techniques have been employed to identify eloquent brain tissue during presurgical planning and intraoperatively. Current patient management comprises the use of brain mapping techniques. However, their influence on treatment varies depending on the neurosurgery department's experience and methods developed from their own translation clinical studies.

The present work was conducted to obtain the third cycle of academic education degree from-Faculdade de Ciências Universidade de Lisboa (Portugal). The main purpose of this thesis was to develop experimental conditions for patients with brain tumors involving speech-related regions to either detect or preserve such function. Knowledge and tools based on neuroimaging techniques and neurophysiological methods were used. This thesis is divided into four sections where speech and language function was evaluated using tractography and connectivity neuroimaging methods during speech processing, and using an accelerometer-based method for speech recording. The introductory chapters review each section's background and methodology, discussing how it may influence current clinical practice. Experimental conditions developed along the three sections focused on reconstruction of anatomical axonal bundles using diffusor

kurtosis imaging, graph-theory connectivity analysis using functional magnetic resonance imaging and detection of language disturbances with an accelerometer and a conventional electromyography apparatus. Functional magnetic resonance imaging was performed in Sociedade Portuguesa de Ressonância Magnética (Hospital da Cruz Vermelha, Lisboa) and the experiments were performed either in Neurosurgery Department at Hospital Garcia de Orta (Almada) or in Electromyography unit (Neurology Department) of the Hospital Clinic of Barcelona.

This thesis aspires to help clinicians and graduate students, serving as a reference to complement patient evaluation in presurgical and intraoperative stages regarding speech and language brain function.

Joao Leote

ACKNOWLEDGMENTS

I would like to thank to:

Josep Valls-Solé, the greatest Mentor of all times, for the guidance and patience and for driving me into ambitious goals.

Mafalda Perez, the Wife, for the love and resilience.

Manuel Cunha e Sá, the Chief, for the unconditional support of my management in the neuromonitoring field at his Neurosurgery Department (Hospital Garcia de Orta).

Rita G. Nunes and **Hugo A. Ferreira**, the research Tag team, for their patience and effort to provide mentoring without constraining my arborous goals.

Isabel Fernandez Conejero, the First person, for receiving me abroad, for sharing her knowledge and neuromonitoring passion with me.

João Costa, Faculdade de Medicina, Universidade de Lisboa and Fundação Calouste Gulbenkian (**GAPIC program**) for the opportunity and the economic support, respectively, in 2014.

NOTA PRÉVIA

A presente tese contém capítulos já publicados de forma integral ou parcialmente (capítulos IV, VI, VII, XI), e outros preparados para ser submetidos de acordo com o Regulamento de Estudos Pós-Graduados da Universidade de Lisboa, e no Despacho nº 4624/2012 do Diário da República II série nº 65 de 30 de Março de 2012. O candidato realizou os trabalhos em colaboração, mas liderou e participou integralmente na conceção dos mesmos, desde a obtenção dos dados, análise estatística, discussão dos resultados e redação dos manuscritos.

Lisboa, 18 de Dezembro de 2019

João Leote

LIST OF CONTRIBUTORS

Catarina Viegas, MD
Neurosurgery Department, Hospital Garcia de Orta, Almada.

Cátia Gradil, MD
Neurosurgery Department, Hospital Garcia de Orta, Almada.

Hugo A. Ferreira, MD, PhD
Instituto de Biofísica e Engenharia Biomédica, Faculdade de Ciências da Universidade de Lisboa, Lisboa, Portugal.

Joana Monteiro, MD
Neurosurgery Department, Hospital Garcia de Orta, Almada.

Jordi Casanova-Molla, MD, PhD
EMG and Motor Control Unit. Neurology Department. Hospital Clinic, University of Barcelona. Barcelona, Spain. Universitat de Barcelona, IDIBAPS. Barcelona, Spain.

Juan M. Castellote, MD PhD
Department of Physical Medicine and Rehabilitation, Universidad Complutense de Madrid, and National School of Occupational Medicine, Instituto de Salud Carlos III, Madrid, Spain.

Judith Navarro-Otano, MD
EMG and Motor Control Unit. Neurology Department. Hospital Clinic, University of Barcelona. Barcelona, Spain. Universitat de Barcelona, IDIBAPS. Barcelona, Spain

Josep Valls-Solé, MD, PhD
EMG and Motor Control Unit. Neurology Department. Hospital Clinic, University of Barcelona. Barcelona, Spain. Universitat de Barcelona, IDIBAPS, Barcelona, Spain

Martin Lauterbach, MD, PhD.
Neuroradiology Department, Hospital da Cruz Vermelha, Lisboa, Portugal.

Luís Cerqueira, MD
Neurosurgery Departament, Centro Hospitalar Central de Lisboa. Lisboa. Portugal.

Ricardo Loução, MSc
Institute of Neurosciences and Medicine – INM 3, Forschungszentrum Jülich, Jülich, Germany.

Rita G. Nunes, PhD
Department of Bioengineering and Institute for Systems and Robotics (ISR/IST), LARSyS, Instituto Superior Técnico, Universidade de Lisboa. Lisboa. Portugal

ABSTRACT

Speech processing can be disturbed by primary brain tumors (PBT). Improvement of presurgical planning techniques decrease neurological morbidity associated to tumor resection during awake craniotomy. The aims of this work were: 1. To perform Diffusion Kurtosis Imaging based tractography (DKI-tract) in the detection of brain tracts involved in language; 2. To investigate which factors contribute to functional magnetic resonance imaging (fMRI) maps in predicting eloquent language regional reorganization; 3. To determine the technical aspects of accelerometric (ACC) recording of speech during surgery.

DKI-tracts were streamlined using a 1.5T magnetic resonance scanner. Number of tracts and fiber pathways were compared between DKI and standard Diffusion Tensor Imaging (DTI) in healthy subjects (HS) and PBT patients. fMRI data were acquired using task-specific and resting-state paradigms during language and motor tasks. After testing intraoperative fMRI's influence on direct cortical stimulation (DCS) number of stimuli, graph-theory measures were extracted and analyzed. Regarding speech recording, ACC signals were recorded after evaluating neck positions and filter bandwidths. To test this method, language disturbances were recorded in patients with dysphonia and after applying DCS in the inferior frontal gyrus. In contrast, HS reaction time was recorded during speech execution.

DKI-tract showed increased number of arcuate fascicle tracts in PBT patients. Lower spurious tracts were identified with DKI-tract. Intraoperative fMRI and DCS showed similar stimuli in comparison with DCS alone. Increased local centrality accompanied language ipsilateral and contralateral reorganization. ACC recordings showed minor artifact contamination when placed at the suprasternal notch using a 20-200 Hz filter bandwidth. Patients with dysphonia showed decreased amplitude and frequency in comparison with HS. ACC detected an additional 11% disturbances after DCS, and a shortening of latency within the presence of a loud stimuli during speech execution

This work improved current knowledge on presurgical planning techniques based on brain structural and functional neuroimaging connectivity, and speech recording.

Key-words: Speech; Language; Brain Tumor; Awake craniotomy; Presurgical planning

RESUMO

A função linguística do ser humano pode ser afetada pela presença de tumores cerebrais (TC) A melhoria de técnicas de planeamento pré-cirurgico diminui a morbilidade neurológica iatrogénica associada ao seu tratamento cirúrgico. O objetivo deste trabalho é: 1. Testar a fiabilidade da tractografia estimada por difusor de kurtose (tract-DKI), dos feixes cerebrais envolvidos na linguagem 2. Identificar os fatores que contribuem para o mapeamento linguagem por ressonância magnética funcional (RMf) na predição da neuroplasticidade. 3. Identificar aspetos técnicos do registo da linguagem por accelerometria (ACC).

A DKI-tract foi estimada após realização de RM cerebral com 1.5T. O número e percurso das fibras foi avaliado. A RMf foi adquirida durante realização de tarefas linguísticas, motoras, e em repouso. Foi testada influência dos mapas de ativação calculados por RMf, no número de estímulos realizados durante a estimulação direta cortical (EDC) intraoperatória. Medidas de conectividade foram extraídas de regiões cerebrais. A posição e filtragem de sinal ACC foram estudadas após vocalização de palavras. O sinal ACC obtido em voluntários foi comparado com doentes disfónicos, após estimulação do giro inferior frontal, e após a adição de um estímulo sonoro perturbador durante vocalização.

A tract-DKI estimou um elevado número de fascículos do feixe arcuato com menos falsos negativos. Os mapas linguísticos de RMf intraoperatória, não influenciou a EDC. Medidas de centralidade aumentaram após neuroplasticidade ipsilateral e contralateral. A posição supraesternal e a filtragem de sinal ACC entre 20-200Hz demonstrou menor ruido de contaminação. Este método identificou diminuição de frequência e amplitude em doentes com disfonia, 11% de erros linguísticos adicionais após estimulação e diminuição do tempo de latência quando presente o sinal sonoro perturbador.

Este trabalho promoveu a utilização de novas técnicas no planeamento pré-cirúrgico do doente com tumor cerebral e alterações da linguagem através do estudo de conectividade estrutural, funcional e registo da linguagem.

Key-words: Linguagem; Tumor Cerebral, Planeamento pré-cirúrgico, Craniotomia Acordada.

PUBLICATIONS

Chapter II

Peer reviewed Journal (Impact factor 3.7). Invited Editorial.
- J. Leote, R.G. Nunes, H.A. Ferreira. Editorial on "Improved Quantification of Myelin Water Content Using Joint Parametric Group-wise Sparsity of T2* Decay". Journal of Magnetic Resonance Imaging. 31; 1-2, 2020.

Chapter IV

Peer reviewed Journal (Open Access)
- J. Leote, R. Loução, L. Cerqueira, R.G Nunes, H.A Ferreira. "Reconstruction of white matter fibre tracts using diffusion kurtosis tensor imaging at a 1.5T: presurgical planning of patients with gliomas". European Journal of Radiology Open, 28; 5: 20-23, 2018.

Chapter VI

Peer reviewed journal (Impact factor 1.1)
- J. Leote, R. Loução, C. Viegas, M. Lauterbach, A. Hick-Perez, J. Monteiro, R.G. Nunes, H.A. Ferreira. "Impact of navigated task-specific fMRI on direct cortical stimulation." J Neurol Surg A Cent Eur Neurosurg. Accepted for publication. Proof-readed at May 2020.

Chapter VII

Peer reviewed Conference Proceedings
- J. Leote, R. Loução, M. Lauterback, J. Monteito, R.G. Nunes, C. Viegas, A. Pérez-Hick, A. Silvestre, H.A. Ferreira. "Understanding network reorganization after glioma regrowth: comparing connectivity measures from functional magnetic resonance imaging to direct cortical stimulation." IEEE 6th ENBENG, 1-5, 2019.

Chapter VIII

Conference Abstract
- J. Leote, R. Loução, R.G. Nunes, C. Viegas, M. Lauterbach, A. Silvestre, J. Monteiro, A. Pérez-Hick, H.A. Ferreira. "Connectivity analysis of glioma patients with language disturbances." Clinical Neurophysiology, 129: 1, e53-54, 2018.

Chapter IX

Conference Abstract
- J. Castellote, J. Leote, J. Valls-Solé. "Accelemetric recording of changes in voice production in teachers after daily task." European Journal of Neurology 25; 2, 623, 2018.

Conference Abstract
- J. Leote, J. Castellote, C. Viegas, C. Lopes, M. Silva, R.G.Nunes, H.A.Ferreica, J. Valls-Solé. "Accelerometer speech recording: technical aspects, reliability, clinical and intraoperative utility" European Journal of Neurology. Waiting for publication.

Chapter X

Peer reviewed Journal (in Portuguese)
- C. Viegas, J. Leote, A. Silvestre, A. Pérez-Hick, L. Albuquerque, M. Cunha e Sá. "Ressecção de um Gliossarcoma com Cirurgia Acordada para Mapeamento da Linguagem." Gazeta Médica, 4 (3), 2017.

Conference Abstract
- J. Leote, J. Valls-Solé, J. Costa, J. Casanova-Molla, L. Oleaga, J. Foncesa, R.G.Nunes, H.A.Ferreira. "Vocal accelerometer recording of TMS evoked language disturbances: preliminary study for awake surgery application." Brain Stimulation: Basic, Translational, and Clinical Research in Neuromodulation, 10; 2, 352, 2017.

Chapter XI

Peer reviewed Journal (Impact factor: 2.7)
- J. Leote, J. Castellote, J. Casanova-Molla, J. Navarro-Otano, R.G. Nunes, H.A Ferreira, J. Valls-Solé. "Motor preparation in picture naming tasks." Brain Lang. 180-182:24-30, 2018.

Conference Abstract
- J. Leote, J. Castellote, J. Casanova-Molla, J. Navarro-Otano, R.G. Nunes, H.A Ferreira, J. Valls-Solé. "Motor preparation in picture naming tasks." Clinical Neurophysiology. 129: 1, e222, 2018.

CONTENTS

LIST OF FIGURES

LIST OF TABLES

LIST OF ACRONYMS

3D – Three Dimensional

ACC – Accelerometer

AD – Axial Diffusivity

AF – Arcuate Fascicle

AG – Angular Gyrus

AI - Asymmetry Index

AK – Axial Kurtosis

BET – Brain Extraction Tool

BOLD – Blood Oxygen Level Dependent

BST – Brain Tumor Subjects

CM – Cortical Mapping

CMRR – Common Mode Rejection Ratio

Cop – Central Operculum;

CST – Corticospinal Tract

DCS – Direct Cortical Stimulation

DI – Deviation Index

DK – Diffusion Kurtosis

DKI - Diffusion Kurtosis Imaging

DKI-tract – DKI-based Tractography

DTI – Diffusion Tensor Imaging

DTI-tract – DTI-based tractography

DWI – Diffusion-Weighted Images

eCM – Electrical Cortical Mapping

EMG – Electromyography

EPI – Echo Planar Imaging

FA – Fractional Anisotropy

FLAIR - Fluid-Attenuated Inversion Recovery

fMRI - Functional Magnetic Resonance Imaging

FSL – FMRIB Software library

FWHM – Full Width at Half Maximum

HS – Healthy Subjects

IFG – Inferior Frontal Gyrus;

IS – Imperative Stimuli

LW – Learned Word condition

mCM – Multimodal Cortical Mapping

MD – Mean Diffusivity

MK – Mean Kurtosis

MMT – Mouth Motor Task

MRI – Magnetic Resonance Imaging

MTG – Middle Temporal Gyrus

nfMRI – Navigated Functional Magnetic Resonance Imaging

NVSDt - Non-verbal Visual Semantic Decision task

opIFG – Opercular part of Inferior Frontal Gyrus;

orbIFG – Orbitalis part of the Inferior Frontal Gyrus

PBT – Primary Brain Tumor

PNt – Picture Naming task

PoG – Postcentral Gyrus

PrG – Precentral Gyrus

r-nTMS – Repetitive Navigated Transcranial Magnetic Stimulation

rs – fMRI – Resting-state functional Magnetic Resonance Imnaging

RD – Radial Diffusivity

RK – Radial Kurtosis

RMT – Resting Motor Threshold

ROI – Region-Of-Interest

RT – Reaction Time

RW – Random Word

RW – Randomly Word condition

SAS – Startling Auditory Stimulus

SCA – Seed Correlation Analysis

SD – Standard Deviation

SFG – Superior frontal Gyrus;

SLOG – Superior Lateral Occipital Gyrus;

SMG – Supramarginal Gyrus

SNR – Signal-to-Noise Ratio

SPG – Superior Parietal gyrus,

STG – Superior Temporal Gyrus

SW – Same Word condition

TE – Echo time

TR – Repetition time

trIFG – Triangularis part of the Inferior Frontal Gyrus

UDKI – United Diffusion Kurtosis Imaging Toolbox

VGt – Verb Generation task

VSDt – Verbal Semantic Decision task

SECTION A: INTRODUCTION, INSTRUMENTATION AND METHODOLOGY

CHAPTER I

SPEECH AND LANGUAGE FRAMEWORK

Complex brain functions are now systematically studied using a whole-brain network perspective (i.e. axonal pathways between functional regions) after evolving from a paradigm structure-related function. A progressive disruption of the brain neuronal networks is caused by primary brain tumors (PBT), such as gliomas representing a significant health problem worldwide. Current studies estimate between 30,000 and 35,000 new cases of PBT per year in United States of America and an incidence of 5.0 per 100.000 in Europe.[1]

Overall an increase in incidence was noted related in part to the advances in neuroimaging and to a higher access to health care system in non-industrialized countries.[1] However, the prognosis and survival of patients remains poor, depending on the histological type and age of presentation. Tumors with high malignancy cells are refractory to almost all modalities of treatment. In fact, the median survival time varies from 18 months for patients with a high malignancy tumor (i.e. glioblastoma multiforme) to 10 years for patients with a low grade malignancy tumor (i.e. astrocytoma).[1] . Surgical intervention is a common initial therapy mainly for reduction of tumor burden, control of seizures, relief of neurological deficits and mass effect. Most surgeons aim to achieve the gross tumor resection defined by the enhancing tumor volume and regionally infiltrated brain identified by magnetic resonance imaging (MRI) sequences. Anatomical scans are commonly used for tumor volume delineation based either in contrast-enhanced images after peripheral contrast injection or in fluid-attenuated inversion recovery images. Gross tumor resection is non-curative but has previously been correlated with longer progression free survival and improved quality-of-life.[1]

Recent advances in neurosciences allowed a technology expansion in neurosurgery departments improving the cortical and subcortical mapping of eloquent brain tissue. Techniques such as: transcranial magnetic stimulation (TMS); tractography derived from diffusion weighted magnetic resonance imaging; functional magnetic resonance imaging (fMRI) at the preoperative period; or direct cortical stimulation (DCS); neuro-navigation; and monitored tumor resection in the awake patient at the intraoperative time; permit to delineate tumor margins with greater acuity. In addition, cortical mapping (CM) techniques allow to identify redistribution of eloquent areas after cortical reorganization, known to be induced by slow growing low-grade gliomas. Overall the

availability of these techniques has allowed tumor resection closer to healthy surrounding brain regions and vascular structures.

The relevance of each technique for the patient treatment management remains inconsistent across studies, depending on the function aimed to be mapped and the experience of the neurosurgical team. Therefore, there is no worldwide consensus. In fact, most of the protocols used to implement a specific technique evolved from "home-made" research studies done at some point along the clinical practice.

This thesis presents an introductory speech and language background comprising a summary of the multiple works performed to test different experimental conditions. Along this volume, the term speech refers to how sounds and words are produced (i.e. articulation, voice and fluency) whereas language refers to the words used and how we use them to share ideas (including meaning, syntax and phonological connotation). Before describing the experimental conditions, a review of the instrumentation and methodology used to study speech and language is provided in more detail (section A). It combines different methods used to study speech and language such MRI techniques as diffusor tensor imaging (DTI) and kurtosis tensor imaging (DKI) for white matter pathways reconstructions (tractography) and fMRI with conceptual approaches incorporating maps calculated from the general linear model and effective connectivity using graph-theory. Moreover, TMS and DCS were used to study causal interactions within the language network and accelerometer (ACC) based speech recording. The aim of this thesis was to develop preoperative and intraoperative methods used to map speech and language within the brain tissue.

Speech processing and production

Eloquent cortex is defined as a region indispensable for certain cortical functions.[2] Current knowledge about language function define a framework with distinct neural circuits and regions involving a high order network.[3] The language network classically consists in an area controlling expressive (i.e. Broca's area) and receptive aspects of language (i.e. Wernicke's area) connected by white matter axonal bundles. The dual-stream model described by Hickok and Poeppel (2004)[4] to explain speech processing gained support in the last decade and is now generally accepted (figure 1). This perspective evolved from the traditional Wernicke–Lichtheim–Geschwind "house" model, which suggests a center that stores the sound-based representations of words with two pathways projections, one to the center that stores the meanings of words and another to the center for speech planning and production.[3,5] Speech perception is initially made in cortical superior temporal regions and further comprehension processing projects to temporal regions

(ventral stream) while auditory to motor coding and speech production projects to tempoparietal and frontal regions (dorsal stream). These brain functional areas are connected via inferior fronto-occipital fasciculus, middle longitudinal fasciculus, and inferior longitudinal fasciculus for semantic processing, and via superior longitudinal fasciculus for phonological processing, respectively.[6] In fact, the dorsal stream was previously defined as the pathway connecting the posterior frontal and superior temporal lobes described by Burdach and later confirmed by Dejerine who referred to the pathway as Burdach's arcuate fasciculus (AF).[3] AF are known to connect directly Wernicke's area with Broca's area, and to connect indirectly Broca's territory with the inferior parietal lobule (anterior segment) and the inferior parietal lobule with Wernicke's territory (posterior segment).[7] Ontological development of human language may be related with dorsal stream maturation. Early leftward asymmetry of the AF is already present in early life.[8,9]

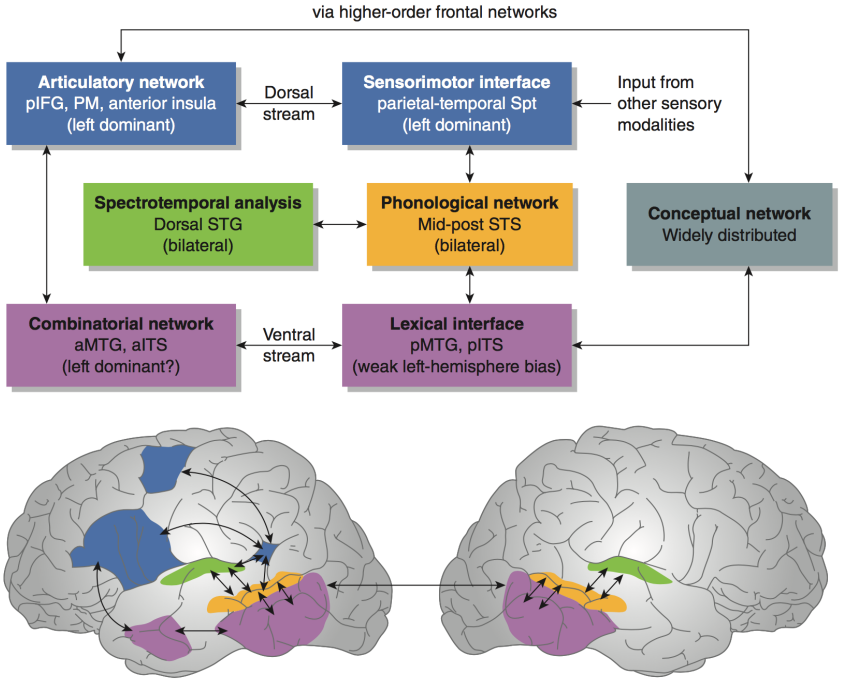

Figure 1.1 – The dual stream model of speech processing adapted from [6]. The ventral stream is responsible for speech perception whereas the dorsal stream is known to be involved in speech production. aMTG - Anterior middle temporal gyrus; aITS - anterior inferior temporal sulcus; pIFG - Posterior inferior frontal gyrus, pITS - Posterior inferior temporal sulcus; PM - precentral motor area; pMTG – Posterior middle temporal gyrus; Spt - Sylvian parietal temporal region (left only); STG – Superior temporal gyrus; STS – Superior temporal sulcus.

1. Tractography

Speech processing white matter pathways studies are based either in axonal bundles characterized after human brain dissection or in vivo non-invasive tractography assessed from MRI. Anatomical pathway connections are perceived using diffusion weighted imaging (DWI) which measure the random motion of water molecules and through DTI, its three-dimensional orientation is estimated.[3] The disconnection of white matter tracts may produce permanent neurologic deficits

and therefore surgeons increasingly incorporate tractography in routine operative planning. The main tracts reconstructed were the corticospinal tract (CST) and language processing involved pathways (including AF). In patients with brain neoplasms, tractography results may be interpreted as the following: signal with altered position (displacement); and loss of signal i) with normal tract positions (increased water diffusion i.e. edema) ii) with tract interruption (such as in tumor infiltration) and iii) with corresponding fiber destruction.

In section B, a study is presented describing the estimation of tracts using DKI as an extension to DTI, to which it is also compared. Thereafter, healthy subjects were recruited to develop an MRI protocol able to estimate kurtosis metrics using a conventional 1.5T scanner. Applicability in patients with PBT at the presurgical planning stage evaluating CST was also assessed. DKI-based tractography (DKI-tract) of CST and AF was performed and compared to DTI-based tractography (DTI-tract) in patients with PBT. The purpose was to verify if DKI and DTI-based motor and language streamlined tracts showed quantitative or qualitative (i.e. interpretation of tract patterns) differences in presurgical planning. The estimation of tracts was made using MATLAB (Mathworks, USA) using algorithms previously developed to guarantee a short time period dispended in data processing (see chapter II for further details). These experiments tried to cover the limitations of DTI-tract in patients with brain neoplasms which infiltrate cerebral white mater parenchyma, imposing a complex microscale architecture. Thus, the value of DKI-tract to depict false negative tracts (not streamlined by DTI) compromising the evaluation of anatomical brain connectivity and explaining possible neurological symptoms was assessed.

2. Brain functional language mapping

Functional MRI provides high spatial resolution maps of brain function by measuring changes in cerebral blood flow as a surrogate for neuronal activity. Behavioral tasks (paradigms) are intended to be performed by subjects in the magnetic resonance (MR) scanner in order to localize functionally specialized regions that activate in response to a specific aspect of behavior. In patients with PBT, successful surgical treatment is somewhat dependent on the determination of eloquent cortical areas, predicting deficit in cognitive (such as language) or sensorimotor functions. Furthermore, asymmetries in the activation pattern mainly in language function indicates the lateralization which may facilitate the localization of a functional deficit zone. fMRI of language processing aims to anticipate language function regions to minimize postoperative language deficits. Moreover, it may be integrated with other imaging modalities for preoperative planning.[10]

Speech and language mapping with non-invasive fMRI at the presurgical stage helps surgeons to plan the tumor resection. However, fMRI does not enable to distinguish essential from participating language areas. Thus, DCS is considered the gold standard for accurate brain language mapping while the patient performs language tasks during asleep-awake-asleep surgery (i.e. awake craniotomy). This anesthesia modality allows to awake patients to perform behavioral tasks after using a combination of local anesthetic field block and short-acting general agents. DCS during glioma awake craniotomy resulted in 2% persistent language deficit 6 months after surgery, in a series of 250 patients with low grade gliomas.[11] However, the efficiency of these anesthesia protocol in patients with high grade gliomas remains to be studied.

Invasive stimulation of the human brain provides unique opportunities to study fundamental processes with a high temporal resolution. DCS of the brain was found to be safe and current practice suggests its use for language mapping while the patients with PBT perform language tasks as during presurgical fMRI studies. Intraoperative language tests usually consist in counting or picture naming tasks (PNt) which test the integrity from visual stimuli interpretation to name generation while the surgeon stimulates the cortical surface. Essential language sites are usually localized to spatially discrete areas in DCS mapping compared to the broader regions identified by fMRI. Moreover, fMRI's acuity to detect areas with language function in comparison with DCS in patients with left perisylvian tumors has been associated with a lower sensitivity (about 30%) and high specificity (about 90%). In contrast, for brain areas without tumor but with language function, fMRI showed a sensitivity and specificity of about 60% in comparison with DCS.[16]

In section C, speech and language connectivity was investigated through fMRI and DCS. The purpose of the section was to investigate: i) the influence of presurgical language functional methods on the technical aspects of DCS and ii) the value of graph theory based connectivity analysis of language to map network reorganization after glioma regrowth and iii) the possibility to detect functional language areas using resting state fMRI (rs-fMRI).

In chapter VI, the impact of methodological issues of imaging processing, language task selection, the surgeon's attitude in DCS are debated. Patients with PBT were recruited to perform either multimodal cortical language mapping (mCM) with DCS and navigated fMRI or electrical cortical language mapping (eCM). The goal was to perceive the influence of the fMRI data from three language paradigms on practical aspects of the DCS. The scope of the developed experiments was to record if such data availability decreased the number of stimuli given intraoperatively, the number of after discharges, seizures and the time dispended for CM. In addition, the correspondence between fMRI and DCS language mapping was assessed.

i. Language network connectivity

Current data shows that language epicenters (or "hubs") encompass other frontal, temporal, parietal, and occipital regions in the left and right hemispheres in a wide-ranging network. Interaction patterns observed in the brain are far from regular and far from random. MRI offers the possibility to map interactions such as observed in other technological, social and biological systems, leading to the development of the statistical mechanics of complex networks and measures.[17]

White matter fibers do not have a function on its own, but their lesion causes structural and functional changes in connected grey matter areas. Moreover, localization of functional brain areas is possible through task-based fMRI. The integration of both types of knowledge allows to study functional (and effective) connectivity. Similarity of the BOLD signals from different brain regions is likely to mean that the regions are passing on information.[18] Thus, in order to study connectivity, current methodology often looks at spontaneous fluctuations in the signal when there are no specific cognitive demands for the subject. Connectivity perspective is based on the construct that a higher oxygen consumption occurs by a self-organized framework processing (i.e. group of interconnected areas) if a subject adopts a rest posture in comparison with an active posture (i.e. performing a task). Such spontaneous fluctuations of brain activity present a low frequency signal between 0.01-0.08 Hz which can be depicted by fMRI due to low concentration of deoxyhemoglobin during a rs-fMRI.[19,20]

rs-fMRI helps to understand the brain's intrinsic architecture and the level of communication whereas task-specific fMRI relies on a difference in the MRI signal between an active and a rest state considered as baseline. In presurgical planning, rs-fMRI could be a viable alternative to task-based fMRI in brain tumor operative planning due to the short scan duration and absence of cognitive demands in patients unable to collaborate during fMRI scans.

In chapter VII, a small group of patients with PBT involving language related areas were followed since the diagnose to tumor recurrence after receiving surgical treatment. A graph analysis was made using task-based fMRI at the presurgical stage. Connectivity measures were extracted from language related areas and were compared to task fMRI and DCS results, to understand language functional reorganization during tumor development. The purpose of this experiment was to perceive the relation of the connectivity measures from language regions (defined by DCS) and to recognize how these changes from task fMRI and DCS results.

A continuum graph analysis[21] was performed in chapter VIII but using rs-fMRI. Presurgical neuroimaging data from patients with PBT was retrospectively analyzed using a data driven approach after defining a region of interest using DCS results from language functional areas. A mixture of voxel and node-based analysis was performed to perceive if the functional language areas could be identified without using a task paradigm during the fMRI presurgical study. The goal was to test if the graph theory method could identify relevant language-related areas at the presurgical stage in non-cooperative patients during rs-fMRI.

3. Speech recording

Speech production is part of speech processing and involves the language dorsal stream within the frontal brain regions which are responsible for muscles activation and phonation. Clinical assessment of speech is based on patient history and comprehensive physical examination. However, reliable and objective analysis of the speech is also an essential part of a physical examination. Objective measures of phonatory ability are helpful in the treatment of patients with voice disorders and in assessing the results of surgical therapies.[22, 23]

After the initial use of kymograph and oscillography to perform physiological measurements of speech, engineering developments led to the use of digital frequency analyzer and sound level meters. Current methodology used for speech recording in voice laboratories involves high quality microphones, amplifiers, acoustically shielded booths with sound-absorbent walls and dedicated software to manipulate speech acoustics.[23,]

Conventional computer driven analysis is used to generate a waveform (i.e. amplitude by time display) which consists in a sum of frequencies with different amplitudes and phase relations from the acoustic signal. Spectral analysis of frequency and amplitude are often performed from short segments of prerecorded voice samples to extract phonation measures. However, waveforms can also be generated by measuring vocal tract vibration with transducers such as electromyographic signal or another time-varying signal able to be transformed into voltage variation.[23, 24] Laryngeal waveforms can also be generated using an ACC placed over the patient's throat transforming vocal tract vibration into a signal waveform. ACC recordings provide signals that are relatively free of contamination by resonance effects of nonlaryngeal structures and that are less costly, despite their lower specificity and lower accessibility to reproduce speech during a taped session. However, when patients complain of harsh or hoarse voice, an important clinical decision must be reached about its pathological or functional aetiology. Therefore, the major applications of automatic, low budget, and sensible methods to detect frequency and amplitude speech variations are i) priority assessment and referral of patients for laryngeal examination by specialists, ii) diagnostic support with acoustic signal quantification and iii) monitoring of speech changes over

time (i.e. radiotherapy, surgery, speech therapy).[24] Therefore, ACC recordings made in the neurological field using conventional (available) equipment such as electromyography (EMG) apparatus can be a useful clinical tool. However, such recordings made using these electronics (amplifiers, electrodes types, vocal tract position) remain to be studied.

In section D, a PNt was used in healthy subjects and patients in order to evoke word pronunciation. Different experiments were developed focusing on the articulatory network for speech production. The aim was to develop a speech recording method useful in presurgical and intraoperative stages of the current patient management which would be able to detect an evoked disruption of the language dorsal stream. To study the effects on speech production, language disturbances were induced by brain stimulation techniques.

In chapter IX, ACC based recordings were studied in more detail in healthy subjects. The descriptive experiments intended to understand the technical and physiological factors influencing the ACC recordings of the vocal tract vibration using a conventional EMG equipment. ACC signals were decomposed into parameters such as latency to phonation, amplitude, duration and frequency. Furthermore, technical aspects (such as position and bandwidth filtering) were studied and reliability was tested. Experiments in patients with infectious laryngitis were also made in order to investigate deviation in ACC parameters from healthy subjects.

In chapter X, the ACC recording method developed was used to detect language disturbance evoked by repetitive and a navigated TMS (r-nTMS). The stimulation was used to perturb neuronal activity and disrupt speech processing at inferior frontal gyrus (IFG). Navigation across subject brain anatomical scans was possible after co-registration of structural MRI scans with a TMS coil using a based stereotactic method. Moreover, an ACC based speech recording methodology was used in the intraoperative theatre to record language disturbances evoked by DCS while patients performed a PNt after awaked from sedation.

Along this journey studying speech production, a set of experiments focused on understanding speech execution were also developed and described in chapter XI. Speech execution is performed as a voluntary motor movement in contrast to speech production (with previous cognitive processing). Therefore, modified versions of PNt with random versus known picture were showed to healthy subjects whereas a loud sound was randomly presented with picture presentation. The goal of this chapter was to demonstrate that for speech execution, cognitive processing does not occur if the subject is able to anticipate a word to be pronounced. For speech recording the ACC based method developed was used.

Finally, concluding remarks concerning the development of the themes approached along this work are provided. The aim of this final chapter is to promote future lines of investigation on each theme.

This page was intentionally leftt blank

CHAPTER II

NEUROIMAGING AND SPEECH PROCESSING

Magnetic Resonance

1. Basic principles

MRI is a non-invasive method that enables soft tissue imaging of the human body and metabolic processes allowing to diagnose conditions of people of almost any age. An image is generated using protons and their magnetic properties. The term magnetic refers to the use of magnetic fields whereas resonance refers to the need to match the (radio) frequency (RF) of an oscillating magnetic field to the frequency of the nuclear spin (i.e. circular motion of the axis of rotation in relation to another fixed axis) in a tissue molecule.[26]

MRI takes advantage of the abundance of water constituting up to 90% of the human tissue. Hydrogen is a single-charged spinning nucleon with an orbiting negative electron. The balance and opposite charges within its structure forms a dipole exhibiting electromagnetism proprieties (i.e. intrinsic magnetic moment). Hydrogen has just one proton in its nucleus (i.e. odd mass number) imposing a net spin or an angular momentum in addition to the conventional atomic nuclear spin. These characteristics enable to maximize the amount of available magnetization in the body.[27]

When hydrogen atoms are exposed to a static magnetic field (B0), some of the intrinsic magnetic moments of the nuclei align parallel with the magnetic field (in the same direction), while a smaller number of the nuclei align anti-parallel to the magnetic field (in the opposite direction).[27] The alignment of these magnetic moments produces a significant net magnetization vector that is used in for clinical MRI. At high field strengths fewer nuclei have enough energy to join the high-energy population with an anti-parallel direction to the stronger B0 field, resulting in a higher magnetization vector.[27]

When the magnetization vector deviates from the B0 direction (i.e. following an excitation for example), it will start moving around B0 in a type of motion called precession, which causes the tip of the magnetization vector to follow a circular path around B0. This (precessional) path has a speed (frequency) which depends on both the B0 field intensity and on the specific nucleus. The term precession (motion) reflects the interaction between the spinning magnetic field and the mass of the proton.[27] The precession angular frequency ($\omega 0$) for the proton magnetic moment vector is given by the Larmor equation:

$$\omega 0 = \gamma B0 \quad (2.1)$$

where γ is a constant called the gyromagnetic ratio (MHz/T). This ratio expresses the relationship between the angular momentum and the magnetic moment of the active nucleus. It is specific to each nucleus and it is expressed as the precessional frequency at 1 Tesla (T). The unit of precessional frequency is megahertz (MHz) and the γ of hydrogen is 42.57 MHz/T. Since each element has its own γ, this allows to specifically image hydrogen and ignore other magnetic active atoms in the body.[27]

The RF pulse at the resonant frequency (Larmor frequency) of the precessing hydrogen nuclei changes the proton energy through nuclear resonance producing: 1. Deviation angle (flip angle) of the net magnetization vector from previous B0 aligned vector with a magnitude that depends on the amplitude and duration of the RF pulse (i.e. transverse magnetization plane); and 2. The same precessional path position is imposed to the hydrogen nuclei.[27] Therefore, the nuclei resonance imposes a transverse plane magnetization vector that is in phase and precesses at the Larmor frequency. This resonance leads to an RF emission that is the primary MRI signal received by the MR coils. The signal amplitude decreases with time as the proton spins begin to dephase and to longitudinal transverse magnetization, returning to the equilibrium condition and alignment with B0 field, respectively (i.e. free induction decay).[28]

Image reconstruction is performed by correlating a series of signal measurements with the spatial locations of the different sources. The RF signal received, suffers a two- or three-dimensional Fourier transformation which converts a graph of signal intensity versus time, into a spectrum, a graph of signal intensity versus Hertz (Hz).[26,28] If an additional external magnetic gradient is added to the field, the spatial location of the received RF signals can be estimated. Thus, across the sample of RF signals, a varying signal frequency is described according to:

$$\omega(x) = \gamma(B0 + x.G(x)) \quad (2.2)$$

where x denotes the spatial coordinate along the direction of the gradient of the added field. Overall, the spectral components received have spatial information (K-space matrix) offering the possibility to reconstruct the physical object (in an image).[26, 28]

2. Image contrast

The process by which spins lose energy and return to an equilibrium state after receiving an RF pulse, is called relaxation. During this process, an increase of the longitudinal net magnetization occurs (i.e. recovery), and at the same time, nuclear spins lose their coherence (same precessional

position), decreasing the amount of transverse magnetization (i.e. decay). Hence, the recovery of the longitudinal magnetization is described by a process termed T1 recovery and the decay of transverse magnetization is called by T2 decay, respectively. The former relates to the energy exponentially released to the surrounding atoms with a recovery time constant called T1 relaxation time after applying a 90ª RF pulse. The latter relates to an exponential decay of coherent transverse magnetization, with a decay time constant called T2 relaxation time, which takes up the time required for 63% of the transverse magnetization to be lost.[27] The brightest pixels in an image originate from a high amplitude and coherent transverse magnetization vector, which depend on tissue characteristics.[26] Thus timing parameters are used to enhance contrast after an RF pulse. The time between two RF pulses is known as repetition time (TR) and determines the amount of longitudinal relaxation (T1 relaxation) that is allowed to occur before the signal is read. In contrast, echo time (TE) is the time interval from the RF to the signal peak detected by the coil. This determines how much decay of transverse magnetization (T2 relaxation) is allowed to occur until the signal is read. Hence, the magnitude and timing of RF pulses are set based on the relaxation time constants for enhancing tissue contrast.[27]

T1 and T2 weighted images depend on the tissue proprieties because physiological factors such as inherent energy of the tissue, space within molecules and molecular Larmor frequency influence the relaxation times of the atoms. When energy transference within excited atoms occurs, the longitudinal relaxation time is shorter (i.e. spin-lattice time), whereas transference efficiency is greater when atoms share a similar Larmor frequency. In addition, packed atoms tend to dephase more rapidly and show a shorter T2 decay.[27] T1-weighted images were used in this work as anatomical or structural scans. For tap water, T1 is about 2500 ms whereas for fat T1 can be as short as 200 ms and for white matter tissue it can be as long as 500 ms (at a 1.5 T static magnetic field). Relevant for T2-weighted images, water has a relaxation T2 of 2500 ms, and white matter tissue shows a T2 of 100 ms. Additionally, the time from an RF pulse to the signal decay after the loss of spin coherence is called T2* decay and depends on the T2 decay and on the presence of magnetic field inhomogeneities. Inhomogeneities are areas within the magnetic field that do not exactly match the external magnetic field strength. These areas influence the precessional frequency of the surrounding atoms and their relative rate of acceleration/deceleration which causes also an exponential and fast spin dephasing. Therefore, the signal decay occurs in a faster way, decreasing the level of available signal which may compromise the MRI image quality.

3. *Echo and gradient echo pulse sequence*

In order to increase signal amplitude and to sensitize the signal to the microscopic magnetic field inhomogeneities, signal echo may be evoked. [27] In this thesis, T1 and T2* weighted images were acquired using an echo produced after the application of magnetic field gradients.

An echo gradient pulse sequence uses an RF excitation which flips the longitudinal net magnetization by any angle (i.e. flip angle). Thus, when a flip angle other than 90° is used, only part of the longitudinal magnetization is converted to transverse magnetization, which precesses in the transverse plane and induces a signal in the receiver coil. After the RF excitation, the signal starts to decay and the magnetic moments to dephase. In order to avoid this, an additional magnetic field is produced by a gradient. Magnetic field gradients are generated by coils of wire situated within the bore of the magnet. This gradient field is superimposed with the B0 field, so that the magnetic field strength along the axis of the gradient coil is altered in a linear way, but the middle of the axis of the gradients (magnet isocenter) remains at the field strength of the B0 field. The application of a gradient induces a polarization of the magnetic moments according to the direction axis of the applied gradient. Therefore, the precessional frequency of the spins increases if alongside with the applied gradient direction (axis) and decreases if following the opposite direction. The precessional frequency increases when the magnetic field increases and decreases when the magnetic field decreases.

In order to obtain an echo within the magneton axis, two gradients of opposite polarity must be applied to equalize accrued phase. The first gradient will promote a speed up of the nuclear magnetic moments in one end (along gradient direction) of the magneton, and the second a speed up in the nuclei at the opposite side. This sequence allows to measure protons signals (transverse net magnetization) in a shorter period of time, because the flip angles used are less than 90º degree. With low flip angles, full recovery of the longitudinal magnetization occurs sooner than with large flip angles. The TR can therefore be shortened without producing saturation. However, short scan periods come with the presence of additional "extrinsic" magnetic field inhomogeneity whose effects cannot be eliminated (i.e. T2' effects). The total relaxation is termed T2* (combined T2 and T2') and in gradient echo imaging this type of weighting is termed T2* weighting.[27,28]

To obtain a T1 weighted image using a gradient pulse sequence, neither the fat nor water vectors must have had time to recover full longitudinal magnetization. To avoid full recovery, the flip angle must be neither large (more than 70ª) nor very small (less than 20º) and the TR should be short (less than 50ms), so that the fat and water vectors are still in the process of relaxing when the next RF is applied. In contrast, to obtain a T2* weighted image, the differences in the T2* times of the tissues are maximized and the differences in the T1 times are minimized. To

maximize T2* decay, the TE is long (more than 25ms) so that the fat and water vectors have had time to decay sufficiently to show their decay differences. To minimize T1 recovery, the flip angle is small and the TR long (more than 1000ms) - enough to permit full recovery of the fat and water vectors.[26,27,28]

In sections B and D, volumetric and three dimensional (3D) T1 weighted images were acquired using magnetization prepared rapid gradient echo technique. A sequence with the following parameters was used: repetition time = 1880 ms; echo time = 3.09, inversion time= 1100, 256 x 256 matrix, pixel width = 130, flip angle= 15º and a 1 × 1 × 1 mm^3 voxel size.

In section C, fMRI experiments were conducted using a higher static magnetic field (3 Tesla), and included a volumetric T1-weighted acquired using a turbo field echo sequence which consisted in 160 slices with a repetition time = 11 ms, echo time = 4.6 ms, 256 × 256 matrix, pixel width = 142, flip angle =8º, FOV= and also using 1 × 1 × 1 mm^3 voxel size.

The strength of magnetic field influences the Larmor frequency at which the protons precess and the signal-to-noise ratio (SNR). RF signals show a quadratic growth with B0 strength but are also accompanied with a linear growth of noise.[27] A static magnetic field of 1.5 Tesla was used for sections B and D. In contrast, section C fMRI experiments were made using a 3 Tesla magnet.

Diffusion Weighted Imaging

Gradient diffusion is based on Fick's first law, which relates molecular motion (J), in which flow (from high to low concentration environments (C)) to the diffusion coefficient (D), intrinsic propriety of the medium (dependent on the temperature, size of the particles and on the microstructural features of the environment). This concept enabled to explicit the relationship between the mean-squared displacement ($<x^2>$) of Brownian (molecular) motion during a diffusion time (Δ) and the diffusion coefficient (D) mentioned in Fick's first law.[29]

$$< x^2 > = 2D\Delta \tag{2.3}$$

The microscopic random thermal Brownian motion of water molecules in the human body can be inferred through DWI. The diffusion coefficient has been measured for many body fluids (mm^2/s). The sensitivity of a given MRI sequence to diffusion (termed b), depends only on gradient magnetic fields, is computed for MR images (s/mm^2).[30] In order to describe water diffusion, an echo must be produced by a diffusion gradient, which consists in energizing at least one of the three gradients used in spatial localization (i.e. encode gradients: frequency, phase and readout).

The readout echo train may consist of spin echoes (generated by a train of 180° RF pulses) termed single shot spin echo or a train of gradient echoes termed echo planar imaging (EPI).

Either sequences begin with an excitation pulse and is followed by EPI readout of the gradient echoes which in this scenario, lead to images acquisition within one TR. To achieve this, each echo is phase-encoded by a different slope of gradient. A high amplitude magnetic field gradient switch is needed, evoking a train of echoes combined with rapid signal sampling of the echo's envelope. After a single RF pulse, the phase encoding gradient waveform consists of a string of short blips, whereas the frequency encoding gradients are turned on allowing signal acquisition following each blip. The acquisition data into k-space starts with the read gradient pulse, which moves the k-space sampling path from left to right (encoded by read-out gradient) whereas the blip pulse shifts the path up one row (phase-encoded gradient). Subsequently, an opposite polarity read gradient pulse is applied moving the path from right to left and the process goes on.[31] For performing such sequence, rise and fall times of approximately 100 μs and gradient magnetic fields exceeding 25 mT/m are required. Caution is needed because rapidly changing magnetic field (dB/dt) may result in nerve stimulation through magnetic induction, leading to muscle contraction.

In section B, DWI were acquired with 64 or 32 non-collinear gradient sensitizing directions using b-values of 0, 1000, and 2000 s/mm^2 with a spin echo EPI sequence with the following parameters: repetition time = 5800 ms, echo time = 107ms, 518×518 acquisition matrix resolution; pixel bandwidth = 1275 Hz, with a 3×3×3 mm^3 voxel size. Whereas for connectivity analysis, made in section C experiments, DWI were acquired with 32 non-collinear gradient sensitizing directions using b-values of 0 and 1000, s/mm^2 with a spin echo EPI sequence with the following parameters: repetition time = 8400 ms, echo time = 65ms, 320×320 acquisition matrix resolution, pixel bandwidth = 3000Hz, with a 2×2×2 mm^3 voxel size.

1. Diffusion tensor imaging

The most common method used to estimate the water molecules motion with a three-dimensional orientation is provided by DTI. The diffusion-weighted signal (S) and the non-weighted signal (S0) are related according to:

$$ln\frac{S}{S0} = -\sum_{i=1}^{3},\sum_{i=1}^{3} bijDij \qquad (2.4)$$

where b_{ij} is the *b-matrix* and D_{ij} the diffusion tensor.[30] The *b-matrix* effectively replaces the *b-value* and is calculated based on the diffusion gradients in the acquisition sequence (*b-vectors)*. The principal eigenvector of the diffusion tensor corresponds to the direction of maximum diffusivity depicting the dominant diffusion axis in each voxel.[32] The diffusion tensor comes in the following form:

$$D = \begin{bmatrix} Dxx & Dxy & Dxy \\ Dyx & Dyy & Dyx \\ Dzx & Dzy & Dzz \end{bmatrix} \quad (2.5)$$

Each diffusion gradient direction enables to estimate water diffusion along that gradient direction.[32] Therefore, the precision when estimating the diffusor tensor increases with the amount of gradient directions, but this also leads to longer acquisition times; a minimum amount of 6 different non-collinear gradient directions are required to estimate D_{ij}. [32,33]

Water molecules within the brain move mainly in the direction parallel to axonal bundles resulting in a anisotropic diffusion in regions of compact white matter tracts. Anisotropic diffusion within tracts can be described by a tensor aligned along the direction of greater diffusion.[32] Its main axis represents the main diffusivity direction, the eccentricity of the ellipsoid representing this tensor relates to the degree of anisotropy and its symmetry and length show the distance travelled as a result of diffusion. Therefore, after DT estimation, rotational invariant parameters may be calculated based on the eigenvalues of the DT. Metrics such as mean diffusivity (MD), fractional anisotropy (FA), axial diffusivity (AD) and radial diffusivity (RD) yield information used to infer on the microstructures present in each voxel.[30]

FA traduces the anisotropy inherent to each voxel ranging between 0, which means the diffusion is isotropic, and 1, which means that the diffusion happens in one direction only. In brief, to calculate the FA, the eigenvalues of the diffusion tensor must be calculated first. By convention, the first eigenvalue $\lambda 1$ gives the AD, and reflects the magnitude of diffusion along the principal component of the diffusion ellipsoid. Whereas the eigenvalues $\lambda 2$ and $\lambda 3$ are used to calculate the RD, reflecting diffusion along the other two components of the diffusion ellipsoid. Therefore, voxels where white mater tracts with one direction are predominant associated with FA values closer to 1.[30, 32]

DTI is based in some assumptions. The model uses a Gaussian distribution to describe the water diffusion motion within the biological tissues. Nonetheless, the high complexity of the brain structures shows a sharper and non-Gaussian water motion resulting in imprecise fiber estimation.[30] Furthermore, DTI assumes only one fibre population per voxel of the brain image.

However, currently it has been estimated that at least 30% of the brain voxels contain at least two different crossing fibre populations. Consequently, voxels with multiple fibres are assigned lower FA (anisotropy intrinsic to each voxel) than the real one.[33,34] To mitigate this limitation, several models are currently available to estimated diffusion within the brain. These approaches use either extended or refined models with multi-shell acquisitions (i.e. multiple b-values) which are often compatible with the deterministic methods available for brain fibre tracking.[35]

2. Diffusion kurtosis imaging

DKI was developed to address the DTI limitations ensuring a multi-shell acquisitions suitable for clinical use. DKI abandons the Gaussian model by including a kurtosis statistical measurement which calculates the degree of deviation from a Gaussian distribution. Furthermore, DKI successfully addresses the crossing fibres' issue showing increased sensitivity for fiber detection.[36,37] DKI is also compatible with the clinical routine with mean acquisition times of 5 minutes with 3 b-values, slightly increased when compared to those of DTI (mean acquisition time of 3 min with 2 b-values).[36] The kurtosis tensor (KT) is a 3×3×3×3 matrix and allows a characterization of the non-Gaussian diffusion. To estimate such a tensor, at least 15 non-collinear diffusion gradients must be applied with at least three *b-values*. The DKI studies in this work used a constrained linear least square method to estimate KT. This estimates plausible biological values besides finding the optimal solution that minimizes the sum of squared differences error.[36] The signal acquired by the receiver coils is quantified using:

$$ln\frac{S}{S0} = -b\,D_{app} + \frac{1}{6}\,b^2\,D_{app}^2\,K_{app} \tag{2.6}$$

where D_{app} and K_{app} are the apparent diffusion value and kurtosis value along a spatial direction (n):[36-39]

$$K\,(n) = \frac{MD^2}{D_{app}(n)^2}\sum_{i=1}^{3}\sum_{j=1}^{3}\sum_{k=1}^{3}\sum_{l=1}^{3} n_i n_j K_{ijkl} \tag{2.7}$$

$$D(n) = \sum_{i=1}^{3}\sum_{j=1}^{3} n_i n_j D_{ij} = n^T D n \tag{2.8}$$

Invariant rotational metrics can also be extracted in a similar way to the diffusor tensor (DT), in order to characterize diffusivities along the structures. A common metric (Mean Kurtosis - MK) uses the mean value of kurtosis along the three main axes. In contrast, FA_K measures kurtosis anisotropy and is close to 1 when there is a value of kurtosis (along the principal direction) that is substantially larger than the other two, and close to 0 when all three values of kurtosis are similar to each other.[37,38]

3. *Tractography*

DT and KT information on the direction of diffusion may be used to perform fibre tract reconstruction. The aim of tractography is to determine intervoxel connectivity based on the anisotropic diffusion of water. Deterministic methods are based on the assumption that the principal eigenvector is parallel to the dominant direction of the fibre, integrating information from neighboring pixels to define smooth trajectories. Such methods start in one point and consequently follow the diffusion path through the main diffusivity direction for each voxel, given by the DT's greatest eigenvalue.[30,33] However, DTI-based assumptions (see above) may introduce both false positives and false negatives tract connections in DTI-based tractography reconstruction.[33]

DKI-based tractography (DKI-tract) was recently studied[36-38] due to its ability to estimate a forth order tensor, and contributing to better spatial characterization of tissue microstructure. The first method to reconstruct fibres from DKI was based on the diffusion orientation distribution function that characterizes the spatial orientation of the displacement's distribution (i.e. water diffusion).[39] However, an algorithm based on kurtosis maxima was recently shown to detect multiple fibre populations within a voxel.[40]

In section B, CST and AF fibres were streamlined using DKI based kurtosis maxima tractography. Currently, DKI applications increased in literature due to the greater sensitivity to microstructural brain tissue.[36,] However, white matter fiber reconstructions using DKI are yet few in numbers probably because of their i) own limitations (greater sensitivity to multi-compartmental model parameters that may lead to instability when reconstructing white mater fibres); and ii) lack of routine protocols applicable to the clinical environment.[39] In spite of DKI be an advantageous method for studying the structural organization in a healthy brain,[39] studies on the influence of pathological neoplasms in kurtosis metrics remain sparse.[37]

In order to perform tractography from DWI, data preprocessing must be made to handle image artifacts. This arise from head motion, physiological factors, Nyquist ghosting from timing errors between sampling and gradient application, eddy currents (from high amplitude gradient switching). For this purpose, a careful data preprocessing was made, and a constrained fitting method was used to estimate DKI based fibres.

For DWI data processing and reconstruction of white matter fibres, the united DKI (UDKI) toolbox (v1.2) based in Matlab (MatlabWorks, USA) was used.[41] Non-brain tissues were removed from all DWI volumes with the brain extraction tool (BET), and eddy current correction was

made, using the FMRIB Software Library (FSL; v.4.2).[42] For MRI noise reduction, DWI data were smoothed with a Gaussian kernel with full width half maximum of 2.5 mm. Afterwards, DT and KT estimates were obtained by fitting the DWI data to the DKI model (see above) using an constrained linear least squares fitting approach. Standard MD and FA maps were then estimated and fibre direction estimation obtained from the KT. Fibre direction was directly estimated after defining the average perpendicular kurtosis along the spatial direction. In order to visually inspect and validate the tractography results, a 3D tractography visualization software named *TrackVis* (www.tracvis.org; v0.64) was used.[43] In section B of this thesis, a clinical routine protocol for DKI based fibres estimation was developed (chapter IV) and a comparison between DTI based tractography using the same methodology was tested (chapter V).

Functional Magnetic Resonance Imaging

T2* weighted images are closely related to T2-weighted ones, as both reflect relaxation of the transverse magnetization. The T2* relaxation time combines the real T2 of tissue plus the effect of magnetic field inhomogeneities (see above).[30] Gradient echo or multi echo approach may acquire a series of signals at different TE for T2 quantification, in order to analyze the distribution of different water compartments within brain tissues (i.e. such as in vessels or in myelin). In presurgical planning, T2* weighted images were used to provide functional information about brain regions activated during task and rest periods. The contrast mechanism (i.e. BOLD contrast) reflects a complex interaction between blood flow, blood volume, and hemoglobin oxygenation.[44] At the microscopic level, a neuron receives input through dendrites generating action potentials which propagate through axonal tracts to other cells, resulting in a localized increase in blood flow. Neuronal activity may be measured by either looking at their firing rate or by measuring the summation of the synchronized post-synaptic activity.[44] Current knowledge correlate the BOLD signal more strongly with post-synaptic activity than firing rate. Thus, neuronal post-synaptic activity reflects the release of vasoactive substances in which effective vasodilators are likely to increase blood flow at local gray matter with oxygenated blood (neurovascular coupling).[44] The magnitude increase of blood flow during cognitive or sensorimotor tasks, contrasts with the subject's brain at a resting-state or low-level control state.[10]

In each voxel, the MR signal reflects the proportion between oxyhemoglobin (negligible effect on T2 relaxation due to hemoglobin diamagnetic proprieties) and deoxyhemoglobin (which accelerates the rate of T2 relaxation due to iron paramagnetic proprieties).[44,45] Thus, after a hemodynamic demand from brain activity, deoxyhemoglobin forms (reducing MRI signal intensity) and consequently oxygenated inflowing of blood displaces the deoxyhemoglobin. By other words, during activity, blood flow to the cortex increases, causing a drop in deoxyhemoglobin, which results in a decrease in dephasing and a corresponding increase in signal intensity. However, the change in MR signal is small, and to obtain an acceptable SNR, an average over multiple repeat trials is performed.[10]

Cognitive tasks such as used to evaluate speech processing consists in a 0.5-1% signal change with a latency of 0.5-1.5s (and with a peak 4-8s after stimuli).[45] Such time scale to depict BOLD signal is one of the drawbacks of the technique, because it is a long time compared with that of neural firing (milliseconds).[46] In this thesis, for conduction tasks during MRI signal acquisition, a block paradigm was selected. It consists of alternating cycles between the task (active state) and the breaks (rest state). These alternating cycles consisting in trials and rest periods were repeated for 5 times enabling better statistical power due to acquiring more images per acquisition and

allowing signal averaging.[10] Once pairs (active vs rest periods) of BOLD images have been acquired, highlighted images were produced using the sets of baseline and with stimuli. Thus, they are co-registered with each individual T1 weighted anatomic scans. Alternatively, an event-related stimulus was used to perform a single event task (e.g. finger taping or mouth movement task) that has shorter duration and higher hemodynamic response.

For testing speech processing, we selected a verbal semantic decision task (VSDt), syntactic judgment. In the sentence processing task, the subject was instructed to interpret the meaning or to detect a syntactic error. We also used a verb generation task (VGt), where the patient was instructed to generate a verb in response to a noun. The tasks were showed on a screen mounted over the MRI head-coil and the responses were given by a button press. This high demand tasks were contrasted with baseline recordings which consisted in a simplified cognitive task where the participant had to perform a symbol search task. Two distinct symbols had to be found in a random letter string. Motor paradigms of the hand (finger tapping) and mouth (opening and closing jaw movements) were also used, however due to high imaging contrast (BOLD response amplitude of 5%), just 8 blocks were acquired.

In contrast to task-specific paradigms, the localization of brain regions involved in a given function may be performed by comparison the BOLD signals between regions when the subject was in rs-fMRI. In section C, resting periods of 150 volumes were also used acquired along 14,65 minutes. T2* weighted imaging was acquired using a gradient echo sequence with the following parameters: TR= 2000ms, TE= 23ms, flip angle= 90º degree, 128 × 128 acquisition matrix resolution, and 3 × 3 × 3 voxel size mm^3 with a gap of 0.5mm.

1. Noise in fMRI sequences

Functional brain regions results depend on data acquisition settings, preprocessing algorithm and connectivity analysis approach.[18] A drawback of gradient echo images is that with the increased magnetic field susceptibility and induced artifacts become more prominent with the use of increasing echo time values. The noise characteristics of fMRI data can pose a great challenge for the analysis process because MRI BOLD signal represents less than 2% or 3% of the total MRI signal.[10] Noise is originated by subject physiology factors, subject movements (structured noise) while some artifacts result from the scanner hardware.[46]

The majority of the hardware artifacts are easily avoided (RF noise or ghosting), but some need to be addressed during preprocessing. These artifacts occur as a result of inhomogeneities in the static magnetic field in the brain and are the following: scanner drift, very slow change in the baseline BOLD signal over time; distortions, as spatial warps in the image; and drop out, of the MR signal in certain anatomical regions. In addition, structured noise has its origin from

physiology factors (i.e., breathing) and movement of the subjects while they are in the scanner. Taking a breath results in small movements of the chest and abdomen, resulting i) head motion, and ii) increased susceptibility artifact due to chest air variation and consequent influence in the B0 field. These are depicted in image by aliasing of the MR signal (i.e., spread over all sampled frequencies). Head motion due to subject movement may be more problematic because it affects the data with spatial misalignment from one volume to the next, and with partial volume effects, spin history, and varying field inhomogeneities. However, dedicated algorithms have been developed for fMRI data preprocessing.

2. fMRI data preprocessing

A stable trade-off must be selected to achieve acceptable fMRI scans spatial resolution without a negative influence in noise and consequently on data analysis. Data analysis included motion and distortion correction, high pass filtering, spatial smoothing and specific noise reduction processing allowing BOLD MR signal isolation and analysis.

In section C, fMRI data preprocessing was done using either BrainVoyager (v.2.8, Brain Innovation, Maastricht, The Netherlands) for task-specific fMRI,[47] or using functional connectivity toolboxes, such as multimodal modal imaging brain connectivity analysis (v.1.0, MIBCA) toolbox,[48] and CONN toolbox (v.18.1)[49] developed in Matlab (Mathworks, USA). With these tools, DICOM files were either converted into "fmr" data or into nifti data format, in BrainVoyager and in Matlab-based toolboxes using the *dcm2nii* function available in the MRIcron package,[50] respectively. For task-specific fMRI scans, slice time correction was applied using sync interpolation and the order of slice scanning was considered as ascending interleaved. Mean intensity adjustment was performed with a cubic spline, 3D motion correction with trilinear interpolation, spatial smoothing with a Gaussian full-width-at-half-maximum (FWHM) filter of 7 mm. For drift removal, a linear trend removal of low frequency was used consisting in a nonlinear drift of 3 or less cycles (0.0063Hz) per time course for the block design. Then, a low pass Gaussian temporal filter with FWHM of two data points was applied.[47]

T1 weighted images were also corrected for spatial intensity inhomogenities. In addition, spatial transformations were combined and applied to transform the images into Talairach standard space. The two affine transformations and isovoxel scaling transformation were concatenated to form a single 4×4 transformation matrix.[47] For each voxel coordinate in the target (Talairach) space a piecewise affine "Un-Talairach" step was performed, followed by application of an inverted spatial transformation matrix. Consequently, the computed coordinates were used to sample the data points in the original 3D space using sync interpolation. For 3D visualization, the brain was segmented from surrounding head tissue which was removed. fMRI data were then

normalized followed by the application of the same transformation steps as performed for the 3D anatomical data set. This step resulted in normalized 4D volume time course data which was coregistered with the subject's 3D anatomical data set.[47]

For the calculation of the contrast, covariates of interest were used for hemodynamic frequency response prediction and sampling.[10,47] An average representation of the MR signal across healthy subjects was implemented using Statistical Parametric Mapping (SPM from Welcome Department of Imaging Neuroscience, London, UK),[50] as a third party tool of the BrainVoyager software, for pattern prediction of neural activity evoked by the experiment in a single voxel (i.e., univariate statistical technique). Therefore, the results from each patient after applying a 3D motion correction and a brain mask to the brain tissue were introduced as predictors consisting in 3 linear translation factors and 3 rotational factors in comparison with the data from the null hypothesis (i.e. experimental block with rest volumes).

The statistical fixed threshold was calculated using a false discovery rate with an alpha of 0.05. This intended to estimate a true-positive brain region for the eloquent function tested with a 95% confidence interval controlling the proportion of false-positive voxels present within a single map. Instead of controlling the false-positive rate at a map-wise level.[10] Correction for multiple voxels comparisons was also made to ensure that positive activations were only considered if surpassing the threshold. Statistics were implemented also taking into account the presence of noise and the consequential low temporal frequencies. Therefore, statistical analysis was conducted using Keith Worsley and Karl Friston's "modified" (1995)[52] general linear model instantiated in SPM.[51] In chapter VI, BOLD activation map was calculated with the simultaneous activation in at least two out of three language tasks used during fMRI. This "final" map was registered with anatomical scans which were implemented in an optical based surgical navigation system (StealthStation, Medtronic) to perform navigated Cortical Mapping (CM) procedures. This system is based on the satellite navigation and have two infrared cameras with a fixed relationship in space which detect passive markers (i.e. spherical reflectors) and calculate distance through triangulation method.[53] In chapter VI, we aimed to perceive the influence of navigated multiple language tasks BOLD activation on DCS.

MIBCA was used for performing connectivity analysis either using task-specific fMRI (Chapter VII) of rs-fMRI scans (Chapter VIII) due to is ability to aggregate different processing steps in one tool.[48] In addition, for DTI data preprocessing analysis was used the *dwidenoise* function of MRtrix,[54] and for rs-fMRI, the *denoising* function and a seed-based analysis function of the CONN toolbox.[49]

MIBCA uses third party software, such as FSL,[55] Freesurfer,[56] Diffusion toolkit,[43] and SPM[50] to

perform the data processing.[48] T1 weighted images processing consisted in BET[42] and then a brain mask was created using FSL's function. Sequentially, the Freesurfer function *recon-all* was applied, consisting in spatial alignment of the subject's brain to a standard space (MN1_152_1mm), which generated transformation matrices. These were used to transpose each region of interest (ROI) into the DWI and fMRI space. Then, this data was non-linearly registered to the anatomical images and the align of the parcellated ROIs was made. The brain segmentation and parcellation was made using the Havard-Oxford brain atlas.[57]

For DWI data processing, additional eddy current motion correction was made after applying BET. Denoising of DWI data were made using *dwidenoise*,[54] which estimated a noise map by exploiting data redundancy in the primary component analysis domain based on Marchenko Pastur distribution.[58] The DT was then reconstructed using *dti_recon* of Diffusion Toolkit[43] which computed the following maps: main eigenvector, apparent diffusion coefficient, FA and b0. Subsequently, the *dti_tracking* function was used to deterministically streamline fibres with *n* interpolated streamline method of fixed step-length. In addition, the *spline_filter* function was used to smooth the final tract. Between pairs of ROIs segmented in anatomical scans, the number of fibers, mean fiber length and mean fiber orientation were calculated, generating 3 different matrices, of which only the matrix of the number of fibers is defined as the structural connectivity matrix.[48]

fMRI data preprocessing performed with MIBCA was carried out using the FSL function, FEAT (FMRI Expert Analysis Tool).[55] The processing involved the following steps: MCFLIRT was used for motion correction,[59] slice-timing correction was applied using Fourier-space time-series phase-shifting; non-brain removal using BET; spatial smoothing using a Gaussian kernel of FWHM 8 mm; 4D data intensity normalization using a single multiplicative factor; and a high pass temporal filtering based on Gaussian-weighted least-squares straight line fitting, using a sigma of 50s. Then, after extraction of functional time series data from each ROI, statistical processing was made by calculating Pearson correlation between each pair of ROIs'. For the rs-fMRI data (Chapter VIII), the CONN toolbox data preprocessing algorithm was used. CONN data preprocessing also included some already mentioned steps for fMRI time series: spatial preprocessing, slice-timing correction, realignment, coregistration, normalization, spatial smoothing and segmentation. In addition, this algorithm dealt with MR signal noise which was implemented to increase the validity and the robustness of functional connectivity MRI analysis. An anatomical aCompCor strategy[60] is used to estimate a user defined number of orthogonal time series. By using principal component analysis of the multivariate BOLD signal within each of these noise ROIs. Therefore, it allows the possibility to define temporal confounding factors that may arise from indirect sources of noise (i.e. respiration cycles within a subject sessions), or from

BOLD signals obtained (white matter and CSF masks) ROIs. For each defined temporal confounding factors, first- and higher- order derivatives of the associated time series, and regression from the BOLD time series at each voxel were made and the resulting residual time series were band-pass filtered (0.009 to 0.08 Hz).[49]

3. Functional connectivity

Fine-scale connectivity occurs between neurons in local circuits in multiple adjacent cortical layers consistent with segregated subcolumnar cortical structures.[18] Selective activation of local areas via microstimulation triggers sparse patterns of activity when using a large-scale recording of multiple brain units.[61] Therefore, recent methods were adapted to study connectivity using rs-fMRI and are now available. They aim to detect similarities among distinct regions of the brain inferring connectivity. The problem of inferring connectivity between neurons may be described by the following equation:[62]

$$S = [S_i]_{NT} \tag{2.9}$$

S denotes the digital form of spike trains, of N neurons during an interval with length *T*. The paradigm of connectivity aims to identify the set of neurons, πi, out of the N neurons observed that affect the firing of the neuron *i*, or *Si*, in a statistical sense. S assumes a digital form of spike train with a firing range width Δ (usually 1–3 ms). This form assumes that at time *m*, $S_i(m\Delta) = 1$ indicates a spike while $S_i(m\Delta) = 0$ indicates no spike. Therefore, functional connectivity refers to the statistical dependence observed between the neuronal spike trains. This can result from the presence of a synaptic link between the neurons or it can be observed when two unlinked neurons respond to a common driving input. Effective connectivity refers to the causal relationships governing this dependence and involves identifying the pre- and post-synaptic neurons in the observed mixture activation.[61-63]

The methods available to study functional connectivity based on rs-fMRI[20] can be divided into voxel-based (such as seed-based correlation analysis) and node-based methods (like graph theory analysis).[64-65] In this thesis, both methods were used in chapters VII and VIII.

Seed-based correlation analysis (SCA) aims to obtain a whole brain map that describes the strength of functional connectivity of each voxel in the brain with the (seed) ROI. Such methods are used to make group-level analysis in order to compare the spatial organization of large-scale resting state networks. The node-based method used in Chapter VII defines a set of regions in the brain and looks at connections between these regions, but does not fully address how integration of information is structured between distinct functional regions (i.e. strength of connections).

In chapter VIII, a SCA were performed using the CONN toolbox. To define seed ROIs, information about cortical surface positive DCS sites for motor and language function were gathered from surgical navigation system and cortical brain surface photographs. These were defined in each subject anatomical scans with a 6x6x6 mm^3 (see chapter III). Seed-to-voxel analysis consisted in computing the temporal correlation (bivariate correlation) between the mean BOLD signals from a given ROI to all other voxels in the brain. Consequently, it was applied a statistical fixed threshold for the bivariate correlation maps and was calculated a false discovery rate with an alpha of 0.05 corrected for multiple voxels comparisons. The resulting activation maps were superimposed with connectivity fMRI matrices originated by MIBCA, and using the BrainConnectivity toolbox (incorporated as third-party software in MIBCA),[21] graph theory measures were extracted from significantly correlated brain regions ($p< 0.05$) using the coordinates of the correlation maps superimposed in atlas-based data-driven from fMRI matrices.

Node-based methods investigate connections defined as edges, between a larger number of functional regions defined as nodes (spatially smaller).[17,21] Data from fMRI are converted in weighted or unweighted matrix. In the former, a correlation is made to calculate matrix edges and subsequently thresholds are applied converting it into a binary matrix where 20% of the strongest connectivity edges are retained. The latter uses the original and unthresholded data of the network.[64] In order to describe properties of large or whole-brain networks the data can be represented in the form of a graph.[65] The graph theory-based approach relies on the perspective that brain macroscale networks are topologically organized in a non-trivial manner (e.g., small-world architecture and modular structure).[65] Therefore, a virtual graph represents a network where nodes are connected by edges, and are organized within in a specific module (such as cognitive system). From this network, metrics may be extracted revealing quantitative measures which may characterize the underlying organizational mechanism. In chapter VII, graph theory measures were extracted from task-specific fMRI data, from an atlas defined brain regions involved in language function and analyzed from the DCS perspective. Whereas, in chapter VIII, the connectivity metrics were extracted from rs-fMRI data, from regions defined by SCA from DCS positive sites for language function.

4. Functional connectivity data analysis

Functional connectivity analysis was made by calculating a correlation matrix for every ROI pair combination using the Pearson correlation within BOLD time series data.[49] Statistical threshold was applied for a significance level of 0.05 with Bonferroni correction. The correlation results were organized in a fMRI matrix studying connectivity and to perform graph theory analysis.[49] Further, binary matrix (weighted data) was generated using also the number of fibers (from DWI data) and functional correlation coefficient with *p*-values < 0.05 using fMRI. For each image

modality (DWI, fMRI and hybrid matrix), the mean of graph theory metrics was calculated using a third party Brain connectivity toolbox.[21] In addition, individual ROI graph theory measures were also calculated using unweighted matrix analysis.

In this thesis, a small range of graph theoretical measures were selected according with the hypothetical definition of each measure and to the experience from other authors and contributors to this work. Such metrics may be divided in segregation, functional integration and centrality measures. Segregation refers to the degree to which network elements form separate clusters (functional related brain areas) and correspond to clustering coefficient. A high clustering coefficient means that if nodes A and B are both connected to node C, they are also likely to be connected to each other.[21] Node degree is defined by the number of other nodes it is connected to. Nodes with a degree that is larger than the average degree in the graph are called hubs.[65] Functional integration measures refers to the capacity of the network to become interconnected and exchange information; it is defined by the characteristic path length (shortest path between nodes) coefficient. Whereas global efficiency is inversely proportional to the average minimum path length (i.e., one divided by mean path length), and is a measure of the efficiency of the graph as a whole.

Centrality measures consists in relevant brain regions (such as hubs) that often interact and facilitate functional integration in network resilience to a insult. Therefore, they are based in the construct that central nodes participate in many short paths within a network controlling network information. The participation coefficient assesses the diversity of interconnections of individual nodes within a specific network (module). A node with a low participation coefficient is also called a provincial hub facilitate the modular segregation whereas a node with high participation coefficient (connector hub) facilitate intermodular integration. Another centrality measure is betweenness centrality, defined as the fraction of all shortest paths in the network that pass through a given node.[21] Despite of providing local and long range connectivity information, an important challenge is to find meaningful ways to characterize brain networks such as language for current practice use (see chapter VII and VIII).[61]

CHAPTER III

BRAIN STIMULATION AND SPEECH RECORDING

Direct cortical and electrical stimulation

Invasive stimulation of the human brain provides unique opportunities to study fundamental processes with high temporal and spatial resolutions. The first electrical stimulation of the human brain was done by Roberts Bartholow (1874) but it was Penfield (1930s) who defined detailed maps of the homunculus on the primary motor and sensory cortex in patients with epilepsy.[67] The speech areas were described later and included anterior frontal areas, posterior temporal areas and superior parietal language areas. The purpose of the mapping procedure is to reliably identify cortical areas and subcortical pathways involved in motor, sensory, language, and cognitive functions.[2,67] In this thesis, DCS was used in Section C and D during intraoperative experiments for language mapping function.

1. Electricity principles and stimulation device

Conventional intraoperative neuromonitoring equipment is furnished with constant current and voltage stimulators. To understand such difference, basic electricity principles must be evoked. While MRI techniques are based on reorientation of positively charged nucleus particles named protons, electrophysiological techniques rely mainly in the negatively charged particles orbiting around the nucleus, the electrons. Materials that allow electrons to move freely are known as conductors like metals such as cooper, silver and platinum. Therefore, an amount of charge (Coulomb) is composed by approximately 6.24×10^{18} electrons.[68] In order to produce movement of electrons through a conductor, an electromotive force is needed (Voltage). This electromotive force results from a fundamental property of physics, which is that oppositely charged particles attract each other. Thus, when a difference in voltage exists between two points, the excess of electrons will move to the point with least electrons. Electron movement itself (current) may be measured in amperes (1 Coulomb passing a point in a conductor in 1 second). *Resistance* opposes the flow of electrons. Examples of resistance to electron flow are non-conductive particles such as rubber, ceramic, etc. The intensity of current I can be calculated using Ohm's law:

$$I = \frac{E}{R} \tag{3.1}$$

where E is the voltage from the battery (an electromotive source of electrons) and R is the resistance. A circuit also has a "reservoir" of current that is ideally a true electrical zero (connected to the earth).[69] The electric charges move from the positive side of the battery to the negative (deficiency), but electron flow occurs from the negative to the positive point.

Electricity is created by attaching a coil (a conductor shaped as a loop) to a mechanical rotation, with the coil placed perpendicular in a strong magnetic field.[70] As the conductor rotates in the magnetic field, electricity is generated and flows to an attached device. If current always flows in the same direction, it is named *direct current*, which describes electrons flow through a conductor to an electrical device and back to the power source.[69] *Alternating current* is used in wall sockets in hospital offices to provide energy to biomedical devices. In such case, electrons follow the path of a sine wave, flowing first in one direction and then reversing in the opposite direction. The current reverses polarity many times a second (cycles per second in Hertz). However, this energy source is not applied directly to human tissue.[69]

A more complex electrical circuit also takes into account *capacitance* (the property of a circuit which allows it to store an electrical charge) in which the amount of charge stored is proportional to the voltage across the circuit. *Inductance* is the property of an electrical circuit that causes it to oppose any change in current. This generates a magnetic field around the conductor, induced by the current. Inductive and capacitive reactants to current flow directly oppose each other. *Impedance* incorporates the total opposition to current flow in a circuit, including resistance, capacitive reactance, and inductive reactance. Impedance (measured in Ohm's) is equal to resistance in circuits with no inductance or capacitance or in circuits where inductive reactance equals capacitive reactance.[69]

The stimulators available in clinical practice produce a direct current either by delivering an adjustable voltage across the stimulating electrodes independent of the stimuli current (constant-voltage stimulator), or by delivering an adjustable current through the stimulating electrodes, essentially independent of their impedance (constant-current stimulator). In electrical cortical mapping, the latter is used, because when using the latter method, a decrease in impedance can dramatically increase the stimulation current.[2,70]

2. Current, local potentials and stimulation parameters

In section C and D, electrical stimulation of the brain tissue was applied with a handheld bipolar stimulator probe which has a cathode and anode side by side (DCS).[70,71] Current flow occurs from the anode (positively charged) to the cathode (negatively charged). Due to that, the extracellular space beneath these two points suffers changes in current: inward, i.e., hyperpolarizing near the former, and outward, i.e., depolarizing near the latter. The current between the probe ball tips spreads in a laminar fashion. Assuming the brain as i) a medium with only one conducting material and ii) in the absence of time variations in the electric signal (quasi-static condition), the electrical field in a volume conductor is represented as:[70]

$$\vec{\nabla} . \left(\sigma \vec{\nabla} V\right) = 0 \tag{3.2}$$

$$\vec{\nabla} = \frac{\partial}{\partial x}\hat{\imath} + \frac{\partial}{\partial y}\hat{\jmath} + \frac{\partial}{\partial z}\hat{k} \tag{3.3}$$

where $\vec{\nabla}$ is the gradient vector, σ is the electrical conductivity and V is the scalar electric potential (Voltage) in unit vectors in the 3 planes.[71] C*urrent density* is the ratio of the charge that flows in 1 second through a surface perpendicular to the flow, divided by that surface area. The SI units for current density, electric field and conductivity are amperes per square meter (A/m^2), volts per metre (V/m), and siemens per metre (S/m), respectively. The relevance of the current density for calculating the electrical field in the brain comes from the fact that, in the quasistatic regime, the amount of charge reaching a small volume in a given time interval must be equal to the amount of charge leaving it.[71] Assuming a uniform conductivity from (3.2), results from Laplace equation state:

$$\sigma . \left(\frac{\partial^2 V}{\partial x^2} + \frac{\partial^2 V}{\partial y^2} + \frac{\partial^2 V}{\partial z^2}\right) = 0 \tag{3.4}$$

In (3.2), V = Vo reflects the applied voltage at the point of contact of the electrode and in (3.3) a derivative of the scalar potential is zero at all other points. Therefore, the electrical field problem through Ohm's law may be stated as:

$$J = -\sigma \frac{\partial V}{\partial x} \tag{3.5}$$

where J is the current density, V is the scalar voltage potential, σ is the electrical conductivity and x is the position.[70] Therefore, because the electrical field can be derived from the scalar potential:

$$E = -\vec{\nabla} V \tag{3.6}$$

The current density may also be calculated from the electrical field as

$$J = \sigma . E \tag{3.7}$$

where J is the current density, is the conductivity and E is the electrical field.

Experiments based on these assumptions showed that bipolar stimulation technique produces a maximal current density below the 1mm spherical metal electrodes of 0.05 A/cm^2, if spaced by 5mm when using a 10mA intensity current. Therefore, the current density decreases with increasing distance from the stimulation electrode. Stimuli are more effective when the stimulation electrodes are aligned transversally to the axon. However, because the electrical resistance is rather unpredictable (resistance of the pia mater is not measurable after a few minutes

of air exposure) and of high value (gray matter resistance is about 4–6 times greater than in white matter), constant-current stimulation is used.[70]

The current applied evokes a potential difference at the local neuronal membrane, which may origin an action potential. The neuron membrane is continually bombarded with neurotransmitters, which produce either excitatory postsynaptic potentials or inhibitory postsynaptic potentials of varying duration. When the membrane potential reaches its threshold (needing around 20mV), an action potential is generated.[71]Briefly, local potentials result from the flow of current through the membrane with a change in channels that are open or closed in response to a chemical agent, mechanical deformation or an applied voltage.[72]

Synaptic potentials occur through either a depolarization or hyperpolarization mechanism. After chemical molecules enter the synaptic cleft, depolarization may result from increased conductance of i) sodium (fastest process) or potassium (slowest process) channels, ii) both sodium and potassium channels and iii) calcium channels. Local potentials may be generated either in soma, dendrites or axonal body of neurons and in addition show unique characteristics in transferring electrical information without decreasing signal amplitude.[72] The local potential is a graded potential and its signal is proportional to the size of the stimulus and hence they may be summated. Most synaptic potentials range from 10 to 15ms in duration, and the longer the duration, the greater the chance for *temporal summation* (generator cell integrates signals that arrive at different times). In addition, *spatial summation* may occur within a few millimeters around the neuron area in which the local potential is generated. Simultaneous application of a second stimulus near the first results in spatial summation of the potentials in the border zones.[72]

Generator potentials occur primarily by the opening of both sodium and potassium channels and increasing conductance of both ions leads to an action potential if the local potentials´ voltage overcome the neuron threshold. This is defined by the membrane excitability, in which suddenly many sodium channels open. In this way, information can travel long distances without being lost. Their all-or-none feature also allows coding of information as frequency, rather than the less stable measure of amplitude.[72]

The ion flux and diffusion under an electrical field (from synapse) may be described by converting flux (molecules diffusion) in electrical current density when multiplied by the number of charges in each mole (number of ion molecules) using the *Nernst–Planck* equation (not describe here).[68] In ion diffusion term of such equation, current arises the movement of an ion under the influence of an electric field. An example, for sodium may be stated as:

$$\overline{J_{NAK}^{e}} = FC_{NAK}\{\mu_{NA} + \mu_{K}\}\bar{E} \qquad (3.8)$$

the ion type is designated by the subscript *Na* and *K*, while the superscript *e* signifies that the current is due solely to an electric field, F the Faraday constant, and μ the ion mobility. Assuming that conductivity (σ) is proportional to ionic concentration, hence using the Ohm's law, ion's conductance may be calculated as follows:[68]

$$\sigma = FC_{NAK}\{\mu_{NA} + \mu_K\} \tag{3.9}$$

For brain mapping, a low frequency paradigm has been established, consisting of the application of short pulse trains with frequencies of 50Hz in Europe (Penfield technique).[73] The individual pulse is rectangular and either monophasic or biphasic. Lower intensity is needed to evoke an effect if anodal current is used (from anode to cathode). Experiments from motor cortex stimulation showed that excitatory postsynaptic potentials produced after an anodic stimulus are not only accumulated, but also enhanced by the pulse sequence.[12,13] In humans, conduction of the pyramidal fiber tracts is slow in 90% (thickness of 1–4μm) and fast in only 1.7% (thickness 11–22μm). Between 60 to 94% of the fibers are myelinated, and show conduction velocities between of 50 to 80m/second. However, this only represents about 20% of the fifth layer of the primary motor cortex (Betz cells). Therefore, using a high-frequency pulse sequence (around 250Hz), not only *direct waves* from pyramidal cells stimulation are recorded, but also additional *indirect waves* (transmitted to pyramidal cells through intracortical connections), particularly after the third stimulus of the sequence.[74]

Bipolar stimulation pulses have 0.3-0.5ms duration and alternating polarity with first phase being anodal and then cathodal. The charge applied to the brain using a biphasic pulse is twice as that applied using the same current but with a monophasic pulse.[73] The current entering the cortex via the electrode elicits an electrochemical reaction that alters tissue pH and leads to organic oxidation, impairing cellular homeostasis through changes in intra- and extracellular concentrations of K^+ and Ca^{++}. The maximum stimulation intensity should not exceed 40μC/cm^2/phase and is commonly limited to 20mA.[73] DCS of the brain was found to be safe with intermittent cortical stimulation being carried out over several days and not resulting in any cortical damage.[13]

3. Stimulation probe

The use of a bipolar probe with 2 tips separated by 6–10mm has become standard. An interelectrode distance > 10mm favors the activation of large pyramidal tract neurons. This creates an electrical field in which the current density is more homogeneous and the electrical field lines between both poles are close to parallel. Alternatively, a monopolar probe with a frontal reference electrode can be used. Given the same stimulation intensities, a monopolar probe provides a homogeneous radiant spreading electrical field, which leads to lower current densities in the area

surrounding the reference electrode, but the probability of stimulating nervous tissue at a more distant site increases.[75]

DCS and awake craniotomy

Current evidence recommends using DCS for language mapping while the patients perform language tasks after sedation withdrawal (asleep-awake-asleep anesthesia protocol). Language mapping with DCS remains the gold standard technique for language localization[11] This assumes greater relevance specially in the setting of a tumor that induces neuronal plasticity. Awake craniotomy surgery increases gross total resection with less neurological language deficits.[11,13] Once the scalp, skull, and dura are opened, sedation wears off so that the patient may cooperate with behavioral testing.

In this thesis, intraoperative language tests consisted in counting, PNt (which tests the integrity from visual stimuli interpretation to name generation) and non-verbal semantic association tasks (NVSDt) carried out while the surgeon stimulates the cortical surface.[13] The threshold of action (intensity) was stablished before language mapping. DCS was applied to the motor cortex (i.e. to the primary motor and the ventral precentral gyri) with intensity increases in 0.5mA steps, while the patient carried on a counting task until speech arrest was detected (i.e. anarthia). In language mapping, patients were asked to simultaneously perform a movement of flexion and extension of the contralateral arm while doing a PNt or NVSDt. For PNt, the same set of pictures was used in all experiments in this thesis (section C and D), either in the presurgical planning, intraoperative testing or laboratory speech recording (section D). Pictures of object nouns consisting of one to two syllables were presented each 4s. Subjects were instructed to use the phrase “this is a ...” before saying the object’s name during intraoperative testing. In addition, the NVSDt consisted in a palm-three test where the subject had to choose a picture semantic related to the presented object. This test was used for presurgical planning and some intraoperative testing (section C).

The stimulation of an area essential to language function induced several forms of alterations due to disrupting the normal neuronal firing, from speech arrest to paraphasias.[73] All sites were stimulated at least 3 non-consecutive times and the following responses were defined as either: (1) positive brain region: a region for which DCS evoked language disturbances such as paraphasia, hesitation, anomia or speech arrest regardless of the error type; or a (2) negative brain region: a brain region that, having undergone at least 2 stimulation trains, did not evoke speech deficits. However, while paraphasias are easily identified due to the phonological or semantic form of the error, speech arrest may occur due to the following mechanisms: i) stimulation of a

positive area evoking responses in muscles used for speech production (i.e. anarthria) as occurs in the primary motor area; ii) stimulation of a negative motor area responsible for speech production such as the IFG or in the supplementary negative motor area (anterior to supplementary area); iii) brain stimulation which elicits distracting symptoms such as visual or auditory; iv) alteration of consciousness, as it occurs during partial seizures (i.e. possibly after discharges); v) and stimulation of an area with language processing function.13,14,71 Therefore, such mechanisms must be excluded before ascribing language function to the stimulated cortex. Electrocorticography or scalp electroencephalogram was used to detect paroxysm activity evoked by DCS (i.e. after discharges). After their detection, cortical surface irrigation with cold ringer lactate and a pause in stimulation were sufficient to promote their disappearance in the reported experiments.

Language network from fMRI maps are known to be influenced by methodological artefactual image acquisition and processing, paradigm selection and statistical approach used. Therefore, correspondance between DCS and fMRI incluiding sources of bias were discussed during section C in chapter VI.

Transcranial magnetic brain stimulation

Experiments involving TMS of brain structures are designed to establish the relationship between a cortical area and a behaviour by measuring the behavioural consequences of transiently altering neuronal firing in the stimulated site.[25] TMS may be used to stimulate neuronal activity and evoke a motor response (i.e. motor evoked potential) or to inhibit neuronal electrical activity to disrupt cognitive processing (such as speech arrest).[25] TMS delivers non-invasively, highly effective and painless magnetic stimuli (1 to 2 Tesla) to generate supra-threshold current in the brain. The current intensity discharged over the skull depends on the magnetic strength field, which induces a perpendicular electric field through the skull, resulting in an electric current in the cortex.[75]

1. Transcranial electrical current density and conductivity

As stated before, the electrical stimulation exerts a force on charged particles and sets the free ones, particularly ions, in coherent motion. In contrast to DCS, electrical properties of the tissues that lay between the TMS coil and the depolarized neurons can be described in terms of their electrical conductivity and relative permitivity.[75] TMS coils use a low frequency to generate electrical current with an approximately constant conductivity. However, brain tissue conductive properties differ from site to site, which may alter the distribution of the electrical field, whereas

permittivity may be neglected.[76] The scalp is mainly made of three different tissue layers: skin, fat and muscle. The stratum cornea shows high resistive properties, 2 x 10^{-5}S/m, whereas skin deep layers show a high conductivity with an average value of about 0.30S/m. Fat tissue has a low conductivity with an average value of 0.036S/m and muscle tissue an average of 0.131S/m. The skull is again made of three layers: two outer cortical layers that enclose a central, cancellous bone. The cortical layers have a lower conductivity and the latter, inner layer, has an anisotropic conductivity with an isotropic value of 0.0056S/m and brain to skull conductivity ratio between 40:1 and 20:1.[76] Cerebrospinal fluid has a value of 1.79S/m at 37ºC, which is constant in the range 10Hz to 10kHz, whereas cortical grey and white maters have a homogenous and isotropic conductivity. These show an average value of "isotropic" conductivity between 0.161S/m and 0.450S/m in the frequency range of 1–10kHz for grey matter and about 0.18S/m for white mater.[76] Therefore, due to different electrical conductivities and heterogeneity, significant effect occurs on the electric field distribution during stimulation.[75-77]

After applying an electrical field, electrical charge accumulates at the interfaces between tissues and gives rise to a secondary electrical field that also contributes to the total electrical field. The secondary electrical field is generated by the charged interface density points which have the same direction as the applied electrical field in the low conductivity tissue, against the high conductivity electrical field. These accumulations are greater when the electrical field is applied perpendicular to the brain tissue. A steady state is reached after about 10μs in which the amount of charge reaching the interface is equal to the amount leaving it (resistive propriety).[75-76] In order to estimate the electrical field distribution in brain tissue with TMS, which uses low frequency from direct current to 10kHz, several of the following approximations are implied: i) quasi-static condition which consists of neglecting the propagation effects of the electrical field (because electromagnetic wavelength in TMS is much larger than the dimensions of the human head), ii) the effect of the magnetic field produced by the currents in the tissue is negligible iii) the capacitive effects are also neglected and the tissue is treated as purely resistive. Therefore, when using rTMS (see chapter I ofr further details), the temporal variation of the electrical field is approximately the same defined in the pulse sequence.[13,77]

TMS induced currents are limited to the head and considering a heterogeneous medium, charge tends to flow tangentially from high conductivity tissues to the boundaries of low conductivity tissues (such as the scalp-air boundary).[76,78] A heterogeneous medium with various tissue interfaces imposes some difficulty to estimate electrical field distribution. The current density was found to be highest in the high-conductivity region and the electrical field highest in the low-conductivity regions.[78] In addition, anisotropy was found to have a small effect on both the site and intensity of stimulation. In an anisotropy medium, the radial component of the electrical field

was found to be not necessarily zero at the interfaces' boundaries, whereas the current density was. Such findings support that the presence of the interface could lead to the activation of neurons that run parallel and close to the interface.[77,78] In contrast do DCS, electrical field does not decrease monotonically with depth, but is determined by the conductivity of the different tissues and by the shape of their boundaries. Stimulation is more effective in depolarizing neurons if the electrical field is parallel to them, tangentially to the skull in the gyri or in the sulci.[76]

2. Coils figure and position

In order to produce a transcranial electrical current to the brain, wires are shaped into a coil figure aiming to evoke a perpendicular magnetic field.[76,79] The TMS hand held coils have many shapes that vary according to the target structure´s depth. In section C, chapter X, we used a figure-of-eight coil to stimulate the motor cortex and the IFG because it allowed to further focus our stimulation.[79] Focality refers to the ability to limit the high intensity region to a small target volume. This double coil has the capacity to evoke a stronger magnetic field tangentially to both coils and perpendicular to the line joining the centers of the two wing coils.[79] The induced electrical field results from the sum of the field from both circular coils and decreases rapidly with distance.[76] For monophasic pulses, a lowest threshold stimulation for the motor cortex is achieved when the coil points in the posterior-to-anterior direction, approximately perpendicular to the central sulcus.[80]

The distribution of the electrical field is also influenced by the position of the coil. For motor cortex stimulation, the best position results from adjusting the coil according to motor evoked potential amplitude.[80] For language mapping, the coil is usually positioned in relation to the standard reference point Cz.[81] In order to optimize coil position, optical surgical navigation was used, allowing for i) coregistration of scans to more accurately determine the delivery of navigated TMS pulses (nTMS), and ii) optimal coil orientation to the brain surface.

In section D, healthy subjects had an MRI scan for three dimensional (3D) T1-weighted image acquisition (1mm^3 isotropic voxel). Thereafter, DICOM data was transferred to the navigation system (BrainSight, NeuroConn, EUA) and 3D skin and curvilinear reconstructions were made. The magnetic coil of the TMS equipment (Magstim Rapid, UK) was calibrated in the navigation system in order to provide the orientation and direction of the coil. For brain stimulation, the coil was placed tangentially to the scalp over the motor area at an angle of 45° to the midsagittal plane with the handle pointing laterally and posteriorly, thus generating a monophasic pulse with posterior-to-anterior direction in the brain. The theoretical center of stimulation was extrapolated from the coil position and projected onto the cortical surface at an angle of 90° by the navigation software. Stimulation intensity was specified as a percentage of the maximum stimulator output.

A single-pulse navidated TMS was used to determine the active motor threshold recorded from felt pad electrodes (rectangular shape, 2 x 6.5mm, separated by 25mm) placed on the right first interosseous. This threshold was defined as the minimum stimulus intensity capable of eliciting a motor evoked potential greater than 50uV at rest in at least half of ten consecutive trials.[80] At such threshold, the electrical field in the cortex is estimated to be about 90V/m for monophasic pulses. Thus, between 90% and 110% of the resting motor threshold (RMT) was used to define the threshold for stimulation of the ventral precentral gyri as in intraoperative testing for language region mapping. For this purpose, a repetitive nTMS pulse protocol (r-nTMS) was used consisting of a train of 5 pulses at 20Hz. The r-nTMS pulse train was automatically triggered by an electronic trigger at the same time as the visual stimulus was presented for PNt during speech processing.

3. Stimulus waveforms

Physiologically, with motor cortex TMS, motor evoked potentials are generated after axon stimulation rather than cell body stimulation.[77] Axons are more excitable at the point where they bend out of the magnetic field (parallel to the surface). This is also the point where the change in electrical field is the greatest.[77] However, the evoked volleys descending in the pyramidal tract at the spinal cord level do not result from a direct activation of the pyramidal tract axons (direct waves), but of premotor neuronal axons running parallel to the cortical surface, i.e., resulting from synaptic inputs to cortical motor neurons (indirect waves).[77,8]. Whether this concept generalizes to all areas of the cortex such as those related to speech is currently unknown.[81] However, TMS is directionally specific because its threshold varies according to current direction and pulse configuration.

TMS pulses have either monophasic or biphasic configuration such as DCS, which produces brief magnetic fields at the orthogonal angles to the coil plane.[81,82] Monophasic pulses have a posterior-to-anterior direction with a duration of 100ms, whereas byphasic pulses have an anterior-to-posterior direction with about 200–250ms duration. The threshold for the motor cortex is lowest when the electrical field is induced in the brain during the initial phase of the waveform, when it points in the posterior-to-anterior direction for the monophasic pulse.[80,82] In contrast, byphasic configuration is more powerful than monophasic (when having the same rise time characteristics), and the second phase is more effective than the first one because of the Na^+ channels inactivation reversal during the hyperpolarizing current.[82] Results from motor cortex stimulation show that monophasic pulses activate a relatively uniform population of neurons and could, therefore, be more effective in producing sustained after-effects.[80] In fact, indirect waves are preferentially recruited , and present a shorter latency (i.e. 1-3ms before) when using an anterior-to-posterior current.[79,82] For this reason, section D r-nTMS experiments were carried out using monophasic pulses for IFG mapping in order to evoke language disturbances.

Subjects were instructed to perform a PNt using pictures of the Snodgrass and Vanderwart collection.[83] The same picture set was used for the fMRI experiment and intraoperative language testing described in chapter II. We selected only pictures with names that are either one or two syllables long in Portuguese or Spanish. Subjects were sitting on a comfortable chair, with their hands resting on armrests, facing a 15-inch computer screen, placed 1m away from the subject's eyes. The experimental setup was constructed with Presentation® (Neurobehavioral systems, U.S.A.), which was used to send a 5V signal to the EMG equipment through a microcontroller (Arduino UNO, Italy). The presented pictures consisted of a white frame occupying the whole screen with a picture of 8x8inches. The images were shown during 4s, every 4s. The screen was left blank between two consecutive images, except for a white "X" letter at the center of the screen, which was used as an attention fixation cue. The image presentation served as an imperative signal for subjects to name the object represented in the picture, avoiding anticipation or misinterpretation errors. Language mapping over the opercular IFG (opIFG) was performed using the same r-nTMS system.[84,85] The r-nTMS pulse train was automatically triggered by the home-made microcontroller at the same time as the visual stimulus for PNt.

Accelerometer based speech recording

Reliable and objective analysis of speech is also an essential part of a physical examination.[23] Phonation is the aerodynamic and acoustic product of a complex vibratory system. Every act of phonation is characterized by a certain degree of apparently random variability of the cycle-to-cycle duration and/or amplitude in pitch periods of the laryngeal periodic pattern vibration. The phonatory process begins with the closure of the glottis and the midline movement of the vocal folds. Thereafter, when the subglottic air pressure increases to exceed the resistance of the vocal folds, air is released producing vibration.[86] In this regard, objective measures of phonatory ability were described as helpful in the treatment of patients with voice disorders and in assessing the results of surgical treatment.[24]

Current methodology to speech recording in voice laboratories involves high quality microphones, amplifiers, acoustically shielded booths with sound-absorbent walls and specific software to manipulate speech acoustics.[24,87] However, they are often available in a restricted number of head and neck departments and cost-effective methods using other transducers to quantify phonation have been developed as alternative methods. In section D, an accelerometer-based method using conventional electromyography equipment is described, aiming to detect evoked voice disturbances due pathology after brain stimulation.

Breathing, phonation, articulation and resonance are the underlying physiological processes of speech production. The vocal tract works like a vibrating column of air, closed at one end. During speech production, the air from the lungs causes vibration of the vocal cords and a basic laryngeal tone. Thus, supraglottic structures act like resonators producing an acoustic sound such as a vowel.[86] The natural frequency of the vocal tract vibration depends on the size and shape of the larynx, naturally varying with gender and age. It has been found to be between 100 and 500Hz. Some microphone speech data of healthy individuals states approximately 120Hz for males and 225Hz for females, despite age-related variations. Phonation intensity in a conversational range is 54dB for males and 51dB for females.[22] However, deglutition maneuvers are known to be associated with frequencies from 500Hz to 8000Hz in addition to the low frequency contamination from involuntary neck muscle activation.[22,86] To prevent distortion of the neurophysiological phonation signal, the recording system which includes the electrodes, must be able to respond to all frequency components, suppressing those that are unrelated to vocal cord vibration.

1. Electromyography equipment

Every electronic instrument consists of active and passive parts. Active parts are dedicated to amplify the biological signal aimed to be recorded (i.e. transistors, integrated circuits) whereas passive parts affect the quality of the signal, such as condensers and transformers. Both parts need an energy supply to function, predominantly the active parts. EMG was developed to record action potentials from nerve, muscle or brain and hardware evolved from this aim[88,89] In section D a speech recording method using an ACC for detection of the physiological movements of the glottis structures was developed in such a way that their disturbance by brain stimulation would be detectable.

Descriptions of electrical signals usually refer to the frequency of the waveform.[22] These descriptions rely on the fact that any arbitrary waveform can be represented as a sum of sine waves of various frequencies, amplitudes, and phases.[22,90] The compound action potentials collected during nerve conduction studies, motor evoked potentials or accelerometer recordings are displayed in two dimensions: voltage on the y-axis and time on the x-axis ($\Delta y/\Delta x$). A Fourier analysis can be made to characterize their different components. Therefore, an EMG amplifier should have an upper frequency limit of no less than 10,000Hz to ensure a distortion-free response.[88,89] However, within the recorded signals some undesired frequencies are also included (electrical noise) such as a 60Hz power line, nearby electrical equipment or even skin tissue (that acts like a low frequency filter). Successful recording depends on the ability to selectively amplify the signal of interest approximately 250,000 times while rejecting the unwanted noise. Figure 3.1 shows a conventional electronic circuit present in a EMG apparatus.

2. *Electrodes and impedance*

In section C and D, an uniaxial piezoelectric ACC was used to record glottis anterior-posterior movements and word pronunciation. The accelerometer is composed by seismic mass attached to the housing by an elastic element. After accelerating the structure in the sensitive direction of the elastic element, a force is applied causing the elastic element to be distorted.[90]

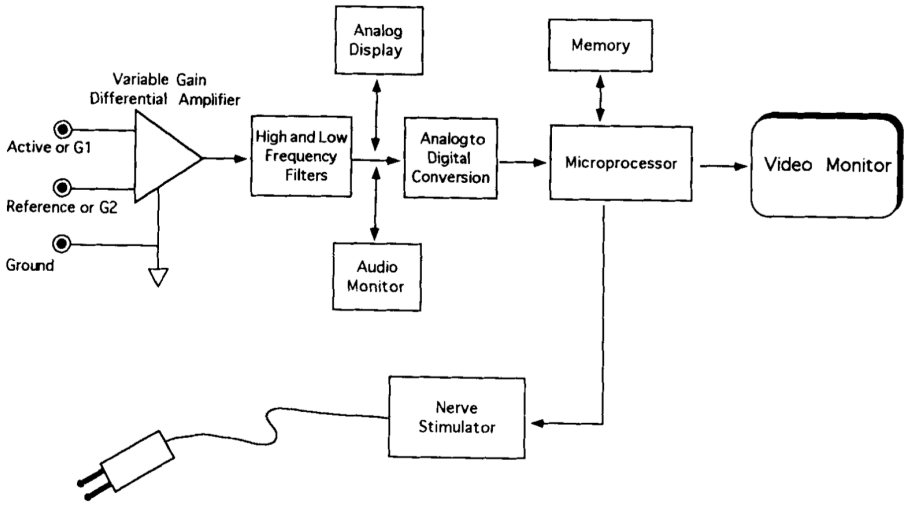

Figure 3.1 – Instruments and computer-controlled data acquisition and display. After recording a neurophysiological signal, follows signal amplification, filtering, conversion to digital values, scaling and analysis by the microprocessor, and display of the waveform on a video monitor. Adapted from Gitter et al.[89]

In this case, the elastic element distortion is measured by a piezoelectric sensor which generates an electrical signal related to the dynamic change of its shape. This sensor can only directly measure time varying forces, and it is, thus, suitable for measuring changes in acceleration.[90] The relationship between displacement and acceleration is found by combining Newton's second law and Hooke's law:

$$a = \frac{k}{m}x \tag{3.10}$$

where x is the measured displacement, m is the known mass, k is the spring constant of the elastic element, and a is the acceleration. We ensured a sampling frequency rate within the physiological range of the fundamental voice frequency (sampling rate of 2000Hz). A ground electrode was used as a safety feature and as a low impedance path to drain electric noise away from signal transducers.

Impedance between skin and transducers plays an important role in neurophysiological signal.[69] Transducers and amplifiers act as series of current (voltage) resistances from the biopotentials.

The transducers' impedance must be as low as possible to ensure that most of the voltage will reach the amplifier. In addition, an EMG amplifier must have an input impedance higher than the transducer´s.[88] For example, to detect 99% of the signal, the amplifier impedance input must be 99 times greater than the transducers impedance. During our experiments, transducers´ impedance were carefully maintained above 5 ohms, using skin abrasive.

3. Amplifiers and filtering

The signal input to the amplifier consists of five components: the biopotential, the undesired biopotentials, the 60Hz power line interference signal, tissue/transductor interface interference and noise.[88] An adequate design of the amplifier provides rejection of a large portion of the signal interferences, which in an EMG apparatus is a differential amplifier. The desired biopotential appears as a voltage between the two input terminals (piezoelectric sensor/mounting mass or active/reference electrode).[90] The voltage measured within such terminals is a preamplified gain of 100 to 50,000 times (1 to 10 V) to provide optimum signal quality.[89] The gain or amplifier sensitivity relates the input voltage to a display scale (e.g., 1mV/cm). A low sensitivity amplifier reduces waveform duration and increases the waveform take off (i.e. leading to longer latencies). Frequency response (or sampling rate) should also be greater than the physiological range of frequencies in order to avoid waveform distortions.[88,89] The preamplifier should also eliminate most of the signals interfering with the biopotential measurements.[91] For this purpose, a differential amplifier will invert and amplify the signal from one reference terminal and add it to the amplified signal from the active terminal. Thus, the interference signals detected in the two electrodes, cause approximately the same potential at both inputs (common mode signal).[92] The common mode signal can be rejected by using the common mode rejection ratio (CMRR). This method increases the SNR by rejecting interference signals, after ensuring that the desired biopotential affects only the active terminal.[92] The CMRR is a function of frequency and source-impedance unbalance; expressed in decibels, the common mode rejection is 20 $\log^{10}$ CMRR. The rejection of the common mode signal in a biopotential amplifier is both a function of the amplifier and the source of signal at both terminal transducer impedances (Z1 and Z2). In an ideal biopotential amplifier with Z1 = Z2, the input impedance (Z_{in}) is equal to Z1-Z2. With an infinite CMRR the output voltage (V_{out}) results from the biopotential signal voltage (V_{bio}) multiplied by the amplifier gain (G_D).[88] However, a real biopotential amplifier output results from a desired differential biosignal output, an undesired component from an incomplete CMRR of the interference signals and an undesired source impedance unbalance (allowing a common mode signal to appear as a differential signal).[88,89] Such output voltage can be defined as:[92]

$$V_{out} = G_D V_{bio} + \frac{G_D V_c}{CMRR} + G_D V_c \left(1 - \frac{Z_{in}}{Z_{in}+Z_1-Z_2}\right) \quad (3.11)$$

where the ground electrode provides a reference potential to the amplifier with a common mode voltage (V_c).

In addition to transducers and electrical interferences, noise is also generated by the amplifier and the connection between biological source and amplifier. As mentioned above, the total source resistance of this system circuit causes thermal voltage noise with a root mean square (rms) value of:[9]

$$E_{rms} = \sqrt{4kTR_SB} \tag{3.12}$$

where k = Boltzmann constant, T = absolute temperature, Rs = resistance in ohms, and B = bandwidth in Hz. Each amplifier also brings up inherent noise which derives from the internal voltage noise source and the voltage drop across the source resistance (caused by an internal current noise generator). Therefore, high SNR requires the use of very low noise amplifiers with acceptable sampling rates.[89] The range of frequency components contained in a neurophysiologic potential can be defined by their own frequency bandwidth. The purpose of the high pass and low pass filters is to i) eliminate interference signals like electrode half-cell potentials and preamplifier offset potentials and to ii) reduce the noise amplitude. Low-frequency filters remove low-frequency, slowly changing components of a waveform whereas high-frequency filters remove the high-frequency rapidly changing components.[89] About 30% of the 10Hz activity is attenuated (amplitude decrease) if a low pass filter of 10Hz is applied. Additionally, the filter changes the phase of a signal passing through which may be interpreted as a time delay occurring in that particular frequency component. In chapter IX, technical aspects of speech recording based

4. Digital electronics

The essence of digital storage is that any waveform can be characterized by a list of numbers.[88] The process of converting a waveform to a number list is done in an analog-to-digital manner, and the waveform reconstruction from numbers uses the reverse process.[88] The waveform and the number list are completely equivalent due to the sampling theorem, stating that a continuous-time signal can be completely recovered from its samples if, and only if, the sampling rate is greater than twice the signal bandwidth.[89,91] An aliasing phenomenon takes place when the sampling frequency is lower than twice the signal frequency, leading to waveform distortion (the sum of the low frequencies with half signal frequency components).[91] Such sampling rate defines the temporal resolution long the monitor´s horizontal axis of the waveform, whereas vertical (axis) resolution is defined by integers allowed. In other words, a sampling rate of 128Hz will capture 128 point in a second to represent the waveform along the horizontal axis. Integers (from 0, 1, 2, and 3) cover *25%* of the entire range of the vertical resolution. Numbers are represented in bits, therefore a 2 bits resolution means the use of four integers.[89] The reconstructed waveform would

only have four possible voltages and a staircase waveform configuration. Digital representation of waveforms allows signal processing techniques such as rectification, filtering (such as for the power line), averaging or others used to interpret the waveforms.[88,89] Computer programs can automatically determine the neurophysiological signal´s latency (time resolution) and amplitude (vertical sensitivity) values.

The speech recording industry has developed since the use of analog tape voice recordings to the use of digital frequency and sound level meters of improved voice laboratories.[24] However, instrumental factors related to the equipments used to acquire physical vocal vibration signals impact the acoustic signal. In addition, descriptive and experimental conditions must be assessed before clinical use when using less costly hardware. In section D, ACC measures such as amplitude and frequency were used to assess speech word pronunciation in patients with vocal cord pathology and PBT.

SECTION B: BRAIN MOTOR AND LANGUAGE AXONAL PATHWAYS

CHAPTER IV

RECONSTRUCTION OF WHITE MATTER FIBRE TRACTS USING DIFFUSION KURTOSIS TENSOR IMAGING AT 1.5T.

Introduction

The first MR scanners used for advanced imaging had a field of 1.5T and are still widely employed nowadays.[93] Among such applications are DTI and DKI, used for studying tissue microsctructure.[94] A recent report found that 3T systems provide similar ability to estimate kurtosis measures when compared to 1.5T systems.[95] The higher discrepancy of 10% was found in the estimation of kurtosis fractional anisotropy reflecting the effect of the signal noise. However, no study had yet assessed the feasibility of reconstructing white matter fibres using DKI at 1.5T.

In this study, we tested whether DKI can provide clinically acceptable whole-brain tractography reconstructions at 1.5T in both healthy volunteers and brain tumor patients. In particular, we wanted to investigate if it could enable to detect high curvature streamlines in the CST. Study of the pyramidal fibers is fundamental in presurgical planning to avoid motor deficits and these fibers or tracts characteristics are well documented in literature.

Methods

1. Subjects and patients

Eight healthy volunteers (two males, mean age 22, ranging from 20 to 26 years old) and three patients (2 males, mean age 27, ranging from 24 to 30) diagnosed with brain astrocytoma were recruited for an MRI scan (Figure 4.1). The study was approved by the hospital's ethics committee and prior informed written consent was obtained from each individual.

2. Magnetic Resonance Imaging Protocol

A 1.5T Avanto (Siemens, Erlangen, Germany) MRI scanner with a 12-channel head receiver coil was used. A standard MRI protocol was acquired in all patients including T1-weighted images, pre- and post-contrast, diffusion-weighted images and T2-weighted images with fluid inversion recovery.[96] DWI were acquired using a single shot spin echo EPI sequence (further details in

chapter II) along 64 non-collinear gradient sensitising directions using b-values of 0, 1000, and 2000 s/mm^2.

3. *DWI Preprocessing and DKI processing*

The preprocessing was detailed in Chapter II. Briefly, all images were corrected for motion,[97] eddy current geometric distortions,[59] and non-brain tissues were removed[39] using FSL.[55] In order to estimate the DT and the DK for all DWI data, an in-house developed toolbox named UDKI was used.[41] The toolbox processes included: spatial smoothing with a Gaussian kernel with FWHM of 1.5 mm; DK estimation was done by fitting DKI's model to the DWI data using linear constrained least squares and DK estimates of fiber directions were done using the maximum kurtosis method. Finally, tractography was processed using the brute force algorithm, as described by Neto-Henriques and colleagues.[41]

Tracking was performed in regions with FA greater than 0.2 and with a maximum curvature of 35º between principal eigenvectors in adjacent voxels. The tractography results were visualized using Trackvis (http://www.trackvis.org/).[43]

4. *Data reduction and statistical analysis*

Whole-brain tractography was performed and its metrics computed (streamline count, voxel count) in all subjects using Trackvis. We isolated the CST by seeding from the cerebral peduncles and the motor pre-central gyrus, using anatomical images and FA maps to evaluate its course in all subjects. We also extracted the CST size for comparison between pathological and healthy hemispheres. The Mann-Whitney U-test was used for comparisons between the pathologic and healthy hemispheres of the patients (a significance level of p=0.05 was chosen). In order to observe the mass effect produced in the reconstructed fibre bundles by the tumor, we calculated the distances between the CST fibre tracts and the brain midline along the z-axis, using FSLView. From these, the highest distance was extracted, for both the pathologic (p) and healthy (h) hemispheres, and the deviation index (DI) was calculated, as defined by:

$$DI = \left|\frac{(deviation\ distance\ h)-(deviation\ distance\ p)}{(deviation\ distance\ h)+(deviation\ distance\ p)}\right| \quad (4.1)$$

Results

1. *MRI processing protocol and tractography*

Figure 4.1 shows representative examples of structural T1, EPI, FA and DK invariant metrics maps of a healthy subject and of all patients. Whole-brain tractography and isolated CST size for a healthy subject and patients can be found in figure 4.2. No significant differences in size were found between healthy and patient groups, in either whole-brain or CST, despite a tendency being observed for the number of depicted voxels (figure 4.2B; p=0.069). In figure 4.2C are showed the delineated CST of a healthy subject and patients.

2. *Analysis of the highest deviation region*

The DTI and DKI metrics extracted from the highest curvature point of the CST are summarized in table 4.1. The DI was significantly larger in pathological hemispheres (p=0.0013). Mean FA values and their asymmetry indices were significantly higher (p=0.01), as well as the radial diffusivity (p=0.026) in healthy subjects when compared to patients. None of the DKI metrics showed significant changes in the group comparison, except for the mean kurtosis asymmetry index which was higher in patients (p=0.04).

Table 4.1 – Diffusion metrics, asymmetry index and deviation of delineated corticospinal tracts

Patients	**FA**	**MD** [b]	**AD** [b]	**RD** [b]	**MK** [b]	**AK** [b]	**RK** [b]	**DI**
1	0.2 (0.4)[a]	0.9 (0.1)	2.3 (0.1)	1.3 (0.1)	1.0 (0.04)	0.7 (0.02)	1.1 (0.1)	0.17
2	0.3 (0.2)	1.1 (0.1)	1.7 (0.2)	1.4 (0.1)	1.0 (0.03)	0.6 (0.01)	1.2 (0.2)	0.12
3	0.2 (0.4)	0.9 (0.2)	1.6 (0.2)	1.4 (0.2)	0.8 (0.04)	0.5 (0.01)	1.0 (0.1)	0.14
Mean±SD	0.23*±0.06 (0.24)*	0.96±0.11 (0.009)	1.8±0.10 (0.008)	1.3*±0.15 (0.18)*	0.89±0.11 (0.14)*	0.60±0.05 (0.09)	1.14±0.11 (0.07)	0.14*±0.03
Healthy subjects Mean±SD	0.54±0.03 (0.04)	0.86±0.06 (0.002)	1.7±0.10 (0.006)	0.8±0.09 (0.05)	1.08±0.10 (0.02)	0.84±0.12 (0.03)	1.28±0.32 (0.03)	0.02±0.03

FA – Fractional anisotropy; MD – Mean diffusivity; AD – Axial diffusivity; RD – Radial diffusivity; MK – Mean kurtosis; AK – Axial kurtosis; RK – Radial kurtosis; DI – Deviation index of corticospinal tract; SD – standard deviation. [a] The values between parenthesis refer to the asymmetry index in comparison with the contralateral hemisphere.[b] Diffusivities are presented in units of 10^{-3} mm^2/s. * Statistically significant ($p<0.05$) differences for evaluated parameter values between healthy subjects and patients.

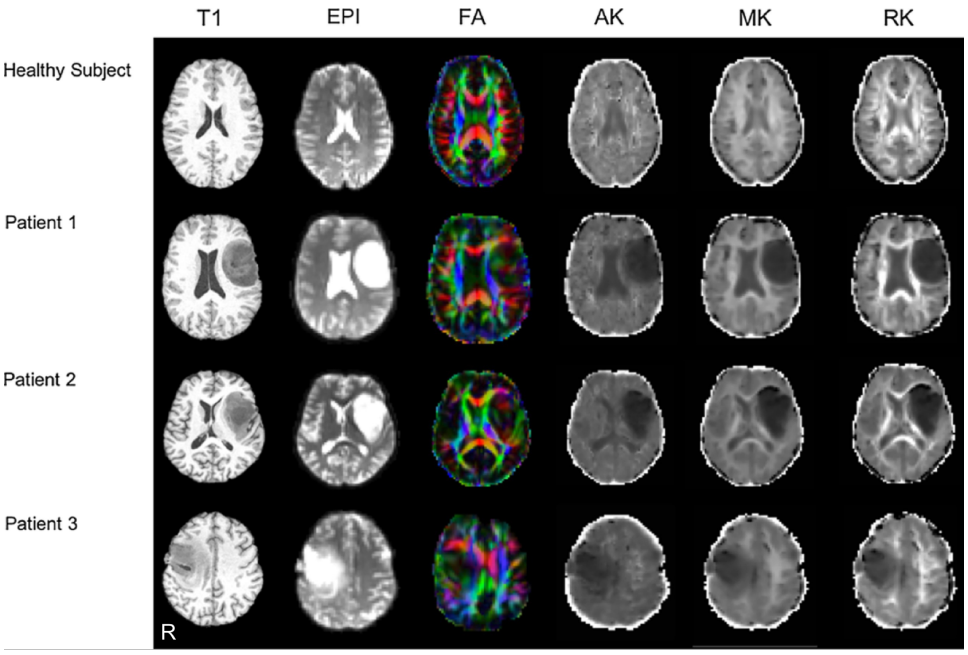

Figure 4.1 – Transverse T1-weighted images (T1), echo planar images (EPI), fractional anisotropy (FA) maps and diffusion kurtosis invariant metrics (AK: axial kurtosis; MK: mean kurtosis; RK: radial kurtosis) maps of a healthy subject and patients with gliomas. In patients, anatomical scans (T1) were contrast-enhanced. Note the distortion of the fibres with cranial-caudal direction (i.e. colored in blue) produced by the tumor in the pathological hemispheres.

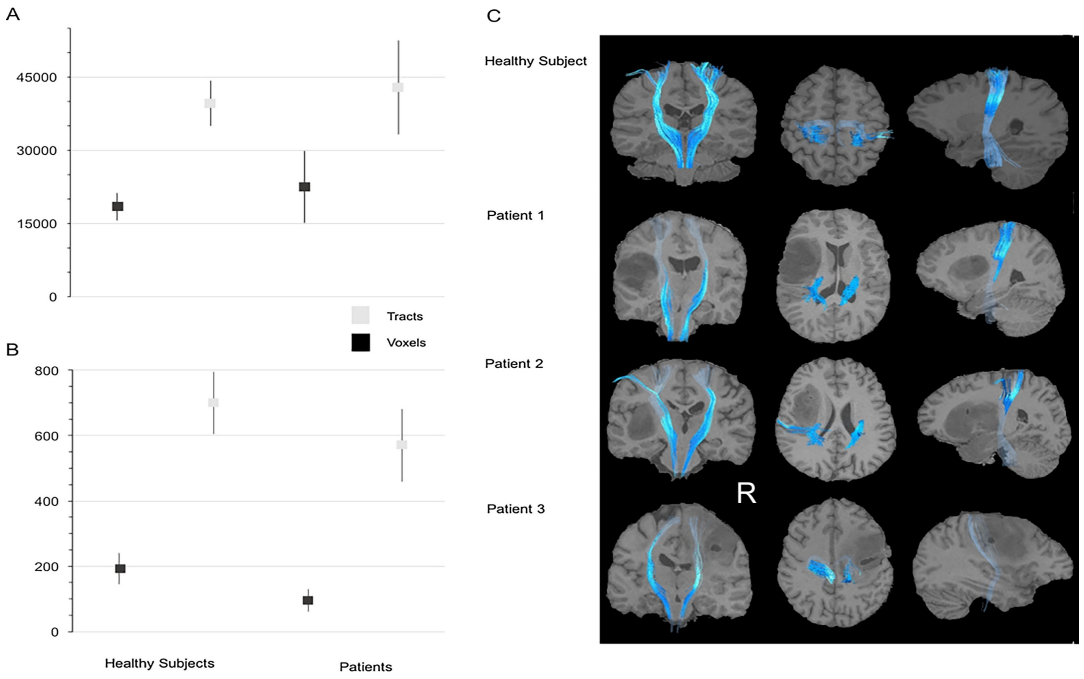

Figure 4.2 – Mean tract sizes for whole-brain (A) and corticospinal (B) tractography of healthy subjects and patient groups (error bars translate standard deviation). Statistically significant differences in tracts and voxel numbers between groups were not found despite the smaller standard deviation in patients' corticospinal tract (CST) size. Representative streamlines of CST are also presented (C). Note the pronounced mass effect imposed by the tumor presence in CST's and their close proximity.

Discussion

1. DWI acquisition and tractography

The white matter streamlines in healthy subjects using DKI has already been reported,[39,41,94,98,99] showing improvements from DTI. However, previous studies were conducted using 3T scanners. We acquired DKI using a 1.5T scanner, and assessed whether tractography reconstruction is affected by the inherently lower SNR. The protocol used in both healthy and tumor patients is compatible with most clinical departments.

Although, many studies point towards the use of several b-values for the DK tensor estimation,[39,41,98] clinically compatible DKI sequences with just 3 b-values have also been suggested. However, none had previously been studied in a 1.5T system. Marrale and colleagues (2015)[94] suggested the use of 32 directions to estimate DKI metrics at shorter scan times. Our protocol used 64 directions, as the higher number of directions increases spatial discrimination of the diffusion profile, relevant for a better characterization of complex tissues.[33,34] Additionally, it can help to mitigate the effects of the lower 1.5T SNR.

2. Effect of brain neoplasm in DK-based tractography

In order to assess if the distortion produced by the tumor affected the number of reconstructed tracts, we compared the size of whole-brain tracts and CST of patients to those of healthy volunteers. We found no statistical differences between the groups. However, due to the small sample size, these results cannot be generalised. In fact, the number of depicted voxels in CST showed a tendency to be diminished in patients (fig. 4.2B).

The presence of a brain tumor causes histological distortion and consequently increases the brain microstructure complexity.[100] Thus, the CST is most likely to be stressed by mass effect at its highest deviation region.[101] Therefore, we analysed the highest curvature point of CST as a higher tissue complexity could affect the DTI/DKI metrics performance and consequently their ability to reconstruct fibres.

We found a significantly increased DI in patient's due to mass effects similar to previous DTI tractography studies[34,101] and significantly decreased mean kurtosis in patients, compatible with an increased Gaussian diffusion behaviour which was not observed in healthy subjects (table 4.1). This hypothesis is supported by the presence of edema surrounding the tumor lowering mean FA values.[102] We also found increased radial diffusivity in patients, which was expected due to the

presence of low grade gliomas with minor neurological involvement and preserved white matter, despite the possibility of some myelin degradation.[100]

We show that at the highest deviation region, the DTI metrics are more affected than DKI metrics, as supported by the higher proportional decrease of mean FA values in comparison with mean kurtosis values in patients (decrease of 0.31 vs 0.19, respectively; table 4.1). This leads us to believe that in the deviation region, DTI's ability to accurately reconstruct fibre tracts is limited. In turn, DKI-based tractography is resilient to this phenomenon, due to DKI's ability to better characterize complex microstructures.[36,39,41,98,99]

Although, the FA values are also influenced by the spatial resolution of the acquired diffusion weighted images. DTI based tractography in a 1.5T scanner for clinical setting, uses higher isotropic resolution (about 2 mm^3 voxel size) with smaller acquisition matrix (between 96 to 128) and smaller echo time (less than 70ms)[33] than those used in this work. During DWI acquisition, susceptibility effects lead to errors in phase encoding and consequently image distortion in the phase-encoding direction of EPI.[17] To minimize this source of errors, decrease of slice thickness and number of echoes by using a smaller acquisition matrix and high receiver bandwidth will reduce echo spacing and the inhomogeneity field.[30] Tractography is highly dependent on the spatial resolution and signal-to-noise quality. In our work DTI extracted metrics may be underestimated due to a diffusion data acquisition optimization for estimation of DKI metrics. However, the balance between greater sensitivity to resolve crossing fibers within a pathological microstructure and optimized DTI performance remain to be studied. This equilibrium should be defined through the relevance of the delineated tracts to surgical planning and decision.

For presurgical planning, distance between the tumor and tracts is of most interest, in order to avoid neurological morbidities. However, this observation remains to be further analysed and tested using direct electrical stimulation, comparing the distance between the point of stimulus and the tracts delineated by DTI and DK-based tractography.

Conclusion

In conclusion, the present study reports the feasibility of the DK-based tractography method in patients with brain gliomas, reconstructed from DWI acquired at 1.5T with a readily-available MRI acquisition protocol.

CHAPTER V

KURTOSIS TENSOR BASED TRACTOGRAPHY IN PATIENTS WITH PRIMARY BRAIN TUMORS: AN EXPLORATORY STUDY COMPARING DETERMINISTIC METHODS

Introduction

Brain lesions such as PBT involving or near the eloquent motor areas are associated with high-risk surgical procedures that may potentially lead to permanent motor disability.[103] The evaluation of water diffusion has been used to track the white matter pathways through the diffusion tensor model using MRI.[104,105] DTI-tract assumes an unrestricted environment where the diffusion displacement probability follows a Gaussian model, assuming furthermore that there is at most a single fiber population within each voxel. However, these assumptions have been shown not to be valid in most of the brain.[106]

Recently, DKI-tract has been described by Lazar et al. (2008),[39] Jensen (2014)[36], and Neto-Henriques et al (2015)[41], demonstrating improved crossing-fiber resolution in comparison with DTI-tract in healthy subjects. The DKI model seems to more closely describe water diffusion in biological tissues than DTI since it can account for complex tissue architectures which lead to a deviation from the Gaussian behavior.[107] Taking into account that PBT tend to evolve through disintegration of brain parenchyma producing edema and anatomical distortion, the method's increased sensitivity to altered tissue microstructure could depict white matter fiber bundles not obtained with DTI-tract. In fact, Neto-Henriques et al (2015)[36] already showed that within a voxel, DKI-tract streamlined crossing fibers in healthy subjects not observed with DTI-methods. However, DKI based tractography PBT remain to be studied in order to evaluate if the pathological parenchyma influences the fibre estimation. DKI-tract of CST using a low magnetic field (1.5T) was recently described in three patients but a comparison with DTI-tract was not provided (further details see chapter IV).[107] Moreover, other white matter tracts with high angulation at their anatomical course remain to be evaluated.

The aim of this study was i) to compare DKI-tract's performance to streamline white matter tracts with DTI-tract ii) to evaluate if DKI-tract depicts additional fibres with different courses to those streamlined by DTI-tract in patients with PBT using routine MRI protocols.

Methods

Patients with a new onset of focal neurological symptoms, diagnosed with gliomas involving or near motor pathways, were selected within 2016 at Hospital de São José (Lisboa, Portugal). The selection criteria for these patients was the localization of the brain tumor or presence of edema, cortically or subcortically, within 2.5cm of anatomical motor landmarks, subjects without cardiac pacemakers and without prosthesis incompatible with MRI. The study was approved by the hospital's ethics committee and a written informed consent was obtained from each subject.

1. MRI Protocol.

All MRI scans were performed in the context of presurgical planning examinations. A 1.5T Siemens MRI scanner and a 12-channel whole-head receiver coil were used. The scanning protocol was described in the chapter IV. At the end of the scanning protocol, and in order to enhance the lesion margins, gadolinium contrast agent was injected and another volumetric T1-weighted sequence was acquired.[96] DWI was acquired using 64 directions in all healthy subjects and in half of the patients, and 32 directions in the rest of the patients (table 5.1). Parameters and pulse sequence details were described in chapter II.

2. DWI preprocessing and tractography.

DWI preprocessing was briefly resumed in chapter IV. In order to estimate the DT and the DK for all DWI data, the UDKI was also used[40] and tracking was also performed in regions with FA greater than 0.2 and with a maximum curvature of 35 degrees.[108] After whole-brain fiber-estimation with DTI and DKI-based tractography algorithms, the results were also visualized using Trackvis.[43]

Seed ROI were then defined in each hemisphere in order to delineate two white matter tracts: the CST and the AF. For the CST, ROI were defined as seed at the point in the cerebral peduncles with the highest concentration of vertical fibers targeting a ROI placed at frontoparietal cortical surfaces. The goal was to include the motor and sensory fibers of the CST allowing for the motor fibers' deviation due to anatomical distortion by the brain tumor. The tracts were identified as CST only if, as well as connecting the two ROI, a route could be visualized reaching the cortical motor region. Whereas for the AF, seed and intermediate ROI were defined in superior, middle and inferior temporal gyri targeting an ROI located at the level of post-central gyrus bilaterally.[109,110] The ROI placement was guided by anatomical images and defined in FA maps. The decision process and placement of the ROI was performed by two contributors (J.L and H.F).

After the definition of the ROI for DTI-tracking, these were imported for DKI-tracking to avoid ROI placement variability.

In the case of the patients, each lesion was segmented and dilated so as to define a surrounding ROI with 10% percent of the lesion. Thus, streamlines targeting the surrounding tumor ROI using as corresponding seed ROI of CST and AF. The goal was to evaluate the presence of tracts in the direct vicinity of the lesion (figure 5.1). Standard directional color-coding was used to aid in the visual inspection of the tractography results, so as to identify the expected cranio-caudal or medial to lateral direction of the delineated tracts. We inspected the anatomical course of these fibers and in a consensus between two contributors (J.L and H.F), decided if they were compatible with CST and AF. The term "false-positive" was used when the reconstructed pathways were considered not to be anatomically compatible reconstructed tracts, while the term "false-negative" was employed when a method failed to track any fibers compatible with CST or AR.

In order to compare each patient CST and AF in pathologic (p) and healthy hemispheres (h), we calculated an asymmetry index (AI) for each tract parameter. The AI set into relation by:

$$Volume\ AI = \left|\frac{(volume\ h)-(volume\ p)}{(volume\ h)+(volume\ p)}\right| \quad (5.1)$$

The CST and AF analysis, and AI's calculation were also obtained in healthy subjects hemispheres (left vs right) with the intention of demonstrating the difference between patients and healthy subjects (i.e. control group).

3. Data reduction and statistical analysis

CST and AF size (streamline count and tract volume (ml) and their respective standard deviation) were calculated using Trackvis. DTI and DKI metrics and their standard deviation were obtained at the strongest deviation of CST in patients and a mean of the same metrics were calculated in healthy subjects. Statistical inference (SPSS Inc., Chicago USA) was made applying either the Kruskal-Wallis test for comparisons between methods and the Mann-Whitney U-test used for comparisons between the pathologic and healthy hemispheres of the patients (a significance level of p=0.05 was chosen), respectively.

Results

This study was undertaken in six patients (mean age 36 years old, range from 24 to 64), who had been diagnosed with primary brain tumors near motor pathways, including astrocytomas (n=4), oligodendroglioma (n=1), and oligoastrocytoma (n=1). The demographic data of patients are summarized in table 5.1. Just one patient presented high grade cancer cells (patient 2). In patient 1 and 3 the neoplasm already involved or compressed CST leading to presurgical neurological deficits. In order to compare the tractography results, 8 right-handers, healthy subjects (three males, mean age 24, range from 20 to 26) were recruited to perform MRI.

Table 5.1 – Demographic characteristics of patients with brain tumors.

Patient	Gender	Age	Hemisphere	Location	Symptoms	Histological finding	DWI acquisition directions
1	Male	24	Right	Frontotemporal	Disarthria	Astrocytoma	64
2	Female	28	Right	Frontoparietal	Seizures	Anaplastic Astrocytoma	64
3	Female	34	Right	Frontal	Hemiparesis	Oligodendroglioma	64
4	Male	30	Left	Frontal	Seizures	Astrocytoma	32
5	Male	39	Right	Frontal	Seizures	Oligoastrocytoma	32
6	Female	64	Left	Frontal	Seizures	Astrocytoma	32

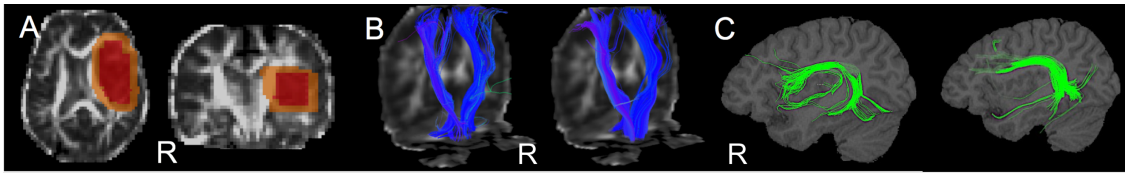

Figure 5.1 – A) Axial and coronal views of the region of interest used in the patient number 2, placed around the previously demarked tumour, and corresponding to 10% of its volume. Note that the ROI were delineated only once in each subject. B) Corticospinal tract and arcuate fascicle (C) streamlined in a healthy subject using diffusor tensor tractography (right image) and kurtosis tensor maxima tractography (left image).

1. Images acquisition and tractography.

On average, MRI acquisition per patient took 34 minutes (ranging from 24 to 41 minutes) including gadolinium injection in all patients. In half of the patients it was possible to acquire DWI with 64 diffusion directions; this lead to an increased acquisition time of 10 minutes in comparison with DWI with 32 directions (mean examination time of 39 minutes versus 28 minutes). Each patient DWI sequence acquisition took 6min58s. Image analysis was performed in about 7 hours for each subject (i5 Core 2.9GHz processor with 4GB RAM), including whole-

brain tractography based in DTI and DKI methods, identifying the CST and AF in the healthy hemispheres and isolating the fibers in the vicinity of the brain tumor in pathological hemispheres. The full analysis took, on average, 2.8 hours for each subject with DTI-tract and 4.7 hours for each DKI-tract method.

2. Diffusion tensor and kurtosis tensor tractography

The CST and AT was streamlined in all subjects using both deterministic methods; tract number and volume are presented in table 5.2. In figure 5.1 an example of the reconstructed CST and AR in healthy subject was showed using both methods. Patients CST's subdivided by tractography method were showed in figure 5.2 and tracts in the vicinity of the tumor were also showed (i.e. targeting surrounding tumor ROI). To evaluate CST fibres, a qualitative inspection of the anatomical course was performed and a low number of false-negatives were identified when using the DKI-tract in comparison to DTI-tract. A higher number of tracts CST were depicted in pathological hemisphere by DKI-tract for CST ($p=0.005$, table 2) in comparison with DTI-tract. Mean tract number and a high AI were obtained in patients using the DTI-tract in comparison with healthy subjects group ($p=0.023$).

Within patients, no differences in CST parameters were identified between those which used 64 directions and 32 directions DWI ($p=0.26$). The AI showed no differences in DTI-tract of DKI-tract of the CST. In three patients (patient 1, 3, 5), the DKI-tract depicted motor fibers were either not delineated (patient 1, 5) or more closely related to the tumor (patient 3) in comparison with DTI-tract. The additional CST pathways were located posteriorly in patient 1 and medially in patient number 5 (fig.5.2).

The AF streamlined by DKI-tract showed a high number of tracts and volume in healthy subjects than DTI-tract ($p=0.01$). Additionally, the AF depicted in left hemispheres were larger (table 5.2) than those depicted in right hemisphere with a high AI ($p=0.022$). In patients, also more voluminous tracts were obtained by DKI-tract in pathological hemispheres in comparison with DTI-tract ($p=0.025$ for tracts number; $p=0.032$ for tract volume). However, despite significant, a smaller AI were obtained in AF parameters when using DKI-tract in comparison with DTI-tract. In figure 5.2, were demonstrated the AF of patient 1, 4, and 5 where DKI-tract depicted tracts not streamlined by DTI-tract.

Table 5.2 – Volume, tract number and asymmetry index (between parenthesis) of the corticospinal tract and arcuate fascicle delineated by diffusion tensor (DTI) and kurtosis tensor (DKI).

Patients	Corticospinal tract				Arcuate fascicle			
	Tract number		Volume (ml)		Tract number		Volume (ml)	
	DTI	DKI	DTI	DKI	DTI	DKI	DTI	DKI
1	106	510	26.4	42.7	128	134	21,2	27,2
2	227	801	33.4	46.3	97	288	21,2	34,4
3	399	478	40.0	45.2	29	136	14,3	21,3
4	381	393	56.4	34.4	34	239	15,3	38,3
5	452	365	55.5	47.2	44	243	15,5	34,2
6	190	373	38.9	41.6	23	76	9,2	16,4
Mean±SD	293±137* (0.19)	487±164* (0.01)	41±12 (0.15)	42.9±5 (0.01)	59±18* (0.55)*	186 ±82* (0.31)	17±6 (0.19)	28±9* (0.17)
Healthy subjects Mean±SD	448±58 (0.06)	412±131 (0.02)	43.3±9 (0.05)	41.6±5 (0.01)	218±106* (0.19)*	325±97* (0.24)*	36±15 (0.16)*	45±9 (0.25)*

The values between parenthesis refer to the asymmetry index in comparison with the contralateral hemisphere. *Statistically significant differences for evaluated parameter values between healthy subjects and patients.

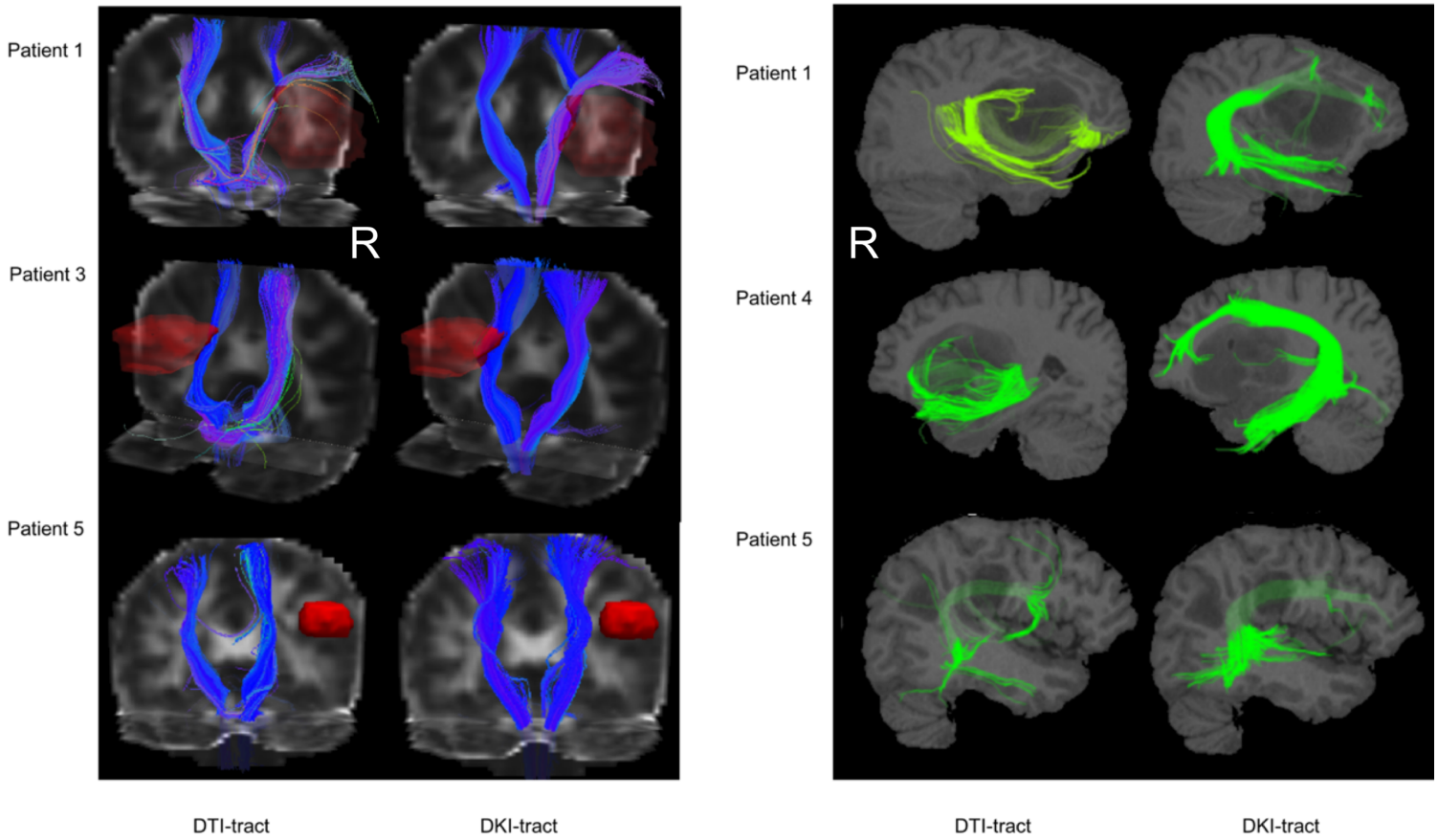

Figure 5.2 – Left image: Corticospinal tract of patients 1, 3 and 5 delineated by diffusor tensor (DTI-tract) and kurtosis tensor tractography (DKI-tract). The tumor is highlighted in red. Note the anatomical course and increased density of streamlines delineated by DKI-tractography near tumour margins. Right Image: Arcuate fascicle streamlined by DTI-tract and DKI-tract. In patient 1 and 4, note the anatomical course of arcuate fascicle since the superior and middle temporal gyri to frontal lobe by DKI-tract not depicted by DTI-tract.

Discussion

The quantification of molecular water motion in the range of micrometers through MRI diffusion imaging made it possible to map the white matter tracts in vivo.[111] To evaluate the usefulness of DKI-tract based on kurtosis maxima in a clinical setting and compare it with DTI-tract, CST and AF tractography were studied in a group of patients with PBT. To our knowledge, the comparison between DTI and DKI-tract performance in presurgical planning of patients with gliomas and the streamline of AF using a DKI method remained to evaluated. Fibre tracking with DKI-tract showed a high number of streamlined tracts in both CST and AF in comparison with the DTI-tract. The performance of both methods was similar in healthy subjects suggesting a negative influence by the brain neoplasm in DTI-performance.

1. Images acquisition and tracts reconstruction.

The tested tractography methods have different requirements regarding the number of diffusion directions sampled and the maximum b-value. This has implications both on the acquisition time, which depends on the number of diffusion volumes (equal to the number of directions times b-values), and on the attainable spatial resolution as higher b-values (higher contrast) result in lower SNR. In this work, the protocol performed used three b-values (0, 1000 and 2000 s/mm^2), with 64 and 32 different gradient directions evaluated and took about 40 minutes to be done. Although there was a penalty in acquisition time and spatial resolution, since this is more demanding than typically used in conventional DTI-tract (two b-values, 0 and 1000 s/mm^2, and 30 directions), it enabled the use of a more complex diffusion model, the DK tensor, accounting for diffusion restriction or tissue complexity.[112] While most studies used at least 5 b-values to perform DK tensor estimation, clinically-compatible DWI sequences with 3 b-values had been suggested to enhance the applicability of this method.[108,] Despite the small sample, there were no significant differences in the CST parameters and metrics extracted from 64 directions DWI acquisition in comparison with 32 directions DWI. Therefore, with our methods we were able to delineate the CST and AT either through DTI or DK methods (table 5.2).

The relatively lower performance of DTI-tract can in part be related to lower resolution DWI data acquired using voxels with isotropic 3 mm resolution in comparison with typically used in DTI-tract (2 to 1 mm isotropic).[113] In addition, slightly high echo time and low matrix resolution were used allowing susceptibility effects to produce echo planar imaging distortion. If the influence of such artefacts for DTI-tract is higher than for DKI-tract are unknown. Additionally, we tried to mitigate such distortion during imaging preprocessing imaging.

The time for reconstruction of the tracts was 2 times longer for DKI-tract than DTI-tract using a personal computer and therefore this can be considered as a disadvantage of the methods. Although, the tools used for tracts reconstruction (i.e UDKI)[40] were simple to use and already reported as reliable tool in literature.[113]

2. Corticospinal and arcuate fascicle tractography.

DTI-tract does no predict reliably the fibre population direction in voxels with two or more intersecting populations. Our results, showed a smaller CST and AF size estimated by DTI-tract in patients in comparison with healthy subjects group. According with other studies,[34,106] such low performance is more evident within the presence of a brain neoplasm due to histological distortion and axonal bundles compression.[114]

In our study, we hypothesised that the DKI-tract method would be more sensitive to these microstructure changes improving the delineation of fibres at high level of complexity.[36] Additionally, we used a recent DKI tractography method to estimate fibres' directions based on the assumption that the maxima of the kurtosis are distributed perpendicularly to the direction of well-aligned fibres.[41] Quantitatively, CST and AF was higher when estimated through DKI-tract in comparison with DTI-tract (table 5.2). Moreover, tracts influenced by the presence of the brain tumor also showed an asymmetry of DTI-tract of CST parameters in comparison with control hemispheres. However, the delineation of AF showed a high asymmetry between left and right hemispheres in healthy subjects. These results are consistent with those reported in the literature which demonstrated that the left AF has twice the volume of the right AF.[109] Such asymmetry was still affected by the low performance of DTI-tract showing higher AI than in AF delineated by DKI-tract. Additionally, the AF volume estimated using DKI-tract were slightly smaller to those estimated using diffusion imaging spectrum.[109]

DKI-tract was also able to streamline fibers in vicinity of the tumor which had not been identified by DTI-tract (false-negatives) in three patients either in CST (patient 1, 3, 5) or AF (patient 1, 4, 5). These fibers were compatible with pyramidal and arcuate pathways as determined by their anatomical course.[109,114] The DKI-tract performance may be explained by the ability to estimate non-Gaussian behavior of water diffusion providing indices of tissue heterogeneity with better characterization of the spatial architecture. However, kurtosis maxima are able to estimate direction of fibres crossing at high intersection angles within a voxel with low angular errors.[41] A high sensitivity to resolve fibres within voxels with complex microstructure (i.e. tumor edema) may explain the delineation of AF fibres in the vicinity of the tumor (fig 5.2).
Although, a larger, more homogeneous groups with direct cortical stimulation should be studied in order to electrophysiologically map the viability of the CST and AF pathways reconstructed

using the DKI-tract methods. Moreover, the location and distance from tumor margin to CST should be investigated to test the functionality of such motor fibres.[114] However, the absence of language disturbances (in patient 4 and 5) suggest a functional AF despite of the presence of anatomical distortion.

Conclusion

The present study reports the usefulness of the kurtosis-based tractography method in the clinical setting, where it is essential to ensure acceptable scanning times. Our results suggest that DKI-tract may be advantageous to estimate fibres for presurgical planning in the presence of gliomas in comparison with conventional DTI-tract.

SECTION C: SPEECH AND LANGUAGE CONNECTIVITY PROCESSING

CHAPTER VI

IMPACT OF NAVIGATED TASK-SPECIFIC FMRI ON DIRECT CORTICAL STIMULATION

Introduction

Awake craniotomy enables communication between the patient and the clinician for assessing cognitive functions while the surgeon performs brain mapping and tumor resection. As stated before, glioma surgical treatment with an asleep-awake-asleep anesthesia protocol improves precision for gross tumor resection within brain functional boundaries.[115,116] Awake craniotomy with DCS is the gold standard treatment for tumors involving eloquent brain areas.[117] However, selection criteria to perform this surgical protocol is based on the patient's qualitative aptitude to collaborate during cognitive tasks evaluated by presurgical neuropsychological tests. Overall, patients seem to tolerate this procedure well, but some report an unpleasant feeling of concern interpreted as anxiety and pain starting mostly from the middle of the surgery, partly due to language disturbances evoked by DCS.[4] Moreover, CM with DCS has also been associated with a high number of intraoperative seizures[118] and increases the total duration of the surgery in comparison with general anesthesia.[116] Thus, this protocol could impose further challenges such as patient fatigue and longer rehabilitation time.[119]

To improve patient comfort without compromising CM performance, the practical aspects of DCS should be addressed, aiming to increase efficiency by shortening its duration, the number of stimuli for which patient collaboration is required, and the number of intraoperative seizures.[118] In fact, approximate locations of eloquent cortical brain regions are already available from presurgical language task-specific fMRI.[120]

The BOLD effect drives the signal obtained with fMRI and this technique can be used in presurgical planning in order to minimize language disturbances resulting from surgery.[121,122] However, the benefits of navigated fMRI (nfMRI) data to identify the resection boundaries remain debatable. In fact, language-specific task fMRI may misidentify or misallocate the fundamental brain regions involved in language function due to the lack of sensibility and specificity[16] showing a limited influence on patients' quality of life.[123] Efforts have been made to deal with this problem by introducing multiple language task paradigms.[124] Together with the continuous improvements in spatial resolution of the fMRI acquisitions,[45] multi task fMRI might provide valuable

information in mapping eloquent locations. However, the application of this technique in the context of brain tumor resection is limited due to the lack of neurovascular coupling in the affected regions.[125,126] This precludes any attempt to use fMRI as a sole tool in CM, where DCS is routinely used. Nevertheless, fMRI might hold pertinent information which could be useful in CM of brain tumor patients.

In this study, we incorporated fMRI results in the navigation system to inform DCS planning when performing CM, evaluating their impact on the number of stimuli delivered, stimuli duration, total time dedicated to DCS, and the number of observed seizures. We hypothesize that the extra "online" information available to the surgeon, given by a nfMRI, regarding the presence or absence of language function will add value to DCS. Our goal was to investigate if presurgical fMRI data acquired using multiple language paradigms could contribute to increased efficiency of DCS during CM.

Methods

Patients with gliomas involving or near the language network including motor areas were selected for awake craniotomy between 2016 and 2018 at Hospital Garcia de Orta (Almada, Portugal). The selection criteria of the patients enrolled were the following: lesions less than 20 mm apart from language brain regions or pathways as evaluated by presurgical MRI; absence of aphasia evaluated clinically and by neuropsychological language tests (i.e. the patients were excluded given an error rate greater than 50% of the trials in any given test) and without cardiac pacemakers. The patients were randomly selected to perform multimodal CM with DCS and nfMRI (i.e. mCM) or to undergo CM using only electrical DCS (i.e. eCM). For the allocation of the patients into each group, a simple randomization method was used. One of two contributors (JL and CV) in the presence of another (HF) would roll a die just once, and if an odd number appeared facing upwards, the patient was allocated to the mCM group. The Ethics committee of Hospital Garcia de Orta gave its approval for conducting this work and prior informed consent was obtained from all participants.

1. Clinical evaluation

Neurological examinations were carried out the day before surgery, 48 hours after surgery, and in consultation regime, 3 to 6 months after hospital discharge. In addition, a battery of neuropsychological tests was performed in the two weeks prior to surgery. For language assessment, a PNt, NVSDt using a pyramid and palm tree test, and a VGt adapted to the Portuguese population were performed.[16] These tests consisted in a total of 80 trials of PNt, 55 of

NVSDt and 35 of VGt that patients were asked to perform as quickly as possible. During awake craniotomy, patients performed PNt and NVSDt with the same pictures shown in presurgical evaluation.

2. Presugical MRI data acquisition

MRI examinations were performed two weeks prior to the surgery. A 3 T Philips MRI scanner (Philips, Netherland) was used, equipped with an 8-channel head receiver coil. A standard MRI protocol was acquired in all patients.[96,128,129] The volumetric T1-weighted sequence was followed by block design BOLD fMRI. The latter sequence was acquired during language and motor tasks already described in chapter II. Briefly, three language tasks were used: VSDt, syntactic judgment, and VGt. Semantic and syntactic paradigm tasks were conducted in 10 design blocks divided in 6 experimental (i.e. test), 2 baseline tasks and 2 rest periods for a total of 160 volumes. The VGt was designed in 8 blocks consisting of 4 experimental, 2 baseline tasks and 2 rest period for a total of 112 volumes. Baseline recordings were made with a simplified cognitive task (i.e. high-level baseline): the participant had to perform a symbol search task, where two distinct symbols had to be found in a random letter string. The motor task consisted of two paradigms: one based on opening and closing the mouth and the other based in finger tapping. These data were recorded in 8 blocks consisting in 4 experimental and 4 rest periods for a total of 80 volumes. For fMRI data, preprocessing was done using BrainVoyager (v.2.8, Brain Innovation, Maastricht, The Netherlands) as described in chapter II.[47] The BOLD and significant activation maps calculated from the general linear model were superimposed and the regions activated by at least two paradigms were defined to be incorporated into the anatomical brain scans (T1-weighted scan) used in intraoperative procedures. Series of language paradigms tasks were excluded and repeated if the patient's collaboration was not considered to be acceptable by a neurologist (author ML). The calculated activation maps were used to assess the dominant hemisphere for language function. The lateralization index was calculated using the data from each activated voxel (i.e. level of activation) with the following formula:

$$Lateralization\ index = \frac{(left\ activation\ map - right\ activation\ map)}{(left\ activation\ map + right\ activation\ map)} \quad (6.1)$$

If the lateralization index was ≥ 0.10, the patient was considered to have a left-dominant hemisphere and if it was ≤ 0.10, right-dominance was considered.[130]

3. *CM during surgery*

Intraoperative mapping was performed by the same surgeon (author CV) using DCS (Inomed Medizintechnik, ISIS IOM System, Germany). Stimulation parameters, probe and current was detailed in chapter III. Recording of muscle burst activation was done in contralateral mentalis, biceps, abductor policis brevis, tibial anterior and abductor of the hallux muscles using 13mm subdermical needles. To detect epileptic seizures and monitor possible inhibition of adjacent cortical areas, a surface electroencephalogram was recorded with 4 channels distributed around the craniotomy limit. For DCS, all sites were stimulated at least 3 times (non-consecutive) and positive or negative brain regions for language function were defined. Threshold of action were defined while the patient performed a counting task which preceded language mapping to establish a stimulation intensity. Language disturbances were assessed by the same neuropsychologist that performed the presurgical evaluation.

Cortical gyri of frontal and temporal lobes were evaluated using neuroanatomical landmarks and nfMRI data (in the mCM group) incorporated in a navigational system (StealthStation, Medtronic, USA). The nfMRI data of the combined language paradigms was used to inform and modulate the effort dispended (time and number of stimuli) for DCS at a specific brain region. For example, within a brain region without nfMRI activation, the surgeon applied only one stimuli (instead of two) before categorizing it as a negative region for language function. On completion of CM, the localization of stimulation effects was based on the assumption that the stimulation is strongest in the tissue in contact with the electrode of the probe used for DCS. The stimulating electrode was localized by transferring the location of positive sites to the navigation system with the navigation pointer.

4. *Anesthesiological procedure*

The standard physiological parameters were monitored during anesthesia and sedation.[131] Analgesia and sedation was maintained by continuous infusion of remifentanil and propofol. The depth of analgesia and sedation was monitored using the Ramsay sedation scale targeting a score of 5: weak response to pain stimuli. Additional bolus doses were administered immediately before incision of the scalp and dura to adjust analgesia to the pain level of the surgical stimuli. Local anesthesia with lidocaine or ropivacaine was also done in skull-pin placement, along skin incision and dura. Intravenous antiepileptic drug loading was done in all patients with 1000 mg of levetiracetam. Analgesia and sedation were discontinued for about 10 minutes before intraoperative neuropsychological testing and CM. Baseline analgesic infusion was continued. The goal during this phase was to achieve a sedation score of 2: awake and alert. After CM, the

surgery continued with tumor resection before reaching its margins, then the depth of sedation was increased and a laryngeal intubation was carried out for hemostasis and closure.

5. *Data reduction and analysis*

For statistical purposes, we considered the patients enrolled for the mCM as the test group and eCM as the control group. Performance of patients in presurgical neuropsychological language tests was quantified as a percentage of correct answers in the total trials per task. Patients who provided 50 to 80% of correct answers in a test were identified as having a low performance. A subgroup analysis (lower vs higher performance) between groups was performed to identify a possible lack of aptitude to collaborate in language tasks.

Intraoperative data for each group and task performed, as the number of cortical stimuli given to the patient, the time of stimulation, the total time required for CM and the frequency of seizures or after-discharges was recorded. Mean and standard deviation for presurgical language tests and DCS parameters were calculated and compared between groups. An independent t-test was used after testing for normality with Shapiro-Wilk test and variances of homogeneity with Levene's test. Statistical analysis was performed using SPSS Statistics (v.24, IBM, USA). A p-value lower than 0.05 was considered statistically significant.

DCS and fMRI data from positive mapping responses and activated brain regions, respectively, were displayed on a cortical surface using a cortical parcellation system.[132] A correspondence analysis between modalities was done considering a positive correspondence region when the DCS probe delivered a stimulus at a point which included an fMRI activation within a 2-mm radius.

Results

In figure 6.1 is shown the presurgical MRI axial scans and in table 6.1 the demographic characteristics, tumor specifications, and presurgical performance of the patients in the neuropsychological tests. Thirteen patients were enrolled for mCM (patients 1 to 13) and eight for eCM. Patients 12 and 13 received a second surgery due to tumor recurrence, which were performed with mCM, 51 and 8 months after the first surgery, respectively. The mean age of the mCM group was 47 years old (y.o.) with a standard deviation (SD) of 9 y.o. in comparison to 51 y.o. (SD = 12 y.o.) for the eCM group. The most common presentation was seizures (62% of the patients). All lesions were located within the left hemisphere. About 31% of patients in the mCM group and 50% in the eCM group presented tumors with high-grade cancer cells located in the

frontal lobe. Oligodendroglioma was the most common tumor histology (33%) and in one patient showed high grade cancer cells (table 6.1).

Patients in the mCM group showed an overall lower performance in PNt and VGt (87% SD = 16% in PNt, 82% SD = 15% in VGt) in comparison to the eCM group (91% SD = 6% in PNt; 87% SD = 5% in VGt), albeit not significantly. In NVSDt, the performance in mCM was higher than in the control group (94% SD = 8% in mCM and 90% SD = 8% in eCM), without statistical significance. Patients 4, 5, 6 and 10 were considered to have a low performance. This subgroup of four patients showed significantly lower performances in PNt (67% SD = 16%) and VGt (69 % SD = 21%) in comparison to the other patients of the mCM group ($p= 0.020$ and $p=0.030$, respectively) and to the control group ($p=0.004$ and $p=0.010$, respectively).

Preoperatively, six patients presented language disturbances (patients 6, 7, 9, 10, 17, and patient 13 before the second surgery) which partially resolved after a five to seven days cycle of oral steroids (dexamethasone 18 mg/day).[103] Patients 6 and 7 also presented a contralateral hemiparesis. Forty-eight hours after the surgical procedure, three patients displayed aggravated language and motor function and two aggravated motor function (table 6.1). Six months after surgery, three patients died due to tumor recurrence (patients 4, 6, and 7). Regarding neurological deficits between 3 to 6 months after surgery, two patients maintained an aphasia (patients 13 and 17), and patients 14 and 18 a mild right hemiparesis and central facial palsy, respectively.

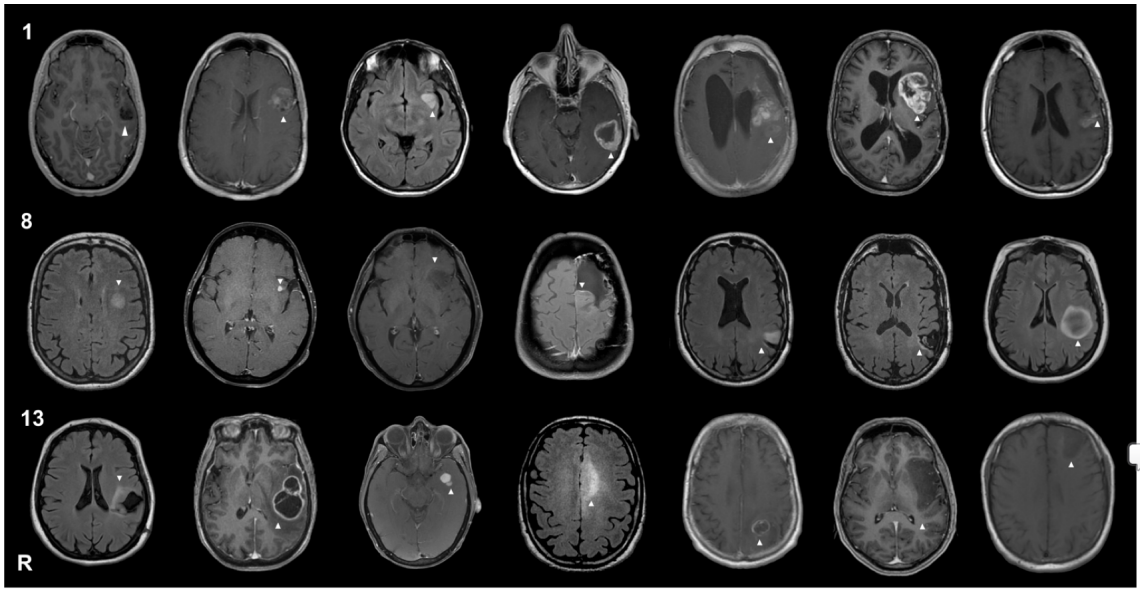

Figure 6.1 – Axial magnetic resonance imaging scans (one per patient, in numerical order from left to right and top to bottom) showing the position of their lesions (indicated by arrows). Different image contrasts were selected according to tumor malignancy in order to better depict the tumor location. Illustrative scans comprise either gadolinium-enhanced T1-weighted images or T2-weighted images with fluid inversion recovery (patients: 3, 8, 12, 13, 17, and 18).

1. *Cortical brain mapping.*

CM was done after awaking the patients and before initiation of tumor approach or resection. A brief interview was made to each patient regarding age, current month, year, and spatial localization to guarantee the awake state (i.e. Ramsay sedation grade 1 or 2). DCS was performed only in the left hemisphere. In figure 6.2 are shown the evaluated parameters extracted from CM with mean and confidence intervals of 95% of mCM, eCM, and mCM with lower performance groups.

In the mCM group, CM was completed in 11.5 minutes (SD = 2.9 min) with a total delivered stimulus duration of 30.2 seconds (SD = 4.9 s) for motor function and 56.7 seconds (SD = 4.6 s) for language function. The number of stimuli delivered for motor mapping and CM intensity identification was 11 (SD = 3) with a mean duration of 2.2 s (SD = 0.4 s). For language mapping, 15 stimuli (SD = 5) with 3.6 seconds (SD = 0.7 s) duration were required. In eCM, CM was performed in 12.2 minutes (SD = 4.4 min) with duration stimulus delivered of 29.5 seconds (SD = 5.5 s) for motor function and 59.9 seconds (SD = 3.1 s) for language function. For motor mapping, 15 stimuli (SD = 4 s) were given with mean duration of 2.4 seconds (SD = 0.7 s) and for language mapping 16 stimuli were required (SD = 4 s) with 3.9 seconds (SD = 0.9 s) mean duration. The mean intensity used in mCM groups was 4.4 mA (SD = 1 mA) in comparison to 4.0 mA (SD = 1 mA) used in the eCM group. No significant differences were found in any of the parameters between mCM and eCM. In two patients per group (patient 4, 6, 14, and 16), after-discharges were identified during CM and cold Ringer's lactate solution was applied directly to the brain. No patient presented intraoperative seizures.

2. *Navigated fMRI in DCS*

All mCM patients were right-handed, attended at least 4 years of primary school (table 6.1) and just 26% were monolingual (patients 6, 10, 14, 15, and 17). All patients used their mother language in presurgical and surgical language tasks (i.e. Portuguese). The positive sites of DCS and fMRI are displayed in figure 6.3, making use of the cortical system described in Corina et al. (2005)[132] with color-coded diagrams.

fMRI data acquired after hands or mouth movement activated bilaterally the precentral gyrus in all the patients. In seven patients, the ventral precentral gyrus was bilaterally activated also by mouth movement. Additionally, DCS of the left hemisphere ventral precentral gyrus evoked hesitations during counting (i.e. anarthria) in 11 patients while motor bursts were evoked in contralateral muscles after stimulation of the precentral gyrus (fig. 6.3).

Table 6.1 – Demographic characteristics of patients (Pt) that received cortical mapping. Neuropsychological performance in language cognitive tests is shown as a percentage of correct answers. Neurological morbidity (unchanged or aggravated) before hospital discharge in relation to presurgical status is presented.

Pt	Gender	Age	Symptom	Location	Histology	Education (years)	PN (%)	NVSDT (%)	VG (%)	Presurgical vs Postsurgical	
										Motor	Language
1	Female	35	Seizure	T	A	9	96	95	80	-	-
2	Male	31	Seizure	F	OD	>13	96	100	94	-	-
3	Male	46	No	I	A	9	94	93	91	-	-
4	Male	57	Seizure	T	GBM	12	68	100	83	-	-
5	Male	58	Seizure	F	OD	>13	89	98	77	Aggravated	-
6	Female	56	Aphasia	F; I	GBM	7	53	73	57	Aggravated	
7	Male	52	Aphasia	F	GBM	9	96	93	86	Aggravated	
8	Female	51	No	F	OD	9	94	96	94	-	-
9	Female	40	Seizure	I	NGT	12	98	98	86	-	-
10	Male	54	Seizure	F	OD	4	76	89	80	-	-
11	Female	46	Aphasia	F	OD A	12	95	95	91	-	-
12	Male	50	Memory loss	P	A	>13	96	95	89	-	-
		52	No			>13	96	95	90	-	-
13	Female	38	Seizure	T	A	12	94	98	89	-	
		39				12	94	98	80	Aggravated	
14	Female	66	Headache	T	GBM	4	74	71	69	Aggravated	-
15	Male	61	Seizure	T	OD	4	81	81	80	-	-
16	Male	40	Seizure	F	A A	9	98	96	91	-	-
17	Male	68	Seizure	P	GBM	4	96	87	91	-	Aggravated
18	Female	61	Seizure	F; T	OD	>13	94	95	89	Aggravated	-
19	Male	48	Seizure	F	A A	10	94	95	91	-	-

A – Astrocytoma, A A – Anaplastic Astrocytoma. F – Frontal, GBM – Glioblastoma, T- Temporal, I – Insular, P- Parietal, NGT – Neuroglial tumor, NVSDT – non-verbal semantic decision task, PN – picture naming task, OD –Oligodendroglioma, OD A – Oligodendroglioma Astrocytoma, " –" unchanged or improved

Bursts in mentalis, abductor pollicis brevis and biceps brachi muscle were evoked with DCS from medial to dorsal precentral gyri according to the motor homunculus. However, DCS at middle precentral gyrus evoked anarthria and interruption of contralateral arm movement in 6 patients. Thus, a correspondence of 100% for precentral gyrus and of 63% for the ventral precentral gyrus was identified.

Left hemisphere language lateralization was identified in 61.5% of the patients. Patient 11 showed a right hemisphere lateralization. Patients 4, 6, and 8 showed a bilateral activation during language tasks. The activation maps for mCM with simultaneous brain activated regions in the three paradigms were used in 61.5% of the patients.

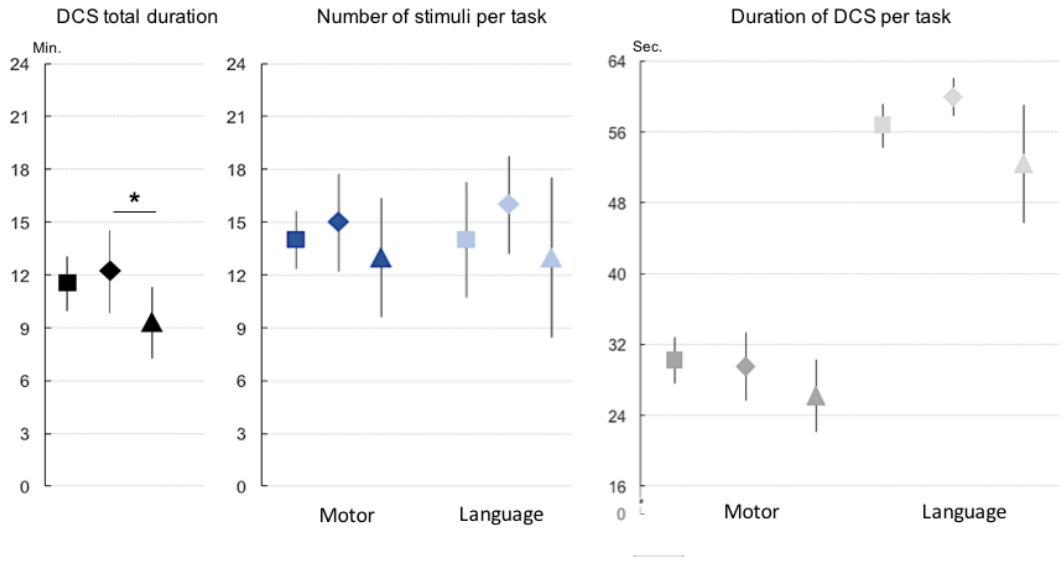

Figure 6.2 – Direct cortical stimulation (DCS) parameters mean (symbols) and 95% confidence intervals (error bars) for 9 patients enrolled in multimodal cortical mapping (square) and 4 patients of the same group but with lower performance in presurgical language tests (triangle). Comparisons were performed with corresponding parameters from 8 patients enrolled for cortical DCS mapping used as a control group (losangle). Total DCS duration in minutes per group are shown using black symbols. Note the statistically significant difference (*) between the lower performance patient group and the control group in the total DCS duration (p=0.02).

In Figure 6.4 is shown an example of mCM used in patient 13's second surgery before resection of the recurrent tumor. A correspondence between nfMRI and DCS positive responses was found in the opIFG (i.e. brain region labeled with number 4), and in the posterior part of the superior temporal gyrus (i.e. number 6). DCS was performed in these gyri while the patient performed a PNt which evoked speech arrest and anomia, respectively. However, a lack of correspondence was seen in the middle part of the superior temporal gyrus (i.e. number 5), while semantic paraphasia was evoked by the DCS.

In the mCM group, the fMRI language paradigms activated the opIGF (in all patients, fig. 6.3), and the posterior superior temporal gyrus (STG ;in 10 patients), with a correspondence with DCS of 84% and 70%, respectively. Conversely, language mapping function in brain cortical areas around these gyri was more dispersed in both fMRI and DCS (figure 6.3). A correspondence of 66% and 30% was found in the supramargincal gyrus (SMG) and in the middle part of STG, respectively. In two patients (8 and 11), no positive responses were evoked with DCS during these tasks.

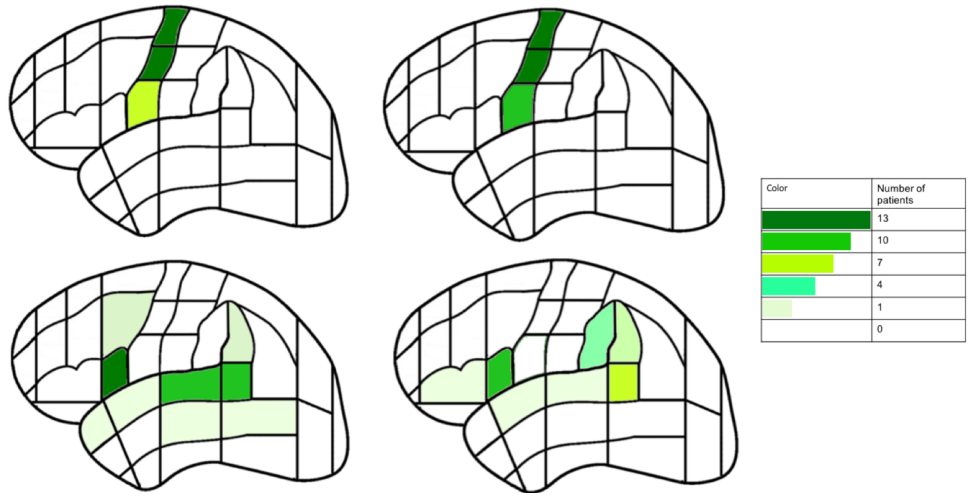

Figure 6.3 – Diagrams illustrating color-coded frequency of cortical activation sites in patients enrolled for multimodal cortical mapping using functional magnetic resonance imaging (fMRI) and direct cortical stimulation (DCS). Left column: fMRI activation maps using finger tapping and mouth movement (top) and language cognitive tasks (bottom). Right column: positive DCS sites for motor function at contralateral hand and face muscles (top) and for language function evoking language disturbances.

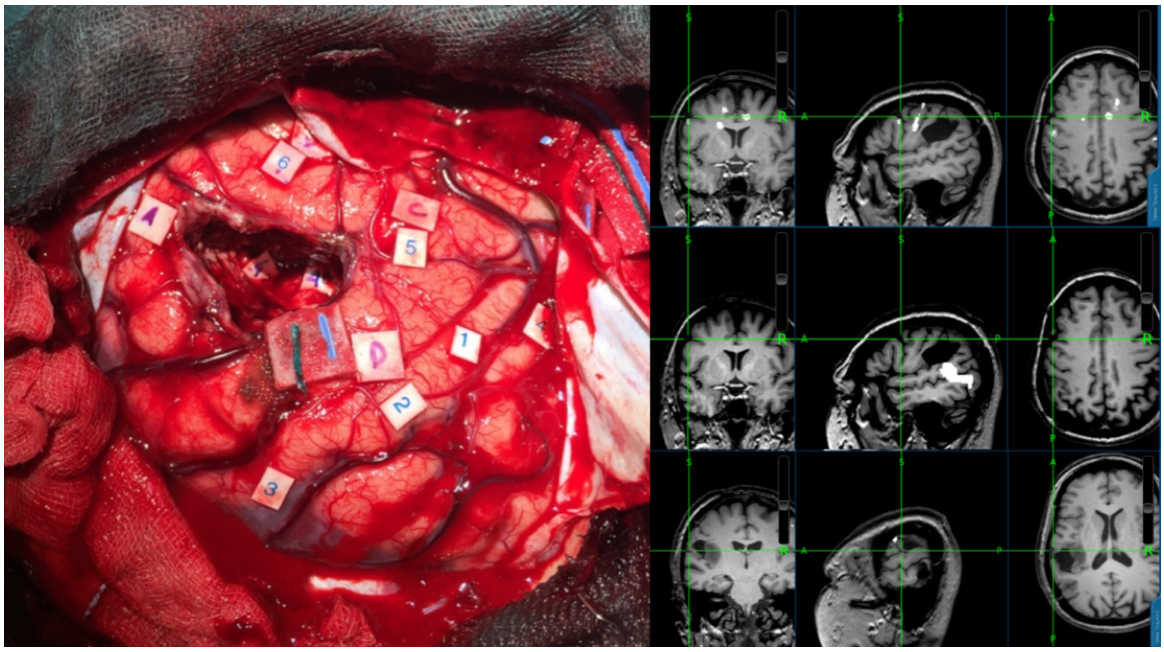

Figure 6.4 – Example of cortical mapping performed in patient 13 during the second surgery after tumor recurrence. Left: photograph after direct cortical stimulation (DCS) was performed with the assistance of navigated task-specific functional magnetic resonance imaging (fMRI) results. The following labels were used to demonstrate: 1 – ventral precentral gyrus in which anarthria was evoked during the counting task; 2 – contralateral mentalis and 3 – abductor policis brevis muscle burst activation at the precentral gyrus; during the picture naming task at 4 a speech arrest was evoked, paraphasias at 5 (middle part of the superior temporal lobe) and anomia at 6 (posterior part of the superior temporal lobe). Right (top to bottom): activation maps shown in white were extracted from mouth and hand movement paradigms (top). Data from three language tasks were also shown (middle and bottom). Note the mismatch between DCS and fMRI in the site labeled as “5” (bottom).

Discussion

CM of eloquent brain functions remains useful in the clinical setting for planning surgical tumor resection to avoid further neurological morbidity.[122,123] The patients recruited suffered from high grade gliomas in more than one third of the cases implying a rapidly progressive pathophysiological mechanism. We aimed to test if allied intraoperative modalities of CM (i.e. nfMRI and DCS) could reduce the effort spent on DCS in awake surgery, reducing patient discomfort. To our knowledge, the practical impact of having prior nfMRI data on DCS during CM remained to be studied. Our work showed that having this information did not reduce the DCS duration, the total number or duration of stimuli delivered to patients, nor the number of after-discharges. However, the duration of CM in patients who showed a low performance in presurgical neuropsychological tests was reduced when using nfMRI in combination with DCS.

The ultimate goal of using presurgical planning with fMRI is to predict postoperative language deficits by assessing the risk of such deficits and minimize their severity.[121,122,133,134] fMRI relies on the BOLD effect, which is based on the assumption that oxidative metabolism and neurovascular coupling leads to an increase in oxygenated blood delivery to task-specific brain regions during activation.[135] However, this technique may suffer from methodological caveats such 1) limited spatial resolution within the region surrounding a PBT,[125,126] 2) differences in task characteristics evaluated during MRI scans acquisition[136] and patient performance, and 3) lack of understanding of the true predictive value of fMRI activation for language function.[133,137] In fact, the reported results from studies in which the language outcome was predicted based on presurgical fMRI varies widely.[16,133,134] Moreover, the specific methodology used by each study must be taken into account to reproduce similar results to detect language eloquent cortex.[137]

In contrast, the implementation of nfMRI data intraoperatively using high-resolution anatomical images gave the opportunity for the surgical team to identify the locations of the cortex typically associated to language functions. Such intraoperative knowledge can lead to avoiding time-consuming neurophysiological tests, but its influence on the length of the operation has not been directly.[138] In our study, the surgeon consulted a map of multi-language task nfMRI activations after identifying a negative brain region for motor or language function following DCS. We hypothesized that having available this three-dimensional information of the cortical eloquent brain could increase the surgeon's confidence, reducing the number of stimuli required and perhaps the intraoperative seizures. However, no differences were seen between mCM and eCM groups despite our effort to minimize some methodological caveats like the spatial resolution of the technique, the selection of the paradigms used, preprocessing analysis, errors in the co-

registration of fMRI data into the intraoperative setting, or the reduced spatial accuracy of the navigation system.

1. fMRI acquisition procedure

The spatial resolution of fMRI is dependent on the brain hemodynamic response and by the images' SNR.[125] In our study, fMRI scans were acquired using an echo-planar sequence based on T2*-weighted contrast which detects dephasing diamagnetic hemoglobin from active brain regions after performing a task.[135] The spatial resolution of the MRI signal is influenced by baseline venous blood vessel and vessel size.[45,125] Therefore, such BOLD signal changes may derive physiologically far from the activated grey matter. In addition, within patients with PBT, the large vessels' contribution to the MRI signal is exacerbated due to tumor vascularity.[45,125,135] Moreover, echo-planar fMRI readouts are affected by susceptibility artifacts, distorting the geometric location of fMRI BOLD activation regions. This effect, combined with the lower spatial resolution of the fMRI, contributes to the mismatch between fMRI and DCS. [138,139] Although, in our study an estimated location with BOLD activation was used to inform the surgeon about the language function influencing the likelihood of repeating the same electrical stimulus again.

For language fMRI mapping a variety of paradigms are sensitive to either more expressive or receptive aspects of language.[124,136] However, these paradigms are not classically used intraoperatively in awake craniotomy because their complexity hinders the patient's collaboration, and due to technical difficulties in the synchronization of the DCS and the presentation of the linguistic task.[136] Despite this, an increasing number of paradigms are being reported as useful for mapping cognitive functions in awake craniotomy.[140-141] In order to decrease the influence of the mismatch between linguistic paradigms used during fMRI and DCS, we computed fMRI probabilistic maps considering brain regions activated by three paradigms. We believed that this method based on the knowledge that some paradigms (i.e. VGt) should activate both expressive and receptive brain regions, could reinforce the relevance of the task design regardless of the type of stimuli. [124,130] However, qualitative differences within language function mapping between fMRI and DCS were found (fig. 6.3) and a higher correspondence of cortical brain regions was reported when using the same paradigms.[136]

Regarding the fMRI acquisition scans, when designing the motor task, we considered that head motion could induce spatial distortions with mouth movements. [138,139] Thus, a stable placement of the head was ensured, and head motion correction was applied in imaging preprocessing to minimize this source of error. In fact, the mapped cortical brain regions for motor function were observed to be similar (figure 6.3) between both CM modalities, as supported by other studies.[133]

In the preprocessing steps, smoothing was applied using a Gaussian filter with a FWHM of 7 mm to reduce noise and increase sensitivity; this could also have contributed to the displacement of the signal depicted by the BOLD sequence.[142] To minimize this error, Strappini and colleagues (2017) [143] reported that using a Gaussian process with voxel-by-voxel smoothing lead to minimal data displacement.

Co-registration to anatomical images showed an accuracy from 1.8 mm to 5 mm based on the same methodology used and reported by others.[144,145] Moreover, surgical drapes, craniotomy, retractors, and increased duration of awake craniotomy are known factors for loss of navigation accuracy.[142] Preventive actions such as the use of bone markers with a second registration before CM were not applied. Yet, CM was performed readily after craniotomy without parenchymal brain interventions and the stability of navigation components was ensured. Additionally, we also considered a 2-mm radius around the pointer coordinates to establish the correspondence between fMRI and DCS. In fact, correspondence in language mapping modalities was similar to those previously reported.[133]

2. Tumor location, grade and neurological involvement

Gliomas tend to infiltrate the surrounding parenchyma and to migrate across the brain. Thus, an a hodotopy approach by surgeons lead to a wider search for impaired neurological functions intraoperatively. Furthermore, about one third of each patient's group presented high grade tumors which develop rapidly, increasing the risk of seizures[118] and resulting in higher neurological morbidity.[115]

In the mCM group, four patients showed a lower performance in presurgical language tests and in this group CM total duration was smaller than in the eCM group. We hypothesize that this result was due to the surgeon's decision to proceed with the tumor resection having into account the systematic errors in language tasks instead of doing a more efficient CM with nfMRI's assistance. Moreover, a comparison between lower performance patients enrolled to eCM was not performed. In fact, during CM, after identification of errors in language tasks without applying DCS, the patients were engaged into spontaneous conversation for language function mapping. This task demands a lower cognitive load, which was not evaluated in fMRI paradigms, and lower stimulus-language task synchronization, explaining the surgeon's decision to stop the CM with DCS. Additionally, the surgeon focused more in negative cortical regions after DCS than in positive nfMRI regions probably because of an unconscious preference for DCS (i.e. gold standard method) for brain eloquent function mapping.[73,103] Patients with lower performance in presurgical neuropsychological language tests also showed rejected test blocks during fMRI data

acquisition in language paradigms (*ad hoc* analysis not quantified in results). These less reliable fMRI data contributed to the lack of confidence in positive brain regions. Moreover, because these evaluations were done within two weeks before the surgery, performance in fMRI was qualitatively similar to neuropsychological.

We subdivided presurgical language tests performance arbitrarily considering a lower performance if in at least one test more than 20% of answers were given incorrectly. In these patients, a maintained clinical aphasia was not present, despite systematic language errors during neuropsychological tests. The evaluation of the patient's aptitude to collaborate intraoperatively (i.e. deciding if the cognitive impairment is evaluated during surgery) is crucial and based on a subjective clinical decision. Intraoperative communication was therefore reported as the main challenge in awake craniotomy failure leading to higher disease progression.[146] Despite three patients having aggravated language neurological status after surgery, only one showed a lower performance in neuropsychological evaluation and had a higher-grade tumor (patient 5). Also, the postoperative outcomes were not worse in mCM than for the control group. In any case, further criteria should be investigated to define patient's aptitude to communicate intraoperatively.

Presurgical fMRI language cortical mapping is used worldwide to avoid additional neurological morbidity.[121] Regarding language mapping lateralization with fMRI, consistent results were obtained. These were supported by DCS' failure to evoke language disturbances due to right hemisphere dominance (patient 11) and neuroplasticity processes with bilateral hemisphere activation (patient 8).
The DCS was helpful to identify motor function in all patients and language function in 84% of the patients. Even in those with bilateral and right hemisphere language processing, DCS evoked anarthria when applied to the ventral precentral gyri (i.e. motor language pathways) during the counting task. Analysis of motor function showed that it was consistently mapped by nfMRI and DCS with higher rate of concordance as expected.[16, 133]

Language mapping by DCS showed predominance for the inferior frontal gyri in comparison to superior temporal gyri, yet with smaller prevalence in comparison with nfMRI results (fig.6 3). The predominance of evoked language disturbances after frontal lobe DCS is explained by a higher neurological morbidity due to tumor location in the majority of the patients. Further involvement of the parenchyma increased the intensity needed to evoke a language disturbance.[73] Additionally, tumor location led to the surgeon's tendency to deliver more stimuli in regions around the tumor to define the resection boundaries.

Correspondence analysis within CM techniques of language function was 84% for the inferior frontal gyri and 70% for the superior temporal gyri, similar to those reported in the literature.[133,147] Lower correspondence was seen in areas mapped with verbal language tasks addressed in fMRI (i.e. such as the posterior middle frontal gyri) and not intraoperatively. Moreover, when using a fixed threshold to construct activation maps in fMRI, tumor malignancy and angiogenesis could impose decreased BOLD contrast through higher local cerebral blood.[45,125,135] In fact, brain tumor resection guided by indirect localization of active brain regions has been associated with mislocalization of functional brain areas additionally to the drawbacks discussed above.[138,139]

3. Limitations

In our study, DCS was used as a gold standard technique for language cortical surface function identification. Despite showing a high specificity and enhancing causality between cortical electrical testing and language disruption, the sensitivity of this method remains difficult to appraise.[137] Moreover, despite our effort to control spatial resolution and increase specificity of fMRI language CM using multi-task language tests, intraoperative neurophysiological language tests was not the same as done during fMRI.

At a deeper level, the mismatch between fMRI and DCS can also be derived from the violation of assumptions behind the BOLD signal. The contrast of fMRI data is based on the neurovascular coupling, instead of electrophysiological gray matter activation. This provides us with only an indirect measure of brain activity. In the case of brain tumor, the neurovascular coupling is impaired in tissues adjacent to the tumor, leading to a loss of task-related contrast. In addition, the co-registration of BOLD activation into high-resolution anatomical scans and into navigation system impose further activation dislocation. In our study, the randomization process of patients could also have suffered from some unbalanced distribution bias because of the small number of patients recruited for each group. This led to a small number of low and high-grade malignancy tumors with different cognitive reserve reflected in neurophysiological language tests performance.

Conclusion

In summary, CM with additional intraoperative information of motor and language tasks data acquired with fMRI did not influence the practical aspects of DCS in presurgical planning. Patients with lower performance in neuropsychological language tests, on the other hand, showed smaller CM duration with nfMRI due to inaptitude to communicate during awake craniotomy

This page was intentionally leftt blank

CHAPTER VII

UNDERSTANDING LANGUAGE NETWORK REORGANIZATION AFTER GLIOMA REGROWTH: COMPARING CONNECTIVITY MEASURES FROM FMRI TO DCS

Introduction

Brain plasticity allows eloquent functions to migrate or be extended to other brain regions during an indolent pathological process such as PBT.[148] Connectome analysis may provide insights about reduction in local and long-range connectivity depending on lesion location.[149] Connectivity analysis may be performed using a variety of tools. Node-based methods investigate connections between functional regions and may provide indirect measures about their "relationship" (i.e. graph based theory).[150] Although, their clinical interpretation remains to be studied in presurgical planning. Further understanding of such measures could for instance show brain regions role in eloquent function network within the presence of pathology, helping to avoid permanent neurological damage.[149]

Our hypothesis was that task-specific fMRI-based connectivity analysis provides insight about the role of a specific brain region (in this case, language-related areas) within networks distorted by a PTB. This knowledge could i) guide the surgeon on how to disrupt its function by DCS and ii) help to predict language network reorganization over time until tumor regrowth. Our aim was to analyze task specific connectivity measures in presurgical planning in patients with low grade glioma.

Methods

We recruited three patients from Hospital Garcia Orta between 2016 and 2018 to undergo awake resection of brain tumor involving frontal, temporal and insular regions (table 7.1). Patients selection was done using the same criteria of the previous chapter. Briefly, patients with occupying brain lesions within or near (i.e. 2 cm) classical brain language regions or pathways and, absence of aphasia (evaluated by neuropsychological language tests) were chosen. The Ethics committee of our institution gave its approval for conducting this work and informed consent was obtained from all participants.

1. *Clinical evaluation*

Neurological examinations were carried out preoperatively, in the intermediate post-operative period and every 3 months until tumor regrowth. We performed a battery of neuropsychological and cognitive tests, and assessed language function with a PNt and NVSDt adapted to the Portuguese population.[127] The selected language tests were done before surgical treatment, during awake craniotomy, before hospital discharge (until five to seven days after surgery) and approximately 3 months after surgery.

2. *Mapping during surgical procedure*

Intraoperative mapping was performed by direct cortical and subcortical stimulation (Inomed Medizintechnik, ISIS IOM System, Germany) for the detection and preservation of eloquent areas during awake craniotomy resection. The methodology used was the same as described in the previous chapter and in more detail in chapter III. Additionally, to the bipolar stimulation for language function mapping, we also mapped motor function with a monopolar probe and using a multipulse technique (5 trains of 500ms duration with 250-500Hz, 1-30 mA). Before resection, the following cortical regions were mapped with the patient awake: opIFG, orbitalis part of the inferior frontal gyrus (orbIFG), triangularis part of the inferior frontal gyrus (trIFG), precentral gyrus (PrG), postcentral gyrus (PoG), superior temporal gyrus (STG), middle temporal gyrus (MTG) and supramarginal gyrus (SMG).

After defining each patient threshold of action, PNt and NVDt were carried out while DCS was applied to define positive and negative brain regions for language function. In addition, cortical and subcortical stimulation was performed during tumor resection to preserve language axonal pathways. Cortical gyri were also assessed using neuroanatomical landmarks and magnetic resonance imaging (MRI) scans using a navigated system (Stealth, Medtronic, USA).

3. *MRI data acquisition and pre-processing*

MRI examinations were performed at 2 different time points: 1) in presurgical planning and 2) after tumor regrowth. After surgical resection, structural MRI was repeated every 3 to 6 months or if patients showed new neurological symptoms.

A 3T Philips MRI scanner (Philips Medical Systems, USA) with an 8-channel head receiver coil was used. The scanning protocol was described in the chapter II and recalled to memory in previous chapter. Functional MRI based on BOLD contrast was acquired during a language and a motor task. The language tasks used during MRI acquisition were VSDt written in a 160-block

design structure. As a rest condition, was used the same high-level task, already described, where the participant has to perform a symbol search task. The motor task used consisted in opening and closing the mouth (i.e motor mouth task – MMT) was compared against rest and also written in a block design with a total of 80 volumes.

Table 7.1 – Patients, tumor characteristics and clinical performance at language tests before and after treatment.

Pt	Gender	Age	1st symptom	Location	Histology	RE (month)	Tumor volume (cm^3)			NVSDt/55*			PNt/80*		
							Pre	Post 3m	RE	Pre	Post 3m	RE	Pre	Post 3m	RE
1	Female	38	Seizures	T; P; I	A II	8	16.7	3.3	4.5	54	55	54	75	76	75
2	Male	32	Headache	F	OD	19	4.3	0	1.1	55	55	54	72	72	74
3	Male	30	Seizure	F	OA II	45	42.6	2.1	4.9	54	**	**	78	**	**

A – Astrocytoma, F – Frontal lobe. I – Insula lobe.; OA – Oligoastrocytoma; OD – Oligodendroglioma; P – Parietal lobe; PNt – Picture Naming tast; Pre – preoperative evaluation; Post3m – Post-operative evaluation 3 months after surgery. NVSDt Non-verbal Semantic Decision task. RE – tumor Regrowth. * no data available due to patient performance. T – Temporal lobe.

For fMRI data, pre-processing was made using BrainVoyager (v.2.8; Brain Innovation, Maastricht, The Netherlands)[47] (see chapter II). The results of one task were used to calculate activation maps using the false discovery rate with an alpha of 0.05.

For connectivity analysis, MRI scans were processed using the MIBCA toolbox.[48] Pipeline and images preprocessing was described in chapter II. Briefly, in the T1-weighted images, non-brain structures were removed using FSL[55] and spatial alignment to a standard space was performed using Freesurfer *recon-all* function,[56] generating transformation matrices. These matrices were used to transpose the analyzed gyrus as a ROI into the fMRI space. After non-linearly data registration, the brain was segmented using the Harvard-Oxford brain atlas. Consequently, fMRI data preprocessing was corrected for motion and slice-timing using Fourier-space time-series phase-shifting. For such imagens, non-brain removal, spatial smoothing (Gaussian kernel with FWHM of 8mm), 4D data intensity normalization, high pass temporal filtering was made. After extraction of functional time series data from each ROI, statistical processing was made by calculating Pearson correlation between each ROI, organized into a matrix for each patient. Using each patient matrix, mean of preselected graph theory metrics were calculated using a third-party Brain connectivity toolbox.[8]

The connectivity metrics extracted were the following: node degree, betweenness centrality, participation and clustering coefficient (see chapter II to further description) were extracted from thirty brain atlas-based regions (i.e. fifteen at each hemisphere).[57] Connectivity metrics were defined as: Node degree – number of links connected to a brain region; Betweenness centrality

– fraction of all shortest paths in the network that pass a given brain region; Participation coefficient – diversity of intermodular interconnections of individual regions; Clustering coefficient – fraction of triangles around an individual brain region.[21]

These metrics were extracted from some ROI (i.e brain regions). We analyzed the connectivity at opIFG, PrG, PoG during MMT. For language function mapping, we analyzed classical anterior and posterior involved brain regions. Therefore, were extracted from opIFG, orIFG, trIFG, insula (i.e considered as anterior language brain regions) and, PoG, STG, MTG, SMG, PoG (i.e posterior) during VSDt.

4. Data reduction and analysis

Normality of data was tested with the Shapiro-Wilk test using SPSS Statistics (v24, IBM, USA). Non-parametric t-test was used to evaluate differences between connectivity measures between anterior vs. posterior brain cortical regions involved in language. Because connectivity data were obtained with the same stimulus in the same individual, we also used paired t-tests for statistical comparison for anterior vs. posterior language involved regions, and left vs. right hemisphere between preoperative and after regrowth fMRI. Because same node comparisons were made multiples times, was not performed correction for multiple comparisons. In contrast, a smaller p-value of 0.03 was considered statistically significant to balance his uncorrection.

Results

1. Clinical evaluation

Demographic and tumor characteristics are showed in table 7.1 and figure 7.1, respectively. Two patients suffered seizures as an inaugural clinical manifestation of the tumor. Neurological examination, non-verbal association task and PN were normal at onset in patients 1 and 2. Patient 3 showed a mild paresis of right arm and face. At discharge from hospital, patient 1 showed right hand paresthesia, patient 2 mild difficulties in repeating sentences and patient 3 right arm paresis and anomic aphasia. After surgical treatment, patient 1 was left with a residual tumor. Tumor volume resection was 81%, 100% and 96% in patients 1, 2, and 3, respectively. All patients performed at least 6 cycles of chemotherapy and 3 months of speech therapy.

At the 3 to 6 months evaluation, only patient 3 maintained a mild anomic aphasia and mild paresis in the right hand. Patients received a second surgical procedure, due to a residual tumor (patient 1) or due to tumor recurrence. All patients' tumor re-growths were detected by repeated MRI scans.

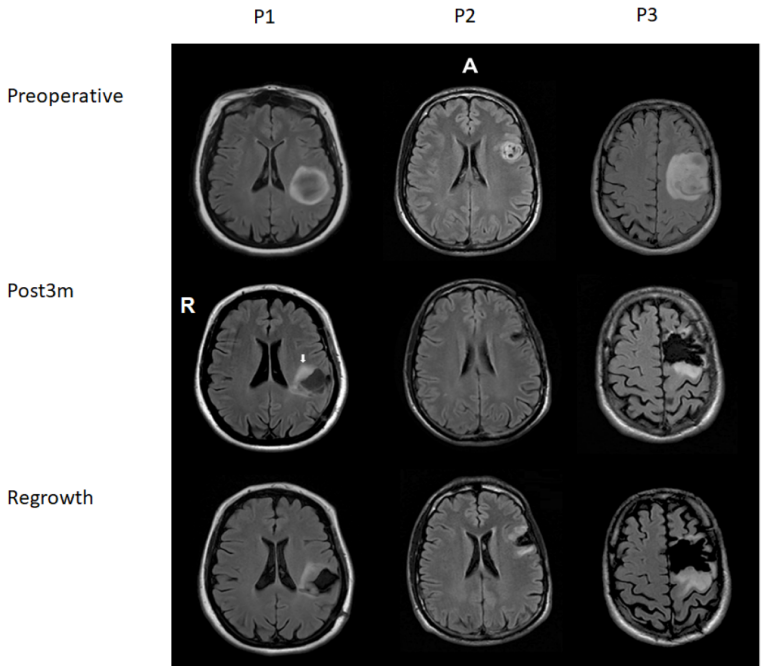

Figure 7.1 – Anatomical magnetic resonance T2 weighted fluid attenuated inversion recovery images of patients (P1-3) at preoperative, 3 months post-surgical treatment (Post3m) and after glioma regrowth. Note the residual tumor in patient 1 (arrow).

2. *Functional MRI, connectivity measures and cortical mapping.*

All patients were right handed (table 7.1) and language was lateralized at the left hemisphere (figure 7.2). Connectivity measures were extracted from fMRI during MMT (table 7.2) and during VSDt (table 7.3 to 7.5 of appendix).

Patient 1 – MMT activated the PrG bilaterally with less intensity at the left hemisphere due to tumor proximity and increased tumor vascularity (i.e around 1 cm anteriorly). Intraoperatively, we evoked a motor potential of the mentalis muscle with DCS using an intensity of 13 mA. At the subcortical level, the pyramidal tract was mapped by recording the abductor pollicis muscle at the posterior tumor boundary using 5 mA. In interruption of counting task, was induced with bipolar stimulation in PrG using an intensity of 4mA. Functional MRI showed similar brain regions activation during MMT in both moments (figure 7.2). Node degree showed a tendency to decrease from 53±2 to 42±3 ($p=0.05$) with a decrease of 11±5.

VSDt activated predominantly the left hemispherical IFG, PrG, and STG. Intraoperatively, we evoked anomia with bipolar DCS of the triIFG and opIFG using an intensity of 3.5 mA. We also evoked paraphasias by stimulating the temporal lobe. At subcortical level, language was disrupted

at medial tumor boundary. Functional MRI was repeated around 8 months later. No differences were identified in connectivity measures between anterior (IGF; Insula; PrG) and posterior language regions. However, a significant increase was verified in participation coefficient at right hemisphere from 0.63±0.08 to 0.72±0.04 (p=0.03); with an increase of 0.09±0.04.

Patient 2 – MMT activated the PrG close to tumor location, approximately 1.5 cm away. Intraoperatively, we evoked a motor potential in the abductor pollicis muscle with DCS at 11 mA and an interruption during counting task with bipolar DCS of the PrG at 4 mA. Connectivity metrics did not show differences after tumor recurrence. Functional MRI during VSDt activated IFG at the left hemisphere which correlated with intraoperatively response elicited with bipolar DCS with 4 mA. We did not evoke language disturbances with DCS of the parietal and temporal lobes. After tumor recurrence, fMRI showed additional activations in the STG and MTG.

Connectivity metrics of cortical language areas showed no differences between anterior (IFG; PrG) and posterior (PoG; SMP, STG, MTG) sites in the left hemisphere. However, after tumor recurrence, node degree of anterior brain regions showed a statistically significant decrease of 23±10 (from 71±3 to 48±7; p=0.01). A betweenness centrality increase of 87 ± 42 (from 94 ± 15 to 182 ± 38; p=0.02) and participation coefficient of 0.12 ± 0.08 (from 0.57±0.09 to 0.68±0.06; p=0.01) was also observed at posterior brain regions.

Patient 3 - During MMT, intraoperative stimulation of the PrG immediately posteriorly to the tumor elicited a motor potential in the right mentalis muscle using an intensity of 14 mA. The counting task was also disrupted with bipolar DCS using an intensity of 3 mA. At the subcortical level, the pyramidal tract was mapped at the posterior tumor boundary and evoked motor potentials of the mentalis and hand muscles were also obtained using stimulus intensities of 3 mA and 9 mA, respectively. After tumor recurrence, there was a significant decrease in the participation coefficient in left hemisphere of 0.12±0.01, (from 0.77±0.01 to 0.65±0.02; p=0.01).

Language assessment with fMRI showed activation of the IFG, PrG, STG and MTG (not shown in figure 7.2). With DCS, we evoked anomia at the IFG and paraphasias at the SMG and STG using an intensity of 3 mA. Medial tumor boundary stimulation also evoked an interruption of VSDt. After tumor recurrence, a greater intensity was seen in STG and MTG during VSDt in comparison to fMRI at preoperative stage. No significant differences were detected in connectivity metrics.

Table 7.2 – Mean connectivity measures of opercular, precentral and postcentral gyrus extracted from patients functional magnetic resonance at presurgical planning (PRE) and after tumor regrowth (RE) during motor mouth movement.

Metrics	Pt.1		Pt.2		Pt.3	
	PRE	RE	PRE	RE	PRE	RE
Node degree	53 (1)	41 (2)	51 (17)	49 (10)	39 (4)	48 (18)
Cluster Coefficient	0.07 (0.01)	0.08 (0.001)	0.07 (0.02)	0.08 (0.02)	0.06 (0.004)	0.07 (0.01)
Betweenness Centrality	93 (29)	21 (2)	76 (5)	169 (98)	127 (74)	102 (67)
Participation Coefficient	0.66 (0.03)	0.68 (0.01)	0.73 (0.06)	0.61(0.14)	0.76 (0.003)	0.06 (0.01)

Discussion

Brain networks are complex and different types of connectivity can be characterized.[149,150] Our work evaluated the use of connectivity measures for tumor pre-surgical planning and after tumor regrowth using a simplified protocol (i.e. only using one and task-specific fMRI). After brain parcellation, we looked for brain regions (i.e. nodes) involved in motor and language tasks and compared them with clinical evaluation, fMRI BOLD activated regions and evoked responses by DCS.

The studied young adult patients presented low grade gliomas and minor neurological impairment despite the tumors' proximity to motor and language brain regions. In pre-surgical planning, motor and language involved regions were mapped with fMRI, as expected, predominantly in the left hemisphere PrG, and in the IFG and temporal lobe, respectively. [122,133]

1. Assessment of motor function

The motor brain region mapped by fMRI correlated with the presence of a motor evoked potential (facial or hand muscle) at anatomical PrG. Lower intensity was used to subcortically evoke a muscle response (i.e. posterior tumor boundary) in patient 3 in comparison to patient 1 (3mA vs 5mA, respectively) leading to lesion of pyramidal tract and right arm paresis during tumor resection. The deficit in patient 3 can be explained due the fact that when performing subcortical stimulation, lower intensity relates to shorter distance between the probe and pyramidal fibers.[151]

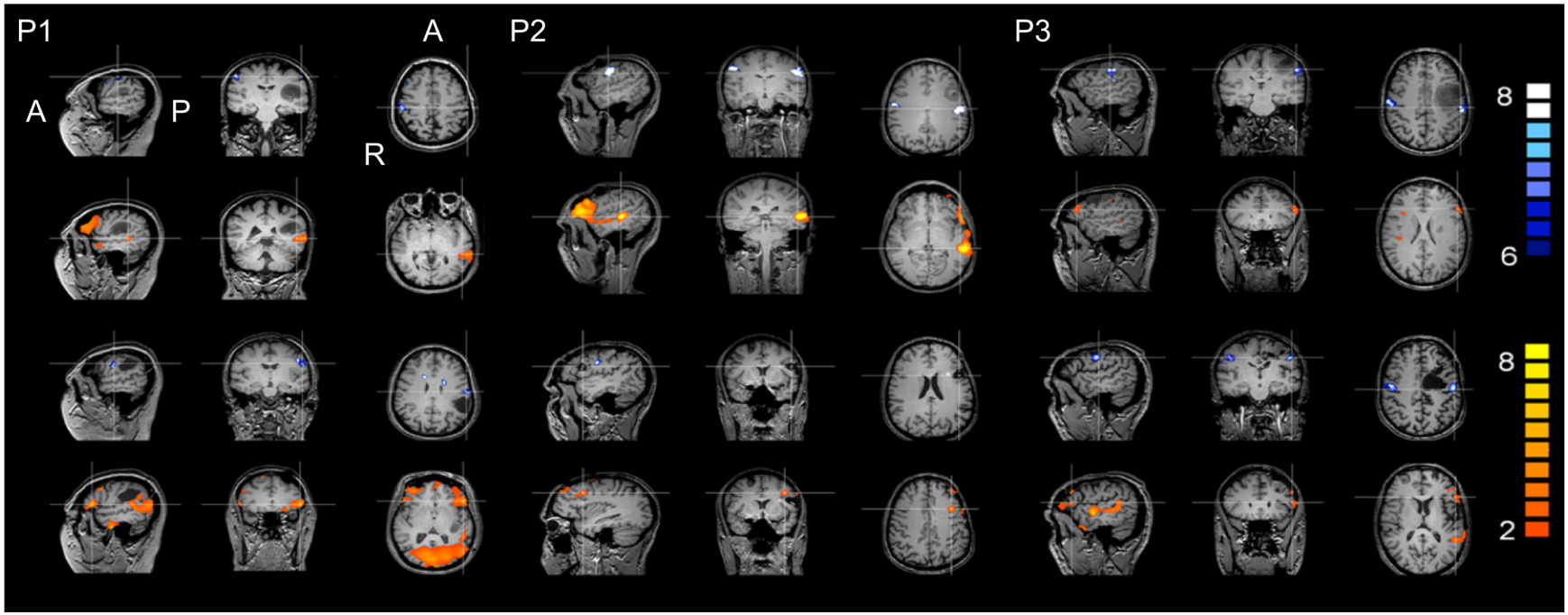

Figure 7.2 - Functional magnetic resonance imaging activation regions (identified using T2*-weighted scans using the blood oxygen level dependent contrast) overlaid on anatomical T1-weighted images performed for pre-surgical planning in patients (first two rows) and after tumor regrowth (bottom two rows). Stimuli included mouth movement task (blue) and performing verbal semantic decision task (orange). fMRI results obtained following tumor regrowth are displayed at the bottom row for each task. A – Anterior; COR – Coronal slice view; P1-3 Patients 1 to 3; R – Right side.

After tumor regrowth, patient 1 showed a smaller node degree (i.e. number of connections) but did not have a permanent motor deficit. Although in contrast, patient 3 showed paresis of the hand 6 months after surgery and presented a participation coefficient significantly reduced. Participation coefficient assesses the diversity of intermodular interconnections of individual nodes and their decrease seem to support a less effective network during a motor task. In fMRI a discrepancy between preoperative and after tumor regrowth functional scans was not evident (figure 7.2). In patient 3, motor deficit probably occurred due to direct lesion of pyramidal tract during resection, instead of only to supplementary motor area.[152]

2. Assessment of language function

Brain language mapping in pre-surgical planning intends to reduce language morbidity post-operatively by identification of eloquent areas through fMRI and their anatomical connection through tractography.[153] However, a better understanding of the brain language regions within the activated network would be desirable. Our fMRI connectivity analysis identified three different reorganization processes after tumor regrowth (figure 7.2): a homologue contralateral (patient 1), ipsilateral temporal lobe (patient 2) and absence of compensation (patient 3) as described in more details below. We advocate that this knowledge can help to predict language functional reorganization considering that gliomas tend to recur.

fMRI activated regions during language task correlated overall well with bipolar DCS. Only in patient 2, DCS missed to evoke language disturbances in the temporal lobe. This mismatch between DCS and fMRI can be explained by different semantic tasks used during clinical and fMRI protocols as discussed in the previous chapter. In our study, a NVSDt was used in operative room to allow higher collaboration by patients in awake state during surgery.

Patient 1 showed some language deficits after surgery despite his full recovery after 3 months. Therefore, we investigated whether preoperative connectivity measures in comparison with after tumor regrowth could indicate a language network compensation. Preoperative mean measures did not differ between anterior and posterior analyzed brain regions. An absence of predominant anterior or posterior language function brain regions with higher right hemisphere activation seemed to support an interhemispheric compensation.

Patient 2 did not present language morbidity after surgery. Lower node degree values were denoted between both fMRI probably due to the tumors' proximity to IFG. However, in contrast to patient 1, a higher participation coefficient and betweenness centrality were denoted in posteriorly involved brain regions instead of right hemisphere. Communication between brain

regions likely occurs in parallel duplication (during a task) not only are direct and efficient connections established, but also indirect and less efficient ones. Betweenness centrality, represents the fraction of all shortest paths that pass through a node and therefore the direct paths in a specific task.[154] We advocate that homolateral reorganization can first be attempted[155] regarding inter-hemispheric compensation.[156] In patient 2, an absence of language deficit correlated with a higher participation coefficient and betweeness centrality supporting a more effective network with predominant ipsilateral reorganization.

In this study, only patient 3 showed anomic aphasia after surgical treatment. This clinical deficit may be explained by lesion of the arcuate fascicle identified by DCS at the medial tumor boundary. We did not address structural connectivity, which could have confirmed this hypothesis. This limitation occurred due to lack a standard protocol for MRI scans acquisition scans at preoperative stage. Functional connectivity analysis led us to hypothesize that, due to the arcuate fascicle lesion, the reduced links between language involved regions decreased the capacity of ipsilateral compensation pattern. Additionally, a non-significant increase of betweenness centrality occurred in the right hemispherical IFG (see appendix) supporting a non-compensated language function, which correlated with moderate anomic aphasia three years after surgery.

3. Limitations

In addition to the small sample size, our study lacks fMRI data from healthy subjects to understand the connectivity measures and to establish normal mean values during motor and language tasks. Also, it is important to bear in mind that interindividual variability of language brain regions activation[9] and tumor characteristics (i.e. location, malignancy) could partially confound the data comparison and its interpretation. Including structural connectivity into the analysis would have been desirable, moreover when tractography results could have helped perceive fascicular damage in patient 3. In these patient, corticospinal tractography could help to identify fibers tracts in posterior tumor boundary at preoperative stage. Non-verbal and verbal semantic tasks were used in clinical and fMRI evaluation, respectively. The activation of brain regions during both tasks can differ,[151] misleading data interpretation and correlation between DCS and fMRI. In fact, in patient 2, DCS do not evoked language disturbances when applied at temporal lobe as suggested by the preoperative fMRI. In spite of, fMRI multiple language tasks be preferred to identify language hemispherical dominance in presurgical planning,[157] may not provide greater correspondence between DCS and nfMRI when performing multimodal CM (see previous chapter).

Conclusion

In this study three adult patients with low grade gliomas were recruited to perform fMRI preoperatively and after tumor regrowth, aiming to relate task functional connectivity measures to motor and language brain reorganization. When compared to standard fMRI, changes in participation coefficient and betweenness centrality of nodes in the functional network contributed to a better understanding of the reorganization of function, which can be used to help preoperative planning.

Appendix

Table 7.3 – Functional connectivity measures of patient 1 extracted from functional magnetic resonance during verbal semantic decision task at presurgical planning (PRE) and after tumor regrowth (RE). Standard deviation (SD) was shown between parenthesis.

PRE	**Hemisphere**	**OpIGF**	**OrbIGF**	**TriIGF**	**Insula**	**PrG**	**PoG**	**SMG**	**STG**	**SMG**	**Mean (SD)**
Node degree	Left	47	76	60	85	71	74	69	78	83	71 (12)
	Right	61	76	76	62	36	76	76	86	89	71 (16)
Cluster Coefficient	Left	0.06	0.09	0.07	0.11	0.09	0.02	0.09	0.10	0.11	0.08 (0.01)
	Right	0.08	0.08	0.08	0.08	0.07	0.08	0.10	0.10	0.10	0.08 (0.01)
Betweenness Centrality	Left	74	250	60	24	64	86	18	54	50	75 (69)
	Right	110	108	128	128	78	106	70	26	36	87 (38)
Participation Coefficient	Left	0.72	0.70	0.651	0.63	0.63	0.71	0.59	0.67	0.70	0.66 (0.04)
	Right	0.51	0.70	0.577	0.61	0.52	0.67	0.70	0.73	0.70	0.63 (0.08)
RE											
Node degree	Left	78	60	83	63	54	75	56	85	76	70 (18)
	Right	49	63	52	61	61	43	81	83	82	64 (15)
Cluster Coefficient	Left	0.10	0.09	0.09	0.07	0.80	0.09	0.08	0.11	0.11	0.17 (0.23)
	Right	0.06	0.08	0.06	0.09	0.10	0.06	0.07	0.12	0.11	0.08 (0.02)
Betweenness Centrality	Left	98	78	86	58	134	194	62	38	24	86 (52)
	Right	168	192	206	66	54	282	106	46	82	134 (82)
Participation Coefficient	Left	0.63	0.52	0.63	0.66	0.70	0.67	0.70	0.67	0.63	0.64 (0.05)
	Right	0.73	0.78	0.79	0.71	0.73	0.70	0.63	0.74	0.72	0.72 (0.04)

MTG - Middle temporal gyrus; opIFG - Opercular part of inferior frontal gyrus; orIFG - Orbicular part of inferior frontal gyrus; PoG - Poscentral gyrus; PrG - Precentral gyrus; SMG - Supramarginal gyrus; STG - Superior temporal gyrus; trIFG Triangulis part of inferior frontal gyrus

Table 7.4 –Connectivity measures of patient 2) extracted from functional magnetic resonance at the verbal semantic decision task at presurgical planning (PRE) and after tumor regrowth (RE). Standard deviation (SD) was shown between parenthesis.

PRE	**Hemisphere**	**OpIGF**	**OrbIGF**	**TriIGF**	**Insula**	**PrG**	**PoG**	**SMG**	**STG**	**SMG**	**Mean (SD)**
Node degree	Left	68	74	72	80	69	65	59	38	67	66 (12)
	Right	49	50	49	69	53	55	59	69	67	58 (9)
Cluster Coefficient	Left	0.06	0.07	0.06	0.06	0.07	0.05	0.06	0.05	0,.5	0.06 (0.01)
	Right	0.04	0.05	0.06	0.08	0.05	0.07	0.07	0.09	0.07	0.07 (0.01)
Betweenness Centrality	Left	94	150	126	64	110	110	88	76	104	102 (26)
	Right	82	138	80	66	176	78	102	50	85	95 (39)
Participation Coefficient	Left	0.75	0.61	0.79	0.74	0.75	0.79	0.78	0.48	0.72	0.71 (0.10)
	Right	0.66	0.63	0.53	0.59	0.70	0.54	0.59	0.42	0.46	0.56 (0.09)
RE											
Node degree	Left	47	38	49	65	56	43	61	51	41	50 (9)
	Right	56	47	51	64	49	40	44	43	53	50 (7)
Cluster Coefficient	Left	0.05	0.04	0.5	0.04	0.06	0.03	0.05	0.04	0.04	0.04 (0.08)
	Right	0.05	0.04	0.05	0.05	0.08	0.04	0.05	0.03	0.04	0.05 (0.01)
Betweenness Centrality	Left	38	148	12	296	296	196	130	220	182	169 (100)
	Right	70	98	56	98	72	82	38	142	76	81 (30)
Participation Coefficient	Left	0.61	068	0.68	0.51	0.69	0.75	0.61	0.61	0.72	0.65 (0.07)
	Right	0.68	0.74	0.63	0.59	0.70	0.78	0.66	0.68	0.76	0.68 (0.05)

MTG - Middle temporal gyrus; opIFG - Opercular part of inferior frontal gyrus; orIFG - Orbicular part of inferior frontal gyrus; PoG - Poscentral gyrus; PrG - Precentral gyrus; SMG - Supramarginal gyrus; STG - Superior temporal gyrus; trIFG Triangulis part of inferior frontal gyrus

Table 7.5 – Patient 3 connectivity measures extracted functional magnetic resonance imaging during verbal semantic decision task at presurgical planning (PRE) and after tumor regrowth (RE). Standard deviation (SD) was shown between parenthesis.

PRE	**Hemisphere**	**OpIGF**	**OrbIGF**	**TriIGF**	**Insula**	**PrG**	**PoG**	**SMG**	**STG**	**SMG**	**Mean(SD)**
Node degree	Left	75	66	52	65	72	40	62	64	75	63 (11)
	Right	71	48	60	61	74	71	37	69	73	55 (12)
Cluster Coefficient	Left	0.07	0.06	0.04	0.06	0.08	0.06	0.07	0.06	0.07	0.06 (0.01)
	Right	0.09	0.05	0.07	0.08	0.08	0.08	0.04	0.05	0.08	0.07 (0.01)
Betweenness Centrality	Left	30	150	404	162	42	78	88	144	98	133 (112)
	Right	94	124	34	20	50	26	232	136	112	89 (68)
Participation Coefficient	Left	0.70	0.53	0.71	0.63	0.64	0.66	0.75	0.67	0.53	0.67 (0.07)
	Right	0.71	0.59	0.71	0.73	0.65	0.65	0.62	0.67	0.53	0.64 (0.08)
RE											
Node degree	Left	81	57	70	76	52	70	64	66	60	64 (12)
	Right	64	58	60	46	57	51	51	79	64	57 (10)
Cluster Coefficient	Left	0.10	0.07	0.09	0.10	0.05	0.05	0.88	0.05	0.07	0.07 (0.02)
	Right	0.06	0.08	0.06	0.06	0.06	0.06	0.05	0.06	0.08	0.05 (0.01)
Betweenness Centrality	Left	72	242	16	18	312	88	88	52	28	119 (103)
	Right	50	52	178	124	116	234	322	176	66	147 (90)
Participation Coefficient	Left	0.68	0.62	0.70	0.71	0.60	0.75	0.63	0.78	0.67	0.68 (0.06)
	Right	0.71	0.60	0.59	0.52	0.54	0.50	0.57	0.80	0.65	0.62 (0.10)

MTG - Middle temporal gyrus; opIFG - Opercular part of inferior frontal gyrus; orIFG - Orbicular part of inferior frontal gyrus; PoG - Poscentral gyrus; PrG - Precentral gyrus; SMG - Supramarginal gyrus; STG - Superior temporal gyrus; trIFG Triangulis part of inferior frontal gyrus

CHAPTER VIII

GRAPH TEORY ANALYSIS OF CORTICAL BRAIN REGIONS WITH LANGUAGE FUNCTION

Introduction

Brain cognitive processing depends on interactions among distributed neuronal populations and brain regions.[159] Advances in neuroimaging allowed to characterize and quantify comprehensive whole brain maps of structural and functional connections involved in cognitive functions.[160] Such maps are based on exploratory multivariate statistical techniques or multivariate pattern analysis and aim to localize brain regions that are differentially activated across tasks.[159] This (connectivity) data can be rendered in the form of a network, describing brain systems as sets of neural elements and their interconnections.[17] Related to this, the eloquent brain region for a specific cognitive task can influence/be modulated by a whole network of regions involved in this type of task.[161] Therefore, focal lesions may result in unexpected or widespread deficits that are not predicted by the local functional properties of the region.[162] In spite of this, to avoid further neurological deficits, surgeons still rely on intraoperative electrostimulation (i.e. DCS) and the most valuable technique for presurgical eloquent brain mapping still remains debatable.[161]

MRI offers the possibility to map anatomic connections (i.e. through DWI) within functional brain regions, firstly detected using the BOLD contrast occurred during a specific cognitive task. However, brain metabolism occurs continuously, even in the absence of a cognitive stimulus, when it is at "rest".[140,162-164]. In fact, spontaneous fluctuations of brain activity, with a low frequency signal between 0.01-0.08 Hz, have been shown by fMRI due to low concentration of deoxyhemoglobin during a resting state.[19,20] rs-fMRI at pre-surgical stage of neurooncological patients could be desirable because it offers the ability to map eloquent functions at primary cortices in populations not suited for task-based experiments.[165]

Recent reports explored the rs-fMRI prospects, firstly to compare accuracy to map primary cortices using DCS as gold standard technique[166-168], and secondly to identify effective connections that are less amenable to DCS.[140,164] In such studies, functional connectivity was investigated using either seed-based analysis or independent component analysis centering either in a correlation map within a ROI or searching for temporal and spatial characteristics underlying whole-brain components within a network, respectively. The use of the seed-to-voxel approach

(or seed correlation analysis – SCA) showed acceptable correlations with DCS for motor and language cortex mapping.[158,165] However, it could be desirable, at the presurgical stage, to have a better understanding of the role of a given brain region within the specific eloquent network. In fact, Alstott and colleagues used functional connectivity data (i.e. tractography and rs-fMRI) to evaluate the impact of virtually "erasing" specific and relevant brain regions within an eloquent network; this evoked a significant decrease in the network's global efficiency. Therefore, brain structure and functional connectivity, which is based on functional segregation and integration principles, may be studied through the application of graph theory. [159,164,169]

The graph theory based approach relies on the idea that brain macroscale networks are topologically organized in a non-trivial manner (e.g., small-world architecture and modular structure).[21] Thus, a highly effective cognitive network is characterized by a high clustering (i.e. number of connections) of brain regions, with short (communication) path length, creating modules (groups) of involved regions.[159] This complex network analysis provides insight into the relationship between brain structure and function as a capable way of transferring information at a low wiring cost.[62] Nonetheless, the ability to study whole-brain functional networks, networks within a restricted number of brain regions, local connectivity disturbance by focal lesions, and reliability of such metrics remains to be investigated.

PBT produces an initial local disruption of white and grey matter which, depending on the cancer cells malignancy, evolves more rapidly, causing neurological symptoms such as speech and language disturbances. Therefore, knowledge of topological small distance network robustness and brain regions participation to a language function could improve presurgical planning. With this information, the surgeon could anticipate each region's centrality (i.e. strength) for the language eloquent network before DCS mapping during awake craniotomy. This data provides a supplementary information to the task-specific activation maps, validating their clinical relevance. Additionally, it could help increase specificity of an activated brain region on task-specific BOLD fMRI by identifying the brain region's role.

In this context, the aims of this study were i) to identify the graph theoretical metrics (based on structural and functional connectivity data) of brain regions in which DCS evoked disturbances in motor and language tasks during awake craniotomy; ii) to identify the eloquent motor and language networks through a seed-based correlation analysis of the rs-fMRI data and iii) to interpret the identified network together with presurgical task-specific fMRI activation maps.

Methods

We retrospectively reviewed patients diagnosed in Hospital Garcia de Orta (Almada, Portugal) with PBT (BTS) between 2016 and 2018 who underwent awake craniotomy for tumor resection. The selection criteria for patient's enrolment were the following: lesions less than 20 mm apart from language brain regions or pathways as evaluated by presurgical MRI; absence of motor deficit or aphasia evaluated clinically and by neuropsychological language tests (i.e. patients were excluded given an error rate greater than 50% of the trials in any given test) and without cardiac pacemaker. In addition, for comparison purposes, data from patients with brain cavernomas subjets (BCS) were also reviewed. The selection criteria were the following: brain cavernomas more than 1 cm apart from the classical brain regions or white matter axonal fibers with language function, absence of clinical aphasia, singular brain cavernoma with a volume less than 2 cm^3. Data were acquired as part of the routine patients' workup and the Ethics Committee of the Hospital Garcia de Orta (Almada, Portugal) approved this study. In addition, subjects signed an informed consent prior to their inclusion in the study.

1. MRI data acquisition

Conventional MRI scans used to diagnose occupying brain lesions consisted of T1- and T2-weighted images combined with additional FLAIR and post gadolinium injection contrast (for further details review chapter II). Patients were then asked to undergo fMRI before awake craniotomy. Structural, DWI and rs-fMRI scans were acquired within two weeks before tumor surgical resection. Gradient echo sequences were used for volumetric T1-weighted images with a 3D resolution with 1×1×1 mm^3 voxel size and T2*-weighted contrast during a resting period of about 5 minutes (i.e. 150 volumes) with a 3×3× 3mm^3 voxel size with a gap of 3.5 mm between slices.

2. DCS mapping

Intraoperative mapping was performed as detailed in chapter III and the previous chapters. Briefly, after durotomy, the cortical surface was exposed and DCS was made by the same surgeon. A conventional bipolar probe with rounded tips 5 mm apart (continuous pulse with 1000 ms duration, 60 Hz, 1-5 mA) was used. Contralateral muscles EMG and phonation ACC was monitored during DCS CM. After identified the threshold of action, PNt and NVSDt was used in all patients while systematically stimulating throughout the exposed cortical surface. Intraoperative evaluation of patient function was made by a neuropsychologist blinded to stimulation. Sites of stimulation that elicited errors in the aforementioned tasks were tested three times for reproducibility and marked with tags. Stimulation points eliciting paraphasias, anomia and perseverations were classified as language stimulation points whereas complete anarthria

(speech arrest) was listed as motor rather than a language impairment. In addition, stimulations causing arrest of movement or involuntary movement were also considered as positive motor sites.

3. *DCS data registration on anatomical scans*

The data from positive cortical stimulation regions were manually defined in structural three-dimensional T1-weighted images of each subject. The stimulating electrode was localized by transferring the location of positive sites to the navigation system with the navigation pointer and by visualizing the positive tags sites recorded on systematic intraoperative photographs according to anatomical landmarks (i.e. sulci, gyri, and cortical veins) and detailed operative reports using FSLeyes from FSL.[55] To ensure the accuracy of positive sites' registrations, the neurosurgeon and the author of this study carried out this work independently. The resulting cortical maps were then compared and modified by consensus if disparities occurred. A current density of 0.05 A/cm^2 was assumed beneath the stimulating bipolar electrode,[70] thus using a maximum current of 5 mA. A current depth diffusion of 2.5 mm beneath the electrode was then estimated. Therefore, with the resulting coordinates of positive sites, a ROI with a $6 \times 6 \times 6$ mm^3 (i.e. two voxels-wide in fMRI scans) was created on the cortical surface excluding non-brain tissue to perform SCA.

4. *fMRI preprocessing*

As described for task-specific fMRI data in chapters VI and VII, the preprocessing of the rs-fMRI was also conducted using MIBCA.[48] This in-house built toolbox, based on Matlab (The Mathworks; MA, USA), incorporates tools from toolboxes such as FSL[55], Freesurfer[57] and Brain connectivity toolbox.[21] MIBCA was used to perform the following preprocessing steps: non-brain tissue extraction,[55] correction of magnetic field distortions,[59] slice-timing correction, head motion correction,[59] spatial smoothing, gray/white matter/CSF segmentation,[56,51] and co-registration to the individual anatomical images. For connectivity graph theory analysis, fMRI matrices were produced using a pairwise correlation[66] between all pairs of cortical and subcortical regions using an atlas-based ROI.[57]

Patients' motor and language stimulation points (i.e. positive sites for anarthria, movement interruption and language disturbances) in distinct gyri were selected (i.e. as seeds) to assess BOLD signal time course similarities between distant nodes of the same functional network. For the seed-to-voxel connectivity maps generation, correlation analyses were performed using the Functional Connectivity (CONN) toolbox[49] implemented in SPM (v.12).[51] Seed-to-voxel analysis consisted in computing the temporal correlation (bivariate correlation) between the mean BOLD signals from a given ROI to all other voxels in the brain. Additionally, to remove possible sources of confounds present in the BOLD signal data, all functional MRI time-series underwent

normalization of the signal from the ventricles, deep white matter and head motion followed by temporal filtering (0.009 to 0.08 Hz) on unsmoothed volumes (i.e. denoising CONN function).[60]

The task-specific fMRI was acquired using the same T2*-weighted contrast sequence and parameters. As stated in chapters VI and II, the motor paradigms used a block design and consisted in language tasks such as the VSDt, syntactic judgment, the VGt and the motor task based in MMT. Data preprocessing and analysis was done using the Brain Voyager software (v.2.8, Brain Innovation, Maastricht, The Netherlands)[47] described extensively in chapter II (methods section). The BOLD activation maps were calculated from the general linear mode and were superimposed volumetric T1-weighted scans. Moreover, the lateralization index (equation 6.1 describe in chapter VI, methods sections) was also calculated to assess the dominant hemisphere for language function (lateralization index $\geq$ 0.10 equaled to a left-dominant hemisphere).

5. DTI preprocessing, tractography and network

Structural connectivity was assessed by reconstructing the tracts using the defined ROI based on DCS positive sites also as seed. The whole brain DTI-based tractography was also estimated using MIBCA,[48] which uses FSL to estimate diffusivity maps and Diffusion toolkit[43] to reconstruct tracts (for further preprocessing details see chapter II or section B). Moreover, an additional step of DWI scans denoising was made by using the *dwidenoise* function of MRtrix.[54] The tract visualization was made using TrackVis[43] and a close inspection of tracts' end points was made to inspect for structural connections between the brain stimulation site and the SCA regions results.

To assess the global efficiency connections mediated by structural white matter axonal bundles graph theory measures were extracted from DTI data. Once the tracts were computed and validated, the connectivity processing took place. Briefly, the labeled ROI and their respective transformation matrices, generated from T1-weighted images, were gathered to perform segmentation of the DWI images. This was accomplished, based on the subject's b0 image, considering the affine transformations between a DWI volume to T1-weighted. Afterwards, non-linear transformation were made to align the ROI and the b0 image using FSL's *flirt* and *fnirt* functions, respectively (i.e. incorporated in MIBCA). An adjacency matrix was then calculated with the information on the number of streamlines connecting each pair of ROIs, and connectivity metrics were extracted (using the brain connectivity toolbox,[21] third party software of MIBCA). Integration and efficiency measures such as characteristic path length (shortest path from node A to node B) and small-worldness index (ratio between effective and random cluster coefficients and characteristic paths length) were computed. A brain small-world topology is defined as an

efficient network demonstrating features of high clustering and short path length reflecting a small-worldness.

6. *Data reduction and analysis*

For better characterization of the focal lesions within each patient brain, the location, histology, and the volume size, was computed for both TP and BCSs. Tumor and cavernomas were manually delineated by one author using Horos software (https://horosproject.org/, USA) for volume computation. Moreover, the location of these lesions was classified as follows: frontal cortex, cortical midline, parietal and temporal cortex, sensory or motor cortex.

Mean and standard deviation of the presurgical neuropsychological language test scores were calculated and compared between the BTS and BCS. An independent t-test was used after testing for normality with Shapiro-Wilk test and variances of homogeneity with Levene's test. Moreover, a bivariate correlation was made using either the point biserial test to test if DTI-based global efficiency metrics correlated with tumor volume higher than 4 cm^3, or Spearman's rho correlation between global efficiency metrics of the BTS. Statistical analysis was performed using SPSS Statistics (v.24, IBM, USA). A p-value lower than 0.05 was considered statistically significant.

Brain regions correlated significantly with DCS sites were identified and displayed using a cortical and subcortical parcellation atlas, already comprised in CONN toolbox.[170] For comparison of task-specific fMRI with language eloquent network resulted from SCA, data from BOLD activated during task-specific fMRI was also parcellated using the Harvard-Oxford atlas.[170] A correspondence analysis between modalities was done considering a positive correspondence region when the task-specific fMRI presented a significant activation at the same atlas region correlated with DCS positive sites. This correspondence was done by a neurologist and neurophysiologist present either in the presurgical fMRI or the intraoperative mapping, respectively. In addition, tracts gyri end-points were also organized using the same parcellation atlas for comparison purposes to infer structural connectivity between DCS sites and significant correlated regions.

Graph analysis were extracted from both group patients. Data gathered from DCS positive sites and related functional network of the BTS compared with connectivity data from the BCS Comparisons of metrics between the BTS (i.e. test) and the BCS (i.e. control) were made within the specific location of the occupying brain lesion. Moreover, a mean measure for each atlas location was calculated within the BCS with similar cavernoma location and a 2 SD range was calculated. The connectivity measure of patients with PBT was considered significantly different from controls' if surpassing the 2 SD value range for that atlas region.

Graph theory measures were extracted from significantly correlated brain regions ($p< 0.05$). The following measures were extracted:[21] degree of a node (i.e. the number of links that are associated to that region considered as a node); segregation measures such as cluster coefficient (i.e. number of links or edges that exist between a node and its neighbors as a proportion of the maximum number of edges possible) and high levels of local efficiency of information transfer; modularity (i.e. statistical measurement that determines the number of non-overlapping modules within a network); centrality measures such as betweenness centrality (the number of times a node acts as a bridge along the shortest path between two other nodes); participation coefficient (i.e. the distribution of a nodes edges between diverse network modules). Hubs are classified as nodes that are positioned to make strong contributions to global network function and their importance has been shown in multiple theoretical graph studies.[171,172] In this work, a brain region hubs connector was defined a brain region with higher node degree or cluster positioned in a central position (participation coefficient or betweenness centrality).[21] A provincial hub was defined as a node with a high level of degree within a specific module.

Results

1. Patient data

Sixteen patients with PBT submitted to awake craniotomy between 2016 and 2018 were enrolled in this study. However, some patients were excluded due to unavailability of intraoperative data regarding DCS positive sites (3 patients), absence of presurgical DWI data (2 patients), development of severe neurological language symptoms after presurgical MRI evaluation (2 patients) and data set processing error in one patient. Demographics characteristics, presurgical neuroimaging and neuropsychological evaluation regarding the 8 subjects of the final cohort is shown in table 8.1 (4 women, mean age of 48 years, range from 35 to 56 years). Moreover, data from 6 patients with cavernomas (mean age of 38 years range from 27 to 55 years) were also gathered. In addition, 5 patients from BCS group submmited to surgical treatment were excluded because presurgical fMRI was not performed.

The main symptom of presentation of the BTS was seizure, in spite of aphasia being presented by two patients (patients 2 and 4). Moreover, patient 4 also showed a mild hemiparesis. These patients' symptoms resolved after either one or two cycles of dexamethasone (18 mg/day) during 5 or 10 days. All patients' PBT were located in the left hemisphere. Histology showed high malignancy cells in half of the PBT group and were located within the frontal lobe in 6 patients, without involving the motor gyrus (3 patients) with a mean volume of 7.5 cm^3 (SD=7; table 8.1). Presurgical neuropsychological language testing is also shown in table 8.1 and none of the BTS showed an error rate greater the 50% of the trials. Patient 4 had a lower performance in

comparison with the other subjects enrolled in the BTS (PNt: 53% vs mean of 94%, SD=3% of other subjects, p=0.0014; NVSDt: 73% vs 96%, SD=2%, p=0.037; VGt: 57% vs 87 SD=6%, p=0.021). Six months after surgery, patient 4 died due to cancer disease recurrence and none of the other patients had neurological motor or language deficits.

Five subjects of the BCS presented with headache and one with personality disorder. Two cavernomas were located in right hemisphere. The majority (4 patients) of the cavernomas involved the frontal lobe, in two occasions were related with the motor gyrus, and in one patient was located at midline. The other two cavernomas, were located in the parietal lobe, one related with the sensory gyrus. The cavernomas' mean volume was 1.5 cm^3 (SD=0.6 cm^3). The BCS showed no motor or language presurgical neurological deficit, moreover, none had seizures. The mean neuropsychological language testing was 94% (SD=2%) for PNt, 89 % (SD=3%) for NVSDt, and 91 (SD=4%) for VGt. Three months after surgery, none of the patients presented neurological symptoms.

2. Direct cortical and subcortical cortical mapping

Intraoperative electrostimulation was performed only in BTS. A mean intensity of 2.8 mA (SD 0.5mA) was used for brain DCS. After completion, intraoperative images of the navigation system and photographs of the cortical brain surface were taken and subsequently analyzed offline. In all but one patient (patient 1), photographs together with navigation data were available for DCS positive sites' identification. None of the patients presented seizures during awake craniotomy electrostimulation. Patients 4 and 7 showed after-discharges during DCS, which disappeared after cortical irrigation with cold ringer lactate. During these electroencephalographic after-effects, the evoked language disturbances were dismissed.

The positive sites of cortical stimulation are shown in figure 8.1 using the cortical parcellation system used for SCA (see below).[170] In all patients, the motor function was found over the precentral gyrus (identified with a + marker in figure 8.1), evoking a anarthria and a negative effect on flexion or extension of the patients' contralateral arms. Additionally, language disturbances, such as paraphasias or speech arrest, were also found in all patients (identified with a marker * in figure 8.1). In two patients (patients 2 and 7), language disturbances were evoked only after subcortical electrostimulation after partial tumor resection identifying functional white matter pathways (i.e. corticospinal tract and arcuate fascicle).

3. Seed correlation analysis, seed based tractography and task-specific fMRI

The significant regions correlated with DCS positive sites of each subject are shown in figure 8.1 for both hemispheres. These functional language networks are comprised of either DCS evoking language motor disturbances or language processing disturbances. Structural connectivity results from seed based tractography between the stimulated brain site and each patient's cortical regions are shown in table 8.3 of appendix. Moreover, examples of functional and structural language network are shown in figure 8.2.

Seed based tractography reconstructions were made using at least two stimulation sites at cortical or subcortical surface. In patients 5, 6 and 8 three or more stimulation sites were used, whereas in two patients two subcortical stimulation sites were used (i.e. patient 2 and 7; figure 8.2). Streamline tracts only involved the left hemisphere and in only two patients' fibers connected with the corpus callosum. From the stimulation sites, part of AF was reconstructed in all patients but one (patient 2; figure 8.2). However, in 5 out of 8 patients, the cortical surface in which was evoked a speech arrest interpreted as anarthria (i.e. stimulation over the PrG) during intraoperative language testing, accomplished to reconstruct part of the AF. Regarding to global efficiency metrics, neither small-worldness index nor path length correlated with tumor volume (0.553 and -0.507 for small worldness index and path length, respectively; $p > 0.1$). A Spearman rho correlation was run to determine the relationship between small-worldness index and mean path length. There was a statistically significant negative correlation ($r = -0.74$, $n = 8$, $p = 0.012$).

All patients of the BTS showed language dominance over the left hemisphere (lateralization index >0.3; equation 6.1 of chapter VI). Five DCS sites over the anatomical PrG showed functional temporal signal correlation either with anterior (opIFG) or posterior (SMG, STG, and angular gyri (AG)) language classical involved gyri. Whereas eight DCS sites distributed between frontal and temporal lobe were related either with anterior or posterior language regions including PrG or PoG (table 8.2). Correspondence between the SCA results and BOLD activated regions during language tasks is also shown in figure 8.1. Correspondence percentage for each patient is shown in table 8.1. Overall, seed based functional network comprised of 34 regions when anarthria was evoked, and 24 out of 34 showed a similar activation in task-specific fMRI (table 8.1). Moreover, 31 significant regions were correlated with DCS sites when a language processing disturbance was evoked, in which 19 regions showed concomitant task-specific BOLD activation. Overall, a mean of 72% (SD=22%) of the regions with DCS positive sites showed activation on the presurgical task fMRI (table 8.1). Combined structural-functional connectivity was achieved in 18 out of 34 functional regions over the left hemisphere (table 8.3). This connectivity was found between the stimulation site and PrG for in four occasions (i.e. subjects DCS sites and correlated regions identified by SCA), and from the stimulation site to middle frontal gyri (MFG) for three

occasions through part of CST. Whereas, connectivity from DCS sites to temporal, parietal or occipital lobe were denoted for 9 times as part of AF.

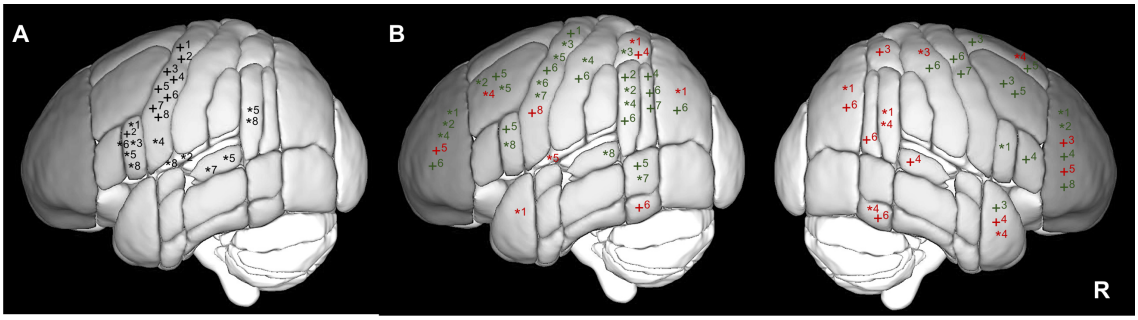

Figure 8.1 – Direct cortical stimulation (DCS) sites displaced in a parcellated cortical surface by Harvard-Oxford atlas.[170] For predominantly evoked motor language disturbances a marker + was used, whereas a marker * was used for cognitive processing disturbances for each patient (marker plus patient number) B – Functional correlated regions with DCS sites showed in A using the same description. In addition, a green marker was used to indicate a positive correspondence with task-specific functional magnetic resonance imaging, whereas a red color indicates the absence of correspondence.

Table 8.1 – Demographic characteristics of patients (Pt) enrolled in this study. Neuropsychological performance in presurgical language tests is shown as a percentage of correct answers. Two global efficiency connectivity measures are shown to provide a perspective from the brain network topology in each patient

Pt	Gender	Age	Sympt.	Location	Histology	Vol. (cm^3)	PNt (%)	NVSDt (%)	VGt (%)	SCA and ts-fMRI	Small-Worldness Index	Mean Path Length
1	Female	51	No	Frontal	OD	1.2	94	96	94	44%	6.02	1.22
2	Male	52	Aphasia	Motor	GBM	1.6	96	93	86	100%	6.08	1.33
3	Male	58	Seizure	Motor*	OD	5.2	89	98	77	75%	7.12	1.11
4	Female	56	Aphasia	Frontal	GBM	15.4	53	73	57	43%	6.47	1.33
5	Female	35	Seizure	Temporal	A	3.8	96	95	80	70%	4.49	1.73
6	Male	46	No	Frontal	A	0.9	94	93	91	67%	4.18	1.85
7	Male	40	Seizure	Frontal midline	AA	17.7	98	96	91	100%	6.25	1.22
8	Female	38	Seizure	Sensory	A	14.1	94	98	89	75%	5.14	1.48

* Tumor recurrence. A – Astrocytoma; AA – Analplasic astrocytoma; GBM – Glioblastoma; NVSDt – Nonverbal semantic decision task; OD - Oligodendroglioma PNt – Picture naming task; Pt – Patient; SCA – Seed correlation analysis; ts-fMRI – task-specific functional magnetic resonance imaging; VGt – Verb generation task,

4. Individual graph theoretical analysis of patients with PBT

Graph theory measures extracted from rs-fMRI for each stimulation site is shown in table 8.2. For understanding such measures, intraoperative photographs, tractography (i.e anatomical connection), rs-fMRI (functional connection) and combined tractography and rs-fMRI

connectivity (i.e. anatomo-functional connection) were reviewed for each patient. Examples of four patients are shown in figure 8.2.

Patient 1 presented a low-grade glioma in the frontal lobe, slightly anterior to the CST and showed no neurological symptoms. DCS evoked disturbances after stimulation at PrG and opIFG. These regions were anatomo-functional connected with superior parietal gyri (SPG) or PrG, respectively. PrG graph measures showed a higher node degree and participation coefficient in comparison with BCS, whereas the opIFG showed a high centrality measure also in comparison with BCS. Therefore, the PrG was classified as a connector hub within this functional network.

Patient 2 presented with a symptomatic glioblastoma over the motor frontal gyri producing aphasia. The DCS sites evoked only motor language disturbances and a anatomo-functional connection was not identified. Despite increased betweenness centrality at central operculum (Cop) gyri, lower participation coefficient was also found which contrasted with PrG stimulation site. The Cop was anatomo-functional connnected to PrG (fig. 8.2) but did not show a high node degree (i.e. not defined as connector hub).

Patient 3 presented with an asymptomatic frontal oligodendroglioma recurrence. The PrG showed hub connector characteristics, with higher node degree and betweeness centrality in comparison with BCS. Similar features were presented by opIFG despite lower magnitude and therefore not significantly different from control group. The DCS sites were anatomically connected to the PrG and SMG through AF.

Patient 4 had a high malignancy and high-volume tumor which conditioned language neurological disability with a lower score in presurgical language testing. The opIFG showed increased betweeness centrality measure (despite non-significant) and showed anatomo-functional connection to middle frontal gyrus, PoG and SMG by part of AF.

Patient 5 was diagnosed with temporal lobe tumor after a seizure. Patient's brain was still organized with a small-word topology (high small worldness index and low path length). Two frontal DCS sites showed a increased betweenness centrality and PrG was anatomo-functional connected to SMG by AF despite a showing low participation coefficient. None of the regions showed significantly different graph measures. Patient 6 was detected with small and asymptomatic PBT. This patient's network also showed a small-world network topology (table 8.1) and the opIFG was located centrally with lower participation coefficient (table 8.2). Moreover, anatomo-functional connectivity was found between opIFG and PrG or PoG, and from Cop to posterior language regions by part of AF.

Patient 7 had a frontal midline anaplastic astrocytoma without significant neurological deficits. DCS of the PrG showed features related to a provincial hub with a high node degree, whereas in the MTG a lower participation coefficient was found. Despite anatomo-functional connection within MTG and STG, these were not connected with the anterior part of the AF (figure 8.2).

Patient 8 showed a low-grade glioma and presented recurrent seizure. The DCS site at PrG showed a lower participation coefficient and was anatomically connected to the STM and SMG. However, anatomo-functional connection was not found between anterior and posterior regions when analyzing the other DCS sites. In contrast to PrG, Cop showed lower participation coefficient and high betweeness centrality, and an anatomical connection to PrG by part of AF.

Table 8.2 – Graph theory metrics of the DCS positive sites (language and motor functions) of patients with primary brain tumor. Note: presence of * indicates a significantly different value cavernoma subjects.

Pt	**Stim. Site**	**Resting State fMRI**			
		Node degree	Cluster Coef.	Participation Coef.	Betweenness Centrality
1	PrG	94*	0.180	0.61*	1709
	opIFG	62	0.120	0.50	13382*
2	PrG	74	0.110	0.28	4792
	COp	77	-0.010	-1.34*	12727*
3	PrG	84*	0.120	-0.54	12700*
	opIFG	72	0.120	-0.07	4803
4	PrG	76	0.100	0.23	696
	opIFG	40	0.060	0.37	8142
5	PrG	70	-0.010	-1.54*	12247*
	opIFG	50	0.003	-1.12	13137*
	STG	45	0.053	0.130	3988
	MTG	72	0.050	-0.83	10302
6	PrG	72	0.120	0.66	2691
	opIFG	62	0.040	-1.45*	12111*
	COp	61	0.053	0.57*	11628
7	PrG	85*	0.080	0.19	6174
	MTG	63	0.022	-3,04*	6098
8	PrG	52	0.025	-2,04*	12186*
	opIFG	41	0.076	0.626	32
	COp	66	0.029	-1.375	15813*
	STG	62	0.013	-0,75	11221

AG – Angular gyrus; Cop – Central operculum; IFG – Inferior frontal gyrus (posterior part); MTG – Middle temporal gyrus (posterior part); PoG – Postcentral gyrus; PrG – Precentral gyrus; opIFG – Opercular part of inferior frontal gyrus; SLOG – Superior lateral occipital gyrus; SMG – Supramarginal gyrus; SPG – Superior lobe gyrus, STG – Superior temporal gyrus (posterior part).

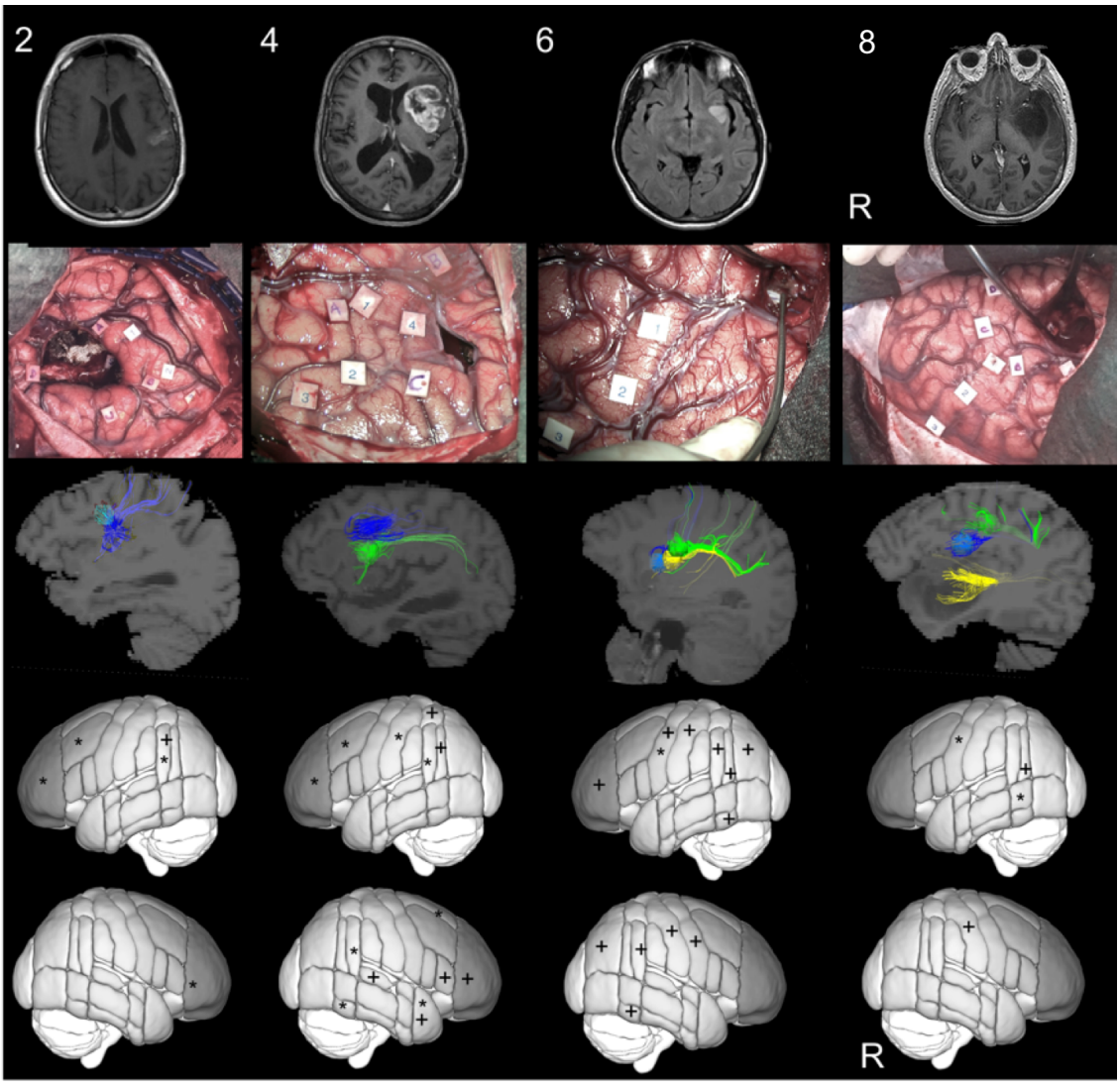

Figure 8.2 – Examples patients' connectivity procedure for evaluation graph theory measures extracted from diffusion tensor imaging and functional magnetic resonance imaging. Each patient with primary brain tumor (first row starting from above; note T1 weighed images were display either with injected contras agent or FLAIR contrast) were submitted to awake craniotomy. Positive direct cortical stimulation sites (second row; letter was used to identify tumors boundaries and number for motor gyri (1,2,3) or language function (4,5,6) were used as seed to either perform tractography (third row; each site was color coded) or correlation analysis using resting state data (last two rows; a + was used to identify regions correlated with motor gyri and * with language function sites).

Discussion

This study aimed to understand how graph theory analysis based on rs-fMRI may provide additional information about eloquent regions within patients with PBT in the presurgical stage. For this purpose, clinical, presurgical and intraoperative data obtained using the conventional algorithm for surgical treatment of PBT were reviewed. Eight patients were included in the test group and electrostimulation brain sites (with motor or processing language function) were used as the gold standard method to reconstruct functional (rs-fMRI based) and structural (DTI-based)

connectivity. Functional regions related to the DCS positive sites using a SCA and a mean correspondence of 72% (which ranged from 22 to 100%) in BOLD language fMRI. Moreover, part of CST and AF were reconstructed from electrostimulation sites and connecting about 59% of the functional related regions within the left hemisphere. Graph theory measures were extracted from previously segmented brain regions according with a standard atlas with 132 regions available in MATLAB based connectivity toolboxes. Individual patient connectivity was evaluated, and the main significant features in comparison with BCS (with lesions smaller than 2 cm^3) were: a few brain hubs with connector and provincial features, and regions centrally located within the network (i.e. betweenness centrality) with a decreased participation and cluster coefficient (despite non-significant). To our knowledge, this study firstly reports the graph theory features of DCS positive sites for motor and language eloquent network. Moreover, it provides further understanding about graph theory measures which may complement the information given by task-specific BOLD fMRI or rs-fMRI for presurgical planning.

1. Clinical evaluation and global network measures

Lesions of the anatomical brain networks result in functional disturbances of behavior which often depend on the lesion site.[170,173, 174] The understanding behind brain dynamics and networks during cognitive processing evolved from a reductive approach to an analysis of multivariate relationships.[164, 175, 176] However, network modeling of a brain occupied by a lesion, such a PBT or a cavernoma, remains undescribed in the literature probably due to the location variance. In this study, brain network modeling by PBT was investigated and compared with brain cavernomas modeling with 20% of the PBT volume. PBT invades the surrounding parenchyma and multiple factors, such as the type of proliferating cells, cellular and nuclear pleomorphism or atypia, mitotic figures and vascular hyperplasia, lead to different delineations of tumor margins and infiltration degree.[1,173] On the other hand, cavernomas have their origin in intracranial hemorrhage after being contained by an inflammatory and chronic response which evolves to hemoglobin digestion by macrophages from the periphery to the center.[173] This study aimed primarily at understanding the graph theory measures in different subsets of modeling.[21,160,] Therefore, patients with brain-occupying lesion were used as a control to identify significant differences in comparison with invasive modeling of brain networks. In fact, previous reports showed different brain topology even in younger subjects versus aging subjects or in subjects with a low nonverbal IQ which bring up difficulties to select an appropriate "control" group.[177-179] Moreover, simulation of lesions in the brain networks showed that lesion volume and location drive network changes the most [160] which was controlled by selecting a control group with 20% of tumors volume and a comparison between BTS and BCS was made within patients with lesions at similar locations.

Both BTS and BCS presented brain lesions predominantly in the frontal lobe.[178,179] Despite the fact that, for research purposes, a more heterogeneous lesion location is more desirable, frontal lobe lesions remain the most studied regions in a presurgical stage, due to their relationship to the motor and language function.[121,180] In the BTS, global efficiency measures do not correlate with tumor volume which could resign the idea of a less organized network when a brain lesion evokes modeling by occupying space. A better understanding is likely to come from high malignancy tumors, which develop rapidly evoking high neurological symptoms and deficits.[1,178] In fact, the BTS was not more symptomatic than the BTS. Despite this, a few tumor patients showed high malignancy and further neurological symptoms, but these were in a small number to draw more conclusions regarding brain network topology. Moreover, BTS obtained a score of about 90% in presurgical neuropsychological language testing but one patient (patient 4), which was not sufficient to relate with global efficiency measures. However, patient 4 showed a large volume and high malignancy tumor which may explain the high neurological impairment and small-worldness index but yet a similar path length in comparison with patient number 7. The time for a gradual development of the PBT play a role in the neuroplasticity process and should implicate different magnitudes of brain network modeling and reorganization with reflection on global efficiency measures.[126,181, 182]

2. Seed-to-voxel analysis of functional and structural data

The intrinsic connectivity between functionally related parts of the brain allows for the mapping of neuronal networks. In this study, a seed-to-voxel analysis was used to relate rs-fMRI temporal correlation of low-frequency BOLD signals in order to measure intrinsic functional connectivity between brain regions.[182-185] The seed-based approach driven upon the DCS positive sites with the prior knowledge of the language network.[182,185] For this purpose, photographs and intraoperative navigation snapshots were used to define the ROI and superimposed them in volumetric 3D T1-weighted images. However, some displacement of the ROI location was expected despite of the agreement between authors, the main reasons was due to navigation displacement error of about 2 to 5 mm (aggravated in subcortical electrostimulation), and some (not quantified) anatomical mislocalization driven from the authors' placement. Thus, the ROI size was doubled in relation to the expected current density dispersion on cortical surface for the intensity used, representing two voxels width in fMRI data and three voxels width in DTI scans. The estimated size was smaller than the used in other studies,[156,179] which may explain the decreased frequency of correlated regions observed in patients 7 and 8. Despite of less probable, a misidentification of language processing disturbances may have occurred due to patient inattention or not detected electroencephalographic epileptiform activity. In fact, in patient 8, opIFG and STG do not show streamlined axonal bundles with other regions.

A structural network is defined by a set of regions which are connected to each other via axonal bundles. Depending on the links' characteristics, the network can be classified in binary undirected (bidirectional links with the same weight); weighted undirected (with an additional weight to each link).[21, 186, 187] Links should be directed and weighted in order to better reflect the underlying neurological function.[175] The seed based tractography in this study was interpreted as unweighted data (i.e. presence or absence of connection between brain regions) because the magnitude (tracts volume and number) were not taken into account during results analysis. This analysis could impose boundaries to the type of information extracted from DTI because anatomical links with a low number of tracts may represent false-positive or spurious tracts.[181] A similar approach was used for functional connectivity analysis in which the correlation magnitude of the regions was not made.[182] To reduce this methodological caveat, binary matrices were used to reconstructed tracts (more than 20% of the fibers between each brain region) and a false discovery rate below 0.05 was used for constructing SCA activation maps.

Combined structural and functional connectivity was found only for 18 times (i.e DCS sites links to brain regions identified in SCA through DTI), which impose a decrease either in functional or structural brain regions identified from seed-based correlation or tractography. Despite 65 functional regions recognized to be related with DCS sites. However, presurgical language network identification using seed-to-voxel analyses were reported as highly correlated with rs-fMRI independent component analysis with an overall good performance.[168] In this work, in spite of a 72 % correspondence between SCA and language task-based fMRI, DCS was not guided by SCA results and therefore their relevance for intraoperative language mapping remain to be studied. Although, similar rs-fMRI and task-specific fMRI correspondence were also reported in literture. [175,176]

3. Graph theory analysis

Brain network characterization has been used for research purposes, but before considering graph theory measures as a potential tool to aid the presurgical mapping of eloquent cortical regions, an understanding and validation of the measures provided is needed.[158] In fact, studies assessing the function of connectivity measures, such as brain hub, obtained from MRI are scarce. [188-190]

The graph theory measures were extracted from rs-fMRI which showed anatomo-functional connectivity to language eloquent brain regions within the left hemisphere. Lesions are modeled as structural perturbations with specific dynamic effects. Therefore, we expected to perceive that different regions of the cerebral cortex have specific effects on the pattern of endogenous functional connectivity. According to Alsttott and colegues (2009)[160] lesions at the cortical midline, the temporo-parietal junction and the frontal cortex result in the largest and most

widespread effects on functional connectivity. In contrast, lesions location within sensory and motor gyri imposes a specific neurological damage related to cortex function.[189] In this study lacked a more homogenous sample and conclusions about location influence in graph theory measures could not be drawn.

Graph measures traduced that DCS was able to perturb regions located centrally within the language module despite of their node degree, or participation coefficient. Our results were in accordance with the simulated effect on brain function according with the brain lesion location.[160, 188, 190]Actually, simulated brain networks showed to be negatively influenced if connector hubs were targeted and removed. Physiologically, regions with node centrality are connected to the baseline metabolic activity and neurodegenerated nodes have been associated with higher metabolic activity.[188] Therefore, function disruption may occur more easily within a region centrally located with low physiological reserve and already decrease participation in eloquent network.

4. Limitations

This study retrospectively reviewed data from patients submitted to awake craniotomy. The absence of presurgical and intraoperative led to a small patients' sample. In addition, some difficulties to control variables (i.e. such as the tumor malignancy) were inherent to the research typology and led to a heterogenous sample. For this purpose, just eight patients were enrolled in the test group and the selection of a control group was limited by the data availability. Moreover, DCS was used as the gold standard technique for identification of language motor and cognitive function. DCS allows to study casual and real-time relationships between the stimuli and the cognitive impairment but fails to reveal the entire architecture of the cortical network.[174] In addition, isolated language disturbances such anarthria occurred when stimulation the primary motor gyri may be difficult to recognize as believed after identifying the PrG. Seed based tractography of 6 patients led to AF reconstruction after applying the DCS in ventral part of the PrG which was not differentiated by the parcellation atlas used. Therefore, the methodological aspects of neuroimaging processing may impose some challenges. Using individual neurons as nodes and synapse as links would be desirable to traduce brain connectivity and dynamics. However, this is not technically feasible and therefore the choice of a parcellation method has some limitations.[181,190] Nodes should be homogeneous units and brain tumors may disrupt regions boundaries during automatic algorithm processing. Moreover, the influence of the number of regions used for brain cortical parcellation should be studied. As mentioned above, large regions may decrease spatial resolution of reconstructed connectivity within atlas regions underestimating real functional data. Also, the criteria used for graph theoretical measures is not well established and definition such as connector brain hubs is not consensual in literature.[162] Lastly, conservative

statistical thresholds impose relevant constraints to data which increase the studies type 2 error (i.e. false negatives) and previous graph theory measures experience should be gathered before draw rigid conclusions.[189]

Conclusion

The graph theory measures provided some insight about specific brain regions and their role in a functional network, detected by seed correlation analysis and tractography. Brain hubs with connector or provincial function, and central location within the network module were predominant features of the brain stimulated regions language motor or processing function.

Appendix

Table 8.3 – Functional (♦) and structural (Δ) connectivity between the intraoperative electrostimulation sites over left hemisphere and brain cortical regions after cortex parcellation using Harvard-Oxford atlas. [170] Functional connectivity regions were located based in seed correlation analysis whereas structural regions were located by seed based tractography.

Pt	Stim. site	FP	SFG	MFG	opIFG	Cop	PrG	PoG	TP	STG	MTG	ITG	SMG	AG	SPG	SLOG
1	PrG							Δ							Δ	
	opIFG	♦	Δ				♦	Δ	♦		Δ				♦Δ	♦
2	PrG												♦			
	COp	♦		♦			Δ	Δ					♦		Δ	
3	PrG							Δ		Δ	Δ				♦	
	opIFG						♦Δ	Δ					Δ	Δ		
4	PrG			Δ				Δ						♦	♦Δ	
	opIFG	♦		♦Δ		Δ		♦Δ					♦Δ	Δ		
5	PrG	♦		♦Δ	♦Δ			Δ			♦Δ	Δ	Δ		Δ	Δ
	opIFG		Δ	♦Δ												
	STG					♦Δ					Δ		Δ		Δ	
	MTG						♦			Δ			Δ			Δ
6	PrG		Δ		Δ			♦Δ							Δ	Δ
	opIFG		Δ				♦Δ	♦						♦		
	COp				Δ		♦						♦Δ		Δ	♦Δ
7	PrG*							Δ						♦Δ	Δ	
	MTG				Δ	Δ				♦Δ						
8	PrG							Δ			Δ		Δ	Δ	Δ	
	opIFG						♦Δ									
	COp				♦											Δ
	STG												♦			

* Data from two simulation sites at PrG. AG – Angular gyrus; Cop – Central operculum; IFG – Inferior frontal gyrus (posterior part); MTG – Middle temporal gyrus (posterior part); PoG – Postcentral gyrus; PrG – Precentral gyrus; opIFG – Opercular part of inferior frontal gyrus; SLOG – Superior lateral occipital gyrus; SMG – Supramarginal gyrus; SPG – Superior lobe gyrus, STG – Superior temporal gyrus (posterior part).

This page was intentionally left blank

SECTION D: SPEECH AND LANGUAGE RECORDING

CHAPTER IX

ACCELEROMETER RECORDING OF SPEECH: TECHNICAL ASPECTS AND RELIABILITY

Introduction

Functional methods for assessment of speech in clinical practice are qualitative, which entails difficulties in the analysis of causative mechanisms and effects of therapy.[191] Video and microphone voice recordings can give high quality reproducible data, covering a large frequency range of signals and high sampling rates.[192] However, these recordings require expensive hardware and complex software installations, and are still prone to contamination by environmental noise or electrical signals arising from the articulatory muscles during voice production.[193] In fact, voice production assessment in candidates for thyroidectomy is made in most instances through audio recording during laryngeal EMG or laryngoscopy.[194] To avoid invasive techniques, surface cricothyroid EMG recording was proposed to evaluate patients with dysphonia.[195,196] Still this has demonstrated limited sensitivity for vocal cord pathology because of contamination by non-specific neck muscles activity.[197]

Speech production implies the activation of the vocal cords modulating the air passing through the trachea, which has the ability to resonate. This phonation process generates vibration of the vocal tract which allows the possibility to use an ACC to record such oscillatory repetitive movement.[198] ACC recordings are able to reflect the fundamental frequency and the pitch range of speech, recorded with a microphone. [192,197,198]

Vitikainen and colleagues (2015)[199] used a three axis ACC placed at submandibular level to detect phonation and developed an automatic algorithm capable of identifying the onset of vocal tract oscillations while mapping cortical brain regions with r-nTMS. Similar use of the ACC has already been reported by other authors, focusing either on the latency to phonation (i.e. reaction time)[200] or on the decrease of amplitude[201,202] and fundamental frequency in vocal cord pathology.[203] However, none of the studies looked at the practical aspects of glottis ACC recordings nor the correlation between the data obtained and the words or syllables pronounced. Moreover, ACC recordings show different characteristics between males and females, mainly in the pitch or fundamental frequency.[192] The understanding of such ACC phonation characteristics

is a necessary step towards making this method clinically useful for monitoring several interventions related to speech, such as identification of language disturbances, or to evaluate rehabilitation therapy in patients with vocal cord pathology. We advocate that speech recording should be done by a readily accessible tool in clinical practice. Besides, it should offer the possibility to store recordings and extract parameters, which can be used to document and compare speech features. The analysis of such recordings might help in the clinical assessment of voice disorders, mitigating interpretation errors.

The present study was designed to investigate specific technical aspects of the vocal tract vibration recording during word pronunciation. Our primary goal was to answer the following questions: a) are recordings different if obtained far from the "point" of higher vibration at the neck (e.g. cricothyroid cartilage)? b) does the activation of surrounding neck muscles impose artifacts preventing reliable vibration recordings? c) are the recordings reproducible within the same subject in different sessions? d) are ACC recordings of the same word reproducible between subjects? Secondly, we also carried out a proof of concept study of the robustness of the technique to show changes generated in speech by vocal cord infectious pathology in patients with laryngitis.

Methods

The study was carried out in 25 healthy subjects (16 women; mean age of 30 years, ranging from 21 to 42 years; body mass index of 24.0±2.0 kg/m^2) and 7 patients with laryngitis (5 women; mean age of 28 years, ranging from 20 to 31 years; body mass index of 23.6±3.1 kg/m^2). The patients with laryngitis were recruited by chance during consultation and selected if met the following criteria: history of previous pharyngitis or laryngitis and hoarsens and/or croup in the last 5 days prior to consultation, audible voice and without fever, dyspnea, sputum or history of allergic or food reactions.

The Ethics Committee of the Hospital Garcia de Orta (Almada, Portugal) approved the study protocol and all subjects signed an informed consent prior to their inclusion in the study.

1. Recording word pronunciation

Subjects were presented with the same set of for PNt in the previous section of this thesis.[83] We selected only pictures which names are either one or two syllables long in Portuguese. Subjects were asked to inspect the set of 24 selected pictures (see appendix) to ensure that picture-name agreement reached 100% before starting the experiment. Subjects were sitting on chair facing a

computer screen placed 1 m away from the subject's eyes. A white frame with a picture of 8x8 inches was presented (i.e. imperative signal) every 4 s and were shown during 4 s. A black screen with a white "X" letter at the center of the screen was shown during 4 s after the picture disappearance as attention fixation cue. The fixation cue disappearance was used as a forewarning signal before the next picture presentation.

There are physiological factors known to influence the vocal tract vibration, such as speech loudness,[204,205] subject's readiness,[200] length of phonation,[206] swallowing,[207] activation of neck muscles[195,208] and the level of attention during the experiment. Therefore, we tried to maintain the same experimental conditions by asking the subjects to articulate correctly the syllables and pronounce words with a normal volume mimicking a spontaneous conventional conversation. In addition, we performed five trials of each word, to obtain the standard pronunciation of the words by each subject. The latency of the response (i.e. the time from visual cue display to onset of the first ACC burst) was considered an indirect measure of attention level and, whenever latency to vocalization varied more than 20% beyond the subject's mean, we stopped the test to continue after a short resting period, during which we reinforced the instructions to each subject.

2. ACC recordings experiment setup

Briefly, a uniaxial ACC (piezo crystal sensor, Pro-Tech, U.S.A.) was used to record word pronunciation. Signals were fed to a conventional EMG (KeyPoint Net, Natus, U.S.A; Inomed Medizintechnik, ISIS IOM System, Germany) with a resolution of 16 bits, sampling rate of 2000 Hz, time resolution of 200 ms per division (up to 4 seconds) and amplitude of 1 mV per division. A ground adhesive electrode was placed at the forearm.

In healthy volunteers, we recorded from three different sites using four different bandpass frequency filters. The glottis sites tested to record ACC vocal tract vibration were selected according to previous voice and dysphagia studies[208, 209] and were 1) a medial point over the cricothyroid ligament (medial cricothyroid), 2) a point 1.5 cm to the left (lateral cricothyroid), and 3) a point 2 cm above the sternal notch, between both sternal heads of sternocleidomastoid muscles (suprasternal). Filter frequency bands were chosen on the bases of physiological frequency of vocal tract vibration (i.e. between 1 to 500 Hz) and were, 1-100 Hz, 1-200 Hz, 20-200 Hz 1-500 Hz.

3. *Procedure and subject's data analysis*

Subjects were asked to select a picture and to pronounce the related word four times for each one of the three recording sites and filter frequency bands. We defined the following criteria for good quality recordings: i) minimum number of artifacts within and between oscillation cycles; ii) optimal signal amplitude; iii) clarity of the onset and end of each burst, and iv) repeatability of the graphical representation with pronunciation of the same word. Scores (0, 0.5 or 1 for each quality criterion) were separately and blindly provided by six subjects, but each one unaware of the scores given by the other. The recording site and bandwidth that received the largest score were considered the optimal ones for quality ACC recording. The optimal recording site and bandwidth were then used throughout the rest of the study: In healthy subjects, we recorded 24 words from the PNt set and tested their reliability between them. Additionally, eight subjects of this group were also recruited to perform another session in order to test reliability of same word within the same subject.

Patients with infectious laryngitis who presented with hoarseness or croup started for three or four days were recruited to perform ACC recordings. We selected a set of 5 pictures to be named, randomly presented, avoiding further voice use and fatigue (each picture was named twice). The results of patients' experiments were compared with baseline recordings and the same quality criteria, technical and practical aspects of ACC recordings were ensured.

4. *Data reduction and analysis*

The following parameters were evaluated in all recordings: burst latency, as the onset of consistent oscillations after the visual stimulus; peak to peak amplitude of the oscillations; burst duration and internal frequency of the bursts. We ignored deviations from the baseline of less than 50 μV and bursts of less than 5 consecutive oscillation cycles.

Normality of data was tested with the Shapiro-Wilk test using SPSS Statistics (IBM, USA). Non-parametric Mann-Whitney tests were used to analyze if mean parameters of ACC recordings varied in each condition tested within each word and subject. To assess inter-rater variability, ACC baseline recordings were evaluated by two observers (JL and JVS) and parameters were tested using two-way mixed intraclass correlation coefficient. Additionally, intra-rater variability within different sessions of the same subject was tested using a one-way random intraclass correlation coefficient. Statistical difference was considered significant if the p-value was below 0.05.

Results

All subjects tolerated well the experiment and there were no missing data. The total scores per condition (position per filter bandwidth) is shown in table 9.1 and a graphical example of each combined condition is shown in figure 9.1.

1. Influence of recording site of vocal structures

The scoring system designed showed a higher score for the suprasternal notch position using a filter bandwidth of 20 – 200 Hz (sum of 80.5), secondly for the suprasternal notch using a filtering of 1-500 Hz (sum of 77), and thirdly for the ACC recordings at the median cricothyroid position with 1-200 Hz filtering (table 9.1, sum of 75.5). In the later, the artifacts contamination led to less score, despite the higher recording signal amplitude (mean 2.3±0.5 mV; p=0.02) in comparison with suprasternal notch recordings (table 9.2). ACC oscillations frequency was lower in the suprasternal notch recording site than in both sites (over the median ligament, p=0.032; or laterally, p=0.027) at the cricothyroid level (mean frequency in males 184±9 Hz, and females 218±8 Hz). This was more frequent in males than in females (table 9.2). Neither duration nor latency showed significant differences (table 9.1). Recordings showed an increased amplitude when using a 1-500 Hz but also-more artefact contamination (table 9.1). The abrupt onset and end of the phonation burst was the parameter that less varied among the subjects scoring.

2. Influence of physiological factors

At the start of each experimental block, the examiner performed about 5 trials in order to instruct the subject to conversation rhythm and readiness, and tone (i.e. volume). The presence of pauses within a burst of ACC recordings was more frequent when subjects were relatively unready. An example is shown in figure 9.2 where the decrease in readiness led to an increase of latency and to the disappearance of the pause between bursts. Amplitude was higher when subjects made a louder pronunciation. An increase of 10 dB (from 20 to 30 dB) in loudness caused an increase in peak to peak mean amplitude of 467 μV (SD = 124 μV). The recordings at the median cricothyroid ligament showed different artifacts contamination and parameters variability when recording the same word pronunciation, in the same subject, after repositioning the ACC trials.

Table 9.1 – Sum of the accelerometer recordings scores of each position per filter bandwidth tested. Six blindly subjects classified a pair of traces of each word made in two sessions by patients.

Position/Filter	**1-100 Hz**					**1-200 Hz**					**20-200 Hz**					**1-500 Hz**				
	A	Amp.	O/E	R	**T**	A	Amp.	O/E	R	**T**	A	Amp.	O/E	R	**T**	A	Amp.	O/E	R	**T**
Median cricothyroid	11.5	2	9.5	11	**34**	13.5	20	19.5	14	**67**	16.5	20	22.5	16.5	**75.5**	9.5	22.5	2.5	13	**67.5**
Lateral cricothyroid	9	3	7	10	**29**	12	12	13	14.5	**51.5**	12	9.5	11.5	10	**43**	10.5	18	12	7.5	**48**
Suprasternal notch	12	1	9.5	9.5	**32**	12	14	17	14	**57**	17.5	20	22.5	20.5	**80.5**	11.5	24	23	18.5	**77**
A - Artefacts; Amp. - Amplitude; O/E – Onset and burst end. R – Repeatability; T – Total score.																				

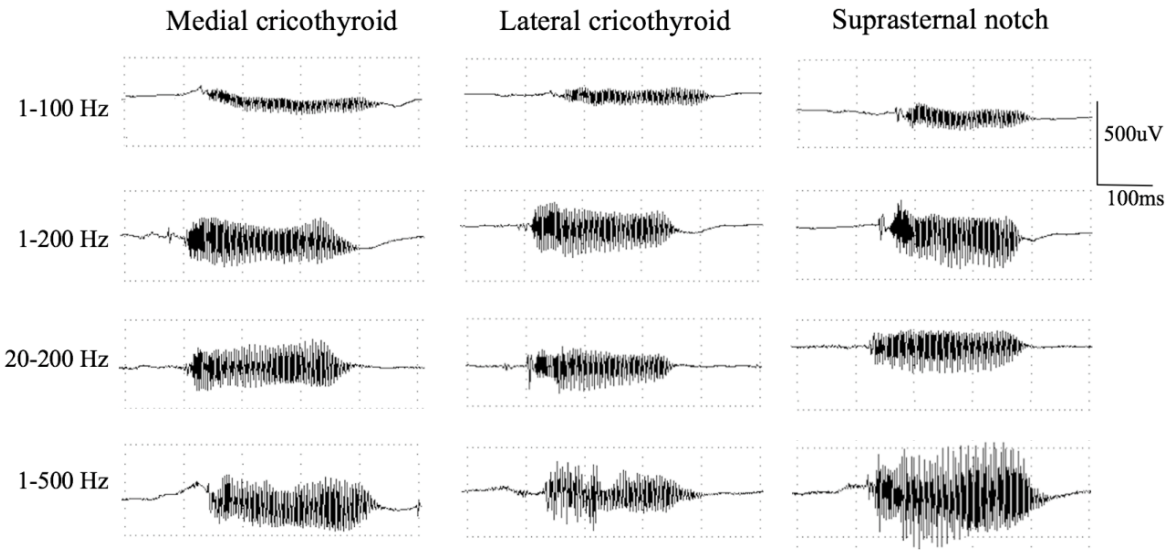

Figure 9.1 – Accelerometer recordings of a female subject after the pronunciation of the word foot ("pé" in Portuguese) during a picture naming task. Note the variations of the amplitude, artefacts at recording baseline and abrupt onset or end of the recorded burst.

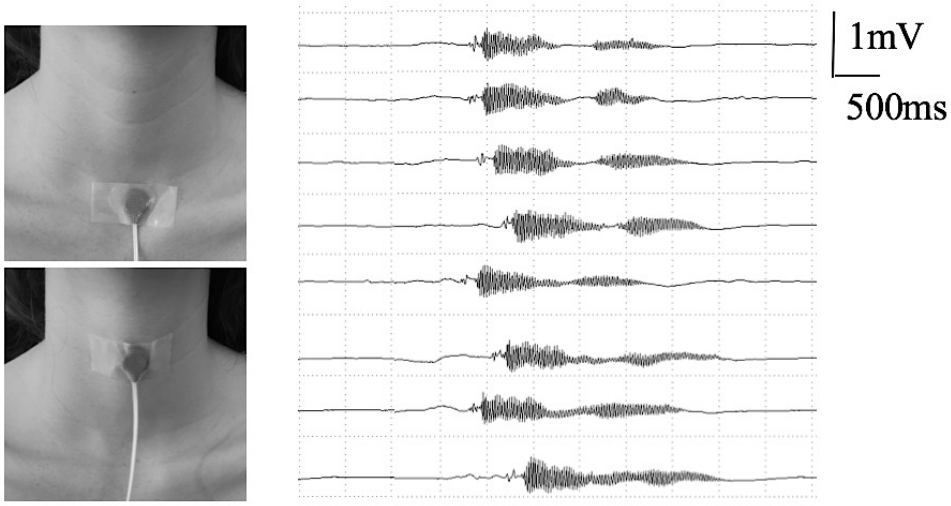

Figure 9.2 – Accelerometer (ACC) position for recordings of the word pronunciation. Left: The placement of the ACC around the neck influence the recordings parameters. Note the placement at suprasternal notch. Right: The subject was instructed to perform a picture naming task (word pencil "lápis"), as faster and as correctly as possible after visual stimuli. After the 4th trace, the subject lowered the readiness to phonation which led to a variable latency to pronunciation and the disappearance of an abrupt pause within the burst recorded.

Table 9.2 – Mean accelerometer parameters from words pronunciation of the enrolled healthy subjects (baseline recordings) and patients with laryngitis. The recordings were made after placing the accelerometer at the suprasternal notch with a 20-200 Hz filter bandwidth. Reliability testing of the same word between subjects and within two different sessions of the same subjects (eight subjects) is also shown. Standard deviation is shown within parenthesis.

Baseline recordings					**Patients**	
Parameters	Gender		Reliability		Gender	
	Male	Female	Within	Between	Male	Female
Latency (ms)	518 (82)	535 (147)	0.92 (0.06)	0.91 (0.08)	504 (102)	554 (124)
Duration (ms)	246 (94)	257 (99)	0.94 (0.03)	0.92 (0.07)	185 (61)	175 (52)
Amplitude (μV)	1295 (256)	1184 (379)	0.89 (0.10)	0.87 (0.12)	447 (78)*	374 (52)*
Frequency (Hz)	125 (9)*	176 (8)*	0.95 (0.03)	0.96 (0.03)	96 (14)*	113 (14)*
* *Statistically significant differences for evaluated parameter values either within healthy subjects or between healthy subjects and patients.						

3. Accelerometer baseline and patient's recordings

Baseline recordings were made using the technical settings with higher scoring. Baseline ACC recordings parameters made after placing the ACC at suprasternal notch are shown in table 9.2.. ACC recordings showed significant reliability between recordings of the same word made by the same subject in different sessions (table 9.2). Examples of ACC recordings at suprasternal notch

of the same word by a subject in two different sessions are shown in figure 9.3. Baseline ACC recordings were also evaluated for inter-variability estimation with significant mean intraclass correlation in ACC parameters. These, reliability was higher within the same subject in comparison to across subjects. The parameter with smaller SD was the frequency and with the larger SD was the amplitude of the graphical burst.

Mean data of ACC parameters are shown in table 9.2 and a recording example is shown in figure 9.4 (of appendix). ACC recordings from five selected words of patients with laryngitis showed a decreased amplitude (p=0.011) and frequency (p= 0.022) in comparison with baseline recordings. The total duration showed a tendency to decrease (p=0.064). Frequency suffered a greater decrease in female patients than in males (table 9.2), when comparing to the baseline recordings. There were no statistically significant differences in latency.

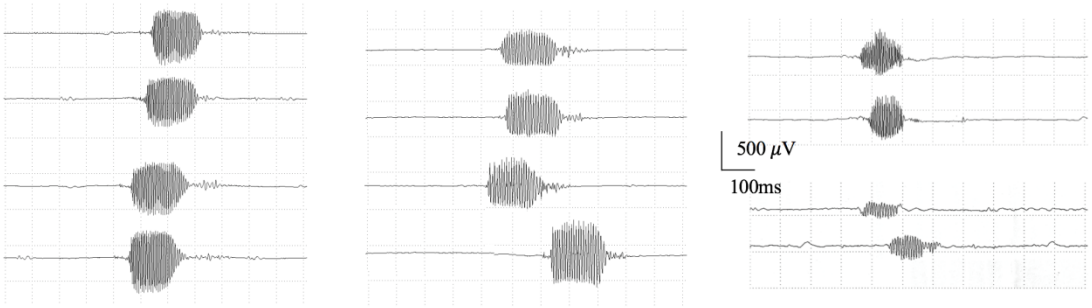

Figure 9.3 – Accelerometer recordings after pronunciation of the word car ("carro") using a 20-200 Hz bandwidth filter at suprasternal notch. Left: Recordings of the same male subject made in two different sessions (two traces in each). In the middle is shown the word car pronounced by two different female subjects. Note the similar graphical representation of the recordings despite the smaller frequency. Right: Recordings of the word boat ("barco" in portuguese) of a female subject in comparison with recording made by a female patient (bottom two traces) with laryngitis. Note the smaller amplitude and frequency.

Discussion

Our work aimed to study the technical and physiological aspects influencing vocal cord vibration recording during phonation with a uniaxial ACC using a conventional EMG amplifier. To our knowledge, this study is the first to evaluate reliability of the method, which may open the way for its clinical applicability. We described the methodology and identified possible caveats before characterizing differences between healthy subjects and patients with phonation disturbances.

1. *Accelerometer recording of vocal tract structures*

The vocal tract works like a vibrating column of air, closed at one end. During swallowing or speech production, vibration occurs in the soft frontal walls of such column of air.[207] In healthy subjects, glottis movement is produced during speech, reflecting the vibration generated at the larynx. The natural frequency of vocal tract vibration depends on the size and shape of the larynx (i.e. females vs males) but has been found to be between 100 and 500 Hz also known as fundamental frequency.[204,207] An odd multiple of this frequency can also be picked up by an ACC attached to the soft tissues of the neck. [202,203]

Most voice studies in which the authors used ACC for glottis movement detection were performed using specific biomedical equipment. These used ACC and amplifiers with high sampling rate (i.e. between 8 Khz to 44 Khz), digital input to record audio signals to microphone recordings and complementary input with 16 to 32-bit (analog-to-digital converter) resolution for EMG or ACC signals.[192,202,204] However, in neurological field, the ACC use started with the recording of low frequencies oscillations (range from 1 to 100 Hz) as occur in tremor,[208] muscle vibration[209] and snore detection.[210] Therefore, only recent EMG apparatus have similar capacity of such biomedical equipments, despite of the common use of a simpler ACC (i.e. one axis movement).

Hence, speech ACC signal evaluation in EMG laboratories to our knowledge remains to be investigated. The understanding and knowledge of pitfalls and drawbacks of vocal tract vibration ACC recording during phonation without additional hardware may improve his clinical applicability. Future applications such as diagnostic or monitoring of vocal tract vibration in a variety of pathophysiological and rehabilitation processes remain unstudied.

2. *Accelerometer technical settings after words pronunciation*

The ACC position to record words pronunciation can be performed in a variety of places at the neck due to vocal tract resonance. Oscillations during phonation are recorded with different amplitude and frequencies depending on the site where the ACC is placed.[211,212] Therefore, we looked for a reliable place to minimize significant parameters variation between subjects and within sessions made by the same subject. For the selection of optimal ACC settings, we used a four-quality criteria score performed blindly by six contributors.

The greatest score was achieved using the suprasternal notch site despite of higher amplitude recordings at median cricothyroid ligament (table 9.1). Greater amplitude and frequency at glottis level may be justified by the proximity to the vibration generator. However, also more parameters variability and less repeatability recordings after repositioning the ACC were found at this level (figure 9.2). Studies performed in dysphagia patients showed a high variability in amplitude (or

magnitude) and frequency when testing different positions around the cricothyroid cartilage[211] which is in accordance with our results. In fact, swallowing studies in dysphagia patients have been mostly conducted at glottis level due to greater sensibility to record irregular axis movements with high frequencies range. [207,211, 213]

The score system used classified the suprasternal and the median cricothyroid level as the optimal sites to place the ACC using either a bandwidth filtering of 20-200 Hz or 1-500 Hz. In addition, words pronunciation was also tested by placing the ACC lateral to the cricothyroid median ligament. However, presumably due to swallowing, neck muscles activation and subcutaneous structures, recordings after repositioning the ACC at that site showed higher variability in the evaluated parameters. In our study, the subjects were also laid on a bed angulated between 30-45º degrees in order to support the head and minimize neck muscles activation. Moreover, studies using supraglottic sites to record vocal tract vibration were only conducted due to commodity during polysomnography[210] and based in a subjective evaluation of higher vibration sites.[199] Additionally, showed minor magnitude vibration and increased mandibular artifacts contamination.[212] Therefore, according to these theoretical underpinnings, sites above cricothyroid level were not tested in our study.

Different signals bandwidth filtering was also tested. Repetitive oscillations of the neck after vocal folds activation measured by ACC signals are closely correlated with human natural vibration frequency evaluated through microphone recordings.[202] The frequencies recorded during speech production depend on the airway system function and shape including length, wave velocity, mechanical proprieties of glottis and trachea and vocal load.[203,214] In our study, authors considered the 20-200 Hz as optimal bandwidth with minor contamination of artifacts in comparison with other frequencies filtering. In spite of the slightly signal decreased amplitude (table 9.1) after increasing the high filter from 1 to 20 Hz. Such artifacts, may arise from the disappearance of the carotid pulse, neck muscles vibration,[209] breathing[207] and tissue to tissue transmission.[215]

The use of 20-200 Hz may also exclude signal amplitude (table 9.1) from physiological activation of vocal cords. In fact, recordings above median cricothyroid cartilage showed an increased SNR and a capacity to measure components related to tissue-to-tissue transmission of vocal fold collision forces through the thyroid cartilage.[215] However, the frequency of the signals did not differ between 20-200 Hz and 1-500 Hz. The number oscillations per time were manually measured without time or frequency domain magnitude spectrum analysis. Therefore, this method did not allow the identification of vocal tracts resonances and may be less accurate to identify frequency due to the presence of components with higher and smaller acceleration during the

words pronounced. In spite of using the same method to infer frequency, smaller values were obtained in suprasternal notch in comparison to cricothyroid cartilage. This result is in accordance with the higher magnitude activity of 150 Hz in suprasternal notch in comparison with the magnitude of 250 Hz in cricothyroid cartilage.[212] In fact, the recorded frequencies of ACC recordings were similar to those reported when measured by a similar ACC at suprasternal notch and glottis level.[203,212,216]

3. Influence of physiological factors in accelerometer recordings

Volume tone and loudness are known to increase the amplitude of ACC recordings and comparisons to microphone recordings showed a linear correlation.[203] In our study, we controlled subjectively the loudness instructing the subjects to maintain their voice effort using a natural conversation volume. In order to quantify this effect, we measured the peak to peak amplitude of the ACC signal after an increase of about 10 decibels showing a linear correlation. Signals of lower amplitude were obtained in suprasternal notch and laterally to cricothyroid cartilage in relation to cricothyroid cartilage midline. The decrease in amplitude alongside the distance to the generator (i.e. vocal fold) enhance the ACC capacity to record air-to-tissue transmission of aerodynamic energy through the trachea.[216] When the ACC was placed laterally to cricothyroid cartilage, it recorded similar amplitudes as in suprasternal notch hence greater proximity to the vocal fold. Nolan and colleagues (2009)[212] showed higher magnitude of 200 Hz signals during vowels pronunciation when a three axis was placed laterally at glottis level. A more detailed distance was reported by Mamun and colleagues (2014),[211] who showed a lower ACC energy signal about 1cm laterally to midline at glottis level during a swallowing task. The lower amplitude may be explained by the increase of thyroid and other neck soft tissues with lower vibration memory in comparison to cartilage.[211,216]

The latency to words phonation depends on the task and instructions, the experimental conditions and the performance of the subjects. In other studies, when the subjects were instructed to say one or two syllables words after an electrical stimulus applied at the finger, the time to react was about 200 ms. In our study, using a PNt with random pictures presentation, the latency to phonation of about 500ms in baseline recordings was similar to those reported in literature which used an ACC to voice detection.[199]

We instructed the subjects to pronounce the picture name with a correct syllable articulation and with conversation volume tone. In other words, in comparison with to other reported experiments,[201] we suggest a words pronunciation prioritizing an efficient phonation and just secondly the velocity. Considering these differences, when performing the experiments, pitfalls related to level of attention, readiness to pronounce and articulation of the words were identified.

The readiness to pronounce words and syllables articulation also exerts effects on duration and consequently the graphical representation of ACC signal (fig 9.2). When subjects do not articulate syllables, an incorrectly phonation due to anticipation or increased velocity may decrease the duration of ACC recordings. Conversely, phonation of words with increased pauses between syllables led to increased duration and a pause between ACC bursts recordings. In studies where a microphone is used to record voice, these caveats are already take into account because of the availability of subjects' pronunciation sound. Thus, examiner experience with microphone voice recordings may improve the control these factors during phonation ACC recordings.

4. Phonation accelerometer recordings reliability and utility

The use of the ACC to record the vocal vibration has been applied to study vocal resonances and deglutition in comparison to microphone recordings, which is considered the gold standard technique.206 Despite of the less hardware being needed to perform ACC recordings, most of the laboratories that have done these studies were equipped with both techniques and therefore gained experience in microphone recordings analysis before making ACC recordings of phonation. In our study, comparisons with microphone recordings were not performed, but instead we tested the recordings variability within and between subjects after defining baselines. We advocated that after testing the practical aspects of the ACC settings, we would be able to adapt the methodology to record words pronunciation and assess the reliability of the technique.

In this study, ACC recording of words pronunciation was considered a reliable technique. The variability was greater when performing recordings of the same word between distinct subjects than within the same subject (i.e. amplitude variability within subjects of 0.89 SD=0.10 vs between subjects of 0.87 SD=0.12; duration variability within subjects of 0.94 SD=0.03 vs between subjects 0.92, SD=0.07). Lien and colleagues (2014)192 assessed similar reliability of ACC recordings at suprasternal notch to identify the vocal tract physiologic vibration frequency. However, slightly variations of the ACC position around sternal notch showed different recordings magnitude,[212] which may obscure the reproduction of these experiments. Besides, when performing the baseline recordings in patients, the conditions of the experiments should be kept the same between sessions.

The fundamental natural frequency identified in our adult subjects was 120 Hz for males and 170 Hz for females at suprasternal notch (table 9.2). This frequency is known to be altered by age, height213,214 and pathophysiological conditions.198 Higher frequencies were seen in women and in younger population (i.e. 300 Hz between 6 to 12 years of age), probably due to smaller vocal tract length and diameter. [198,213] We also ensured a similar body mass index and age within

the healthy subjects and patients. To our knowledge the baseline collected data was the first described in the Portuguese population.

In the neurological field, some studies have already reported the use of ACC in voice production experiments to detect phonation after repetitive magnetic brain stimulation during a PNt.199 However, none investigated their clinical application to detect dysphonia. In our study, to provide proof-of-concept, we recorded words pronunciation in patients with voice hoarseness during laryngitis. Our goal was to detect the expected decreased amplitude and test the ACC capacity to detect a decreased frequency (table 9.2). In fact, duration was also decreased but without statistical significance. Other authors, already reported the decreased natural frequency in patients with dysphonia[202,204] and our results are in accordance. Despite the inability to identify resonance, vocal effort and other voice measures due to simpler hardware and software used, the pathological characteristics imposed by dysphonia were easily detected.

5. Limitations

We evaluated the ACC signal as a representative of vocal cord vibration during word pronunciation. We defined criteria to select which was considered an optimal biomedical signal derived from phonation. Therefore, a selection bias may have occurred. For example, the variation of the ACC signal was minimized by the criteria defined to increase repeatability. Although, physiological contribution of surrounding structures involved in phonation could also be excluded. In fact, the parameters evaluated may not reflect the burst morphology. For example, the word leg or finger showed a minor amplitude in the onset in comparison with the burst end (see appendix) which does not translate in the maximum peak-to-peak amplitude. Moreover, the methodology for parameter extraction from ACC recordings was handmade and not exact, mainly regarding to the frequency analysis. For frequency evaluation, recordings were analyzed by using a 50 μsec per division sweep. The scoring was evaluated and counted using a 500 μV per division which may mitigated the presence of low frequency artifacts (i.e, due to decreased amplitude). Additionally, patients just pronounced five words of the 24 words set which may affect duration if, by chance, words of smaller duration were chosen (which was not the case). The number of days after the initial hoarseness detection by the subject were also not controlled, which explains the increased SD (table 9.2) of the ACC parameters in comparison with baseline recordings, due to the different grade of vocal cords edema. At last, the sample of patients recruited was small, mainly regarding the male subjects and therefore, data should be confirmed using greater sample.

Conclusion

The vocal cord vibration during speech recorded by a uniaxial ACC showed an optimal setting using the suprasternal notch site with a bandwidth filter of 20-200 Hz. Using this setup, ACC baseline recordings showed a high reliability between and within subjects when pronouncing the same word. This technique was able to detect the expected decreased amplitude and frequency in patients with laryngitis.

Appendix

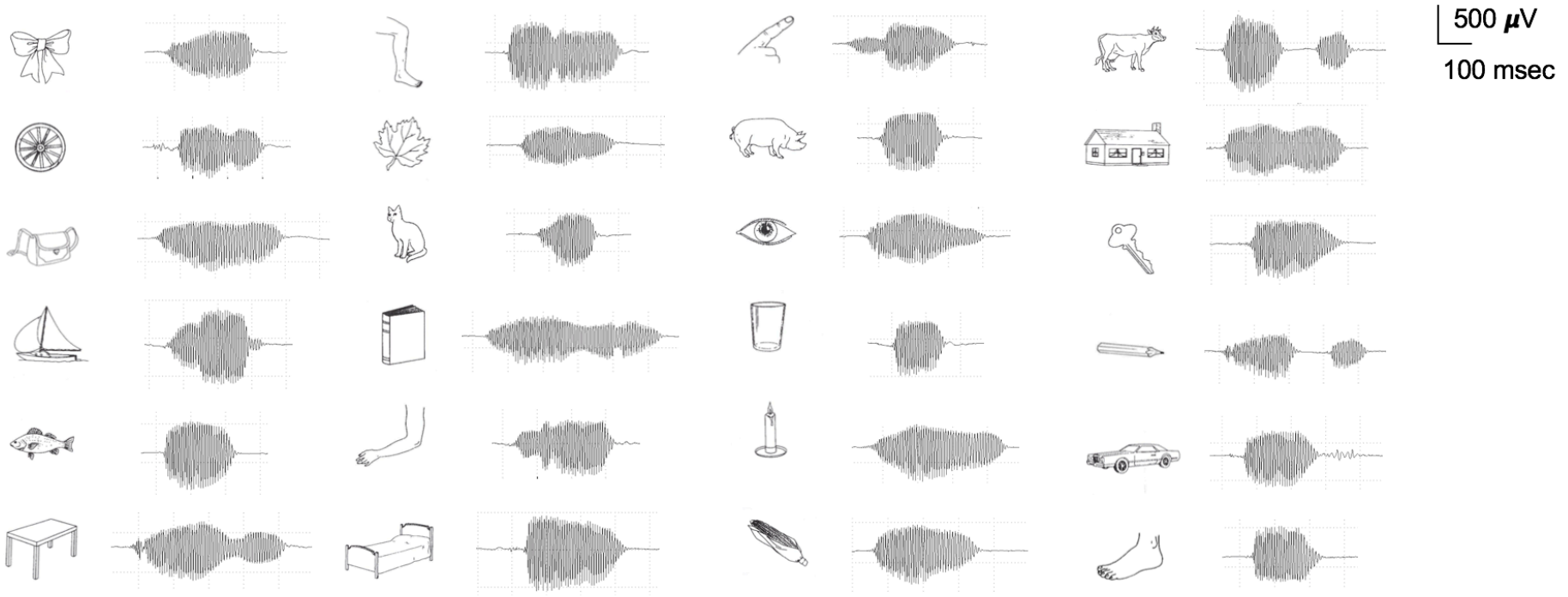

Figure 9.4– Graphical representations of accelerometer signals recorded after words pronunciation in Portuguese. The words defining each picture were said as following described (left to right within the same row, English and Portuguese word): lace-laço; leg-perna; finger-dedo; cow-vaca. Second row: wheel-roda; leaf-folha; pork-porco; house-casa. Third row: purse-mala; cat-gato; eye-olho; key-chave. Fifth row: boat-barco; book-livro; glass-copo; pencil-lápis. Sixth row: fish-peixe; arm-braço; candle-vela; car-carro. Seventh row: table-mesa; bed-cama; corn-milho; feet-pé. Note that the word table in Portuguese may have two bursts depending on the subject readiness.

This page was intentionally left blank

CHAPTER X

ACCELEROMETER BASED SPEECH RECORDING AFTER BRAIN STIMULATION

Introduction

Speech implies activation of a complex brain network that normally reaches full development at pediatric age. Many brain lesions may cause speech disturbances. Therefore, patients with PBT should undergo presurgical planning to anticipate the location of sensitive regions.[115] For the study of human language function preoperatively, Pascual-Leone et al. (1991)[25] proposed the use of rTMS, to non-invasively identify language sensitive brain regions. This method in combination with optically tracked stereotactic navigation system (r-nTMS), has led to the identification of language processing regions and lateralization, minimizing the risk of iatrogenic lesions during surgery. [16,217,218] Recently, Sollmann et al. (2018)[16] showed an additional improvement of outcome from surgery of patients with gliomas by adding tractography to preoperative r-nTMS.

DCS is presently applied to conscious and cooperative patients during speech in order to produce transient language disturbances to identify eloquent regions. However, even if awake craniotomy has had a positive impact on postoperative outcome,[220] the reliance on false negative sites may result in permanent language deficits.[221] Moreover, language disturbances evoked by DCS in the operative theater are, conventionally, qualitatively evaluated by a neuropsychologist or a neurologist, which is a relevant weakness of the procedure. Speech can be recorded using a microphone, which implies increasing cost and complexity of the procedure due to of additional software and hardware.[206] We advocate that to enhance speech recording and speech analysis in clinical setting, a conventional and inexpensive equipment should be available. Furthermore, for intraoperative setting, microphone recordings are difficult to be implemented due to signal noise. An ACC attached to the anterior wall of the neck can, indeed, record a surrogate aspect of speech, i.e., the vibration generated by the passage of air in the vocal cords. [199,223] The ACC recordings show at some extent reproducible and word-specific high frequency oscillations.[223] However, they have not been analyzed regarding to the type of language disturbances evoked.[199] In addition. the utility of ACC recording of DCS-induced language disturbances during surgery remain to be investigated.

The goal of our study was to evaluate the value of the ACC vocal tract recording in demonstrating transient language disturbances provoked by r-nTMS in classical linguistic areas during PNt in healthy patients and examine the utility of ACC recording during DCS in awake patients during surgery.

Methods

We carried out two different studies with the same procedure: The first study included 7 healthy subjects (HS), in whom we applied r-nTMS over IFG. They were 4 men and 3 women, all right-handed, with a mean age of 30 years, ranging from 26 to 31 years. Their body mass index was 22±2 kg/m^2; The second study involved 15 BST undergoing awake craniotomy for removal of PBT. The selection criteria were similar to those mentioned in chapter VI. Patients with PBT near motor or language, absence of aphasia, without known contraindication for TMS and MRI (i.e. pacemakers, ferromagnetic prosthesis), and in addition, with left language lateralization as evaluated by presurgical fMRI. They were 10 men and 5 women, with a mean age of 47 years, ranging from 31 to 68 years, and a body mass index of 24±3 kg/m^2.

HS experiments were carried out in Hospital Clinic (Barcelona, Spain) and patient experiments were carried out in the Hospital Garcia de Orta in Almada (Portugal). Ethics Committee of each hospital approved the study protocol and an informed consent was signed by all healthy subjects prior to their inclusion in the study. Subjects were briefed on the effects of single and r-nTMS and were encouraged to ask for a pause in case of any discomfort. They were also instructed that speech arrest could occur and were given reassurance that any language disturbance caused by stimulation would spontaneously resolve without any consequences. Because of the possibility that the stimuli could spread and activate cranial nerves, we recorded EMG activity from masseter muscles: Recording silver cup electrodes were placed in the masseter muscle (reference electrode in the ear lobe) with filter settings between 2 Hz and 5 kHz, a time resolution of 1ms per division and a gain of 10 μV per division. Also, subjects were asked to report any feeling of interference in word pronunciation by unintended mandibular or temporal muscles contraction. Whenever subjects' sensation of interference or motor evoked potentials were evident on the EMG recordings, the trial was repeated after slight adjustment of the stimulation characteristics (see below).

1. Recording word pronunciation

The experimental procedure, PNt and the ACC used for word pronunciation was the same described in previous chapter. Five pictures were also selected from the 24 set showed in appendix

of the chapter IX. In addition, the ACC was attached in the optimum site, 2 cm above the suprasternal notch, in the midline between the two sternal heads of sternocleidomastoid muscle, and optimum filter bandwidth (i.e. 20-200 Hz).

2. Imperative stimulus and time to word pronunciation

The protocol used for image presentation is schematically represented in figure 10.1. Subjects were instructed to wait for the visual stimulus and name the object represented in the picture, as fast and as correctly as possible. We also ensured a high level of attention during the experiments by controlling the latency to word pronunciation after visual stimuli.

3. Mapping of the motor and language areas with r-nTMS

HS made a MRI for 3D T1-weighted images aquisiction that were then transferred to the navigational system (BrainSight, NeuroConn, EUA). 3D skin and curvilinear reconstructions were made for IFG localization. We then calibrated the magnetic coil of the TMS equipment (Magstim Rapid, UK) in the navigation system in order to provide the orientation and direction of the coil.

Initially, the central sulcus was used as a landmark to ensure that the direction of the current flow was anterior-posterior and orthogonal. Surface felt pad electrodes mounted on a plastic support with a fixed separation of 2.5 cm were placed to record motor evoked potentials from the right 1º dorsal interosseous muscle. The left precentral gyrus was mapped with single pulse TMS, applied following a grid pattern of 5 mm spacing and systematically varying the rotation, tilt and yaw of the magnetic field to search for the motor evoked potential of maximum amplitude at each stimulation point. After finding the motor "hotspot", we decreased the stimulus intensity to identify the lowest intensity that evoked 5 out of 10 motor evoked potentials with at least 50 μV amplitude, to define the resting motor threshold intensity.

Language mapping over the opercular part of IFG (i.e. opIFG) was performed using the r-nTMS system, with a protocol of a 5 pulses train, 20 Hz stimulation frequency and the subject's 100% RMT.[220,224] The r-nTMS pulse train was automatically triggered by an electronic trigger at the same time as the visual stimulus for PNt.[225] A 10% decrement of intensity was made if subjects were unable to tolerate the cortical mapping. Stimulation sites (i.e. primary motor cortex and opIFG) were identified in an offline session using a cortical parcellation system[15] and used to guide cortical mapping. The landmarks of all points stimulated were recorded online for later review. Several stimulation trains within IFG and the corresponding r-nTMS induced behavioral changes were videotaped. We run 50 trials in each subject of HS, 7 of them were test trials per

each word selected (picture presentation plus r-nTMS), which were interspersed randomly among the control trials**.**

4. DCS mapping

We recorded word pronunciation in patients submitted to awake craniotomy while they performed a PNt for brain language eloquent cortical mapping. All patients had a preoperative MRI and craniotomy was planned using a navigation system (Stealth, Medtronic, USA) to include the extension of the tumor and a 3-cm margin of healthy surrounding brain tissue. After craniotomy and durotomy, the patient was woken-up and the primary motor cortex was mapped while the patient performed a counting task to establish the appropriate DCS intensity. For language mapping, the defined threshold was used to map the patients' opIFG as they performed a PNt.

DCS was a biphasic square current of 60 Hz, delivered over the opIFG with a bipolar probe (see chapter III for further details). The protocol used for brain stimulation is also shown in figure 10.1. Language cortical areas were mapped before tumor resection. Patients were proficient in using the Portuguese language. Instructions during PNt involved the inclusion of the matrix sentence *"This is a..."* to be completed with the name of the object presented in the image. A rehearsal was done previously to avoid any possible confusion with the words defining each object. They were asked to use a voice conversational volume and tone of voice in their responses. In addition, subjects and patients were instructed to name the picture as correctly as possible despite of the time to react**.** In BST, 30 trials were performed, and 3 test trials per word were given randomly. In addition, at operative room, the visual stimulus was shown simultaneously with an auditory sound. The surgeon was instructed to apply the probe (and DCS) over the IFG after the produced auditory sound. Each visual stimulus was presented for 4s, which implied a rhythm for the PNt that allowed the surgeon to know and expect the auditory sound.

5. Data reduction and statistics

The presence or absence of language disturbances in test trials were evaluated by the author and either a neurologist or neuropsychologist in both groups. We detail the language disturbance type founded. These were grouped, and the following consensual criteria, was used for recognition of evoked language disturbances: 1. no-response (subjects did not utter a word, in which case, the ACC recordings were expected to be flat), 2. imperfect pronunciation (words were slurred or imprecisely articulated, in which case, the ACC recordings would be expected to differ from mean control trials), 3. hesitation (delayed onset of naming, in which case, the ACC recordings would be expected to be delayed) and 4. others (including semantic or phonologic paraphasias and circumlocution errors, in which case, the ACC recordings would be expected to show a pattern

not pertaining to the word related to the presented image). Initially, after each test trial, two opinions were given by the specialists regarding the presence and type of a language disturbance evoked before ACC and videotape recording review. In case of discrepancy, the case was debated together with the examination of the videotape until reaching consensus or dismissing the case.

For each one of the recordings, we measured onset latency, mean amplitude, total duration and internal frequency of the vibration-induced oscillations related to each word. Whenever the word-related recordings showed more than one burst, data were gathered for each burst separately (burst 1, burst 2, etc) and a mean was shown. We ignored deviations from the baseline with less than 50 μV and bursts of less than 5 consecutive oscillation cycles. For each word, we recorded 4 traces and calculated the means for each parameter. We considered the data in control trials as the individual baseline recordings, which were used as reference values for data in test trials. Differences with respect to control trials were required to be larger than 2 SD from the controls' mean value to be considered a disturbance.

We used the SPSS Statistics (v.24, IBM, USA) for the statistical analysis of data. Normality was tested with the Shapiro-Wilk test and homogeneity was examined with the Levene test. We ran descriptive statistics of mean and standard deviation of the ACC parameters. Comparisons between healthy subjects and patients or between control and test trials were done using (parametric) paired t-tests.

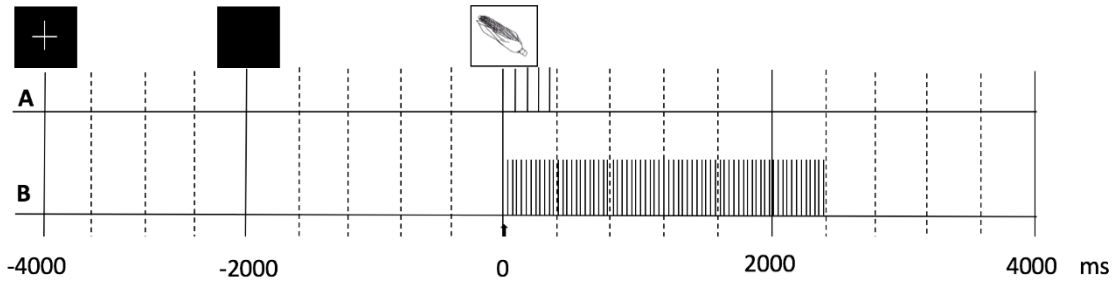

Figure 10.1 – Picture naming task protocol used to evoke language disturbances by brain stimulation (arrow). The protocol A was performed with transcranial magnetic stimulation. For each trial, a black background screen was presented first, containing a centered white "X" letter, as an attention fixation cue. The "X" disappeared as a forewarning sign and the picture appeared 2 s later. In a test trial, repetitive transcranial magnetic stimulus at the opercularis part of left inferior frontal gyrus was applied. The protocol B was used during direct cortical stimulation at the left inferior frontal gyrus. The patient was to name the picture with the introductory sentence "This is" while a train of byphasic 1 ms duration pulses was applied at a frequency of 60 Hz and an intensity of 5 mA, until a language disturbance occurred or up to a maximum duration of 4 s.

Results

1. Data obtained in healthy subjects

The words selected to perform the PNt were the following: car *"carro",* finger *"dedo"*, pencil "lápis", leg *"perna"*, and foot *"pé"*. Examples of the ACC recordings is shown in figure 10.2. These were selected randomly. In control trials, the ACC recordings were word-specific, individually patterned and with just a few differences between subjects, as expected. The complete set of recordings is shown in appendix, where recordings are kept for gain and resolution but aligned at onset, after eliminating the intra- and interindividual differences, for better visual identification of the similarities between word-specific recordings. There were no significant interindividual differences in control trials per word (repeated factors ANOVA; $p>0.05$ for each word) after ensuring conversational tone and correctly articulation of the syllables. However, when separated by gender, females had a higher frequency of oscillations than males. For the words 'carro' and "pé", the mean frequency was 174 Hz with a SD of 8 Hz and 180 Hz (SD=6 Hz) for females and 135 Hz (SD=8 Hz) and 140 Hz (SD=6 Hz) for males, respectively (t-test; $p=0.001$). Parametric mean data in control and test trials for each word are summarized in Table 10.1.

None of the healthy subjects had to be excluded from the experiment due to non-tolerability or adverse reactions to TMS. No subject exhibited emotional disturbance, headache, tongue bites or seizures during or after cortical mapping. However, two healthy subjects reported discomfort due to strong facial muscle contractions with brain stimuli, which disappeared after adjusting the intensity to 80% of RMT.

Speech disturbances were observed in at least one test trial per subject and for two times per word, for a total of 16 language disturbances out of 105 test trials (15.2%). Examples are shown in figure 10.2. We identified: 5 no response, 5 hesitations, 4 words pronunciation imprecision and 2 semantic paraphasia. In four trials with hesitation error, the two evaluators had a discordant judgement, which was solved by checking the videotapes. In these cases, was decided in favor of performance errors. Retrospectively analyzing both ACC recordings, was noted in both a latency increase of 112 ms and 128 ms in comparison to the subject's mean of control trials (more than 2 SD). In test trials with no response errors, latency increased and amplitude decreased significantly in comparison to control trials (table 10.1). No significant differences were found in duration or frequency in test trials.

The masseter muscles were activated in 94% of the trials. Ipsilateral masseter activation response was obtained with 2.2 ms (SD= 0.8 ms) with a peak to peak amplitude of 31 μV (SD=12 μV) and contralateral motor evoked potentials with 13.4 ms (SD=1.3 ms) with 84 μV (SD=14 μV). We managed to decrease the masseter muscle activity to below 100 μV either by aligning the coil with temporalis muscle or decreasing intensity by 10% of the maximal output (i.e. in three patients). Although, a total of 23 test trials were excluded due to masseter muscles activity.

2. *Data obtained from BTS*

Demographic characteristics of the 15 craniotomy patients that were examined in the operating room are shown in table 10.2. All patients were right-handers and had Portuguese as their mother language.

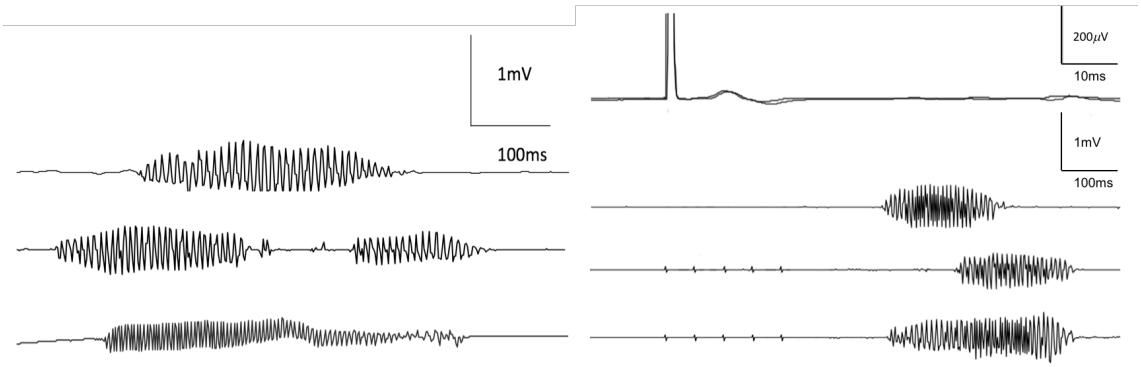

Figure 10.2 – Examples of accelerometer (ACC) recordings placed in suprasternal notch using a filter bandwidth 20-200 Hz. Left: words pronounced from top to bottom are finger (in portuguese, "dedo"), pencil ("lápis") and leaf (in portuguese, "folha"). We measured the total duration present, the maximum amplitude and the frequency (phases divided with burst duration) for each word. Note the increased frequency of the bottom trace acquired in female subject. Right: ACC recordings of words phonation and language disturbances (i.e. traces with stimuli artifact) evoked during a picture naming task (PNt) after brain magnetic. In top traces, ipsilateral masseter compound muscle action potential of both test trials was superimposed. In test trials it was possible to identify a latency increase (i.e. hesitation) in comparison to the control trial. Also note a semantic paraphasia (bottom trace) with the subject saying hand "mão" instead of finger.

Seven patients (46.7%) presented tumors localized in frontal lobe, six (40.0%) in the temporal lobe and two in the insula. Forty-eight hours after surgery patient number 6 showed a conduction aphasia which resolved 3 months after surgery.

Cortical mapping was done after anesthesia withdrawal, with the patient in a comfortable position, without pain and with an adequate visual field for PNt. DCS was performed using a mean intensity (i.e. threshold of action) of 3.7 mA (range from 3 to 5.5 mA). None of the patients presented seizures or tongue bites during or after DCS. However, in four patients were recorded after discharges which resolved with a prolonged pause of DCS and brain cold ringer lactate. Therefore, these were excluded from language disturbances analysis

Table 10.1 – Accelerometer recordings parameters evaluated after brain stimulation at opercular part of the inferior frontal gyrus with navigated magnetic transcranial stimulation in healthy subjects. Standard deviation is presented between parenthesis.

	Onset latency		**Mean amplitude**		**Total duration**		**Mean frequency**	
Word	Control	Test	Control	Test	Control	Test	Control	Test
Car	493 (32)	697 (58) p=0.023	855 (144)	574 (202) p=0.032	240 (21)	213 (35)	151 (8)	157 (13)
Finger	515 (38)	723 (42) p=0.012	879 (158)	425 (189) p=0.021	320 (31)	282 (42)	149 (9)	137 (16)
Pencil	482 (29)	684 (49) p=0.029	1005 (125)	595 (212) p=0.011	378 (15)	347 (49)	156 (7)	159 (11)
Leg	534 (43)	692 (63) p=0.042	1195 (112)	674 (231) p=0.018	360 (21)	339 (31)	154 (10)	145 (18)
Foot	497 (31)	659 (54) p=0.038	875 (123)	467 (176) p=0.014	216 (13)	189 (56)	161 (7)	151 (17)

Table 10.2 – Demographic characteristics, presentation symptom, tumor location and histology of the patients enrolled to intraoperative direct cortical stimulation (DCS) in awake craniotomy.

Patient	**Gender**	**Age**	**Symptom**	**Location**	**Histology**	**DCS intensity (mA)**
1	Female	35	Seizure	T	A	3
2	Male	31	Seizure	F	OD	3.5
3	Male	46	No	I	A	3.5
4	Male	57	Seizure	T	GBM	5
5	Male	50	Memory loss	P	A	4
6	Male	68	Seizure	P	GBM	4
7	Female	31	Seizure	T	A	3
8	Female	66	Headache	T	GBM	3
9	Male	48	Seizure	F	A A	5.5
10	Female	40	Seizure	I	NGT	3.5
11	Male	54	Seizure	F	OD	3
12	Male	38	Headache	F	OD	3.5
13	Female	38	Seizure	T	A	4
14	Male	61	Seizure	T	OD	4
15	Male	40	Seizure	F	A A	3.5

A – Astrocytoma, A A – Anaplastic Astrocytoma. F – Frontal, GBM – Glioblastoma, T- Temporal, I – Insular, P-Parietal, NGT – Neuroglial tumor, OD –Oligodendroglioma, OD A – Oligodendroglioma Astrocytoma.

DCS was able to evoke language disturbances in all the patients at opIFG but one (i.e. patient number 9). An error rate of 57.0% was obtained in the total 150 test trials, leading to a mean of 5.6 positive test trials per patient for language function. Two examples of DCS evoked language disturbances are demonstrated in figure 10.3. In total, 84 language disturbances were evoked after DCS consisting in 28 hesitations, 21 pronunciation imprecisions, 16 no response errors, 2 neologism and 3 semantic paraphasia. Similar to HS analysis, for 10 occasions, the authors disagreed on the presence of a language disturbance (11% of the test trials). In these cases, videotapes were consulted. In 2 cases, were identified hesitation errors. However, in the other 8 test trials (occurred in patient 2, 3, 11 and 15) imprecise pronunciation errors were identified. To reassure a language function at that sites, DCS was repeated after a mean intensity increase of 0.8 mA (SD= 0.3 mA) resulting in 4 speech arrest, 2 hesitation errors and 2 semantic paraphasia. In these cases, before adjusting intensity, the following latencies and amplitude were obtained: 1143 ms, 1227 ms, 1089 ms and 643 μV, 697 μV, 584 μV, respectively. Despite of the latency increase and amplitude decrease in comparison with control trials, no statistical significance was obtained (p=0.067). ACC evaluated parameters are summarized in table 10.3. As in HS, significant differences were seen in amplitude and latency of the test trials in comparison with control trials.

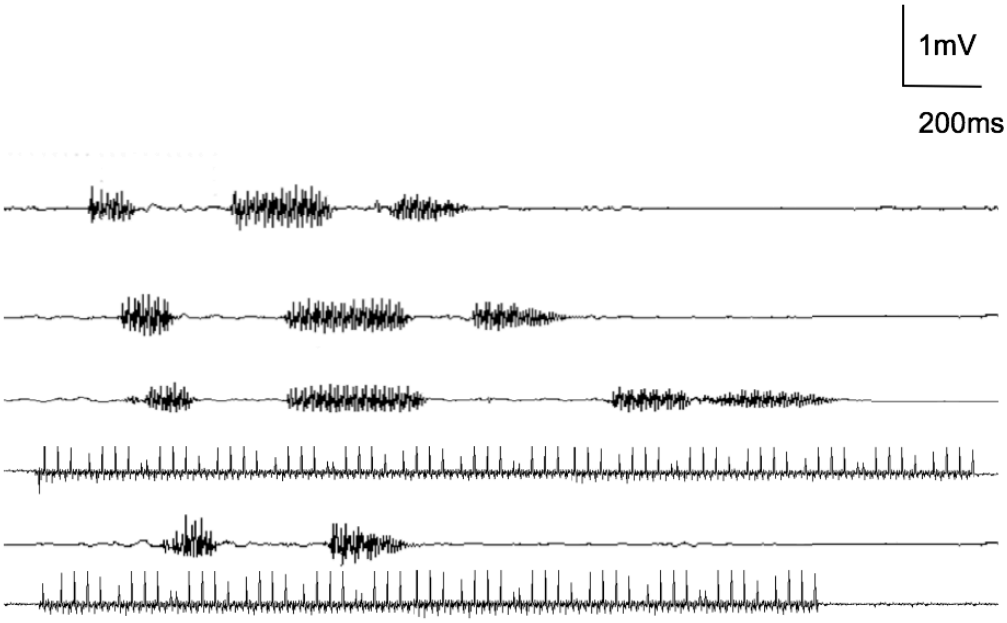

Figure 10.3 – Accelerometer recordings made during awake craniotomy direct cortical stimulation. From top to bottom: the first two traces were made after the patient pronunciation “this a foot, this is an arm” without brain stimuli (i.e. control trials). In last two traces are shown test trials with a stimuli artefact below accelerometer recordings In the third trace is shown a example of a hesitation error with an increase latency between the introductory sentence “this is” and the word” leg”. Also note an example of speech arrest after brain stimulus at the bottom trace with just the pronunciation of the word “this is”. Note also the smaller burst regarding the word “is”.

Table 10.3 – Accelerometer recordings parameters of word pronunciation after direct cortical stimulation at opercular part of the inferior frontal gyrus patients during awake craniotomy. Standard deviation is presented between parenthesis.

	Onset latency		**Mean amplitude**		**Total duration**		**Mean frequency**	
Word	Control	Test	Control	Test	Control	Test	Control	Test
Car	934 (234)	1632 (185) p=0.019	1032 (284)	364 (141) p=0.024	342 (47)	376 (82)	158 (6)	154 (11)
Finger	1134 (238)	1863 (342) p=0.025	982 (253)	397 (152) p=0.036	422 (67)	483 (98)	151 (7)	147 (14)
Pencil	869 (229)	1322 (149) p=0.041	993 (196)	381 (79) p=0.016	457 (58)	493 (78)	152 (10)	155 (9)
Leg	1231 (383)	1721 (133) p=0.029	1024 (229)	582 (196) p=0.028	438 (81)	485 (67)	147 (9)	143 (11)
Foot	996 (376)	1432 (301) p=0.038	793 (211)	295 (96) p=0.029	284 (53)	317 (88)	159 (12)	154 (12)

Discussion

Language disturbances evoked during presurgical and intraoperative brain mapping remain only qualitatively appraised. In our study, a ACC signal recorded from infraglottic structures using a EMG equipment was used to detect language disturbances. This method traduced phonation vocal tract oscillations, word-specific at some extent, providing a reliable quantification of the evoked language disturbances. For this purpose, healthy subjects and patients were recruited to perform a PNt while received r-nTMS and DCS at a opIFG (i.e. Broca area), respectively. Brain stimuli perturbed speech processing noted by increasing the time to word pronunciation (hesitation errors) and by slurring or decreasing the speech volume tone (articulation imprecision errors) in addition to speech arrest errors. ACC recordings correlated with clinical errors in the identification of language disturbances. In our study, we showed the utility of ACC words pronunciation recordings in presurgical planning. We also stressed out his complementary role in awake craniotomy during language brain mapping by clarifying and then identifying 11% more language disturbances.

1. Speech recording with an ACC signal

The vocal tract resonances after vocal cord activation, induces oscillation movements in the adjacent glottis structures.[226] These can be documented by using a piezo crystal sensor to record movement during a certain time (i.e. accelerometry). ACC use to record speech was already

described in voice studies[227,228] and to detect words or syllable phonation. [199,200] However, in these studies vocal tract accelerometry was used aiming to detect movement as a gross motor activation. Therefore, authors analyzed individual parameters such as frequency or time from IS to phonation without studying the signal pattern during a specific word phonation. Our work group argue that within a controlled environment and trained instructions, subjects pronounce the same word in a similar way without significant changes in ACC recordings of appendix (figure 10.4), review previous chapter for further details).[223] Therefore, we hypothesized that ACC recording characteristics should be used in clinical circumstances where speech production data remained to be quantified and their analysis could alter the course of clinical interpretation.

In this study, we placed a uniaxial ACC to record speech 2 cm above the suprasternal notch using a filter bandwidth of 20-200 Hz. We selected this setting in order to enhance recordings amplitude avoiding artefact contamination by neck muscles activation at intraoperative electrical hostile environment in comparison with cricothyroid level. The recordings were made while subjects and patients took a PNt using 5 pictures set presented randomly where within the control trials was given a brain electrical stimuli.

In order to individualize the effect of the brain stimuli, subjects "baseline" recordings were first made. The mean frequency obtained in ACC recordings was about 30 to 60 Hz lower in males and females respectively, than those reported in voices studies also performed with adult subjects.[227] We attributed this difference to the low magnitude of higher frequencies in suprasternal notch in comparison with other neck sites.[213] Nevertheless, the gap between males and females subjects found showed similar magnitude (between 30 to 40 Hz) to the reported studies.[215]

The mean latency to words pronunciation in PNt control trials is also in accordance to those previously reported. [199,226,227] A greater latency was observed in patients performing PNt during awake craniotomy (table 10.1 and table 10.3). Such difference may be explained by the use of an introductory sentence in order to distinguish the etiology of a no response errors.[141] Additionally, BST are under pharmacologic effects of analgesics (i.e. remifentanil), anti-convulsive drugs (i.e levetiracetam) and at some extent, sedation (i.e. propofol) not used by HS. Moreover, the former group is exposed to an environment where the experimental instructions given regarding to readiness and tone volume are less rigorous.

2. *r-nTMS mapping in healthy subjects*

Evaluation of motor function in patients with PBT using single pulse and navigated TMS, showed either to increase gross tumor resection when performed presurgically[228] or to predict functional outcome when performed after surgery.[229] In addition, almost perfect correspondences were reported between sites with motor function identified by navigated TMS and DCS.[219] However, language function in most instances are not disturbed by single nTMS and a repetitive train of stimuli must be used. [25,27,230] Still, the correspondence between sites with language function identified by r-nTMS and DCS remains sparse. Nevertheless, presurgical r-nTMS for language function influence in about one third of a decision-making process of neurosurgical patients. [231,232] For this purpose, data quantification review of the language disturbance evoked by brain stimuli may support the clinical evaluation in addition to videotape recordings.

We recruited a HS, right-handers to perform language function mapping with r-nTMS. No previous knowledge about language lateralization of the selected subjects was gathered. Yet, a high proportion of right handers subjects are known to have a left hemispheric language lateralization.[233] The protocol used for stimulation was optimized according with the recent reported studies.[220, 225, 233-236] In order to obtain a high error rate, we selected an object naming task and applied r-nTMS at opIFG.[233] Moreover, due to the lower number of test trials, we selected a high stimuli frequency (i.e. 20 Hz) with a train of 5 pulses.[79, 234] In our study a similar error rate was obtained in comparison to those already reported, consisting the majority in hesitations errors and no response errors.[219, 233-236] However, the error rate evoked by TMS was less than half obtained with DCS in BST. In accordance with Krieg et al (2017),[225] numerous stimulations of r-nTMS are needed at the same site to perturb cortical circuits involved in language function. Therefore, trained and independent specialists should evaluate the presence of disturbances to minimize misinterpretations in addition to session videotape review.

Vitikainen et al. (2015)[199] suggested a ACC based method to automatically and quantitatively detect the voice onset after r-nTMS. They recorded an analog signal from a three axis ACC placed at submandibular level where the vibration of vocal tract was considered higher than other neck sites. They used a EMG system built in TMS equipment with a 10-500 Hz bandwidth filter and 3 kHz sampling rate. Using this method, a sensitivity of 96% and a specificity of 71% was reported for the voice onset detection in comparison with the language specialist offline evaluation. The low specificity of the method was attributed to the throat, extra voice movements before the response and to trigger related problems. In spite, of some similarities with our methodology, we advocate that the ACC based method is useful to either detect the onset of vocal tract vibration and to appraise signal oscillations in a way that one could recognize pronunciation activation

patterns. In such a way, that speech recording showed word-specific oscillations if the influence of physiological factors such as tone and articulation velocity was reduced. Once the control trials were performed, a visual oscillation signal (with a set of baseline parameters) was provided and differences were more easily recognizable whenever a discordant evaluation was given by specialists. Our results showed that ACC recording method was able to detect errors where the latency to onset was either absent (i.e. no response) or delayed (i.e. hesitation errors). The no response errors are known to be more frequent when a high frequency r-nTMS is used.[236] Whereas hesitation errors are frequent when mapping the IFG, [223,236] but both type of errors were easily identified in real time clinical evaluation. In addition, the described method also detected a similar rate of errors where subjects imprecisely articulated syllables, lower their tone or substituted them for other sounds. These errors possibly led to a discrepancy between specialists' evaluation and led to ACC recordings consultation, depicting a mean latency or amplitude deviation greater than 2 of the mean obtained in control trials. These types of errors led in BST to clear no response errors after increasing DCS intensity which evoked an additional 11% language disturbances. We also recorded the masseter muscles to exclude an anarthria due to peripheral nerve activation and ACC artefact contamination (through volume conduction). In our study about 90% of the r-nTMS showed activation of the masseter muscles which were reduced by optimizing the stimulation technique.[237]

The influence of physiological aspects such as readiness, correct syllables articulation, level of attention and loudness in ACC recordings parameters also contribute to ACC parameters deviations. The mean latency to words pronunciation was expected to increase less than 20% of the individual mean latency obtained in control trials if he denied lack of attention. Similar evaluation was made to keep the subjects volume tone during words pronunciation equivalent to the mean control trials. However, the physiological factor more challenging was the velocity and correct syllables articulation which was reflected in burst duration. In order to decrease this factor influence, a series of control trials were made, before applying a test trial, instructing the subject to maintain similar word pronunciation velocity and readiness. We advocate that for further signal oscillation analysis based in ACC recording to recognize word-specific waveforms, detailed control of these physiological factors should be performed (see discussion of the previous chapter).

3. DCS mapping in patients

PBT surgical treatment aims the gross resection. Within the preserved brain tissue, eloquent parenchyma with cognitive or sensorimotor functions remains identifiable by DCS in awake craniotomy surgery.[11,238] Recent automated setups have been described with time synchronization between electrical navigated stimuli and language task with videotape and sound recording built

on an improved software.[239,240] Although, in most neurosurgery departments language DCS is performed with simpler setups while a language specialist in real time evaluate the presence and type of the language disturbances.[103,240]

In our study, a selected set of pictures was intraoperatively presented to patients with PBT. The PNt in operative theater slightly differed from the one used in HS. Intraoperatively, the time to the word defining the object presented was measured from the moment that the probe contacted the brain tissue. Therefore, the electrical stimulus was not triggered simultaneously with visual stimuli. Such technical limitation should not have influenced negatively the number of language disturbances. In fact, recent studies showed a similar ability of the r-nTMS at opIFG to evoke language disturbances when delivering the stimuli 300ms after picture presentation in comparison with simultaneously presentation.[224] In our setup, we estimate a similar delay of the electrical stimuli (in relation to the visual stimuli), yet the evoked error rate and patient outcome was similar to the previous reported studies.[219,239] Additionally, about 300ms after the visual stimuli presentation in a PNt, the word production is undergoing and may be accelerated if a loud stimuli is given (see next chapter for further discussion).

The disruption of language functions was possible in all patients but one (patient 9) after defining a higher threshold of action (minimum intensity to evoke a speech arrest during a counting task). However, in our study, the electrical stimuli did not evoked language disturbances using individual threshold of action (patient 2, 3, 11 and 15) but evoked with slightly higher intensity stimuli (mean of 0.8 mA). In these test trials, ACC recordings detected some (imprecision) errors which showed a non-significant parameters deviation after an assessment discrepancy between language specialists. These findings which could be interpreted as a DCS "false negative" for language function may in part be explained by: lack of sensitivity of the method used for language disturbances detection; tumor involvement of the opIFG in the frontal lobe[73] and neuroplasticity process's (patient 9)[237] not revealed in preoperative functional neuroimaging. Despite of the etiology, the ACC recoding's were able to detect a deviation from the mean parameters from control trials. Changes in the waveform pattern during control trials as and synchronic evaluation between stimuli and phonation, allowed further ACC recording's analysis instead of just voice onset (latency). Therefore, when occurring mild and articulation imprecision errors, quantitative and online data readily accessible from ACC demonstrated parameters deviations.

Conclusion

In this study, we recruited healthy subjects and patients to perform a PNt while brain stimulation was applied to infer the ability of an ACC to record infraglottic phonation pattern variations. ACC of words pronunciation was able to detect errors either through latency increase and oscillation pattern deviation in presurgical planning after r-nTMS. In awake craniotomy, a complementary role of the ACC allowed to detect subtle changes in latency and amplitude recordings in addition to the clinical evaluation.

Appendix

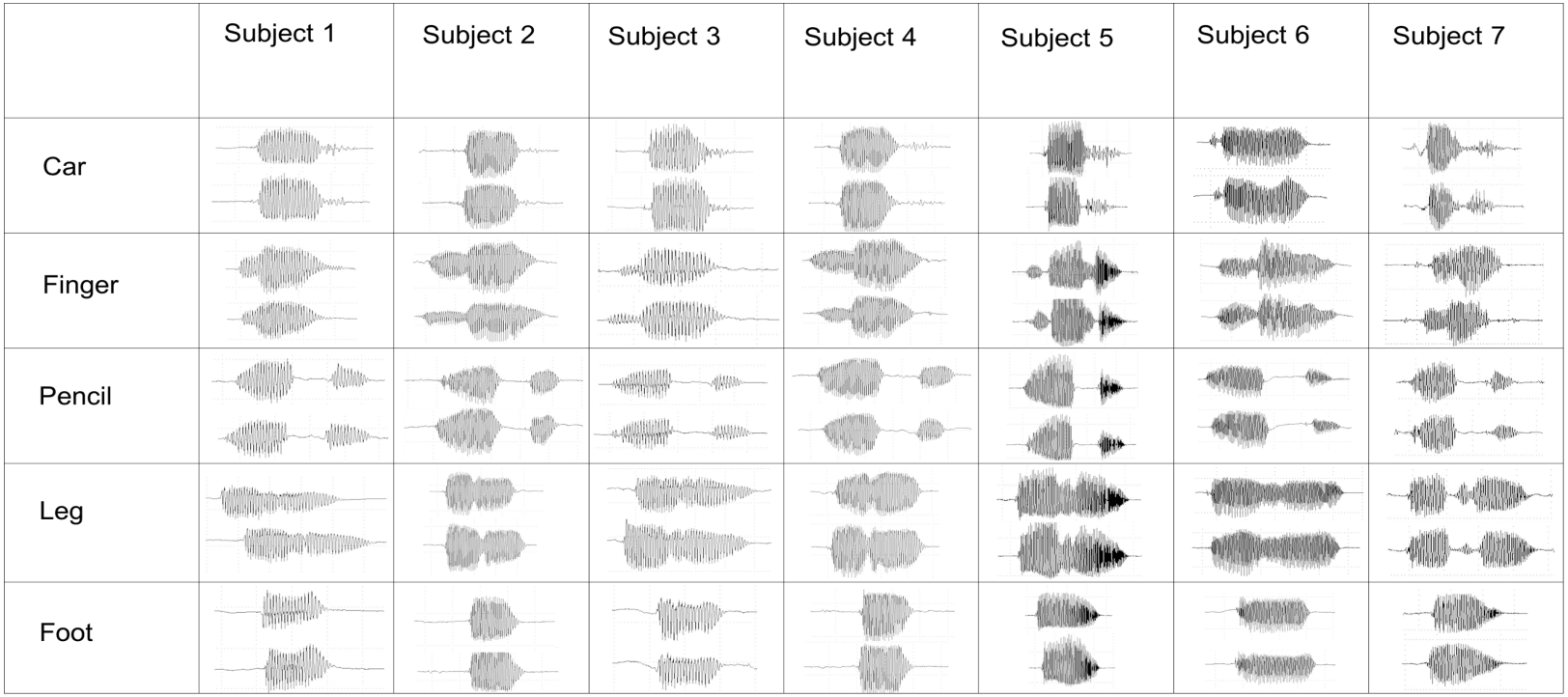

Figure 10.4 – Accelerometer recordings of five pronounced words by healthy subjects (3 female, from fifth to seventh subjects). Recordings were made after placing the acc at midline, 2 cm above the above sternal head, using a filter bandwidth of 20-200 hz.

CHAPTER XI

SPEECH EXECUTION: PREPARATION AND READINESS

Introduction

Preparation to perform a simple motor task implies enhancement of excitability in the structures required for its execution. In simple reaction time (RT) tasks, the readier the subject is for task execution, the lesser should be the requirement for cognitive processing.[241] It is under these conditions that the StartReact effect may appear, [242,243] i.e., a significant shortening of RT when a startling auditory stimulus (SAS) is presented together with the IS (i.e. visual stimuli).

A task undoubtedly involving cognitive activity is speech. [244,245] In one of their experiments, Stevenson et al. (2014)[200] showed that the StartReact effect was present in vocalization of a syllable, using this observation to support cortical involvement in the physiology of the StartReact effect. Indeed, speech is a motor task requiring more cognitive processing than moving a limb segment.[246] However, the relationship between cortical processes and speech production is not straightforward. There are example conditions in health or disease in which utterance of a word may be an automated action. This is the case with recurring utterances in aphasia patients,[247] some phonic tics in patients with Gilles de la Tourette syndrome,[248] mantra-type practices[249] or swearing in response to pain.[250] In all these examples, words can be uttered without intervention of cognitive processes or dedicated thinking.

We reasoned that through experimental manipulation it would be possible to diminish the cognitive processing needed for speech production to a minimum; this would allow subjects to prepare the articulatory channels for word pronunciation in advance and up to the extent that the StartRact effect could be made evident. We used the Snodgrass and Vanderwart (1980)[83] picture naming set to arrange for word pronunciation tasks with varying requirements of cognitive processing. In this type of test, when pictures are presented randomly, subjects require a high degree of cognitive processing to retrieve from memory the word corresponding to the object represented in the picture. [251,252] Consequently, we should not expect a StartReact effect in these cases since execution circuits cannot be prepared beforehand. However, we predicted that if we allowed subjects to know what picture to expect, then they could prepare the articulatory mechanisms corresponding to the selected word beforehand. If this is the case, the StartReact effect would be fully expressed.

Our aim was to improve our understanding of the relationship between cognitive and executive aspects of word pronunciation, considering the StartReact effect as a probe for the degree of preparation. We further checked the influence of preparation in word utterances by repeatedly presenting the subjects with a set pattern of three subsequent images thus allowing them to learn what picture to expect after a few repetitions. We hypothesized that, as described for limb movements,[253] the StartReact effect would appear only when subjects have learned the sequence and are able to fully prepare the task-specific execution channel in advance.

Methods

A group of 27 healthy, right-handed subjects participated in the study (aged 25 to 66 years, 10 women, 34 ±12 years old - mean age ± standard deviation). The Ethics Committee of the Hospital Clinic of Barcelona approved the study protocol and all subjects signed an informed consent prior to inclusion in the study.

1. Recording pronunciation

We attached an ACC (Pro-Tech, U.S.A) with a sampling rate of 2000 Hz over the cricothyroid cartilage with a filter bandwidth between 1 Hz and 200 Hz and a 16-bit resolution amplifier incorporated within a EMG equipment. We selected these technical parameters in order to detected phonation onset due to signal high amplitude (see chapter IX for further details).

2. SAS

The SAS was obtained by discharging the magnetic coil of a magnetic stimulator (MagStim, London, UK) over a metallic platform at an intensity of 100% of the stimulator's capacity. This delivered an auditory stimulus of 130 dB (sound-pressure level), suitable for eliciting the auditory startle response).[242] This was monitored by surface EMG recording from orbicularis oculi and sternocleidomastoid muscles, with pairs of silver cup electrodes (2 Hz to 5 KHz). We chose these muscles because their activation indicates that the subject has normal startle responses.

3. Experimental procedure and study conditions

The study conditions used for the PNt were similar to those described in the previous chapters of this section, and were schematically presented in Figure 11.1. Briefly, there were control trials, containing only the IS, and test trials, in which the presentation of the IS was accompanied by the delivery of a SAS. We created blocks of thirty trials presented with an inter-trial time of 20 s (from trial onset to trial onset). For each trial, the same sequence of black background, attention cue ("X" letter) and forewarning signal ("X" disappearance), prepared the subject to the visual

stimuli (picture) 2 s later. The IS was presented as a visual stimulus (i.e. picture). The picture was shown for 3 s and, therefore, the whole trial lasted 9 s, allowing for 11 s of rest from the end of one trial to the beginning of the next one. We divided the study in three consecutive sessions in different days (at least one day apart). The set up and experimental settings were the same in all three sessions. We ensured the quality and similarity of the recordings through measuring and comparing the electrodes impedance at the beginning of each session. We also selected only pictures whose names are either one or two syllables long, but this study was conducted in Spanish, instead of Portuguese.

Subjects were also asked to inspect the set of 24 selected pictures before starting the experiment and in this case, to pronounce aloud the word as early as possible at presentation of the picture. The correctness of the word articulation was not evaluated, but imperceptible pronunciations were automatically rejected. In every condition, test trials containing a SAS were presented simultaneously with the IS in 6 out of the 30 trials. Presentation was semi-random, as no SAS were presented in any of the first 3 trials, nor after another test trial.

i. First session

For the first condition in the first session, subjects were asked to select one pictur and memorize the word defining the selected picture. This picture was used as the IS for all 30 trials. Therefore, subjects were expected to fully prepare beforehand the motor structures needed for pronunciation of the expected same word in all trials (SW condition). In the second condition, which we ran after a period of rest of 20 minutes after ending the SW experiment, we used the same paradigm but subjects were presented with the whole collection of 24 pictures shown randomly, with no possibility to prepare the word to pronounce (RW condition). Subjects were often reminded that they had to pronounce the word defining the object shown in the picture as fast as possible along the test.

ii. Second session

Subjects were presented with the images for the PNt, as in the second condition of the first session. However, test trials were presented with varying intervals between IS and SAS in 6 different blocks of 30 trials each (6 test trials per block). Intervals IS-SAS were -100, 0, 100, 200, 300 and 400 ms. If signs of boredom were detected, subjects were scheduled to continue the test in another session. With this experiment, we aimed to identify the change from cognitive to executive mode in the process of word pronunciation. We reasoned that, at a given interval, subjects could be ready for uttering the selected word after finishing cognitive processing. This might be made evident by the StartReact effect being significantly different for that interval with respect to others.[254-256] On top of that, replication of the block of trials with 0 ms interval was used for the

evaluation of consistency of data between this session and the first one. The order of presentation of the 6 blocks was also semi-random.

Subjects were told that this session was just a short version of one part of the second session (i.e., presentation of random pictures), with some variation. We used, instead, only three pictures, presented repeatedly in perfectly sequential order for 30 trials. The purpose was for the subjects to learn the sequence and, therefore, come to know the word to be pronounced at due time (learned word - LW - condition). We selected three pictures in such a way that the corresponding words to be pronounced would have a similar number of letters. This was intended to minimize potential differences in brain processing requirements for retrieval of each word.[257] As in the other conditions, subjects were told at the beginning of the experiment to respond as accurately and rapidly as possible. In this particular condition, they were reminded to do so at the presentation of the 10^{th} picture, as we considered this time sufficient for subjects to have learned the sequence.

4. Data reduction and statistical analysis

The primary outcome measure, RT, was the latency of onset of the first oscillation after the stimulus, as measured by the ACC. We also evaluated the overall shape of the response, characterized by number of bursts, maximum burst amplitude and duration, as secondary measures. These parameters were largely phoneme-specific and were expected to differ between words but to be rather consistent for each word. Therefore, we limited the measurement of amplitude, duration and number of bursts to conditions SW and LW, where there was the possibility to compare the outcome for each word between control and test trials. We also measured latency and size of the responses to SAS recorded in the orbicularis oculi and sternocleidomastoid muscles in test trials, using the automated area measurement method provided by the EMG equipment.

For each condition, data were grouped separately in control and test trials. We defined the StartReact value as the mean percentage shortening of RT in test trials with respect to control trials, according to the formula:

$$\text{StartReact Value (\%)} = 100 - \left(\frac{mean\ test\ trials\ RT}{mean\ control\ trials\ RT} * 100\right). \quad (11.1)$$

Before performing statistical tests, we made sure that the extracted data complied with all assumptions required. A p-value lower than 0.05 was considered statistically significant. Data comparison between control and test trials was made using one-factor ANOVA, separately for

each condition. For comparison of the StartReact values among conditions, we normalized the data by assigning 100 to the mean value of RT in control trials per subject and condition.

For the condition RW, we first confirmed no differences between data obtained in the first session and data obtained in the second session for the interval 0 ms. These data were grouped to obtain a robust baseline for comparison with data obtained for the various IS-SAS intervals. For that, we used repeated measures one-factor ANOVA and, in case of significant differences, the Bonferroni's post-hoc test.

In the LW condition, in which different results were expected according to sequence learning, we subdivided the trials in two groups according to whether the subjects had learned the sequence or not. Learning was determined by the observation of consistent RT shortening in control trials (shorter than 25% of the mean RT for the first three control trials). To avoid uncertainties, we excluded from the analysis the four trials that followed the one for which learning was assumed. The two groups of trials (before learning; LW-1 and after learning; LW-2) were treated as two different sub-conditions for calculation of the StartReact value. We compared the StartReact value between the two sub-conditions using the paired t-test.

In SW and LW conditions, the comparison of secondary measures between control and test trials were used to ascertain if SAS had any effect on the characteristics of ACC recordings (i.e., modified word pronunciation). For this purpose, we represented the data from test trials as a percentage of the mean among control trials for each individual and condition (counting LW-1 and LW-2 as two separate conditions), to obtain separate StartReact values for each condition. Data comparison was done on the grand mean from all individuals and conditions, using a one-factor ANOVA.

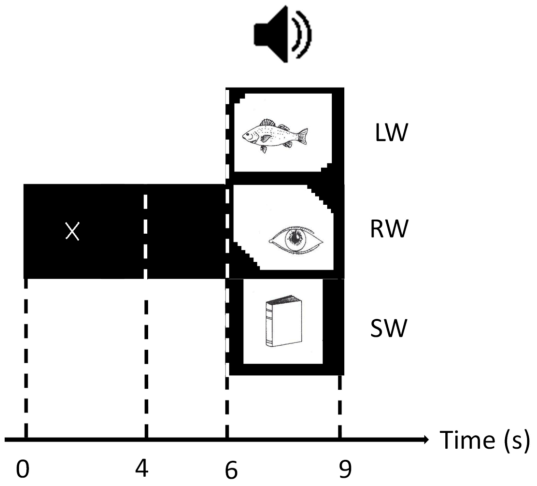

Figure 11.1 – Schematic representation of the experimental procedures. Subjects were instructed to utter as soon as possible the word defining the picture that was shown as imperative signal (IS) in the computer's

screen. Trials commenced with subjects fixating their gaze on the letter 'X' in the center of a black background. Disappearance of this symbol was the forewarning for the IS to be shown 2 s later. There were three different conditions: presentation of the same picture, requiring pronunciation of the same word in all trials (SW), randomly presented pictures, requiring pronunciation of words that subjects had to retrieve from memory at random (RW), and a perfect sequence of pictures, leading to learning the word to pronounce (LW). A startling auditory stimulus (SAS) was semi-randomly applied together with the IS in 6 out of 30 trials for each condition.

Results

All subjects tolerated well the experiment with no signs of boredom or fatigue, as per direct questioning. The number of rejected trials was less than 5% per subject with no accumulation in any condition. Reasons for rejection were movement artifacts during ACC recordings (37.3%), noise in the laboratory environment during the experiment (38.7%), errors due to lack of attention (i.e., 25.0%). There were sternocleidomastoid muscles' EMG bursts in all trials with SAS, at a mean latency of 76.9 ms (standard deviation, SD=10.5 ms) and in the orbicularis oculi muscles at a mean latency of 46.7 ms (SD= 8.7 ms). Representative examples of the ACC recordings are shown in Figure 11.2 for SW and RW conditions. As seen in that figure, shape of the accelerometric oscillations and number of bursts composing the response were consistent in repeated utterances of the same word. Data in all conditions had normal distribution (Kolmogorov-Smirnov test $p>0.05$) and homogeneity of variance (Levene's test $p<0.05$) was found in each condition.

1. SW

Pictures preferred for this experiment were "libro" (book) and "pez" (fish), selected respectively by 44.4% and 27.8% of the subjects. We carried out a multiple comparisons ANOVA to analyze possible differences between control and test trials. Significant differences were found for RT ($F[1,25]=9.94$; $p=0.004$) and for response amplitude ($F[1,25]=7.19$; $p=0.013$) but not for duration ($F[1,25]=0.80$; $p=0.373$). Table 11.1 shows the absolute mean values for all measures. The StartReact value was 29.5% (SD=7.3%). Mean amplitude was 157.5% (SD=16.1%), and mean duration was 96.9% (SD=5.2%), in test trials with respect to control trials. In test trials, SAS induced bursts of EMG activity in the orbicularis oculi and sternocleidomastoid muscles, with mean sizes of 75.2 mV.ms (SD=12.8 mV.ms) and 83.2 mV.ms (SD=38.9 mV.ms), respectively.

2. RW

As expected, mean RT in control trials was longer in the RW than in the SW condition (paired t-test; $p=0.005$). At 0 ms interval, pooled data from the two sessions showed no significant differences in mean RT between control and test trials (509 ms with SD=40 ms in control trials, vs 505 ms with SD=32 ms in test trials; $p>0.05$). However, repeated measures ANOVA showed

significant differences when comparison involved all intervals examined in the second session ($F[5,21]=5.89$; $p<0.02$). The Bonferroni post-hoc test showed shorter RT in test trials than in control trials only at the interval of 300 ms between presentation of the picture and application of the SAS ($p=0.013$), with a StartReact effect value of 9.0% (SD=4.9%). Figure 11.3 shows the mean results in the RW condition for each interval in percentage of baseline. The orbicularis oculi and sternocleidomastoid muscles' bursts in SAS trials were present with no differences in size with respect to the SAS trials in the SW condition ($p>0.05$).

3. LW

The first control trials in which subjects showed signs of learning (i.e., shortening of RT for more than 25% of the first three trials) were between the 10th and the 13th trial. Therefore, depending on the individual performance in learning, LW-1 included 10 to 13 trials while LW-2 included 12 to 15 trials (those remaining after excluding 4 trials following the one showing the first signs of learning for each individual). Table 11.1 shows the mean values for each of the two sub-conditions. By definition, RT in control trials of LW-1 was significantly longer than in LW-2 (unpaired t-test; $p<0.001$). The StartReact value was almost absent in LW-1 (see Table 11.1) but reached 25.1% (SD=6.2%) in LW.2. Figure 11.4A shows selected control and test trials and Figure 11.4B shows the mean RT absolute values for LW-1 and LW-2. The ACC response amplitude was larger in test than in control trials for both sub-conditions, with statistical significant difference in LW-2 (147.0%; SD=17%; $p<0.027$), but not in LW-1 (127.4%; SD=23.1%; $p>0.05$). Mean duration was not different between control and test trials in both subconditions. The size of the orbicularis oculi and sternocleidomastoid muscles' bursts was not different between LW-1 and LW-2 ($p>0.05$).

Table 11.1 - Reaction time, amplitude and duration of each condition tested. The values represent the mean (and standard deviation) of reaction time, amplitude and duration in control and test trials for each subcondition.

Trials	**Control trials**			**Test trials**		
	SW	LW-1	LW-2	SW	LW-1	LW-2
Reaction time (ms)	282 (40)	437 (38)	311 (30)	200 (20)*	438 (21)	233 (10)*
Amplitude (uv)	322 (84)	237 (90)	218 (114)	443 (54)*	302 (70)	320 (38)*
Duration (ms)	194 (9)	249 (13)	258(14)	190 (10)	247 (10)	247 (6)

* Statistical significance (i.e using a $p<0.05$ level) in the comparison of the corresponding conditions between control and test trials is marked with an asterisk.
SW: Same word condition; LW-1: Trials in which the subjects have not yet learned the pictures' sequence; LW-2: Trials in which the subjects have already learned the pictures' sequence.

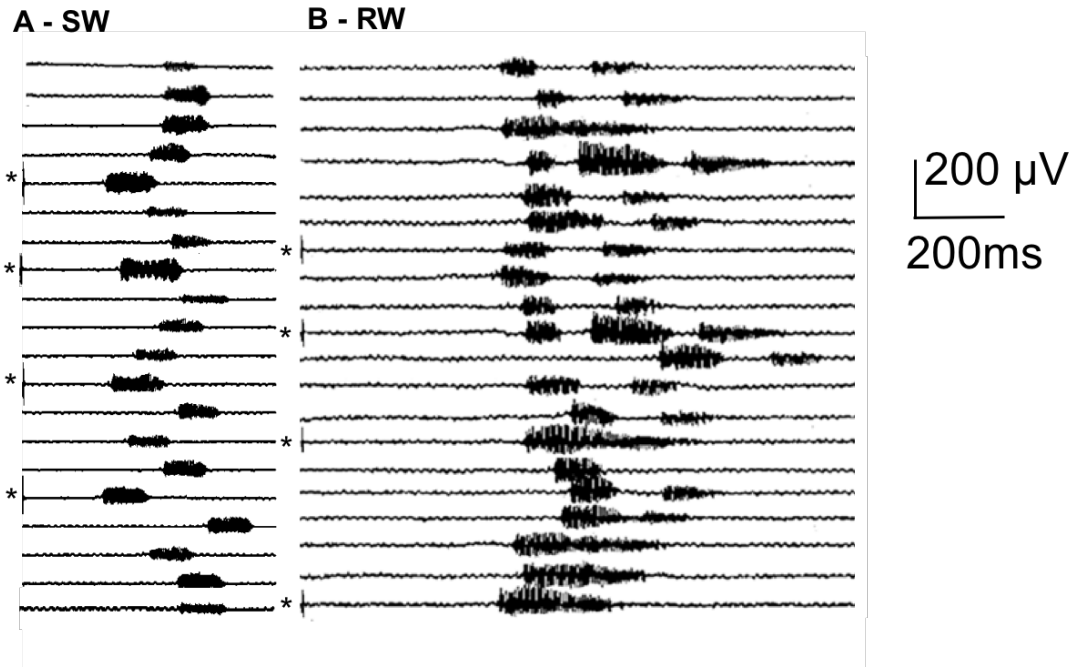

Figure 11.2 – Example of accelerometer recordings of the word uttered in conditions: same word (SW) and random word (RW). In 4 trials a startling auditory stimulus (SAS) was randomly presented together with the IS (trials marked with a small bar at onset and an asterisk). In the SW condition, the word was uttered significantly faster in trials with SAS than in those with no SAS (left side trials). However, there was no significant effect of SAS in RW trials (right side trials)-

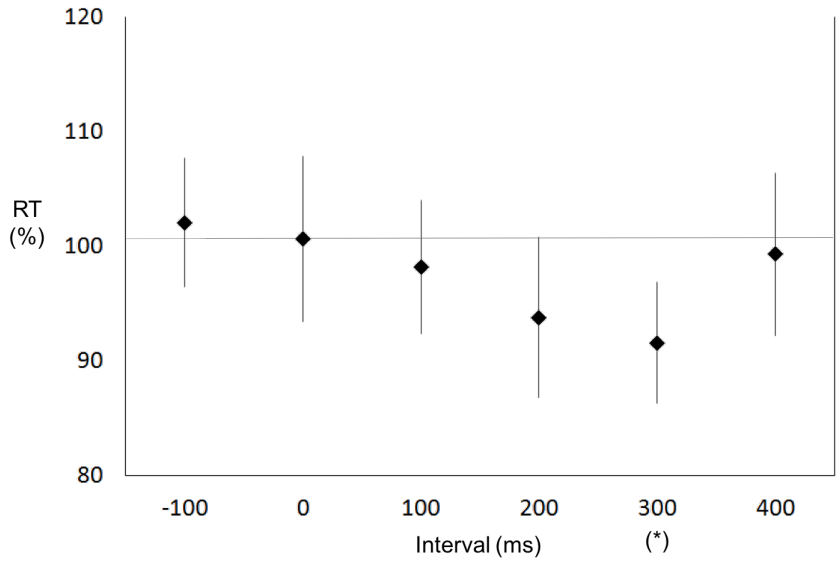

Figure 11.3 –Effects of startling auditory stimulus (SAS) on reaction time (expressed in percentage of the mean at 0 ms in the vertical axis) in the random word (RW) condition, with respect to the interval between the imperative signal and SAS presentation (expressed in ms in the horizontal axis). The asterisk is indicating the only interval for which there was a significant effect of SAS.

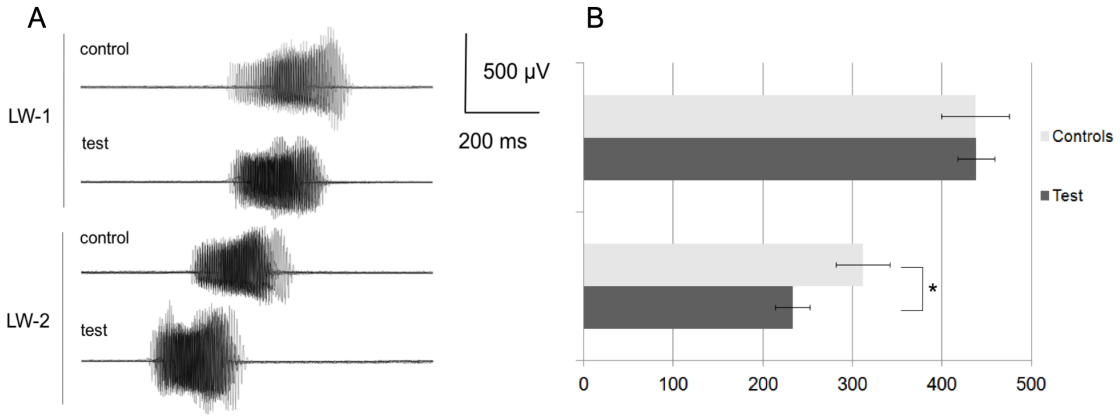

Figure 11.1 - A) Example of superimposed accererometer recordings from uttering the same word in the learned word (LW) condition. We show the superimposition of 10 representative control traces and of 5 representative test trials (from different subjects) in each of the two subconditions. Note the variability of reaction time (RT) in control trials, shown by the light grey color, and the marked decrease of RT in test trials of the LW-2 subcondition in comparison to those of the LW-1 subcondition. B) Bars showing the grand mean RT values and their standard deviation for control and test trials in each subcondition. The comparison between control and test trials showed statistical significance only in LW-2 subcondition (asterisk).

Discussion

The main conclusions extracted from the results of our study are: 1. The StartReact effect takes place in word pronunciation tasks as in other motor tasks, provided that preparation has been possible; 2. The StartReact effect is inhibited during cognitive tasks related to word retrieval from memory, but reflex startle reaction can still take place; and 3. Prediction of subsequent stimuli after learning entails sufficient preparation of articulatory mechanisms for the StartReact effect to appear with word pronunciation.

1. The StartReact effect and motor preparation

The need for fully prepared motor circuits to express the StartReact effect has been reported in many previous publications but not for the tasks used in this study. Speeding-up the pronunciation of a word by a SAS has implications for better defining the cognitive and executive aspects of speech production. We think that in the conditions SW and LW-2 of our study, words were uttered after full preparation of the execution channel, in many ways similar to a ballistic hand movement. In fact, the mean StartReact value was similar to that observed for limb tasks.[258-260]

In the task of vocalization of a syllable, Stevenson et al. (2014)[200] reported a slightly less marked StartReact effect than when performing hand movements. However, these authors used a microphone for voice recording and the difference relative to limb motor tasks could be attributed to the delay in reproduction of the syllable. Although our results are similar to those reported by Stevenson et al. (2014)[200] and Maslovat et al. (2015),[261] our interpretation differs: in contrast to these authors, we think that there is no need to invoke cortical activity to explain the StartReact effect when vocalization of words is already fully prepared. This does not mean, though, that participation of cortical circuits can be ruled out. Obviously, various cortical sites are involved in speech production but some speech constructs can be accessed and executed with no or little previous cognitive processing. This seems to be the case, for instance, in some reflex expressions, usually swearwords, which are used when in rage or disgust in spite of being socially inappropriate. It is the case also with the speech utterances of patients with non-fluent aphasia after a left hemisphere stroke, [247,262-264] possibly generated in a post-lexical prearticulatory structure accessible by various inputs even if the main language connections are interrupted. These repetitive utterances are considered to be stored in sites beyond the inhibitory control of descending tracts and, therefore, they may behave as reflex responses in non-fluent aphasia patients.[191,247,263,] Moreover, spontaneous speech may be observed at onset of speech recovery in patients with aphasia after a left-hemisphere stroke and who are not completely conscious of their utterance.[247] We have not found a study on the origin of reflex swearwords or other utterances that healthy subjects may pronounce in certain conditions such as pain, disgust, emotional stress or sports competitions (both players and spectators), but it is possible that subcortical centers related to word pronunciation beyond cognitive control may also be responsible for them.

2. *Cognitive vs executive modes of word pronunciation*

Another relevant finding of our study is the absence of the StartReact effect in the pronunciation of the same words by the same subjects when cognitive engagement was required, as in RW or in LW1. This is likely due to the lack of motor preparation for task execution in those conditions. [243,258] Indeed, the process of word pronunciation in PNts could arbitrarily be divided in two phases: cognitive and executive. These could be understood as two modes in which the brain works according to speech production requirements. In the cognitive-mode subjects' attention is focused on understanding the image shown in the picture and retrieving from memory the word appropriate for its definition. This process, which we may relate mostly to cortical activity, is likely to be blinded to interfering inputs.[265] We hypothesized that, at some point between picture presentation and word pronunciation, a StartReact effect could occur indicating a high level of preparation for task execution. In fact, in the RW condition, SAS applied at most intervals neither shortened nor lengthened RT. The exception was a barely significant shortening of RT (9%) at the interval of 300 ms after picture presentation, and a non-significant tendency to lengthen RT

at the interval of -100 ms. The latter indicates that an early SAS could potentially disturb the cognitive process as it was the case in some previous work.[266] The RT shortening seen at an interval of 300 ms is compatible with an effect of the SAS at a time when subjects might have been ready for word pronunciation. An alternative to consider is intersensory facilitation. [267,268]

In fact, it is difficult to completely separate in practice the StartReact effect from intersensory facilitation, even if the two phenomena have rather different physiology: intersensory facilitation is understood as a reinforcement of the sensory signal activating the motor circuits through a conventional route, while the StartReact effect is thought to occur within the motor pathway, either at the motor cortex[200,269, 270] or in subcortical centers. [242,271,272]

In any case, the size of the effect was small, not comparable with what would be expected for a standard StartReact effect. This raises the possibility that during the RW condition, the brain does not totally disengage from the cognitive-mode, but is, instead, expecting to continue the task as instructed. We therefore believe that the StartReact effect can only be elicited in full when the brain is engaged in an executive-mode and there is no simultaneously ongoing cognitive task. Cognitive tasks may entail some inhibition or control of inputs to the central nervous system in order to protect the process from potentially disturbing stimuli. A relevant observation is that SAS application in RW induced startle responses in the orbicularis oculi and sternocleidomastoid muscles. The dissociation between the startle reaction and the StartReact effect is already known[273] but, in the context of our study, it may indicate that inputs to the central nervous system can be conveniently gated to protect cognitive processes. Because the whole RW task was demanding regarding cognitive processes, preparation of subcortical motor structures could not be completed prior to IS presentation and so the execution of the task only benefited from the SAS to a very limited degree.

3. Effects of learning on preparation for word pronunciation

Probably the most relevant finding of our study is the fact that the StartReact effect was observed with values similar to SW when subjects learned the sequence of words presented in LW. A similar finding was reported by Maslovat et al. (2011)[253], where the authors examined how preparation of unimanual movements changed as a result of practice. We extend the observations of Maslovat et al. (2011)[253] to the speech area. We considered PNt very convenient form of motor activity for the study of changes occurring in the degree of preparation with learning. By presenting only three selected pictures sequentially repeated, we expected subjects to learn the presentation pattern. They were reminded at due time that they were required to utter the word defining the picture as fast as possible, which might have been of help to some subjects to realize that there was a sequence present. Repeated presentation of the same pictures might have caused

a downgrade of cognitive demands up to the extent that the brain could disengage from the cognitive-mode and enter the executive-mode. In PNt a large cortical area is activated where speech processing takes place.[274-276] It has been demonstrated that task repetition and training leads to reduction of task-related brain activity. [277,278] In our subjects, learning might have enhanced the transition from a cognitive process devoided of preparation to an executive process in which the task is more rapidly and automatically executed.

A recent neuroimaging study showed significantly reduced brain activity in cortex (i.e left IFG, right dorsal anterior cingulated cortex, left superior lobule) and bilateral caudate nuclei, in healthy subjects after learning the appropriate name of pictures presented in both chinese or english language after a 8-day training sessions.[279] A reduced RT to response and cognitive control was also reported after learning.[279] In fact, would be expected that activity in many cortical centers at the beginning of the task would lead to a pattern of activity suppression, similar to the one seen with SW repetition[276] indicating lesser relevance of speech-related cortical areas in uttering a fully prepared (or learned) single word. The basal ganglia-thalamo-cortical loops are known to have important functions in planning and executing actions.[280-282] These primitive functions[283] are likely to be independent from higher cognitive processing. In cases where cognitive process is present (i.e., unprepared actions) more time is needed to input these data to basal ganglia for configuration of the appropriate planning of action.[280,281] Other findings from animal experimentation suggest that there is greater influence of nuclei of the basal ganglia in the delivery of inputs to reach the point of no return in RT.[284] These aspects point to the basal ganglia nuclei as the most likely site where motor preparation for fast responding is set. From there, an increase in excitability may occur to facilitate responding upstream towards the motor cortex and the corticospinal tract, as well as downstream to the reticular formation and the reticulospinal tract, through the pedunculopontine nucleus and the nucleus *reticularis pontis caudalis*.

4. *Implications of our findings for the interpretation of the physiology of the StartReact effect*

The exact pathways followed by the SAS inputs for the StartReact effect to occur are still a matter of debate. So far, studies on the physiology of the StartReact effect have not distinguished between the processes needed to retrieve and express the motor program. We thought that, if a cortical route is engaged, there should be a different effect when subjects are involved in a cognitive task than when they are fully ready for task execution. We demonstrated that this is the case with PNts in which subjects could be led to prepare conveniently the execution of the task after learning.

It would be an oversimplification to attribute to a single descending motor tract the execution of a task that involves anticipatory activity, prime movers and readiness of various circuits to prepare for a feedforward compensation for the inputs provoked by the execution of the task. Therefore, our view is that the prepared task is executed through activation of a pack of tightly linked commands issuing from cortical and subcortical centers. We advocate that what is relevant for the StartReact effect to occur is motor preparation, a concept that involves enhancement of excitability in various levels of the motor system. [285,286] At such a stage, the slightest excitatory input may activate the whole system with minimal delays between cortical and subcortical motor centers and it is possible that both circuits in fact work together with mutual potentiation and reinforcement.

This page was intentionally left blank

GENERAL DISCUSSION AND CONCLUSIONS

Human speech and language function performed using a diversity of brain, respiratory and pronatory structures. Such cognitive function is probably more explored than other cognitive functions because of the human's aptitude to communicate in society. In patients with PBT, the maintenance of this function allows an increased quality of life in comparison with those patients with a compromised language function. Therefore, presurgical planning in patients with tumors near or involving known brain language network[6] proposed for tumor surgical resection, should include neuroimaging and neurophysiological tools usage such as DTI, fMRI and nTMS.[137,123] However, evidence based on randomized double blind clinical trials remains to be shown.[287,230] Despite widely use of neuroimaging tools, the navigated TMS utility increased in the last few years and European groups report a strategy chance in about one third of the patients during surgical treatment.[123]

In section A, an effort was made to revise the fundamental and updated knowledge about the biomedical technology used in clinical experiments. Overall, during clinical routine, the appraisal of the methods and equipment used to diagnose or to investigate a pathophysiological process is out of the most relevance. The knowledge about the "basics" of each technique allowed 1) to select the technology for that specific clinical doubt, 2) to modify and redirect the technique used for clinical applicability, 3) to exclude such technology from other applicability's, and 4) to overthink the experiments results taking into account each limitation.

Neuroimaging is based on biophysics, but if during clinical practice, this type of knowledge is secondary due to standardization of imaging aquisiction,[96-288] in research, the signal origin and processing may represent different physiological phenommns.[30] In addition, due to the development of tools which offers the opportunity to process signal imaging without financial and software constraints, mathematical and programing knowledge is desired. In this dissertation, such knowledge allowed 1) adapt Matlab based tools to perform kurtosis based tractography, 2) development of scripts either to perform effective connectivity analysis based on graph theory model or to connect a EMG to a TMS equipment in order to perform a PNt in a synchronized fashion between recording and magnetic or visual stimuli. In neurophysiological field, electronics, electrical fields and current distribution understanding is also desired. Because along the developed experiments an electronic device based on a Arduino microcontroller was used to deliver a 5V o amplifier signal recording during PNt. Connectivity analysis was also based after estimating a ROI with 6x6x6 mm^3 which derived from the current density (0.025 cm/m^2) beneath the bipolar electrode used for DCS (5mm apart, using 5mA). Lastly, a speech recording method

was developed using a uniaxial ACC and "conventional" amplifiers present in available EMG equipment's and its utility, reliability and caveats were studied. In conclusion, nowadays clinical assessment knowledge based on purely anatomical and physiological fundaments, is needed but is yet not sufficient to perform clinical translation research.

In section B, kurtosis based tractography of the CST and AF was estimated in healthy subjects and in patients with PBT using a 1.5T MRI scanner. The main purpose was to study the language involved white matter tracts. The DKI based estimated tracts showed a higher consistency (number and volume) in patients when compared with DTI based tractography, mainly for the AF (chapter V). Our clinical experiments intended to show that a alternatively tractography method is available and is compatible with high clinical output of patients. This method compensates some of the DTI caveats, showing a high performance within voxels with crossing fibers with higher microstructure complexity.[40] However, the fibers delineated by DKI-tract in our experiments, were not tested functionally (with DCS) and the methodology used for DTI-tract was the same as used for DKI-tract which may imposed some limitations for the former method. Although, further clinical trials, should be performed using DKI-tract, mainly for CST delineation because when resecting a tumor, a distance of 5 mm evaluated from the point given by a navigation system is proposed by literature[289] in order to avoid neurological motor morbidity. But in our neurosurgery department, just resections within 3mm from the CST showed definitive motor deficit (unpublished data), and in some patients, distances between 5 to 10 mm may evoke a motor permanent deficit.[290] Therefore, these results may reflect the "non" delineated fibers by DTI-tract due to complexity brain microstructure (i.e. edema, cancer cells).

The experiments developed in section C intended study a more cognitive component of the brain language function. The use of nfMRI data derived multi-language tasks BOLD activations at presurgical stage, do not reduce the number of DCS stimuli or decrease the time and therefore the patient discomfort of eCM during awake surgery. This experiment was developed to either perceive the spatial resolution of BOLD activation data from presurgical planning into intraoperative setting. Thus, mCM could minimized the time for language CM by associating an high specificity technique (DCS) to a high sensitivity technique (fMRI). However, no influence was denoted, leading the better understanding of the fMRI caveats regarding spatial resolution in patients with PBT.[45,125] As stated, task-specific fMRI is a sensible tool to brain language hemisphere lateralization and gyrus involved in language network detection. However, the relevance of such identified brain regions for language network is lacking leading at false positive language function brain regions.[291] In chapter VII and VIII, we developed clinical experiments in order to extract connectivity metrics from task-specific and resting state fMRI, respectively, through graph model theory analysis. Patients with PBT performed fMRI at diagnose and after

tumor regrowth, which allowed to identify intra and interhemispheric neuroplasticity mechanism of language function compensation. Therefore, intrahemispheric language related classical regions were associated with higher participation coefficient and betweenness centrality when PTB involved either frontal lobe or the temporal lobe. To perform such analysis, connectivity measures were extracted using an atlas-based approach. However, this method of analysis within a dysmorphic brain hemisphere may show some constraints either due to the absence of brain parenchyma or the presence of the brain tumor. Therefore, a SCA from brain regions with language function identified by DCS was driven in chapter VIII to obtain a more accurate estimation of the connectivity measures. In this chapter, we showed that brain regions with language and motor function, have a central location (i.e. betweeness centrality; participation coefficient) within the eloquent network showing either a high node degree or a low participation coefficient. As in other studies, central features of the brain regions which acts as hubs show an important role for the neurological function tested. Overall, these measures may provide complementary information about the region function within a network. Although, neuroimaging preprocessing and functional connectivity analysis methodology should be standardized to avoid processing errors.

In the last section of this thesis, we intended to ensure and standardize a useful and available technique for speech recording. To achieve this purpose, a transductor ACC was used to record speech phonation during words pronunciation. Caveats and reliability measures were made in healthy subjects, and word-specific recordings were defined. In addition, a graphical atlas was provided at supplementary material of the chapter IX. However, experimental conditions should be controlled to ensure a reliable and reproducible word-specific graphical representation recorded by the ACC. In fact, preparation, readiness and loudness alters the word pronunciation sound (subjectively evaluated) besides language disturbances evoked by infectious laryngitis or brain stimulation at IFG (chapter X). Such method demonstrated to be useful for example for r-nTMS language mapping at presurgical planning. In addition, allowed to detect language disturbances evoked by DCS intraoperatively during patients' neuropsychological language testing. ACC of words pronunciation was able to detect clinical language errors either through subtle latency increase and oscillation pattern deviation. In 11% of the discrepancy cases, current intensity was increased evoking language disturbance avoiding a false negative result. In addition, the method developed allowed to study the mechanisms involved in speech execution. Vocalization may not be a cognitive function, but just a motor action without from speech processing. In the last chapter XI, we showed that a prepared task is executed through activation of a pack of tightly linked commands issuing from cortical and subcortical centers.[242] The StartReact effect was used to demonstrate that when a cognitive processing is prepared or learned

in a way that a subject can anticipate it, speech execution involves various levels of the motor system, but without participation of classical brain regions in speech processing (i.e. IFG).

This thesis aimed to contribute to the understanding of speech and language function. Translational experiments were developed in order to improve simple and reliable methodologies that could enhance speech appraisal and minimize neurological morbidity associated with surgical treatment of patients with PBT. This improvement was applied to presurgical planning and intraoperative stage patients' management using neuroimaging and neurophysiological tools. Overall this thesis results contributed to speech and language pathophysiological understanding from the speech execution, recording to neuroplasticity mechanisms occurred during tumor growth to maintain speech processing capacity.

REFERENCES

1. H. Newton. “Overview of Pathology and Treatment of Primary Brain Tumors,” in Handbook of Neuro-Oncology Neuroimaging, 2nd ed., H. Newton (Ed.). London: Academic Press, 2016, 9-22.
2. H. Luders and I. Awad. “Conceptual considerations.” in Epilepsy Surgery ed., HO Luders (Ed.) New York: Raven Press, 1992, 51–62.
3. M. Catani. “The rises and falls of disconnection syndromes.” Brain, 128, 2224–2239, 2005.
4. G. Hickok and D. Poeppel. “Dorsal and ventral streams: A framework for understanding aspects of the functional anatomy of language.” Cognition, 92, 67–99, 2004.
5. L. Lichtheim. “On aphasia.” Brain, 7, 433-484, 1885.
6. G. Hickok and D. Poeppel. “The cortical organization of speech processing.” Nature Reviews Neuroscience, 8, 393–402, 2007.
7. M. Catani and M. Mesulam. “The arcuate fasciculus and the disconnection theme in language and aphasia: History and current state.” Cortex, 44, 953–961, 2008.
8. A. Friederici. “Pathways to language: Fiber tracts in the human brain.” Trends in Cognitive Sciences, 13, 175–181, 2009.
9. J. Dubois, L. Hertz-Pannier, A. Cachia, J. Mangin, D. Le Bihan, G. Dehaene-Lambertz. “Structural asymmetries in the infant language and sensorimotor networks.” Cerebral Cortex, 19, 414–423, 2009.
10. G. Aguirre. “Experimental design and data analysis for fMRI” in BOLD fMRI, S.Faro and F. Mohamed Ed., New York: Springer, 2010, 55-69.
11. N. Sanai, Z. Mirzadeh, M. Berger. “Functional outcome after language mapping for glioma resection.” N Engl J Med. 358, 18–27, 2008.
12. B. Gordon, R. Lesser, N. Rance, J. Hart, R. Webber, S. Uematsu, R. Fisher. Parameters for direct cortical electrical stimulation in the human: histopathologic confirmation. Electroencephalogr Clin Neurophysiol., 75, 371-377, 1990.
13. L. Schader. “Direct cortical stimulation to localize sensory, motor and language function” in Intraoperative monitoring of neural function, Handbook of Clinical Neurophysiology, 8, M. Nuwer (Ed.) Netherlands: Elsevier, 2008, 150-162.
14. L. Cattaneo. “Language.” In Brain stimulation, Handbook Clinocal Neurology, vol., 116., M. Lozano and M. Hallet Ed. Netherlands: Elsevier, 2013, 681-691.
15. W. Bi, O. Olubiyi, S. Tharin, A. Golby. “Neurosurgical treatment planning.” In Handbook of Neuro-Oncology Neuroimaging, 2nd ed., H. Newton Ed. London: Academic Press, 2016, 217-229.
16. S. Ille, N. Sollmann, T. Hauck, S. Maurer, N. Tanigawa, T. Obermueller, C. Negwer, et al. “Impairment of preoperative language mapping by lesion location: a functional magnetic resonance imaging, navigated transcranial magnetic stimulation, and direct cortical stimulation study.” J Neurosurg. 314-324, 2015.

17. C. Lynn and D. Basset. “The physics of brain network structure, function and control.” Nature Review Physics, 318-333, 2019.
18. K. Van Dijk, T. Hedden, A. Venkataraman, K. Evans, S. Lazar, R. Buckner. “Intrinsic functional connectivity as a tool for human connectomics: theory, properties, and optimization.” Journal of Neurophysiology, 297–321, 2010.
19. B. Biswal, F. Yetkin, V. Haughton, J. Hyde. “Functional connectivity in the motor cortex of resting human brain using echo-planar MRI.” Magn Reson Med. 537-541, 1995.
20. S. Smith, P. Fox, K. Miller, D. Glahn, P. Fox, C. Mackay, N. Filippini, et al. Correspondence of the brain's functional architecture during activation and rest. Proc Natl Acad Sci USA. 13040-13045, 2009.
21. M. Rubinov and O. Sporns “Complex network measures of brain connectivity: uses and interpretations.” Neuroimage. 1059–69, 2010.
22. J. Laver. “Acoustic waveform perturbations and voice disorders.” Journal of Voice. 115 – 126, 1992.
23. R. Sataloff. “Physical examination.” In Clinical assessment of voice, 2nd ed., R. Sataloff (Ed.) San Diego: Plural Publishing, 2017, 29 - 43.
24. J. Romak, R. Heuer, M. Hawkshaw, R. Sataloff. “The clinical voice laboratory.” In Clinical assessment of voice, 2nd ed., R. Sataloff (Ed.) San Diego: Plural Publishing, 2017, 44 - 77.
25. A. Pascual-Leone, J. Gates, A. Dhuna. “Induction of speech arrest and counting errors with rapid-rate transcranial magnetic stimulation.” Neurology. 697-702, 1991.
26. R. Brown, Y. Cheng, E. Haacke, M. Thompson, R. Venkatesan. “Magnetic Resonance Imaging: A Preview.” In Magnetic Resonance Imaging: Physical Principles and Sequence Design. Fourth edition. New Jersey, Willey Blackwell. 2014, 1-18.
27. S. Bushong, G. Clarke. “Fundamentals” In Magnetic Resonance Imaging: Physical and Biological Principles. Fourth ed., S. Bushong, G. Clarke. Eds, Missouri: Elsevier, 2015, 1-57.
28. S. Bushong, G. Clarke. “The Magnetic Resonance Image” In Magnetic Resonance Imaging: Physical and Biological Principles. Fourth ed., S. Bushong, G. Clarke. Eds, Missouri: Elsevier, 2015, 58-109
29. A. Einstein. Über die von der molekularkinetischen Theorie der Wärme geforderte Bewegung von in ruhenden Flüssigkeiten suspendierten Teilchen. Ann. Phys., 322: 549-560, 1905.
30. M. Otaduy. “Physics of Diffusion Weighted and Diffusion Tensor Imaging” In Diffusion Weighted and Diffusion Tensor Imaging: A Clinical Guide. C. Leite, M. Castillo eds., Rio de Janeiro: Thieme, 2016, 1-18.
31. J. Pipe. “Pulse Sequences for Diffusion-Weighted MRI.” In Diffusion MRI from quantitative measurement to in-vivo neuroanatomy, second edition, H. Berg, T. Behrens eds, London: Elsevier, 2014, 63-104.
32. C. Pierpaoli, P. Basser. “Toward a quantitative assessment of diffusion anisotropy.” Magn Reson Med. 36: 893-906. 1996 Erratum in: Magn Reson Med. 37: 972, 1997.

33. P. Mukherjee, S. Chung, J. Berman, C. Hess, R. Henry. “Diffusion tensor MR imaging and fiber tractography: technical considerations.” AJNR Am J Neuroradiol. 29: 843-852, 2008.
34. F. Rueda-Lopes, C. da Cruz, E. Gasparetto. “Diffusion Weighted Imaging in the Evaluation of Brain Tumors” In Diffusion Weighted and Diffusion Tensor Imaging: A Clinical Guide. C. Leite, M. Castillo eds., Rio de Janeiro: Thieme, 2016, 99-111.
35. K. Seunarine, D. Alexander. “Multiple fibers: Beyond the Diffusor Tensor.” In Diffusion MRI from quantitative measurement to in-vivo neuroanatomy, second edition, H. Berg, T. Behrens eds, London: Elsevier, 2014, 105-123.
36. J. Jensen, J. Helpern. “MRI quantification of non-Gaussian water diffusion by kurtosis analysis.” NMR Biomed.; 23: 698-710, 2010.
37. R. Loução. “Structural Connectivity based on Diffusion Kurtosis Imaging”. Instituto Engenharia Biomédica e Biofísica. Faculdade de Ciências, Lisboa. 2015.
38. R. Neto Henriques. “Diffusion Kurtosis Imaging of the Healthy Human Brain.” Instituto Engenharia Biomédica e Biofísica. Faculdade de Ciências, Lisboa. 2012.
39. M. Lazar, J. Jensen, L. Xuan, J. Helpern. “Estimation of the orientation distribution function from diffusional kurtosis imaging.” Magn Reson Med., 60: 774-781, 2008.
40. R. Neto Henriques, M. Correia, R. Nunes, H. Ferreira. “Exploring the 3D geometry of the diffusion kurtosis tensor--impact on the development of robust tractography procedures and novel biomarkers.” Neuroimage, 1; 111: 85-99, 2015.
41. R. Neto-Henriques, H. Ferreira, M. Correia. “United Diffusion Kurtosis Imaging (UDKI) toolbox.” MAGMA, 28: 511-512, 2015.
42. M. Smith. “Fast robust automated brain extraction.” Human brain mapping, 17, 143-155, 2002.
43. R. Wang, T. Benner, A. Sorensen, V. Wedeen. “Diffusion toolkit: a software package for diffusion imaging data processing and tractography “[Abstract 3720]. Proceedings of the International Society for Magnetic Resonance in Medicine 15: 207.
44. C. Kayser, S. Logothetis. “The Electrophysiological Background of the fMRI Signal.” In S. Ulmer, O. Jansen Eds. fMRI. Springer, Berlin, Heidelberg, 2010, 23-34.
45. S. Kim, T. Jin, M. Fukuda. “Spatial Resolution of fMRI Techniques.” In S. Ulmer, O. Jansen. Eds fMRI. Springer, Berlin, Heidelberg. 2010, 15-21.
46. R. Constable. “Challenges in fMRI and Its Limitations.” In S. Faro, F. Mohamed, Eds. Functional MRI. Springer, New York, 2006, 71-89.
47. R. Goebel, F. Esposito, E. Formisano, “Analysis of FIAC data with BrainVoyager QX: from single-subject to cortically aligned group GLM analysis and self-organizing group ICA,” Human brain mapping, 27, 392-401, 2006.
48. A. Ribeiro, L. Lacerda, H. Ferreira. “Multimodal Imaging Brain Connectivity Analysis (MIBCA) toolbox,” PeerJ, vol.3, 1078, 2015.
49. S. Whitfield-Gabrieli, A. Nieto-Castanon. “Conn: a functional connectivity toolbox for correlated and anticorrelated brain networks.” Brain Connect. 2:125-141, 2012.

50. C. Rorden, H. Karnath, L. Bonilha. “Improving lesion—symptom mapping.” Journal of Cognitive Neuroscience 19:1081–1088, 2007.
51. J. Ashburner. “SPM: a history.” NeuroImage, 2011.
52. K. Worsley, K. Friston. “Analysis of fMRI time-series revisited-again.” Neuroimage. 2: 173-181,1995.
53. V. Tronnier. “Functional Neuronavigation.” In Stippich C. (eds) Clinical Functional MRI. Medical Radiology (Diagnostic Imaging). Springer: Berlin, 2007, 149-166.
54. J. Tournier, F. Calamante, A. Connelly. “MRtrix: Diffusion tractography in crossing fiber regions.” Int J Imag Syst Tech, 22 , 53-66, 2012.
55. M. Jenkinson, C. Beckmann, T. Behrens, M. Woolrich, S. Smith.” FSL.” NeuroImage, 62: 782-90, 2012.
56. B. Fischl, A. van der Kouw, C. Destrieux, E. Halgren, F. Segonne, D. Salat, E. Busa, et al. “Automatically parcellating the human cerebral cortex.” Cereb Cortex 14, 11-22, 2004.
57. C. Destrieux, B. Fischl, A. Dale, E. Halgren. “Automatic parcellation of human cortical gyri and sulci using standard anatomical nomenclature.” Neuroimage. 15; 53: 1-15, 2010.
58. J. Veraart, D. Novikov, D. Christiaens, B. Adesaron, J. Sijbers, E. Fieremans. “Denoising of diffusion MRI using random matrix theory.” NeuroImage 142, 394–406, 2016.
59. M. Jenkinson, P. Bannister, J. Brady, S. Smith. “Improved optimisation for the robust and accurate linear registration and motion correction of brain images.” NeuroImage 17: 825–841, 2002.
60. Y. Behzadi, K. Restom, J. Liau, T. Liu. “A component based noise correction method (CompCor) for BOLD and perfusion based fMRI.” NeuroImage 37: 90–101, 2007.
61. P. Rossini, R. Di Iorio, M. Bentivoglio, G. Bertini, F. Ferreri, C. Gerloff, R. Ilmoniemi et al. “Methods for analysis of brain connectivity: An IFCN-sponsored review.” Clin Neurophysiol. Review; 130: 1833-1858, 2019.
62. S. Eldawlatly, K. Oweiss. “Graphical Models of Functional and Effective Neuronal Connectivity.” In Statistical Signal Processing for Neuroscience and Neurotechnology, K. Oweiss Ed. USA: Academic Press, 2010, 129-174.
63. C. Fernandes. “Resting state fMRI experimental and analytical methodology: A functional connectivity analysis.” Instituto Engenharia Biomédica e Biofísica. Faculdade de Ciências, Lisboa. 2013.
64. J. Bijsterbosch, S. Smith, C. Beckmann. “Introduction to Resting State fMRI Functional Connectivity.” Oxford: University Press, 2017, 1-130.
65. J. Wang, X. Zuo, Y. He. “Graph-based network analysis of resting-state functional MRI.” Front Syst Neurosci. 7; 4: 16, 2010.
66. C. Granger. “Investigating Causal Relations by Econometric Models and Cross-spectral Methods. Econometrica, 37, 424-438, 1969.
67. P. Gildenberg. “Evolution of Neuromodulation” Stereotact Funct Neurosurg, 83:71-79, 2005.

68. R. Plonsey, R. Barr. “Bioelectric potentials” In Bioelectricity, A quantitative approach, third ed. New York: Springer, 2007, 45-69.
69. D. Preston, B. Shapiro. “Basics of Electricity and Electronics for Electrodiagnostic Studies” In Electromyography and Neuromuscular Disorders: Clinical-Electrophysiologic correlations. London: Saunders, 2013, 22-33.
70. S. Nathan, S. Sinha, B. Gordon, R. Lesser, N. Thakor. Determination of current density distributions generated by electrical stimulation of the human cerebral cortex. Electroencephalogr Clin Neurophysiol. 86: 183-192, 1993.
71. D. Brocker, W. Grill. “Principles of electrical stimulation of neural tissue” Handb Clin Neurol. Review. 116: 3-18, 2013.
72. J. Daube. “Physiology” Handbook of Clinical Neurophysiology, Elsevier, 8, 2008, 7-43.
73. A. Szelényi, L. Bello, H. Duffau, E. Fava, G. Feigl, M. Galanda, G. Neuloh, F. Signorelli, F. Sala. “Workgroup for Intraoperative Management in Low-Grade Glioma Surgery within the European Low-Grade Glioma Network. Intraoperative electrical stimulation in awake craniotomy: methodological aspects of current practice.” Neurosurg Focus. 28: E7, 2010.
74. H. Journee. “Motor EP physiology, risks and specific anesthetic effects” Handbook of Clinical Neurophysiology. Elsevier, 8, 2008, 218-234.
75. J. Malmivuo, R. Plonsey. “Magnetic stimulation of neural tissue” In Bioelectromagnetism, Principles and applications of bioelectric and biomagnetic fields. New York: Oxford University, 1995, pp. 375-380.
76. P. Miranda. “Physics of effects of transcranial brain stimulation” Handb Clin Neurol. Review, 116: 353-366, 2013.
77. V. Di Lazzaro. “Biological effects of non-invasive brain stimulation” Handb Clin Neurol. Review, 116: 367-374, 2013.
78. M. Stenroos, L. Koponen. “Real-time computation of the TMS-induced electric field in a realistic head model” NeuroImage 203: 116159, 1-12, 2019.
79. P. Rossini, D. Burke, R. Chen, L. Cohen, Z. Daskalakis, R. Di Iorio, V. Di Lazzaro, et al. “Non-invasive electrical and magnetic stimulation of the brain, spinal cord, roots and peripheral nerves: Basic principles and procedures for routine clinical and research application. An updated report from an I.F.C.N. Committee” Clinical Neurophysiology, 126, 6, 1071-1107, 2015.
80. T. Kammer, S. Beck, A. Thielscher, U. Laubis-Herrmann, H. Topka. “Motor thresholds in humans: a transcranial magnetic stimulation study comparing different pulse waveforms, current directions and stimulator types” Clin Neurophysiol. 112: 250-258, 2001.
81. P. Tarapore. “Speech Mapping with Transcranial Magnetic Stimulation” In Transcranial magnetic stimulation. Neuromethods. A. Rotenberg, J. Horvath, A. Pascual-Leone. Ed. New York: Springer, 2014, pp. 361- 379.
82. W. Paulus, A. Peterchev, M. Ridding. “Transcranial electric and magnetic stimulation: technique and paradigms” Handb Clin Neurol. Review. 116: 329-342, 2013.

83. M. Snodgrass and M. Vanderwart. “A standardized set of 260 pictures: norms for name agreement, image agreement, familiarity, and visual complexity“ Journal of Experimental Psychology. Human Learning and memory, 6, 174-215, 1980.
84. R. Comeau. “Neuronavigation for Transcranial Magnetic Stimulation” In Transcranial magnetic stimulation. Neuromethods. A. Rotenberg, J. Horvath, A. Pascual-Leone. Ed. New York: Springer, 2014, 31-56.
85. J. Mäkelä, A. Laakso. “nTMS Language Mapping: Basic 8 Principles and Clinical Use” In Navigated Transcranial Magnetic Stimulation in Neurosurgery, first edition, S. Krieg ed., Switzerland: Springer, 2017, 131-150.
86. D. Fuller, J. Pimentel, B. Peregoy. “Anatomy and physiology of the phonatory system” In Applied anatomy and physiology for Speech-Language pathology and audiology, first edition, D. Fuller, J. Pimentel, B. Peregoy. ed., Baltimore: Lippincott Williams and Wilkins, 2012, 8: 1-100.
87. J. Svec, S. Granqvist. “Guidelines for selecting microphones for human voice production research.” Am J Speech Lang Pathol. 19: 356-368, 2010.
88. D. Barry. “AAEM minimonograph #36: basic concepts of electricity and electronics in clinical electromyography.” Muscle Nerve. Review. 14: 937-946, 1991. Review. Erratum in: Muscle Nerve. 14: 1153, 1991.
89. A. Gitter, W. Stolov. “AAEM minimonograph #16: instrumentation and measurement in electrodiagnostic medicine--Part I.” Muscle Nerve. Review. 18: 799-811. 1995.
90. M. Neuman. Physical Measurements. In The Biomedical Engineering Handbook: Medical devices and systems, third edition, J. Bonzino ed. Boca Raton: Taylor & Francis Group, 2006, pp. 46: 1-13.
91. J. Whitaker. “Logic Concepts and Devices.” In The Electronics Handbook, first edition, J. Whitaker ed., CRC Press, Boca Raton: CRC Press, 2001 , pp. 295–311.
92. J. Nagel. “Biopotential Amplifiers.” In The Biomedical Engineering Handbook: Second Edition. J. Bronzino ed., Boca Raton: CRC Press LLC, 2000, pp. 70: 1-14.
93. L. Martí-Bonmatí, M. Kormano. “MR equipment acquisition strategies: low-field or high-field scanners.” Eur Radiol.; 7 Suppl 5: 263-268, 1997.
94. M. Marrale, G. Collura, M. Brai, N. Toschi, F. Midiri, G. La Tona, A. Lo Casto, C. Gagliardo. “Physics, Techniques and Review of Neuroradiological Applications of Diffusion Kurtosis Imaging (DKI).” Clin Neuroradiol.; 20: 1-13, 2015.
95. C. Shaw, J. Jensen, R. Deardorff, M. Spampinato, J. Helpern. “Comparison of Diffusion Metrics Obtained at 1.5T and 3T in Human Brain With Diffusional Kurtosis Imaging.” J Magn Reson Imaging.; 45: 673-680, 2017.
96. B. Ellingson, M. Bendszus, J. Boxerman, D. Barboriak, B. Erickson, M. Smits, S. Nelson, et al. “Jumpstarting Brain Tumor Drug Development Coalition Imaging Standardization Steering Committee. Consensus recommendations for a standardized Brain Tumor Imaging Protocol in clinical trials.” Neuro Oncol. Review. 17: 1188-1198. 2015.

97. J. Andersson, S. Sotiropoulos. “An integrated approach to correction for off-resonance effects and subject movement in diffusion MR imaging.” Neuroimage.; 15; 125: 1063-1078, 2016.

98. G. Glen, J Helpern, A. Tabesh, J. Jensen. “Optimization of white matter fiber tractography with diffusional kurtosis imaging.” NMR Biomed.; 28: 1245-1256, 2015.

99. G. Glenn, L. Kuo, Y. Chao, C. Lee, J. Helpern, J. Jensen. “Mapping the Orientation of White Matter Fiber Bundles: A Comparative Study of Diffusion Tensor Imaging, Diffusional Kurtosis Imaging, and Diffusion Spectrum Imaging.” AJNR Am J Neuroradiol., 37: 1216-1222, 2016.

100. S. Van Cauter, J. Veraart, J. Sijbers, R. Peeters, U. Himmelreich, F. De Keyzer, S. Van Gool, et al. “Gliomas: diffusion kurtosis MR imaging in grading” Radiology, 263: 492-501, 2012.

101. A. Potgieser, M. Wagemakers, A. van Hulzen, B. de Jong, E. Hoving, R. Groen. “The role of diffusion tensor imaging in brain tumor surgery: a review of the literature.” Clin Neurol Neurosurg.; 124: 51-58, 2014.

102. E. Kaal, C. Vecht. “The management of brain edema in brain tumors.” Curr Opin Oncol. Review. 16: 593-600. 2004.

103. H. Duffau, L Capelle, D. Denvil, N Sichez, P. Gatignol, L. Taillandier, M. Lopes, et al. “Usefulness of intraoperative electrical subcortical mapping during surgery for low-grade gliomas located within eloquent brain regions: functional results in a consecutive series of 103 patients” J Neurosurg. Review. 98:764-778. 2003.

104. P. Basser, J. Mattiello, D LeBihan. “MR diffusion tensor spectroscopy and imaging” Biophys J., 66: 259-267, 1994.

105. P. Basser, S. Pajevic, C. Pierpaoli, J. Duda, A. Aldroubi A. “In vivo fiber tractography using DT-MRI data.” Magn Reson Med., 44:625-632, 2000.

106. B. Jeurissen, A. Leemans, J. Tournier, D. Jones, J. Sijbers J. “Investigating the prevalence of complex fiber configurations in white matter tissue with diffusion magnetic resonance imaging.” Hum Brain Mapp., 34:2747-2766, 2013.

107. J. Leote, R. Loução, L. Cerqueira, R. Nunes, H. Ferreira. “Reconstruction of white matter fibre tracts using diffusion kurtosis tensor imaging at a 1.5T: presurgical planning of patients with gliomas”. European Journal of Radiology Open, 28; 5: 20-23, 2018.

108. S. Smith, M. Jenkinson, M. Woolrich, C. Beckmann, T. Behrens, H. Johansen-Berg H, P. Bannister, et al. “Advances in functional and structural MR image analysis and implementation as FSL.” Neuroimage. Review. 23: S208-219. 2004.

109. J. Fernández-Miranda, Y. Wang, S. Pathak, L. Stefaneau, T. Verstynen, F. Yeh. “Asymmetry, connectivity, and segmentation of the arcuate fascicle in the human brain.” Brain Struct Funct.; 220: 1665-80, 2015.

110. T. Nguyen-Thanh, M. Reisert, C. Anastasopoulos, F. Hamzei, T. Reithmeier, M. Vry, V. Kiselev, et al. “Global tracking in human gliomas: a comparison with established tracking methods” Clin Neuroradiol.; 23:263-275, 2013.

111. Y. Bai, Y. J. Lin. D. Tian, J. Shi, E. Cheng, E. Haacke, X, Hong, B. Ma, J. Zhou and M. Wang. “Grading of Gliomas by Using Monoexponential, Biexponential, and Stretched Exponential Diffusion-weighted MR Imaging and Diffusion Kurtosis MR Imaging” Radiology.; 278: 496-504, 2016.

112. T. Behrens, M. Woolrich, M. Jenkinson, H. Johansen-Berg, R. Nunes, S. Clare, P. Matthews, J. Brady and S. Smith. “Characterization and propagation of uncertainty in diffusion-weighted MR imaging” Magn Reson Med.; 50: 1077-1088, 2003.

113. M. Mandelli, M. Berger, M. Bucci, J. Berman, B. Amirbekian and R. Henry. “Quantifying accuracy and precision of diffusion MR tractography of the corticospinal tract in brain tumors” J Neurosurg. 121: 349-358, 2014.

114. F. Zhu, J. Wu, Y. Song, C. Yao, D. Zhuang, G. Xu, W. Tang et al. “Clinical application of motor pathway mapping using diffusion tensor imaging tractography and intraoperative direct subcortical stimulation in cerebral glioma surgery: a prospective cohort study” Neurosurgery. 71: 1170-1183; discussion 1183-1184. 2012.

115. I. Eyüpoglu I, M. Buchfelder, N. Savaskan. “Surgical resection of malignant gliomas-role in optimizing patient outcome” Nat Rev Neurol. 9: 141-151, 2013.

116. J. Tuominen, S. Yrjänä, A. Ukkonen, J. Koivukangas. “Awake craniotomy may further improve neurological outcome of intraoperative MRI-guided brain tumor surgery” Acta Neurochir (Wien). 155: 1805-1812, 2013.

117. T. Beez, K. Boge, M. Wager, I. Whittle, D. Fontaine, G. Spena, S. Braun, et al. “European Low Grade Glioma Network. Tolerance of awake surgery for glioma: a prospective European Low Grade Glioma Network multicenter study” Acta Neurochir (Wien). 155: 1301-1308, 2013.

118. J. Dineen, D. Maus, I. Muzyka, R. See, D. Cahill, B. Carter, W. Curry, et al. “Factors that modify the risk of intraoperative seizures triggered by electrical stimulation during supratentorial functional mapping” Clin Neurophysiol. 130: 1058-1065, 2019.

119. M. Milian, M. Tatagiba, G. Feigl. “Patient response to awake craniotomy – a summary overview” Acta Neurochir (Wien). 156: 1063-1070, 2014.

120. K. Vakamudi, S. Posse, R. Jung, B. Cushnyr, M. Chohan. “Real-time presurgical resting-state fMRI in patients with brain tumors: Quality control and comparison with task-fMRI and intraoperative mapping” Hum Brain Mapp. 6. 2019.

121. K. Peck, M. Bradbury, N. Petrovich, B. Hou, N. Ishill, C. Brennan, V. Tabar, et al. “Presurgical evaluation of language using functional magnetic resonance imaging in brain tumor patients with previous surgery” Neurosurgery. 64: 644-52; discussion 652-653, 2009.

122. C. Benjamin, P. Walshaw, K. Hale, W. Gaillard, L. Baxter, M. Berl, M. Polczynska et al. “Presurgical language fMRI: Mapping of six critical regions” Hum Brain Mapp. 38: 4239-4255, 2017.

123. M. Jenkinson, D. Barone, A. Bryant, L. Vale, H. Bulbeck, T. Lawrie, M. Hart et al. “Intraoperative imaging technology to maximize extent of resection for glioma” Cochrane Database Syst Rev. 22: 1-50, 2018.

124. W. Gaillard, L. Balsamo, B. Xu, C. McKinney, P. Papero, S. Weinstein, J. Conry, et al. “fMRI language task panel improves determination of language dominance” Neurology. 63: 1403-1408, 2004.

125. A. Holodny, M. Schulder, W. Liu, J. Wolko, J. Maldjian, A. Kalnin. “The effect of brain tumors on BOLD functional MR imaging activation in the adjacent motor cortex: implications for image-guided neurosurgery” AJNR Am J Neuroradiol. 21: 1415-1422, 2000.

126. L. Wang, D. Chen, J. Olson, S. Ali, T. Fan, H. Mao. “Re-examine tumor-induced alterations in hemodynamic responses of BOLD fMRI: implications in presurgical brain mapping” Acta Radiol. 253: 802-811, 2012.

127. A. Castro, I. Gomes, S. Caló, “PALPA-P – Provas de Avaliação da Linguagem e da Afasia em Português,” Lisboa: CEGOC, 2007.

128. R. Soffietti, B. Baumert, L. Bello, A. von Deimling, H. Duffau, M. Frénay, W. Grisold, et al. “Guidelines on management of low-grade gliomas: report of an EFNS-EANO Task Force” Eur J Neurol. 17: 1124-1133, 2010.

129. M. Weller, M. van den Bent, K. Hopkins, J. Tonn, R. Stupp, A. Falini, E. Cohen-Jonathan-Moyal, et al. “European Association for Neuro-Oncology (EANO) Task Force on Malignant Glioma. EANO guideline for the diagnosis and treatment of anaplastic gliomas and glioblastoma” Lancet Oncol. 15: e395-403. Erratum in: Lancet Oncol. 2014; 15: e587, 2014.

130. M. Hund-Georgiadis, U. Lex, C. von Cramon. “Language dominance assessment by means of fMRI: contributions from task design, performance, and stimulus modality” J Magn Reson Imaging, 13: 668-675, 2001.

131. M. Schulte-Tamburen, J. Scheier, J. Briegel, D. Schwender, K. Peter. “Comparison of five sedation scoring systems by means of auditory evoked potentials” 1999. Intensive Care Med 25: 377–382, 1999.

132. D. Corina, E. Gibson, R. Martin, A. Poliakov, J. Brinkley, G. Ojemann. “Dissociation of action and object naming: evidence from cortical stimulation mapping” Hum Brain Mapp. 24: 1-10, 2005.

133. H. Weng, K. Noll, J. Johnson, S. Prabhu, Y. Tsai, S. Chang, Y. Huang Y, et al. “Accuracy of Presurgical Functional MR Imaging for Language Mapping of Brain Tumors: A Systematic Review and Meta-Analysis” Radiology 286: 512-523, 2018.

134. D. Sabsevitz, S. Swanson, T. Hammeke, M. Spanaki, E. Possing, G. Morris, M. Mueller et al. “Use of preoperative functional neuroimaging to predict language deficits from epilepsy surgery” Neurology. 60, 1788–1792, 2003.

135. C. Gauthier, A. Fan. “BOLD signal physiology: Models and applications.” NeuroImage 27: 116-127, 2018.

136. M. Morrison, F. Tam, M. Garavaglia, L. Golestanirad, G. Hare, M. Cusimano, T. Schweizer, S. Das and S. Graham. “A novel tablet computer platform for advanced language mapping during awake craniotomy procedures” J Neurosurg. 124: 938-944, 2016.

137. J. Binder. “Use of fMRI Language Lateralization for Quantitative Prediction of Naming and Verbal Memory Outcome in Left Temporal Lobe Epilepsy Surgery” In: Ulmer S., Jansen O. (eds) fMRI. Springer, Berlin, Heidelberg 2013, 77-93.

138. H. Mehdorn, S. Goebel, A. Nabavi. “Direct Cortical Stimulation and fMRI.” In Ulmer S, Jansen O. eds., fMRI – Basics and Clinical Applications 2013. Berlin, Springer, 169-175.

139. W. Hall, P. Kim, C. Truwit. “Functional magnetic resonance imaging-guided brain tumor resection” Top Magn Reson Imaging. 19: 205-212, 2009.

140. E. De Witte, D. Satoer, E. Robert, H. Colle, S. Verheyen, E. Visch-Brink, P. Mariën. “The Dutch Linguistic Intraoperative Protocol: a valid linguistic approach to awake brain surgery” Brain Lang. 140: 35-48, 2015.

141. E. De Witte, P. Mariën. “The neurolinguistic approach to awake surgery reviewed.” Clin Neurol Neurosurg. 115: 127-145, 2013.

142. F. Roux, D. Ibarrola, M. Tremoulet, Y. Lazorthes, P. Henry, J. Sol, I. Berry. “Methodological and technical issues for integrating functional magnetic resonance imaging data in a neuronavigational system” Neurosurgery 49: 1145-56; discussion 1156-1157, 2001.

143. F. Strappini, E. Gilboa, S. Pitzalis, K. Kay, M. McAvoy, A. Nehorai, A. Snyder. “Adaptive smoothing based on Gaussian processes regression increases thevsensitivity and specificity of fMRI data” Hum Brain Mapp. 38: 1438-1459, 2017.

144. L. Stieglitz, J. Fichtner, R. Andres, P. Schucht, A. Krähenbühl, A. Raabe, J. Beck. “The silent loss of neuronavigation accuracy: a systematic retrospective analysis of factors influencing the mismatch of frameless stereotactic systems in cranial neurosurgery” Neurosurgery. 72: 796-807, 2013.

145. M. Jen, I. Hassan, P. Hou, G. Li, A. Kumar, S. Prabhu, R. Colen, et al. “Comparison of functional localization accuracy with different co-registration strategies in presurgical fMRI for brain tumor patients” Med Phys. 45: 3223-3228, 2018.

146. E. Nossek, I. Matot, T. Shahar, O. Barzilai, Y. Rapoport, T. Gonen, G. Sela et al. “Failed awake craniotomy: a retrospective analysis in 424 patients undergoing craniotomy for brain tumor” J Neurosurg. 118: 243-24, 2013.

147. E. Chang, J. Breshears, K. Raygor, D. Lau, A. Molinaro, M. Berger. “Stereotactic probability and variability of speech arrest and anomia sites during stimulation mapping of the language dominant hemisphere” J Neurosurg., 126: 114-121, 2017.

148. H. Duffau, L. Capelle, D. Denvil, N. Sichez, P. Gatignol, M. Lopes, M. Mitchell, J. Sichez, and R. Van Effenterre, “Functional recovery after surgical resection of low grade gliomas in eloquent brain: hypothesis of brain compensation” J Neurol Neurosurg Psychiatry, 74, 901-907, 2003.

149. M. Hart, S. Price and J. Suckling," Connectome analysis for pre-operative brain mapping in neurosurgery" Br J Neurosurg., 30, 506-517, 2016.

150. R. Alemi, S. Batouli, E. Behzad, M. Ebrahimpoor and M. Oghabian, "Not single brain areas but a network is involved in language: Applications in presurgical planning" Clin Neurol Neurosurg., 165, 116-128, 2018.

151. E. Shiban, S. Krieg, B. Haller, N. Buchmann, T. Obermueller, T. Boeckh-Behrens, M. Wostrack, B. Meyer and F. Ringel, "Intraoperative subcortical motor evoked potential stimulation: how close is the corticospinal tract?" J Neurosurg., 123, 711-720, 2013.

152. M. Vassal, C. Charroud, J. Deverdun, E. Le Bars, F. Molino, F. Bonnetblanc, A. Boyer, G. Herbet, S. Moritz-Gasser et al. "Recovery of functional connectivity of the sensorimotor network after surgery for diffuse low-grade gliomas involving the supplementary motor area", Neurosurg., 126, 1181-1190, 2017.

153. A. Bizzi, V. Blasi, A. Falini, P. Ferroli, M. Cadioli, U. Danesi, D. Aquino, C. Marras, D. Caldiroli et al. "Presurgical functional MR imaging of language and motor functions: validation with intraoperative electrocortical mapping" Radiology, 248, 579-589, 2008.

154. J. Joyce, P. Laurienti, J. Burdette and S. Hayasaka, "A new measure of centrality for brain networks" PloS One, vol. 16, e12200, 2010.

155. J. Leote, R. Loução, R. Nunes, C. Viegas, M. Lauterbach, A. Silvestre, J. Monteiro, A. Pérez-Hick and H. A. Ferreira, "Connectivity analysis of glioma patients with language disturbances", Clinical Neurophysiology (Abstract), e53-e54, 2018.

156. G. Kristo, M. Raemaekers, G. Rutten, B. de Gelder and N. Ramsey," Inter-hemispheric language functional reorganization in low-grade glioma patients after tumour surgery" Cortex, 64, 235-248 2011.

157. N. Ramsey, I. Sommer, G. Rutten and R. Kahn, "Combined analysis of language tasks in fMRI improves assessment of hemispheric dominance for language functions in individual subjects" Neuroimage, 13, 719-733, 2001.

158. Cochereau J, Deverdun J, Herbet G, Charroud C, Boyer A, Moritz-Gasser S, Le Bars E, Molino F, Bonafé A, Menjot de Champfleur N, Duffau H. "Comparison between resting state fMRI networks and responsive cortical stimulations in glioma patients" Hum Brain Mapp. ; 37: 3721-3732, 2016.

159. O. Sporns. "Contributions and challenges for network models in cognitive neuroscience" Nat Neurosci. Review, 17: 652-660, 2014.

160. J. Alstott, M. Breakspear, P. Hagmann, L. Cammoun, O. Sporns. "Modeling the impact of lesions in the human brain" PLoS Comput Biol. 5: e1000408, 2009.

161. H. Duffau. "Mapping the connectome in awake surgery for gliomas: an update" J Neurosurg Sci.; 61: 612-630, 2017.

162. S. Lang. "Cognitive eloquence in neurosurgery: Insight from graph theoretical analysis of complex brain networks" Med Hypotheses. 98: 49-56. 2017.

163. M. Raichle, M. Mintun. “Brain work and brain imaging” Annu Rev Neurosci 29: 449–476, 2006.

164. M. Hart, R. Ypma, R. Romero-Garcia, S. Price, J. Suckling. “Graph theory analysis of complex brain networks: new concepts in brain mapping applied to neurosurgery” J Neurosurg. Review. 124: 1665-78, 2016.

165. M. Hampson, B. Peterson, P. Skudlarski, J. Gatenby, J. Gore. “Detection of functional connectivity using temporal correlations in MR images” Hum Brain Mapp. 15: 247-262, 2002.

166. T. Mitchell, C. Hacker, J. Breshears, N. Szrama, M. Sharma, D. Bundy, M. Pahwa et. al. “A novel data-driven approach to preoperative mapping of functional cortex using resting-state functional magnetic resonance imaging” Neurosurgery. 73 :969-82; discussion 982-983, 2013.

167. C. Rosazza, D. Aquino, L. D'Incerti, R. Cordella, A. Andronache, D. Zacà, M. Bruzzone, G. Tringali, L. Minati. “Preoperative mapping of the sensorimotor cortex: comparative assessment of task-based and resting-state FMRI” PLoS One. 10; 9: e98860, 2014.

168. N. Tanaka, S. Stufflebeam. “Presurgical Mapping of the Language Network Using Resting-state Functional Connectivity” Top Magn Reson Imaging. 25: 19-24, 2016.

169. G. Tononi, O. Sporns, G. Edelman. “A measure for brain complexity: relating functional segregation and integration in the nervous system” Proc. Natl. Acad. Sci. 91, 5033–5037, 1994.

170. R. Desikan, F. Ségonne, B. Fischl, B. Quinn, B. Dickerson, D. Blacker, R. Buckner et al. “An automated labeling system for subdividing the human cerebral cortex on MRI scans into gyral based regions of interest” NeuroImage, 31, 968–980, 2006.

171. M. Kaiser, R. Martin, P. Andras, M. Young. “Simulation of robustness against lesions of cortical networks” Eur J Neurosci. 25: 3185-3192, 2007.

172. A. Barabasi, R. Albert. “Emergence of scaling in random networks.” Science. 286: 509- 567, 1999.

173. I. Arrillaga-Romany, M. Monje, P. Wen. “Neurologic complications of oncology therapy” in Handbook of Neuro-Oncology Neuroimaging, 2nd ed., H. Newton (Ed.). London: Academic Press, 2016, 125-142.

174. F. Miraglia, F. Vecchio, P. Rossini. “Searching for signs of aging and dementia in EEG through network analysis” Behav. Brain Res. 317, 292–300, 2007.

175. G. Herbet, M. Maheu, E. Costi, G. Lafargue, H. Duffau. “Mapping neuroplastic potential in brain-damaged patients” Brain 139, 829–844. 2016.

176. Y. Yordanova, J. Cochereau, H. Duffau, G. Herbet. “Combining resting state functional MRI with intraoperative cortical stimulation to map the mentalizing network” NeuroImage, 186, 628-636, 2019.

177. Y. Iturria-Medina, R. Sotero, E. Canales-Rodriguez, Y. Aleman-Gomez, L. Melie-Garcia. “Studying the human brain anatomical network via diffusion-weighted MRI and graph theory” NeuroImage. 40: 1064-1076, 2008.

178. L. Zhu, Y. Fan, Q. Zou, J. Wang, J. Gao, Z. Niu. “Temporal reliability and lateralization of the resting-state language network” PLoS One; 9: e85880, 2014.

179. P. Branco, D. Seixas, S. Deprez, S. Kovacs, R. Peeters, S. Castro, S. Sunaert. “Resting- State Functional Magnetic Resonance Imaging for Language Preoperative Planning” Front Hum Neurosci.; 10, 11, 2016

180. M. Vigneau, V. Beaucousin, P. Hervé, H. Duffau, F. Crivello, O. Houdé, B. Mazoyer et al. “Meta-analyzing left hemisphere language areas: phonology, semantics, and sentence processing” Neuroimage; 30: 1414-1432, 2006.

181. P. Hagmann, L. Cammoun, X, Gigandet, R. Meuli, C. Honey, V. Wedeen, O. Sporns. “Mapping the structural core of human cerebral cortex” PLoS Biol 6: e159, 2008.

182. O. Sporns, G. Tononi. “The human connectome: A structural description of the human brain” PLoS Comput. Biol. 1, e42, 2005.

183. S. Stramaglia, J. Cortes, D. Marinazzo. “Synergy and redundancy in the Granger causal analysis of dynamical networks” New J. Phys. 16, 2014.

184. M. Rubinov, O. Sporns, O. “Weight-conserving characterization of complex functional brain networks.” Neuroimage 56, 2068–2079, 2011.

185. E.B ullmore, O. Sporns. “The economy of brain network organization” Nat. Rev. Neurosci. 13, 336–349, 2012.

186. M. Cole, J. Reynolds, J. Power, G. Repovs, A. Anticevic, T. Braver. “Multi-task connectivity reveals flexible hubs for adaptive task control.” Nat Neurosci. 16:1348-1355, 2013.

187. A. Zalesky, A. Fornito, E. Bullmore. “Network-based statistic: identifying differences in brain networks” Neuroimage; 53, 1197–1207, 2010.

188. K. Shen, G. Bezgin, R. Hutchison, J. Gati, R. Menon, S. Everling, A. McIntosh. “Information processing architecture of functionally defined clusters in the macaque cortex” J Neurosci. 28: 17465-17476, 2012.

189. G. Zamora-López, C. Zhou, J. Kurths. “Cortical hubs form a module for multisensory integration on top of the hierarchy of cortical networks” Front. Neuroinform. 4, 1, 2010.

190. C. Honey, O. Sporns, L. Cammoun, X. Gigandet, J. Thiran, R. Meuli, P. Hagmann. “Predicting human resting-state functional connectivity from structural connectivity” Proc Natl Acad Sci U S A. 106: 20352040, 2009.

191. W. Campbell. “Disorders of Speech and Language.” In DeJong’s, The neurologic examination, Campbell ed., India: Lippincott Williams & Wilkins, 2013, 87-97.

192. Y. Lien, C. Stepp. “Comparison of voice relative fundamental frequency estimates derived from an accelerometer signal and low-pass filtered and unprocessed microphone signals.” J Acoust Soc Am. 135: 2977-2985, 2014.

193. S. Chandrasekhar, G. Randolph, M. Seidman. R. Rosenfeld, P. Angelos, J. Barkmeier-Kraemer, M. Benninger, et al. “Clinical practice guideline: improving voice outcomes after thyroid surgery” Otolaryngol Head Neck Surg.;148: S1-37, 2013.

194. H. Schliesser. “EMG biofeedback as a function of voice-quality change” Percept Mot Skills, 64: 719-724, 1987.

195. E. Van Houtte, S. Claeys, E. D'haeseleer, F. Wuyts, K. Van Lierde. “An examination of surface EMG for the assessment of muscle tension dysphonia” J Voice. 27: 177-186, 2013.

196. C. Stepp, J. Heaton, M. Braden, M. Jette, T. Stadelman-Cohen, R. Hill. “Comparison of neck tension palpation rating systems with surface electromyographic and acoustic measures in vocal hyperfunction” J Voice. 25:67–75, 2011.

197. N. Vermula. “A study of human throat-wall and vocal tract from input/output measurements”. In N. Vermula ed. Missouri: Washington University. 1979.

198. E. Yiu, F. Chen, G. Lo, G. Pang. “Vibratory and Perceptual Measurement of Resonant Voice” Journal of Voice, 26: 5, 675.e13, 2012.

199. A. Vitikainen, E. Mäkelä, P. Lioumis, V. Jousmäki and J. Mäkelä. “Accelerometer-based automatic voice onset detection in speech mapping with navigated repetitive transcranial magnetic stimulation” J Neurosci Methods., 30; 253: 70-77, 2015.

200. A. Stevenson, C. Chiu, D. Maslovat, R. Chua, B. Gick, J. Blouin, I. Franks. “Cortical involvement in the StartReact effect“ Neuroscience, 269, 21-34, 2014.

201. J. Castellote, J. Leote, J. Valls-Sole. “Accelerometric recording of changes in voice production in teachers after daily task” European Journal of Neurology, (Abstract) 25, 623, 2018.

202. Y. Lien, C. Calabrese, C. Michener, E. Murray, J. Van Stan, D. Mehta, R. Hillman, J. Noordzij, C. Stepp. “Voice Relative Fundamental Frequency Via Neck-Skin Acceleration in Individuals with Voice Disorders” J Speech Lang Hear Res. 58: 1482-1487, 2015.

203. F. Lindstrom, K. Ren, H. Li, K. Waye. “Comparison of two methods of voice activity detection in field studies” J Speech Lang Hear Res. 52 :1658-1663, 2009.

204. R. Hillman, J. Heaton, A. Masaki, S. Zeitels, H. Cheyne. “Ambulatory monitoring of disordered voices” Ann Otol Rhinol Laryngol. 115: 795-801, 2006.

205. V. McKenna, A. Llico, D. Mehta, J. Perkell, C. Stepp. Magnitude of Neck-Surface Vibration as an Estimate of Subglottal Pressure During Modulations of Vocal Effort and Intensity in Healthy Speakers. Journal of speech, language, and hearing research. 60, 3404–3416. 2017.

206. R Coleman. “Comparison of microphone and neck-mounted accelerometer monitoring of the performing voice” J. Voice 2, 200–205, 1988.

207. J. Cichero, B. Murdoch. “Detection of Swallowing Sounds: Methodology Revisited” Dysphagia, 17: 40-49, 2002.

208. M. Morgan, R. Hewer, R. Cooper. “Intention tremor – a method of measurement” J Neurol Neurosurg Psychiatry. 38: 253–258, 1975.

209. M. Zwarts, M. Keidel M. “Relationship between electrical and vibratory output ofmuscle during voluntary contraction and fatigue” Muscle Nerve. 14: 756-761, 1991.

210. R. Berry, R. Budhiraja, D. Gottlieb, D. Gozal, C. Iber, V. Kapur, et al. “American Academy of Sleep Medicine. Rules for scoring respiratory events in sleep: update of the 2007 AASM Manual for the Scoring of Sleep and Associated Events.” Deliberations of the Sleep Apnea Definitions Task Force of the American Academy of Sleep Medicine. J Clin Sleep Med. 15; 8: 597-619, 2012.

211. K. Mamun, C. Steele, T. Chau. “Swallowing accelerometry signal feature variations with sensor displacement” Med Eng Phys. 37: 665-673, 2015.

212. M. Nolan, B. Madden, E. Burke. “Accelerometer based measurement for the mapping of neck surface vibrations during vocalized speech” Conf Proc IEEE Eng Med Biol Soc. 4453-4456, 2009.

213. G. Yeung, S. Lulich, J. Guo, M. Sommers, A. Alwan. “Subglottal resonances of American English speaking children” J Acoust Soc Am. 144: 3437, 2018.

214. S. Lulich, A. Alwan, H. Arsikere, J. Morton, M. Sommers. “Resonances and wave propagation velocity in the subglottal airways” J Acoust Soc Am.130: 2108-2115, 2011.

215. D. Mehta, H. Cheyne, A. Wehner, J. Heaton, R. Hillman “Accuracy of Self-Reported Estimates of Daily Voice Use in Adults With Normal and Disordered Voices” Am J Speech Lang Pathol. 25: 634-641, 2016.

216. J. Lee, C. Steele, T. Chau. “Classification of healthy and abnormal swallows based on accelerometry and nasal airflow signals” Artificial Intelligence in Medicine, 52: 17–25, 2011.

217. P. Tarapore, A. Findlay, S. Honma, D Mizuiri, J. Houde, M. Berger, S. Nagarajan. “Language mapping with navigated repetitive TMS: proof of technique and validation” Neuroimage 82:260–272, 2013.

218. T. Picht, S. Krieg, N. Sollmann, J. Rösler, B. Niraula, T. Neuvonen, P. Savolainen, et al. “A comparison of language mapping by preoperative navigated transcranial magnetic stimulation and direct cortical stimulation during awake surgery” Neurosurgery 72: 808–819, 2013.

219. N. Sollmann, A. Kelm, S. Ille, A. Schröder, C. Zimmer, F. Ringel, B. Meyer et al. “Setup presentation and clinical outcome analysis of treating highly language-eloquent gliomas via preoperative navigated transcranial magnetic stimulation and tractography” Neurosurg Focus., 44: E2, 2018.

220. R. Kilbride. ”Intraoperative functional cortical mapping of language” J Clin Neurophysiol. Review. 30: 591-596. 2013.

221. A. Chacko, S. Thomas, K. Babu, R. Daniela, G. Chacko, K. Prabhu, V. Cherian et al. “Awake craniotomy and electrophysiological mapping for eloquent area tumours” Clin Neurol Neurosurg., 115: 329– 334, 2013.

222. J. Leote, J. Valls-Solé, J. Costa, J. Casanova-Molla, L. Oleaga, J. Fonseca, R. Nunes et al. “Vocal accelerometer recording of TMS evoked language disturbances: preliminary study for awake surgery application” Brain Stimul. Abstract. 2, 352, 2017.

223. S. Krieg, P. Tapore, T. Picht, N. Tanigawa, J. Houde, N. Sollmann, B. Meyer, et al. “Optimal timing of pulse onset for language mapping with navigated repetitive transcranial magnetic stimulation” NeuroImage, 100; 15: 219–236, 2014.

224. S. Krieg, P. Lioumis, J. Mäkelä, J. Wilenius, J. Karhu, H. Hannula, P. Savolainen, et al. “Protocol for motor and language mapping by navigated TMS in patients and healthy volunteers; workshop report” Acta Neurochir (Wien). Review. 159: 1187-1195, 2017.

225. R. Kent. “Vocal tract acoustics” J Voice. Review. 7: 97-117, 1993.

226. M. Rogic, V. Deletis, I. Fernandez-Conejero. “Inducing transient language disruptions by mapping of Broca’s area with modified patterned repetitive transcranial magnetic stimulation protocol” J Neurosurg 120: 1033–1041, 2014.

227. D. Frey, S. Schilt, V. Strack, A. Zdunczyk, J. Rösler, B. Niraula, P. Vajkoczya et al. “Navigated transcranial magnetic stimulation improves the treatment outcome in patients with brain tumors in motor eloquent locations” Neuro Oncol., 16: 1365-1372, 2014.

228. K. Seidel, L. Häni, K. Lutz, C. Zbinden, A. Redmann, A. Consuegra, A. Raabe et al. “Postoperative navigated transcranial magnetic stimulation to predict motor recovery after surgery of tumors in motor eloquent areas” Clin Neurophysiol. 130: 952-959, 2019.

229. C. Epstein, J. Lah, K. Meador, J. Weissman, L. Gaitan, B. Dihenia. “Optimum stimulus parameters for lateralized suppression of speech with magnetic brain stimulation” Neurology 47: 1590– 1593, 1996.

230. J. Jung, J. Lavrador, S. Patel, A. Giamouriadis, J. Lam, R. Bhangoo, K. Ashkan et al. “First United Kingdom Experience of Navigated Transcranial Magnetic Stimulation in Preoperative Mapping of Brain Tumors” World Neurosurg., 122: e1578-e1587, 2019.

231. S. Knecht, M. Deppe, B. Dräger, L. Bobe, H. Lohmann, E. Ringelstein, H. Henningsen. “Language lateralization in healthy right-handers” Brain. 123 (Pt 1): 74-81, 2000.

232. J. Rösler, B. Niraula, V. Strack, A. Zdunczyk, S. Schilt, P. Savolainen, P. Lioumis, et al. “Language mapping in healthy volunteers and brain tumor patients with a novel navigated TMS system: evidence of tumor-induced plasticity” Clin Neurophysiol. 125: 526-536, 2014.

233. N. Sollmann, S. Ille, T. Hauck, S. Maurer, C. Negwer, C. Zimmer, F. Ringel, et al. “The impact of preoperative language mapping by repetitive navigated transcranial magnetic stimulation on the clinical course of brain tumor patients” BMC Cancer. 11; 15: 261, 2015.

234. T. Hauck, N. Tanigawa, M. Probst, A. Wohlschlaeger, S. Ille, N. Sollmann, S. Maurer, et al. “Stimulation frequency determines the distribution of language positive cortical regions during navigated transcranial magnetic brain stimulation” BMC Neurosci. 16: 5, 2015

235. T. Hauck, N. Tanigawa, M. Probst, A. Wohschlaeger, S. Ille, N. Sollmann, S. Maurer, et al. “Task type affects location of language-positive cortical regions by repetitive navigated transcranial magnetic stimulation mapping” PLoS One 10: e012529, 2015.

236. P. Tarapore, T. Picht T, Bulubas L, Shin Y, Kulchytska N, Meyer, M Berger et al. “Safety and tolerability of navigated TMS for preoperative mapping in neurosurgical patients” Clin Neurophysiol. 127: 1895-900, 2016.

237. H. Duffau, L. Capelle, D. Denvil, N. Sichez, P. Gatignol, M. Lopes, M. Mitchell, et al. “Functional recovery after surgical resection of low grade gliomas in eloquent brain: hypothesis of brain compensation” J Neurol Neurosurg Psychiatry, 74, 901-907, 2003.

238. A. Tekriwal, G. Felsen, J. Thompson. “Modular auditory decision-making behavioral task designed for intraoperative use in humans” J Neurosci Methods. 304: 162-167, 2018.

239. Picart T, Duffau H. “Awake resection of a left operculo-insular low-grade glioma guided by cortico-subcortical mapping” Neurosurg Focus. 45 (VideoSuppl2): V1, 2018.

240. S. Hervey-Jumper, J. Li, D. Lau, A. Molinaro, D. Perry, L. Meng, M. Berger. “Awake craniotomy to maximize glioma resection: methods and technical nuances over a 27-year period” J Neurosurg 123: 325–339, 2015.

241. L. Henderson, W. Dittrich. “The cortical organization of uncertainty: I. New perspectives on simple reaction time” British Journal of Psychology, 89, 531-554, 1998.

242. J. Valls-Solé, J. Rothwell, F. Goulart, G. Cossu, J. Muñoz. “Patterned ballistic movements triggered by a startle in healthy humans” Journal of Physiology, 516, 931–938, 1999.

243. A. Carlsen, R. Chua, J. Inglis, D. Sanderson, I. Franks. “Prepared movements are elicited early by startle” Journal of Motor Behavior, 36, 253-264, 2004.

244. F. Pulvermüller, M. Huss, F. Kherif, M. Moscoso del Prado, O. Hauk, Y. Shtyrov. “Motor cortex maps articulatory features of speech sounds” Proceedings of the National Academy of Sciences, 103, 7865-7870, 2006.

245. S. Tremblay, D. Shiller, D. Ostry. “Somatosensory basis of speech production” Nature, 423, 866-869, 2003.

246. B. Grimme, S. Fuchs, P. Perrier, G. Schöner. “Limb versus speech motor control: a conceptual review” Motor Control, 15, 5-33, 2011.

247. I. Rodrigues, A. Castro-Caldas. “Aphasia with recurring utterances: Old syndrome, new perspectives” Aphasiology, 28, 1350-1363, 2014.

248. Y. Worbe, S. Lehericy, A. Hartmann. “Neuroimaging of tic genesis: Present status and future perspectives. Mov Disord, 30,1179-1183, 2015.

249. A. Berkovich-Ohana, M. Wilf, R. Kahana, A. Arieli, R. Malach, “Repetitive speech elicits widespread deactivation in the human cortex: the "Mantra" effect?” Brain & Behavior, 5, e00346, 2015.

250. O. Robertson, S. Robinson, R. Stephens. “Swearing as a response to pain: A cross-cultural comparison of British and Japanese participants”Scand J Pain, 17, 267-272, 2017.

251. T. Schuhmann, N. Schiller, R. Goebel, A. Sack. “Speaking of which: dissecting the neurocognitive network of language production in picture naming” Cerebral Cortex, 22, 701-709, 2012.

252. A. Turken, N. Dronkers, “The neural architecture of the language comprehension network: converging evidence from lesion and connectivity analyses” Frontiers in Systems Neuroscience, 5, 1, 2011.

253. D. Maslovat, N. Hodges, R. Chua, I. Franks. “Motor preparation and the effects of practice: evidence from startle” Behav Neurosci, 125: 226-240, 2011.

254. A. Carlsen, C. Mackinnon. “Motor preparation is modulated by the resolution of the response timing information” Brain Res, 1322, 38-49, 2010.

255. D. Maslovat, M. Carter, A. Carlsen. “Startle neural activity is additive with normal cortical initiation-related activation” Neurosci Lett, 558,164-168, 2014.

256. J. Castellote and J. Valls-Solé. “The StartReact effect in tasks requiring end-point accuracy” Clinical Neurophysiology, 126, 1879-1885, 2015

257. I. Indefrey. “The spatial and temporal signatures of word production components: a critical update” Frontiers in Psychology, 2, 255, 2011.

258. H. Kumru, X. Urra, Y. Compta, J. Castellote, J. Turbau, J. Valls-Solé. “Excitability of subcortical motor circuits in Go/noGo and forced choice reaction time tasks” Neuroscience Letters, 406, 66-70, 2011.

259. M. Fernandez-Del-Olmo, D. Río-Rodríguez, E. Iglesias-Soler, R. Acero. “Startle Auditory Stimuli Enhance the Performance of Fast Dynamic Contractions.” PLoS ONE, 9, e87805, 2014

260. J. Nonnekes, L. Nijhuis, M. de Niet, S. de Bot, J. Pasman, B. van de Warrenburg, et al. “StartReact restores reaction time in HSP: evidence for subcortical release of a motor program” Journal of Neuroscience, 34, 275-281, 2014.

261. D. Maslovat, R. Chua, A. Carlsen, C. May, C. Forgaard, I. Franks. “A startling acoustic stimulus interferes with upcoming motor preparation: Evidence for a startle refractory period” Acta Psychologica, 158, 36-42, 2015.

262. G. Blanken, C. Wallesch, C. Papagno. “Dissociations of language functions in aphasics with speech automatisms (recurring utterances)” Cortex, 26, 41-63, 1990.

263. C. Wallesch, G. Blanken. “Recurring utterances-how, where, and why are they generated?" Brain & Language, 71, 255-257, 2000.

264. M. Fama, C. Baron, B. Hatfield, P. Turkeltaub. "Group therapy as a social context for aphasia recovery: a pilot, observational study in an acute rehabilitation hospital” Topics in Stroke Rehabilitation, 23, 276-283, 2016.

265. K. Scholes, M. Martin-Iverson. “Relationships between prepulse inhibition and cognition are mediated by attentional processes” Behavioural Brain Research, 205, 456-467, 2009.

266. D. Maslovat, N. Drummond, M. Carter, A. Carlsen. “Reduced motor preparation during dual-task performance: evidence from startle” Experimental Brain Research, 233, 2673-2683, 2015.

267. R. Nickerson. “Intersensory facilitation of reaction time: energy summation or preparation enhancement?” Psychology Reviews, 80, 489–509, 1973.

268. S. Gielen, R. Schmidt, P. Van den Heuvel. “On the nature of intersensory facilitation of reaction time” Perception & Psychophysics, 34, 161-168, 1983.

269. L. Alibiglou, C. MacKinnon, “The early release of planned movement by acoustic startle can be delayed by transcranial magnetic stimulation over the motor cortex” Journal of Physiology, 590, 919-936, 2012.

270. W. Marinovic, M. Milford, T. Carroll, S. Riek, “The facilitation of motor actions by acoustic and electric stimulation” Psychophysiology, 52, 1698-1710, 2015.

271. R. Reynolds, B. Day. “Fast visuomotor processing made faster by sound” Journal of Physiology, 583, 1107-1115, 2007.

272. J. Nonnekes, L. Nijhuis, M. de Niet, S. de Bot, J. Pasman, B. van de Warrenburg, B. Bloem, et al. “StartReact restores reaction time in HSP: evidence for subcortical release of a motor program” Journal of Neuroscience, 34, 275-281, 2014.

273. J. Valls-Solé, M. Kofler, H. Kumru, J. Castellote, M. Sanegre. “Startle-induced reaction time shortening is not modified by prepulse inhibition” Experimental Brain Research, 165, 541-548, 2005.

274. A. Friederici. “The brain basis of language processing: from structure to function" Physiological Reviews, 91, 1357-1392, 2011.

275. C. Price. "The anatomy of language: a review of 100 fMRI studies published in 2009“ Annals of the New York Academy of Sciences, 1191, 62–88, 2010.

276. A. MacDonald, S. Heath, K. McMahon, L. Nickels, A. Angwin, S. van Hees, K. Johnson, et al. “Neuroimaging the short- and long-term effects of repeated picture naming in healthy older adults” Neuropsychologia, 75, 170-178, 2015.

277. R. Bapi, K. Miyapuram, F. Graydon. “fMRI investigation of cortical and subcortical networks in the learning of abstract and effector-specific representations of motor sequences” Neuroimage, 32, 714-727, 2006.

278. Y. Kwon, J. Kwon, J. Park. “Changes in brain activation patterns according to cross-training effect in serial reaction time task: A functional MRI study” Neural Regen Res, 8, 639-646, 2013.

279. C. Kang, Y. Fu, J. Wu, F. Ma, C. Lu, T. Guo. “Short-term language switching training tunes the neural correlates of cognitive control in bilingual language production” Hum Brain Mapp., 38, 5859-5870, 2017.

280. O. Monchi, M. Petrides, A. Strafella, K. Worsley, J. Doyon. “Functional role of the basal ganglia in the planning and execution of actions” Annals of Neurology, 59, 257-264, 2006.

281. A. Saunders, I. Oldenburg, V. Berezovskii, C. Johnson, N. Kingery, H. Elliott, T. Xie, et al. “A direct GABAergic output from the basal ganglia to frontal cortex” Nature, 521, 85-89, 2015.

282. F. Tecuapetla, X. Jin, S. Lima, R. Costa. “Complementary contributions of striatal projection pathways to action initiation and execution” Cell, 166, 703-715, 2016.

283. M. DeLong. “Primate models of movement disorders of basal ganglia origin” Trends in Neuroscience, 13, 281-285, 1980.

284. R. Schmidt, D. Leventhal, N. Mallet, F. Chen, J. Berke. “Canceling actions involves a race between basal ganglia pathways” Nature Neuroscience, 16, 1118-1124, 2013.

285. M. Bortoletto, R. Cunnington. “Motor timing and motor sequencing contribute differently to the preparation for voluntary movement” Neuroimage, 49, 3338-3348, 2010.

286. M. Kennefick, D. Maslovat, A. Carlsen. “The time course of corticospinal excitability during a simple reaction time task” PLoS One, 9: e113563, 2014.

287. C. Benjamin, A. Li, H. Blumenfeld, R. Constable, R. Alkawadri, S. Bickel, C. Helmstaedter, et al. “Presurgical language fMRI: Clinical practices and patient outcomes in epilepsy surgical planning” Hum Brain Mapp. 39: 2777-2785, 2018.

288. S. Prabhu, J. Gasco, S. Tummala, J. Weinberg, G. Rao. “Intraoperative magnetic resonance imaging-guided tractography with integrated monopolar subcortical functional mapping for resection of brain tumors” J Neurosurg. 114: 719-726, 2011.

289. A. Moiyadi, P. Velayutham, P Shetty, K. Seidel, A. Janu, V. Madhugiri, V. Singh et al. “Combined Motor Evoked Potential Monitoring and Subcortical Dynamic Mapping in Motor Eloquent Tumors Allows Safer and Extended Resections” World Neurosurg.120: e259-e268, 2018.

290. J. Szaflarski, D. Gloss, J. Binder, W. Gaillard, A. Golby, S. Holland, J. Ojemann et al. “Practice guideline summary: Use of fMRI in the presurgical evaluation of patients with epilepsy: Report of the Guideline Development, Dissemination, and Implementation Subcommittee of the American Academy of Neurology” Neurology. 24;88: 395-402, 2017.